Universidad de Oviedo

Programa de doctorado en Energía y Control de Procesos

Contributions to the Modeling of Resonant DC-DC Converters: Implementation of Control in Programmable Circuits

RWAMURANGWA Evode

Tesis Doctoral

2022

Universidad de Oviedo

RESUMEN DEL CONTENIDO DE TESIS DOCTORAL

1.- Título de la Tesis	
Español/Otro Idioma: Aportaciones al Modelado de Convertidores CC/CC Resonantes: Implementación del control en circuitos programables.	Inglés: Contributions to the Modeling of Resonant DC-DC Converters: Implementation of Control in Programmable Circuits.

2.- Autor	
Nombre: RWAMURANGWA Evode	
Programa de Doctorado: Energía y Control de Procesos	
Órgano responsable: Centro Internacional de Postgrado	

FOR-MAT-VOA-010 (Reg.2018)

RESUMEN (en español)

Actualmente, el costo de los diferentes circuitos de control digital ha disminuido significativamente, mientras que la complejidad y las características han aumentado. En el caso de convertidores de potencia (DC-DC), esto permite implementar diferentes estrategias de control, aprovechando las capacidades de cálculo (análisis de armónicos, etc).

Los convertidores resonantes se caracterizan por no tener un comportamiento lineal; los modelos estáticos suelen ser complejos, y la mayoría de las veces el proceso de diseño involucra ecuaciones complejas que tienen que ser representadas gráficamente. Existen diferentes métodos de análisis que intentan simplificar de alguna manera el proceso, como First Harmonic Approach para modelos estáticos y Extended Describing Function para obtener el modelo de pequeña señal, por ejemplo.

El presente trabajo trata sobre el modelado de convertidores resonantes, con el fin de implementar el modelo estático en circuitos de control digital, tales como Controladores de Señal Digital (DSC) o Arrays de Puertas Programables en Campo (FPGAs). Hay muchos artículos en las revistas más importantes (IEEE Transactions on Power Electronics, IEEE Transactions on Industrial Electronics) que revelan la importancia de esta tendencia. Durante los últimos años se han presentado varios esquemas de control basados en FPGA o DSC.

En los primeros capítulos se presentan los objetivos de la tesis y una breve revisión de los convertidores resonantes. Luego, se seleccionan dos topologías para el proceso de modelado, con el fin de validar el método propuesto: el Convertidor Resonante Serial y el Convertidor Resonante Paralelo. Estas dos topologías se utilizan en diferentes usos: el SRC es la topología típica utilizada en la transferencia de energía inalámbrica (WPT), generalmente de bajo voltaje y alta potencia, y el convertidor resonante paralelo, diseñado para aplicaciones de alto voltaje/potencia de salida. Las topologías seleccionadas están siendo estudiadas y se les aplica el método propuesto, modelado con polinomio. Para ello se siguieron los siguientes pasos, para ambas topologías:

- Modelo estático para la topología, usando análisis en el dominio del tiempo.

- Modelo polinomial obtenido del modelo anterior.
- Validación del modelo propuesto.
- Implementar el modelo en el DSC.
- Validación por simulación.
- Validación por resultados experimentales.
- Implementar el modelo en la FPGA. El modelo se ha implementado directamente en hardware; significa que no se ha utilizado el procesador nativo.
- Validación por simulación.
- Validación por resultados experimentales.
- Control de lógica difusa para el PRC, basado en polinomio. Resultados de la simulación.

Para la obtención de los diferentes modelos así como su implementación en el DSC se utilizaron herramientas de MATLAB; de esta manera, se define un proceso simplificado. El trabajo desarrollado demuestra que el método propuesto es una solución adecuada para obtener modelos de convertidores resonantes para ser implementados en circuitos digitales. En cuanto al código FPGA, se implementó en VHDL, para el SRC, evitando el uso de procesador nativo (En el caso de Altera/Intel, el Procesador Nios): de esta forma se obtiene el código más óptimo, en términos de velocidad. Los polinomios se implementaron en hardware, evitando el uso de cualquier procesador. El documento incluye diferentes resultados experimentales: se probó un PRC con alto voltaje de salida (alrededor de 5kV) y también se construyó un SRC. Los resultados experimentales obtenidos demuestran la validez de los modelos.
La tesis propone diferentes líneas de investigación, en base a los resultados obtenidos, que incluyen el desarrollo de algoritmos de control, evaluar el control de lógica difusa (basado en polinomio) en otras topologías, evaluar el método propuesto en diferentes topologías (convertidores multi-resonantes, PWM, etc.), por ejemplo.

RESUMEN (en Inglés)

Nowadays, the cost of different digital control circuits has decreased significantly, while the complexity and features has increased. In case of power converters (DC-DC), this allows to implement different control strategies, taking advantage of the calculation capabilities (harmonic analysis, etc).

The resonant converters are characterised by no linear behaviour; the static models usually are complex, and most of the times the design process involves complex equations that have to be represented graphically. There are different analysis methods that try to simplify somehow the process, such as First Harmonic Approach for static models and Extended Describing Function to obtain the small-signal model, for instance.

The present work deals with modelling resonant converters, in order to implement the static model in digital control circuits, such as Digital Signal Controllers (DSC) or Field Programmable Gate Arrays (FPGAs). There are many papers in the

most important journals (IEEE Transactions on Power Electronics, IEEE Transactions on Industrial Electronics) that reveal the importance of this trend. Several control schemes based on either FPGAs or DSCs have been presented during last years.

In the first chapters, the thesis goals and a brief review of resonant converters are presented. Then, two topologies are selected for the modelling process, in order to validate the proposed method: the Serial Resonant Converter and the Parallel Resonant Converter. These two topologies are used in different uses: The SRC is the typical topology used in Wireless Power Transfer (WPT), typically low voltage and high power, and the Parallel Resonant Converter, intended for high output voltage/power applications. The selected topologies are being studied and the proposed method, modelling with polynomial, is applied to them. In order to do it, the following steps were followed, for both topologies:

- Static model for the topology, using time domain analysis.
- Polynomial model obtained from the previous model.
- Validation of the proposed model.
- Implement the model in the DSC.
- Validation by simulation.
- Validation by experimental results.
- Implement the model in the FPGA. The model has been implemented directly in hardware; it means that the native processor has not been used.
- Validation by simulation.
- Validation by experimental results.
- Fuzzy logic control for the PRC, based on polynomial. Simulation results.

In order to obtain the different models as well as their implementation in the DSC, MATLAB tools were used; in this way, a simplified process is defined. The developed work demonstrates that the proposed method is suitable solution to obtain resonant converters models to be implemented in digitals circuits. Regarding the FPGA code, it was implemented in VHDL, for the SRC , avoiding the use of native processor (In case of Altera/Intel, the Nios Processor): in this way, the most optimum code is obtained, in terms of speed. The polynomials were implemented in hardware, avoiding the use of any processor. The document includes different experimental results: A PRC with high output voltage (around 5kV), has been tested and a SRC was also built. The experimental results obtained demonstrate the models' validity.

The thesis proposes different research lines, based on the obtained results, which include the development of control algorithms, evaluate the fuzzy logic control (based on polynomial) in another topologies, evaluate the proposed method in different topologies (multi-resonant converters, PWM, etc), for instance.

SR. PRESIDENTE DE LA COMISIÓN ACADÉMICA DEL PROGRAMA DE DOCTORADO EN ENERGÍA Y CONTROL DE PROCESOS

To my parents, Teachers, Siblings, Wife and Children .....

Acknowledgments

In completing this wonderful work, I would like to give Glory to God Almaight. I acknowledge and appreciate the support of my thesis supervisors: **Prof. Dr. Juan Diaz Gonzalez** and **Prof. Dr. Pedro Jose Villegas Saiz**. I wish to appreciate the support from my professional managers: **Jan Vriens**, **Jean Marie Prosper NDAYIRAGIJE** and **Elvis NGARAMBE** for everything you made to personally support this journey. I wish to appreciate **Dr. Albert BUTARE**, your support was necessary to complete such a good work. I strongly thank my wife **Sandra**, my kids: **Benito, Ange, Sacha and Sabel** for being there for me when it hard and easy. I tank my parents and siblings for being there for me. I acknowledge the support from the **government of Rwanda**, **Africa Improved foods** and **Africa Energy Services Group** , the operations' team and technology team in particular, you made it for me. Thank you the **Emmanuel Community** for your love and prayers. Thank you my friends, family and supporters, you did a great job. It was not that easy, but because of your support, I was able to achieve it.

Contents

1 The Outline of the Research, Objectives, Methodology and Structure 31

1.1 The Outline of the Research 31

1.2 The Objectives of the Research 33

1.3 The Methodology of the Research 34

1.4 The Structure of the Thesis 34

1 Esquema de la Investigación, Objetivos, Metodología y Estructura 37

1.1 Esquema de la investigación 37

1.2 Los objetivos de la investigación 39

1.3 La Metodología de la Investigación 40

1.4 La estructura de la tesis 40

2 The High Voltage DC Based Equipment 43

2.1 Introduction 44

2.2 High Voltage DC Applications 44

2.2.1 High Voltage DC in Medical Applications 44

2.2.1.1 Medical Imaging X-ray 45

2.2.1.2 X-ray Production 46

2.2.1.3 Projectional radiography 48

2.2.1.4 Mammography 48

2.2.1.5 Computed Tomography (CT) 49

2.2.2 High Voltage DC in Industrial Applications 50

2.2.2.1 Electron Beam Welding Machine Fundamentals . . . 51
2.2.2.2 Electrostatic Precipitator(ESP) . . . 52
2.2.2.3 Traveling-wave tube(TWT) . . . 53
2.3 High Voltage DC Conversion Sytems . . . 54
2.3.1 DC-DC Resonant Conversion Systems . . . 57
2.3.1.1 Resonant Tank Topology . . . 59
2.3.1.2 Power Transformer . . . 60
2.3.2 Parallel Resonant Converter . . . 61
2.3.3 Series Resonant Converter . . . 64
2.4 The Propositions and Contributions of the Project . . . 67
2.5 The review of the cutting-edge solutions for the implementation of resonant converter control in the programmable circuits . . . 70
2.6 Conclusions . . . 71

3 Overview of PRC and SRC Steady State Models 73
3.1 Introduction . . . 74
3.2 Steady State Model of the Series Resonant Converter . . . 75
3.2.1 Analytical study of SRC Steady State Model . . . 77
3.2.2 Graphical Represention of SRC Steady State Model . . . 80
3.3 Steady State Model of the Parallel Resonant Converter . . . 82
3.3.1 Analytical study of PRC Steady State Model . . . 83
3.3.2 Base and Normalized values . . . 84
3.3.3 PRC Operating Modes . . . 85
3.3.3.1 Mode I . . . 87
3.3.3.2 Mode II . . . 88
3.3.3.3 Optimum Mode . . . 88
3.3.4 Graphical Represention of PRC Steady State Model . . . 90
3.4 Conclusions . . . 93

4 The Polynomial Model of Resonant Converters: PRC and SRC 95
4.1 Introduction . . . 96

4.2 The polynomial model of SRC . . . 96
4.2.1 Data Fitting . . . 97
4.2.2 B-Spline Application . . . 102
4.3 The polynomial model of PRC . . . 107
4.3.1 Data Fitting . . . 108
4.3.2 B-Spline Application . . . 111
4.4 Conclusions . . . 114

5 The Modeling and Simulations of SRC 115
5.1 Introduction . . . 115
5.2 The Matlab Model of SRC . . . 116
5.3 The simulation of SRC . . . 117
5.4 The Simulink model: DSC implementation . . . 118
5.4.1 DSC Configuration . . . 119
5.4.1.1 The Use of TMS320F28335 DSC . . . 119
5.4.1.2 The Model-Based Programming . . . 119
5.4.1.3 The TMS320F28335 Control Program . . . 120
5.5 Conclusions . . . 122

6 The Modeling and Simulations of PRC 123
6.1 Introduction . . . 124
6.2 The Matlab Model of PRC . . . 124
6.2.1 Two inputs model Simulations . . . 125
6.2.2 One input model Simulations . . . 127
6.3 The Simulink model: DSC implementation . . . 129
6.3.1 DSC Configuration . . . 129
6.4 The Resonant converter controls: FPGA implementation . . . 132
6.4.1 Model-Based FPGA programming . . . 133
6.4.2 FPGA configuration to Simulink . . . 134
6.4.3 Implementation in FPGA of the direct calculation of the Frequency and Duty-Cycle . . . 135

6.5 The Fuzzy closed loop control of PRC . . . 140
6.5.1 Fuzzy Control overview . . . 141
6.5.1.1 Membership function . . . 141
6.5.2 Fuzzy closed-loop control of PRC polynomial model . . . 142
6.5.2.1 Structure of the Fuzzy Logic Controller (FLC) . . . 142
6.5.2.2 Control Setting . . . 143
6.5.2.3 Simulink model of Fuzzy controller . . . 145
6.5.2.4 Simulation results . . . 146
6.6 Conclusions . . . 148

7 The Experimental Prototyping and Results 149
7.1 Introduction . . . 150
7.2 The Experimental Consideration . . . 150
7.3 The Digital Control and Discretization . . . 151
7.4 The Experimental Set-up . . . 151
7.4.1 Gate Drivers Board . . . 152
7.4.2 Power stage . . . 152
7.5 The Outline of the experimental Results . . . 154
7.5.1 Series Resonant Converter . . . 154
7.5.1.1 DSC Configuration and PWM tests . . . 154
7.5.1.2 Experimental Power Prototype and Results . . . 156
7.5.2 Parallel Resonant Converter . . . 158
7.5.2.1 Low-Voltage Test . . . 159
7.5.2.2 High-Voltage Test . . . 163
7.5.2.3 Frequency change . . . 167
7.6 Conclusions . . . 167

8 The Conclusion and Future Development 169
8.1 Conclusions . . . 169
8.2 The Publications . . . 170
8.3 The Future Development . . . 171

8 Conclusiones y Futuros trabajos **173**

8.1 Conclusiones . . . 173

8.2 Publicaciones . . . 174

8.3 Futuros trabajos . . . 175

A Tables of Parallel Resonant converter Data **177**

A.1 Introduction . . . 177

A.2 Tables . . . 178

B Tables of Series Resonant Converter Data **193**

B.1 Introduction . . . 193

C PRC and SRC polynomials in Matlab Codes **243**

C.1 PRC Polynomial Codes . . . 243

C.2 SRC Polynomial Codes . . . 248

C.2.1 Initial resonant current polynomial . . . 248

C.2.2 Frequency polynomial . . . 252

D FPGA codes for the PRC polynomial model **257**

D.1 Introduction . . . 257

D.2 The Codes Cuadrado block . . . 258

D.3 The Codes Cubo block . . . 259

D.4 The Codes Motor block . . . 261

D.5 The Codes Motor block . . . 262

D.6 The Codes Sumafin block . . . 264

D.7 The Codes Vectorespos block . . . 265

E Publications **269**

E.1 The list of publications . . . 269

List of Figures

2-1 Illustration of x-ray radiation location in the electronic spectrum[88] . 46
2-2 Illustration of X-ray generation system components[88] 46
2-3 X-ray production by energy conversion[88] 47
2-4 Illustration of the Projectional X-ray working principle[21] 48
2-5 Image acquisition on projectional X-ray[69] 49
2-6 Attenuation of breast tissues on energy[44] 50
2-7 Electron Beam welding machine working principle[50] 51
2-8 Electrostatic Precipitator working principle[33, 9] 52
2-9 Traveling-Wave working principle[56] 54
2-10 Illustration HV DC conversion and energy transfer process 55
2-11 Illustration of (a) hard switching and (b) soft switching, with ZVS and ZCS shown. 56
2-12 Illustration of the complete power conversion stream 57
2-13 Illustration of the resonant converter 57
2-14 Resonant Tank: (a) Series Resonant; (b) Parallel Resonant; (c) Series-Parallel Resonant. 60
2-15 Illustration of equivalent topology to the step-up transformer 61
2-16 Parallel resonant DC-DC converter applied at full with output capacitive filter 62
2-17 PRC voltage conversion characteristics, with respect to the load level and frequency 64

2-18 Series resonant DC-DC converter applied at full with output capacitive filter . . . 65
2-19 SRC voltage conversion characteristics, with respect to the load level and frequency . . . 66
2-20 The process of generating a polynomial model from the PRC's steady state models is depicted in this illustration. . . . 68
2-21 Illustration SRC of the Polynomial model construction from the steady state Model . . . 69

3-1 SRC block with major related waveforms[100] . . . 76
3-2 SRC main waveforms and its equivalent circuits. . . . 80
3-3 Voltage gain vs. period (top) and output power vs. voltage gain, every curve is plotted for initial current different values. All the magnitudes are normalized. . . . 81
3-4 The PRC with the resonant tank components embedded in the Power Transformer. . . . 83
3-5 Output of PRC in terms of voltage and current in optimum mode of operation . . . 83
3-6 Mode I: at (a), Capacitor (C_p) voltage clamps before DT. Mode II: at (b) the capacitor (C_p) voltage clamp is produced after DT. Both the figures (a) and (b) illustrate Mode I and Mode II in Optimum mode[25] 86
3-7 The illustration of Mode I and Mode II in their respective circuitry and expression, both in their Optimum Mode. . . . 87
3-8 Normalized output voltage vs normalized frequency for two values of duty cycles[25] . . . 91
3-9 Normalized frequency vs normalized power and duty vs normalized power in presence of normalized voltage . . . 91
3-10 Illustration of normalized frequency vs normalized power and duty vs normalized power in presence of normalized voltage with the related behaviors . . . 92

4-1 Data fitting application on plot $\hat{v}$ = –0.75 on the figure 3-3 (at the bottom) . . . 98
4-2 Data fitting application on plot $\hat{I}_o$ = –0.01 on the figure 3-3 (at the top). 99
4-3 Illustration of a_0 coefficient through Data fitting and B-spline application. 103
4-4 Data fitting application on Frequency and Duty in presence of $\hat{v} = 1.1$ and $\hat{v} = 1.7$. . . . 108
4-5 Illustration of a_0 plotting, Data fitting and B-Spline application. . . . 111

5-1 The illustration of the Simulink topology of the SRC polynomial model 117
5-2 The SRC inverter output Voltage and Current . . . 118
5-3 Illustration of Texas Instrument (TI) TMS320F28335 DSC[101] . . . 120
5-4 PWM code generation model in Simulink . . . 121

6-1 Illustration of Simulink model with normalized voltage and normalized power as inputs . . . 125
6-2 The voltage and current output of the converter with Normalized output voltage and normalized power as inputs . . . 126
6-3 One input Simulink control model . . . 127
6-4 Inverter voltage, Current and power at fixed load . . . 128
6-5 PWM Generation Model in Simulink . . . 131
6-6 The Arrow DECA Max 10 FPGA . . . 134
6-7 Illustration of the steps to generated the FPGA program from the Simulink Model[68] . . . 135
6-8 Illustration of how numbers are stored in memory. . . . 136
6-9 The illustration of results for $\hat{v}$=1.15, 1.11 and 1.18 . . . 138
6-10 Illustration of results: (a) cubic block and (b) Square block . . . 138
6-11 Illustration of precise clock signals generation . . . 139
6-12 Illustration of FPGA complete model in Altera. The codes for various blocks shown in this figure are detailed in Appendix D . . . 139
6-13 The illustration of fuzzy controller structure . . . 143
6-14 The illustration of fuzzification and defuzzification process . . . 143

6-15 The illustration of fuzzy control design 145
6-16 The illustration of fuzzy controller structure 146
6-17 The illustration of fuzzy controller performance 146
6-18 The illustration of fuzzy controller performance 147
6-19 The illustration of inverter current and voltage 147
6-20 The illustration of power transfer profile 148

7-1 Illustration of the complete model of the practical implementation. . . 151
7-2 Driver Board Schematic 152
7-3 The F4-150R12KS4 IGBTs embedded structure 153
7-4 Illustration of embedded F4-150R12KS4 IGBTs 153
7-5 Illustration of the PWM generated at the normalized power $\hat{p} = 0.10$ and generate a frequency f = 86.87kHz. 155
7-6 The PWM signal for inverter switching with deat-time of 700 ns . . . 156
7-7 The illustration of the inverter current and voltage, based on the operation point 1 in the table 7.2 157
7-8 The illustration of the inverter current and voltage, based on the operation point 3 in the table 7.2 158
7-9 Illustration of the low-voltage prototype 160
7-10 Illustration of normalized frequency and duty at a fixed load of $\hat{\Omega} = 1.387$, corresponding to 10 Ω. 161
7-11 Illustration of the prototype output results as illustrated in table 7.4, Operational point 1 161
7-12 Illustration of the prototype output results as illustrated in table 7.4, Operational point 2 162
7-13 Illustration of the prototype output results as illustrated in table 7.4, Operational point 3 163
7-14 Illustration of the high-voltage prototype. 164
7-15 Illustration of converter output at 2 kV output voltage, following the data on scenario 1, operational point 1 in the table 7.5 166

7-16 Illustration of converter output at 4 kV output voltage, following the data on scenario 2, operational point 1 in the table 7.5 166
7-17 Frequency change from 51.387 kHZ to 26.144 kHz 167

List of Tables

4.1 Coefficients of resulted $\hat{I}_o$ equivalent polynomials by applying Data fitting applied to plots on the figure 3-3 (at the Bottom). 100

4.2 Coefficients of resulted $\hat{T}$ equivalent polynomials by applying Data fitting applied to plots 0n the figure 3-3 (at the top). 101

4.3 Illustration of current polynomial coeficients. 104

4.4 Illustration of coefficients specific to the polynomial coefficients in Table 4.2 after B-spline application. 105

4.5 Illustration of coefficients specific to the polynomial coefficients in Table 4.2 after B-spline application. 106

4.6 The table illustrates various coefficients of different fittings on frequency plots, at specific levels of voltage. a_i: coefficients for frequency fitting. 109

4.7 The table illustrates various coefficients of different fittings on duty plots, at specific levels of voltage. b_i: coefficients for duty fitting. . . . 110

4.8 This table shows the specific coeffiecients retrieved from the coefficients in table 4.6 after B-spline. 112

4.9 This table shows the specific coeffiecients retrieved from the coefficients in table 4.7 after B-spline. 113

5.1 The parameters used to simulate the SRC model in Simulink 117

5.2 Illustration of the SRC simulation results 118

6.1 The parameters used to simulate the model in figure 6-1 with variable load 126
6.2 Simulation parameters and results of the PRC in two inputs case . . 127
6.3 Simulation parameters and results of the PRC in single input case . . 128
6.4 Illustration of ranges for the error and delta error, normalized frequency $\hat{f}$, the normalized output voltage $\hat{v}$, the normalized output power $\hat{p}$ and duty cycle. 144
6.5 This table shows the range of various membership functions respective to the variable i.e. input or output 144
6.6 The illustation of Fuzzy rule base defining the relation between the input and the output 145

7.1 Illustration of the experimental validation of the SRC polynomial model as indicated in figure 5-4 155
7.2 Illustration of polynomial model expermental testing and comparative study to various other models of SRC. 157
7.3 This table shows different operating points in the design operating window of the prototype in Figure 7-9 with the load of $10\Omega \approx \hat{\Omega}=1.387$ 160
7.4 Illustration of low voltage polynomial model experimental testing for PRC with f_r= 33.517 kHz and $\hat{\Omega}=1.387$ 162
7.5 Illustration of PRC polynomial model tests on High Voltage scenarios 165

A.1 Frequency vs Power at the Normalized voltage $\hat{v}$ varying from 1.0 to 1.4 179
A.2 Frequency vs Power at the Normalized voltage $\hat{v}$ varying from 1.5 to 1.9 180
A.3 Frequency vs Power at the Normalized voltage $\hat{v}$ varying from 2.0 to 2.4 181
A.4 Frequency vs Power at the Normalized voltage $\hat{v}$ varying from 2.5 to 2.9 182
A.5 Frequency vs Power at the Normalized voltage $\hat{v}$ varying from 3.0 to 3.4 183
A.6 Frequency vs Power at the Normalized voltage $\hat{v}$ varying from 3.5 to 4.0 184
A.7 Maximum Power, Maximum Frequency and Maximum expected load at each level of Normalize voltage $\hat{v}$. 185
A.8 Duty vs Power at the Normalized voltage $\hat{v}$ varying from 1.0 to 1.4 . 186

A.9 Duty vs Power at the Normalized voltage $\hat{v}$ varying from 1.5 to 1.9 . 187
A.10 Duty vs Power at the Normalized voltage $\hat{v}$ varying from 2.0 to 2.4 . 188
A.11 Duty vs Power at the Normalized voltage $\hat{v}$ varying from 2.5 to 2.9 . 189
A.12 Duty vs Power at the Normalized voltage $\hat{v}$ varying from 3.0 to 3.4 . 190
A.13 Duty vs Power at the Normalized voltage $\hat{v}$ varying from 3.5 to 4.0 . 191
A.14 Maximum Power and Maximum Duty at each level of Normalize voltage $\hat{v}$. 192

B.1 Period vs Normalized output voltage $\hat{v}$ from 0.00 to 0.39 in Presence of $\hat{I}_o$ from –0.01 to –0.09. 194
B.2 Period vs Normalized output voltage $\hat{v}$ from 0.40 to 0.79 in Presence of $\hat{I}_o$ from –0.01 to –0.09. 195
B.3 Period vs Normalized output voltage $\hat{v}$ from 0.79 to 0.99 in Presence of $\hat{I}_o$ from –0.01 to –0.09. 196
B.4 Period vs Normalized output voltage $\hat{v}$ from 0.00 to 0.39 in Presence of $\hat{I}_o$ from –0.10 to –0.18. 197
B.5 Period vs Normalized output voltage $\hat{v}$ from 0.40 to 0.79 in Presence of $\hat{I}_o$ from –0.10 to –0.18. 198
B.6 Period vs Normalized output voltage $\hat{v}$ from 0.80 to 0.95 in Presence of $\hat{I}_o$ from –0.10 to –0.18. 199
B.7 Period vs Normalized output voltage $\hat{v}$ from 0.00 to 0.39 in Presence of $\hat{I}_o$ from –0.10 to –0.18. 200
B.8 Period vs Normalized output voltage $\hat{v}$ from 0.40 to 0.79 in Presence of $\hat{I}_o$ from –0.10 to –0.18. 201
B.9 Period vs Normalized output voltage $\hat{v}$ from 0.80 to 0.95 in Presence of $\hat{I}_o$ from –0.10 to –0.18. 202
B.10 Period vs Normalized output voltage $\hat{v}$ from 0.00 to 0.39 in Presence of $\hat{I}_o$ from –0.19 to –0.27. 203
B.11 Period vs Normalized output voltage $\hat{v}$ from 0.40 to 0.79 in Presence of $\hat{I}_o$ from –0.19 to –0.27. 204

B.12 Period vs Normalized output voltage $\hat{v}$ from 0.80 to 0.91 in Presence of $\hat{I}_o$ from –0.19 to –0.27. 205
B.13 Period vs Normalized output voltage $\hat{v}$ from 0.00 to 0.39 in Presence of $\hat{I}_o$ from –0.28 to –0.36. 206
B.14 Period vs Normalized output voltage $\hat{v}$ from 0.40 to 0.79 in Presence of $\hat{I}_o$ from –0.28 to –0.36. 207
B.15 Period vs Normalized output voltage $\hat{v}$ from 0.80 to 0.87 in Presence of $\hat{I}_o$ from –0.28 to –0.36. 208
B.16 Period vs Normalized output voltage $\hat{v}$ from 0.00 to 0.39 in Presence of $\hat{I}_o$ from –0.37 to –0.45. 209
B.17 Period vs Normalized output voltage $\hat{v}$ from 0.40 to 0.79 in Presence of $\hat{I}_o$ from –0.37 to –0.45. 210
B.18 Period vs Normalized output voltage $\hat{v}$ from 0.80 to 0.84 in Presence of $\hat{I}_o$ from –0.37 to –0.45. 211
B.19 Period vs Normalized output voltage $\hat{v}$ from 0.00 to 0.39 in Presence of $\hat{I}_o$ from –0.46 to –0.54. 212
B.20 Period vs Normalized output voltage $\hat{v}$ from 0.40 to 0.79 in Presence of $\hat{I}_o$ from –0.46 to –0.54. 213
B.21 Period vs Normalized output voltage $\hat{v}$ from 0.80 to 0.81 in Presence of $\hat{I}_o$ from –0.46 to –0.54 214
B.22 Period vs Normalized output voltage $\hat{v}$ from 0.00 to 0.39 in Presence of $\hat{I}_o$ from –0.55 to –0.63. 215
B.23 Period vs Normalized output voltage $\hat{v}$ from 0.40 to 0.77 in Presence of $\hat{I}_o$ from –0.55 to –0.63. 216
B.24 Period vs Normalized output voltage $\hat{v}$ from 0.00 to 0.39 in Presence of $\hat{I}_o$ from –0.64 to –0.72. 217
B.25 Period vs Normalized output voltage $\hat{v}$ from 0.40 to 0.74 in Presence of $\hat{I}_o$ from –0.64 to –0.72. 218
B.26 Period vs Normalized output voltage $\hat{v}$ from 0.00 to 0.39 in Presence of $\hat{I}_o$ from –0.73 to –0.80. 219

B.27 Period vs Normalized output voltage $\hat{v}$ from 0.40 to 0.70 in Presence of $\hat{I}_o$ from –0.73 to –0.80. 220
B.28 Coefficients of resulted equivalent polynomials by Data Fitting application. 221
B.29 Coefficients of resulted equivalent polynomials by Data Fitting application. 222
B.30 Simulation and Practical Test results of the SRC code Model. 223
B.31 Normalized Power $\hat{p}$ vs Normalized initial resonant current $\hat{I}_0$ in presence of normalized output voltage $\hat{v}$. 224
B.32 Normalized Power $\hat{p}$ vs Normalized initial resonant current $\hat{I}_0$ in presence of normalized output voltage $\hat{v}$. 225
B.33 Normalized Power $\hat{p}$ vs Normalized initial resonant current $\hat{I}_0$ in presence of normalized output voltage $\hat{v}$. 226
B.34 Normalized Power $\hat{p}$ vs Normalized initial resonant current $\hat{I}_0$ in presence of normalized output voltage $\hat{v}$. 227
B.35 Normalized Power $\hat{p}$ vs Normalized initial resonant current $\hat{I}_0$ in presence of normalized output voltage $\hat{v}$. 228
B.36 Normalized Power $\hat{p}$ vs Normalized initial resonant current $\hat{I}_0$ in presence of normalized output voltage $\hat{v}$. 229
B.37 Normalized Power $\hat{p}$ vs Normalized initial resonant current $\hat{I}_0$ in presence of normalized output voltage $\hat{v}$. 230
B.38 Normalized Power $\hat{p}$ vs Normalized initial resonant current $\hat{I}_0$ in presence of normalized output voltage $\hat{v}$. 231
B.39 Normalized Power $\hat{p}$ vs Normalized initial resonant current $\hat{I}_0$ in presence of normalized output voltage $\hat{v}$. 232
B.40 Normalized Power $\hat{p}$ vs Normalized initial resonant current $\hat{I}_0$ in presence of normalized output voltage $\hat{v}$. 233
B.41 Normalized Power $\hat{p}$ vs Normalized initial resonant current $\hat{I}_0$ in presence of normalized output voltage $\hat{v}$. 234

B.42 Normalized Power $\hat{p}$ vs Normalized initial resonant current $\hat{I}_0$ in presence of normalized output voltage $\hat{v}$. 235
B.43 Normalized Power $\hat{p}$ vs Normalized initial resonant current $\hat{I}_0$ in presence of normalized output voltage $\hat{v}$. 236
B.44 Normalized Power $\hat{p}$ vs Normalized initial resonant current $\hat{I}_0$ in presence of normalized output voltage $\hat{v}$. 237
B.45 Normalized Power $\hat{p}$ vs Normalized initial resonant current $\hat{I}_0$ in presence of normalized output voltage $\hat{v}$. 238
B.46 Normalized Power $\hat{p}$ vs Normalized initial resonant current $\hat{I}_0$ in presence of normalized output voltage $\hat{v}$. 239
B.47 Normalized Power $\hat{p}$ vs Normalized initial resonant current $\hat{I}_0$ in presence of normalized output voltage $\hat{v}$. 240
B.48 Normalized Power $\hat{p}$ vs Normalized initial resonant current $\hat{I}_0$ in presence of normalized output voltage $\hat{v}$. 241

C.1 Illustration of the practical validation of the SRC polynomial model as indicated in the figure 5-4 255

Chapter 1

The Outline of the Research, Objectives, Methodology and Structure

Contents

1.1 The Outline of the Research 31
1.2 The Objectives of the Research 33
1.3 The Methodology of the Research 34
1.4 The Structure of the Thesis 34

1.1 The Outline of the Research

This Ph.D. thesis is framed within the scope of electrical engineering, specifically in the disciplines of industrial electronics, power electronics, and control systems. The recent developments in power converters, energy conversion, with advances in control strategies and systems are leading a technological revolution to enhance the growth

of High Voltage DC application. This concept is based on the use of various control strategies and topologies applied to various Power electronics energy converters to generate high voltage. The envisaged high voltage is at the level of tens of kilo-volts. Therefore, the energy density, system efficiency, reliable and simple control topology are the major focuses of this work.

A couple of converters to provide DC output voltage were developed for various applications, and very different: High Voltage (HV) and Wireless Power Transformer (WPT). As far as HV converters are concerned, with the drastic increase in high voltage DC applications, the resonant converters' use has known a radical growth. There are various suitable topologies of the resonant converters, depending on the application, the level of output voltage required and the envisaged control strategies. This work considers Parallel Resonant Converter (PRC) and Series Resonant Converters (SRC) topologies for HV and WPT applications respectively. It limits itself to the control part of those, to ensure minimum losses, reliability, and energy density, enable different control strategies, and a larger span of application. Bearing in mind the different digital controllers, it is interesting to consider digital control. In this work, a methodology to implement the converter control, based on a simplified model in digital controllers is proposed. The PRC and SRC will be modeled and analyzed in this work. The steady-state model shall be shown, its advantages are outlined and its complexities in terms of building the control strategies are detailed. For ease of control and the implementation on complex digital circuits, the polynomial model is introduced and implemented in this work. Therefore, the PRC & SRC, their respective steady-state model, their simplified model, and their control built in Matlab-Simulink are outlined in this work. They are validated through simulation and practical implementation. Different programmable circuits. i.e. DSCs and FPGAs are used for control purposes. On the other hand, the closed-loop control using Fuzzy logic is proposed and tackled in this work. More closed loop proposals and deep analysis and the use of gate array circuits shall be considered in future work.

In order to achieve this crucial goal, the objectives set were established in the next section. Then, the methodology for the accomplishment of the set objectives is discussed

and in the end, the structure of the complete thesis is indicated.

1.2 The Objectives of the Research

In order to fulfill the main targets of this work, a number of objectives have to be picked out. Those objectives will be tracked along the chapters and their respective accomplishments will be evaluated at the end of this work. The following are the objectives:

- Outline of High Voltage DC based equipment in various use i.e. Medical and Industrial.
- The review on the use of resonant converters in the High voltage applications.
- Identification and definition of the topologies of study.
- Steady-state modeling and outline of the operating and control points.
- Polynomial modeling of the topology, and open-loop control study.
- Implementation of the models in the programmable circuits.
- Proposing the closed loop control option for the great performance of the model.
- Establishment of the design methodology for validation and implementation of the proposed solution.
- Validation of the proposed solutions through the simulations and experimental test in laboratory prototypes.
- Critical analysis of the results, conclusions and establishment of future development and improvements.

1.3 The Methodology of the Research

The established methodology starts with the revision of cutting-edge solutions for the implementation of resonant converter control in programmable circuits. The major emphasis goes to high voltage DC applications aspects, the energy conversion topologies involved, the potential challenges, and the applied technologies in terms of control, control methods, and strategies. The comparison of the technologies, topologies, and control strategies is performed in order to outline the bases of the research to carry out. The bases performance are evaluated in all operating modes, conditions, and control strategies. The drawbacks and limitations of those bases will be analyzed and highlighted and alternatives shall be proposed as mitigation measures. The performance of critical comparison of the proposed solutions against the bases shall be illustrated by this methodology. Therefore, the design procedure, set conditions, and constraints, for both the bases and proposed solutions will be carried out. The design methods will be given value through the evaluation of the system performance by simulations and experimental results from a laboratory prototype. In the end, the analysis of the results will be done and the conclusions driven from the research will be drawn.

1.4 The Structure of the Thesis

In order to accomplish the outlined objectives of this work, the following lines show the structure of this thesis.

Chapter 2 Introduces High Voltage DC based equipment, the application and the targeted technology. It identifies the high voltage topology of study and its comparison with the rest of the topologies in the same scope. The challenge and gaps of the chosen technology of application and the respective topologies are outlined. The resonant converters are set as the suitable alternative to the identified drawbacks, and their control becomes a humping point. Therefore the hypothesis of the thesis is

established.

Chapter 3 Introduces the resonant converters, with strong emphasis on the Series Resonant Converter(SRC) and Parallel Resonant Converters (PRC). The steady-state model for both topologies is detailed in this chapter, the related control strategies are outlined. However, due to the complexities of both topologies; the graphical representations are used for better understanding and build the control design. Various operating mode were indicated in this chapter, and normalized values are used to avoid limitations on the operating span.

Chapter 4 The polynomial model for both SRC and PRC converter is shown. This comes in as a solution for better illustration of the converter control; mostly when the complex micro-controllers are used. The conversion of graphical data into polynomials using the numerical analysis like Data Fitting and B-spline are illustrated in this chapter. The polynomial model general equations for both converter topologies are illustrated in this chapter.

Chapter 5 and **Chapter 6** show modeling and simulations of SRC and PRC respectively in Simulink. The models for both topologies were built in Simulink and simulated for validation purposes. The Simulink models were done for each of the topologies and the DSC (F28335) and FPGA (Arrow Deca Max 10) are configured to Simulink in these chapters. The model-based programming option for both DSC an FPGA in Simulink was introduced. In **Chapter 6** specifically the PRC closed loop control was introduced using Fuzzy logic controller.

Chapter 7 shows the experimental prototyping, the practical validation of the models built in previous chapters. The components of the prototypes are shown in this chapter. The analysis of the results and comparisons with those of simulations are illustrated in this chapter.

Chapter 8 Shows the conclusions drawn from the results analysis in the **Chapter 7**, the open points in the projects that are suggested for future development and the publications. In those, this chapter indicates the published work related to this thesis, those which are not related to this thesis and those which are in publication

processes.

Chapter 1

Esquema de la Investigación, Objetivos, Metodología y Estructura

Contents

1.1 Esquema de la investigación 37
1.2 Los objetivos de la investigación 39
1.3 La Metodología de la Investigación 40
1.4 La estructura de la tesis 40

1.1 Esquema de la investigación

Este doctorado La tesis se enmarca en el ámbito de la ingeniería eléctrica, concretamente en las disciplinas de electrónica industrial, electrónica de potencia y sistemas de control. Los desarrollos recientes en convertidores de potencia, conversión de energía, con avances en estrategias y sistemas de control están liderando una revolución

tecnológica para mejorar el crecimiento de la aplicación de CC de alto voltaje. Este concepto se basa en el uso de varias estrategias de control y topologías aplicadas a varios convertidores de energía de electrónica de potencia para generar alta tensión. El alto voltaje previsto está en el nivel de decenas de kilovoltios. Por lo tanto, la densidad de energía, la eficiencia del sistema y la topología de control confiable y simple son los principales enfoques de este trabajo.

Se desarrollaron un par de convertidores para proporcionar tensión de salida de CC para diversas aplicaciones, y muy diferentes: Alta tensión (HV) y Transformador de potencia inalámbrico (WPT). En lo que respecta a los convertidores HV, con el drástico aumento de las aplicaciones de CC de alta tensión, el uso de convertidores resonantes ha experimentado un crecimiento radical. Hay varias topologías adecuadas de los convertidores resonantes, dependiendo de la aplicación, el nivel de voltaje de salida requerido y las estrategias de control previstas. Este trabajo considera las topologías de Convertidores Resonantes Paralelos (PRC) y Convertidores Resonantes en Serie (SRC) para aplicaciones de AT y TIP respectivamente. Se limita a la parte de control de estos, para garantizar pérdidas mínimas, confiabilidad y densidad de energía, permitir diferentes estrategias de control y una mayor amplitud de aplicación. Teniendo en cuenta los diferentes controladores digitales, es interesante considerar el control digital. En este trabajo se propone una metodología para implementar el control del convertidor, basada en un modelo simplificado en controladores digitales. El PRC y el SRC serán modelados y analizados en este trabajo. Se mostrará el modelo de estado estacionario, se esbozarán sus ventajas y se detallarán sus complejidades en cuanto a la construcción de las estrategias de control. Para facilitar el control y la implementación en circuitos digitales complejos, en este trabajo se presenta e implementa el modelo polinomial. Por lo tanto, en este trabajo se describen los PRC & SRC, su respectivo modelo de estado estacionario, su modelo simplificado y su control integrado en Matlab-Simulink. Se validan mediante simulación e implementación práctica. Diferentes circuitos programables. es decir, los DSC y los FPGA se utilizan con fines de control. Por otra parte, en este trabajo se propone y aborda el control en lazo cerrado mediante lógica difusa. En trabajos futuros se considerarán más

propuestas de bucle cerrado y un análisis profundo y el uso de circuitos de matriz de puertas.
Para lograr este objetivo crucial, los objetivos planteados se establecieron en la siguiente sección. Luego se discute la metodología para el cumplimiento de los objetivos planteados y al final se indica la estructura de la tesis completa.

1.2 Los objetivos de la investigación

Para cumplir con los objetivos principales de este trabajo, es necesario señalar una serie de objetivos. Dichos objetivos serán rastreados a lo largo de los capítulos y sus respectivos logros serán evaluados al final de este trabajo. Los siguientes son los objetivos:

- Resumen de equipos basados en CC de alta tension en diversos usos, es decir, médicos y industriales.
- La revisión sobre el uso de convertidores resonantes en las aplicaciones de alto voltaje.
- Identificación y definición de las topologías de estudio.
- Modelado de estado estacionario y esquema de los puntos de operación y control.
- Modelado polinomial de la topología de estudio y estudio de control de bucle abierto.
- Implementación de los modelos en los circuitos programables.
- Proponiendo la opción de control en lazo cerrado para el gran desempeño del modelo.
- Establecimiento de la metodología de diseño para la validación e implementación de la solución propuesta.
- Validación de las soluciones propuestas a través de las simulaciones y pruebas experimentales en prototipos de laboratorio.

- Análisis crítico de los resultados, conclusiones y establecimiento de futuros desarrollos y mejoras.

1.3 La Metodología de la Investigación

La metodología establecida parte de la revisión de soluciones punteras para la implementación del control del convertidor resonante en circuitos programables. El mayor énfasis se pone en los aspectos de las aplicaciones de CC de alto voltaje, las topologías de conversión de energía involucradas, los desafíos potenciales y las tecnologías aplicadas en términos de control, métodos de control y estrategias. Se realiza la comparación de las tecnologías, topologías y estrategias de control con el fin de trazar las bases de la investigación a realizar. El desempeño de las bases se evalúa en todos los modos de operación, condiciones y estrategias de control. Se analizarán y destacarán los inconvenientes y limitaciones de dichas bases y se propondrán alternativas como medidas de mitigación. El desempeño de la comparación crítica de las soluciones propuestas contra las bases será ilustrado por esta metodología. Por tanto, se llevará a cabo el procedimiento de diseño, condiciones establecidas y restricciones, tanto de las bases como de las soluciones propuestas. Los métodos de diseño se valorizarán mediante la evaluación del rendimiento del sistema mediante simulaciones y resultados experimentales a partir de un prototipo de laboratorio. Al final, se realizará el análisis de los resultados y se extraerán las conclusiones derivadas de la investigación.

1.4 La estructura de la tesis

Para cumplir con los objetivos planteados en este trabajo, a continuación se muestra la estructura de esta tesis.

Capítulo 2 presenta la Alta Tensión CC, la aplicación y la tecnología objetivo, la identificación de la topología y su comparación con el resto de topologías del mismo ámbito. Se describen el desafío y las lagunas de la tecnología de aplicación elegida y las topologías respectivas. Los convertidores resonantes se configuran como la al-

ternativa adecuada a los inconvenientes identificados, y su control se convierte en un escollo. Por lo tanto se establece la hipótesis de la tesis.

Capítulo 3 introduce los convertidores resonantes, con fuerte énfasis en los convertidores resonantes en serie (SRC) y los convertidores resonantes en paralelo (PRC). En este capítulo se detalla el modelo de estado estacionario para ambas topologías y se describen las estrategias de control relacionadas. Sin embargo, debido a las complejidades de ambas topologías; las representaciones gráficas se utilizan para una mejor comprensión y construcción del diseño de control. En este capítulo se indicaron varios modos de funcionamiento y se utilizan valores normalizados para evitar limitaciones en el intervalo de funcionamiento.

Capítulo 4 Se muestra el modelo polinomial para el convertidor SRC y PRC. Esto viene como una solución para ilustrar mejor el control del convertidor; principalmente cuando se usan microcontroladores pequeños. En este capítulo se ilustra la conversión de datos gráficos en polinomios mediante el análisis numérico como Ajuste de datos y B-spline. Las ecuaciones generales del modelo polinomial para ambas topologías de convertidores se ilustran en este capítulo.

Capítulo 5 y **Capítulo 6** muestran modelos y simulaciones de SRC y PRC respectivamente en Simulink. Los modelos para ambas topologías se construyeron en Simulink y se simularon con fines de validación. Los modelos de Simulink se realizaron para cada una de las topologías y el DSC (F28335) y FPGA (Arrow Deca Max 10) se configuran para Simulink en estos capítulos. En **Capítulo 6** específicamente, se introdujo el control de bucle cerrado PRC utilizando el controlador de lógica difusa.

Capítulo 7 muestra la creación de prototipos experimentales, la validación práctica de los modelos construidos en capítulos anteriores. Los componentes de los prototipos se muestran en este capítulo. El análisis de los resultados y las comparaciones con los de las simulaciones se ilustran en este capítulo.

Capítulo 8 Muestra las conclusiones extraídas del análisis de resultados en el **Capítulo 7**, los puntos abiertos en los proyectos que se sugieren para desarrollo futuro y las publicaciones. En aquellos, este capítulo indica los trabajos publicados relacionados con esta tesis, los que no están relacionados con esta tesis y los que están en proceso

de publicación.

Chapter 2

The High Voltage DC Based Equipment

Contents

2.1 Introduction 44
2.2 High Voltage DC Applications 44
2.2.1 High Voltage DC in Medical Applications 44
2.2.2 High Voltage DC in Industrial Applications 50
2.3 High Voltage DC Conversion Sytems 54
2.3.1 DC-DC Resonant Conversion Systems 57
2.3.2 Parallel Resonant Converter 61
2.3.3 Series Resonant Converter 64
2.4 The Propositions and Contributions of the Project 67
2.5 The review of the cutting-edge solutions for the implementation of resonant converter control in the programmable circuits 70
2.6 Conclusions 71

2.1 Introduction

Nowadays, in modern technologies, High Voltage DC dominates a couple of application environments. The voltage in the level of Kilo-volts is crucial in various application: Medical, industrial, environmental, instrumentation and measurement, etc[82]. In medical practices, X-ray is the right instance of high voltage DC use. Medical x-ray imaging systems are know in series of Mammography, Computed Tomography (CT), Projectional Radiography, etc[10]. The electronic beam welding (EBW) machines, Traveling Wave Tubes (TWT) and Electrostatic Precipitator(EP) make an example of industrial application are powered by high-voltage DC too[65]. This chapter outlines different high voltage DC applications and various switch mode power supply systems illustrating those that are suitable for the mentioned applications. The resonant converters as part of the switch mode power supply will be deeply illustrated in this work. The state-of-art of this project will be shown in this chapter, and more of the core objective and novelty will be illustrated.

2.2 High Voltage DC Applications

As indicated previously, high voltage DC is applied in various domain including medical and industrial. It has been reliable for long distance power transmission[94], in smart welding systems[50] and medical imaging[88]. The most commonly known equipment are medical X-ray imaging systems(Mammography, Computed Tomography, Projectional Radiography) and industrial (Electronic Beam welding machine, Traveling-wave Tubes (TWT), and Electrostatic Precipitator). This section elaborates more on the working principles of indicated equipment , with major focus on the power supply and the technology applied.

2.2.1 High Voltage DC in Medical Applications

In specific use such as medical, a special application of high-voltage DC-DC converter is capital to drive the concerned apparatus[10]. Hence, the medical equipment must

have a specific ability to tune its DC output voltage in order to track the required quality of image[10]. Depending on the application, some equipment are required to operate over a wide range of voltage; the regulation is done through controlling the DC output voltage across the equipment[10]. In most of the cases, the required DC output voltage is generated as low voltage and boosted to the level of use[29]. It involves various type of converters. This part focuses on high voltage DC application in medical equipment. It outlines medical X-ray sytems, with emphasis on: Mammography, Computed Tomography (CT), Projectional Radiography. Their respective principles of functionality shall be elaborated and the role of High voltage DC shall be outlined.

2.2.1.1 Medical Imaging X-ray

The X-ray is a type of electromagnetic radiation (EM) of same category as microwaves, infrared, visible and ultraviolet light[10]. It is periodic and cyclic radiation in characteristics; having in it electrical and magnetic fields, with period and wave-length as its in both time and space representation. The wavelength for diagnostic x-ray is basically from 10nm to 0.01nm as illustrated in figure. 2-1, ranged between ultraviolet light and cosmic rays. Hence, it can be mathematically represented in terms of velocity ($C = \lambda/T$ or $C = \lambda f$) and energy ($E = hf$). With λ standing for wavelength, and h for Planck's constant. The electromagnetic energy mentioned can be viewed in the Einstein's theory of relativity, where $E = mc^2$. Hence, X-rays are results of kinetic energy conversion reached through electron's accelerations under a given potential difference[88]. The X-rays have been in medical use since soon after their discovery by Roentgen in 1896[88]. The use of X-ray in medical practices bases on the X-ray differential attenuation once in contact with the human body. In case of contact with the patient's part of diagnosis, the uniform x-ray beam incident on tissues produces a transmitted x-ray flux that is affected by the attenuation along its path. The shadow of internal targeted anatomy is re-produced.

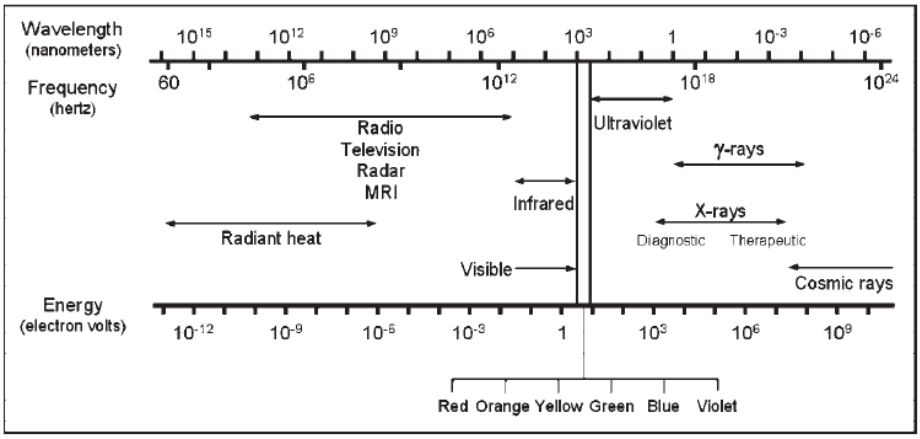

Figure 2-1: Illustration of x-ray radiation location in the electronic spectrum[88]

2.2.1.2 X-ray Production

In X-ray production and control, the X-ray tube and X-generator are capital component. The X-ray tube gives an adequate environment and components to generate X-rays; while the x-ray generator is responsible for the source of electrical voltage and interface controls to energize the x-ray tube. Inside the X-ray tube, two electrodes

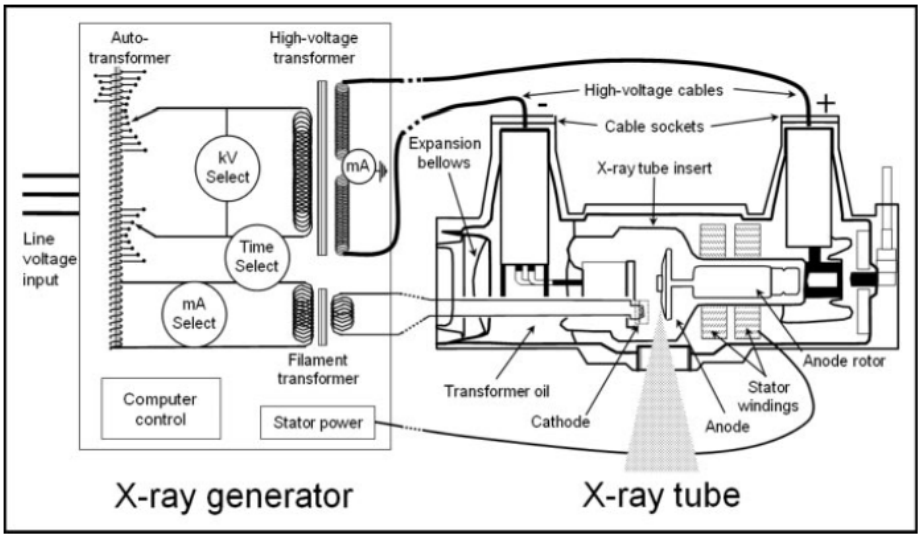

Figure 2-2: Illustration of X-ray generation system components[88]

(cathode and anode) are positioned about 1 – 2cm in a vacuum fold known as insert in either glass or metal. The electrodes are connected to the separate power sources. The filament connected to cathode get intensely heated due its electrical resistance and release alot of free electrons. The generated free electrons build up, saturate the

surface of the filament and prevent the release of more electrons. The presence of high voltage (in range of 50 – 150kV) from the x-ray generator to the electrodes accelerates the free electrons from cathode along the filament to the anode. The electron build up is hence evacuated. Depending on the filament temperature, the electron release will be kept.The number of electrons flowing between the electrodes defines the tube current in terms of milliamperes (mA). The level of tube current defines the type of medical examination required and the quality targeted[88]. Each electron is accelerated to a kinetic energy proportional to the supplied tube voltage. The last is single range that depends on the examination type targeted. Hence the tube voltage, current (power) and the duration of exposure are operator-set parameters[88]. The intensely accelerated electrons, once in contact with x-ray tube anode (target), the X-rays are produced. At the incidence, the kinetic energy of accelerated electrons is converted into electromagnetic radiation, hence the X-rays.

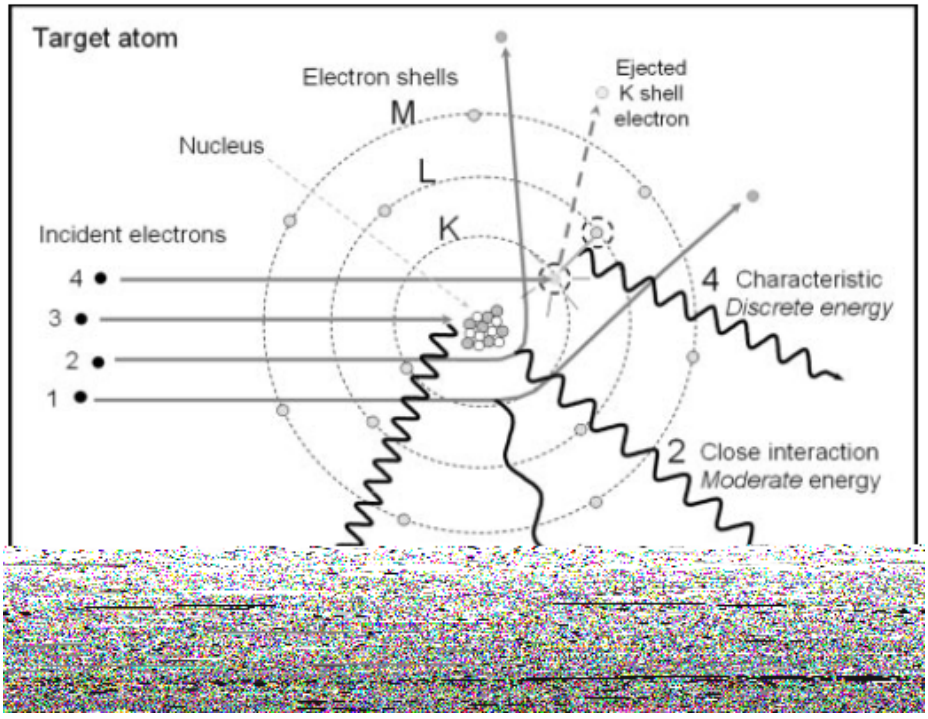

Figure 2-3: X-ray production by energy conversion[88]

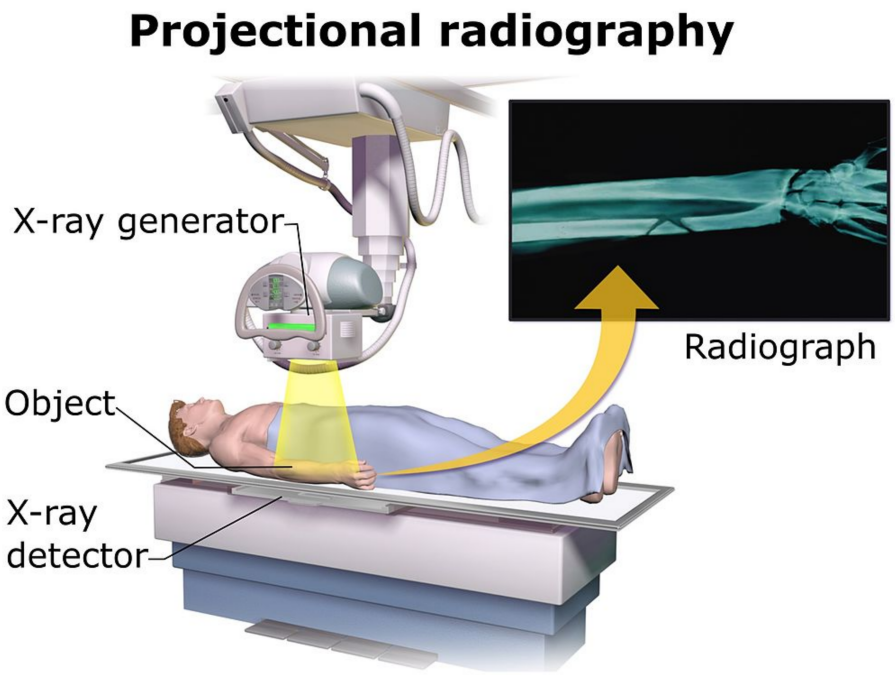

Figure 2-5: Image acquisition on projectional X-ray[69]

signed to breast imaging. Its diagnostic sensitivity has greatly improved over the decades[10]. Due to the fact that breasts are of soft tissues, mammography diagnostic specifications differ from those of the normal x-ray diagnostics. For some specific diagnosis like breast cancer, the equipment needs to have the optimization capability to produce low energy x-rays. The last gives the greatest differential attenuation between the tissues. However, the exposure time has to be optimal to avoid high doses accumulation in the tissues[44]. For the best X-ray energy and exposure control; High-frequency generators are used.

2.2.1.5 Computed Tomography (CT)

The CT imaging is also known as computerized axial tomography (CAT). It is a result of image reconstruction mathematics, that was developed to give cross-sectional of a head diagnostics[63]. The CT scanners have rotating gentry on which x-ray source and solid-state detectors are mounted. The CT images are captured in sequential slices, that are later combined for complete analysis. The data are captured through multi-row detectors spinning around the patient. With CT scanner, the non-destructive accuracy on interior image reconstruction of an object is obtained as a number of

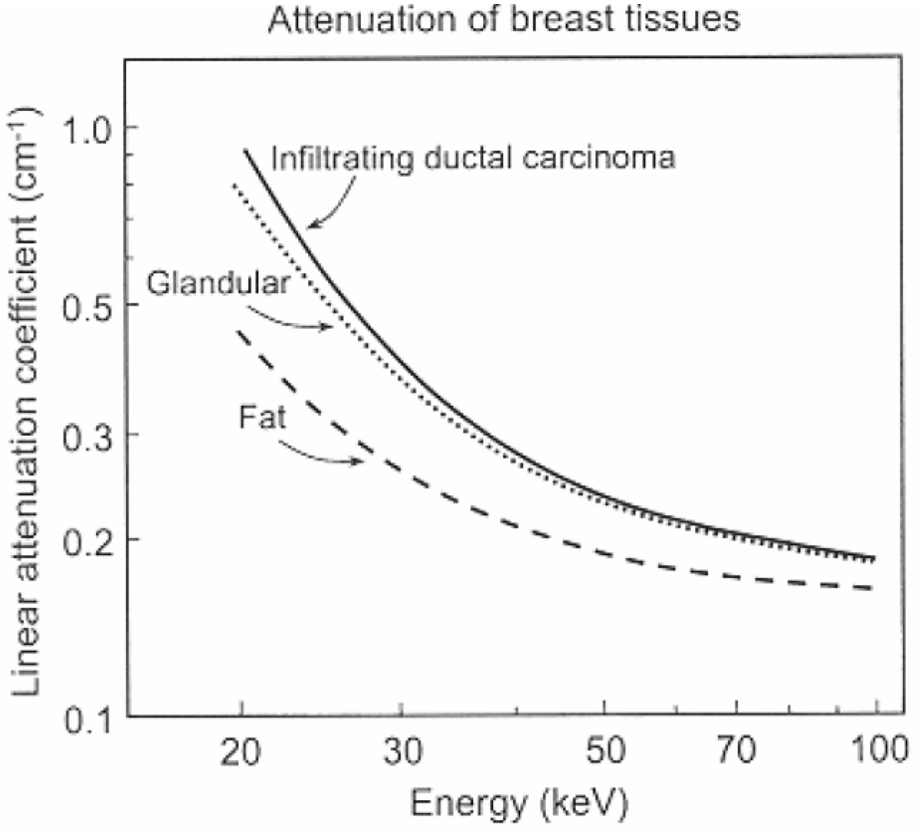

Figure 2-6: Attenuation of breast tissues on energy[44]

various X-ray projections. Various recorded images are iteratively reconstructed based on chosen iterative reconstruction algorithm[105].

2.2.2 High Voltage DC in Industrial Applications

Not only in medical, but also, the High Voltage DC application dominates a wide range of use in industrial practices. In those, the particular use of high-voltage DC-DC converter is crucial to drive the concerned equipment[50, 33, 56]. Depending on the specific application and the output quality envisaged, the same equipment are required to operate over a wide range of voltage. Then, the ability of the equipment to tune DC output voltage and management of the power transfer are key. The voltage regulation is done through controlling the DC output voltage and power transfer across the equipment[9]. The High Voltage DC application in industrial equipment considers the instance of: Electron Beam Welding Machine, Electrostatic Precipitator and Traveling-wave tube and outlines their respective principles of functionality and

the role of High Voltage DC on those.

2.2.2.1 Electron Beam Welding Machine Fundamentals

Electron Beam welding (EBW) is welding technique based on a concept of emitted electrons in the vacuum tube. The welding is basically executed in vacuum. It presents minimized distortions on a wide range of welding applications. The use of EBW machine under low vacuum or by moving electron gun were recently proven[50], hence the expansion of application scope. The cathode in vacuum releases electrons

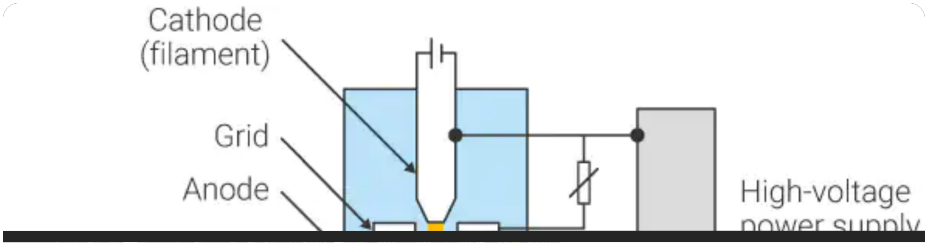

Figure 2-7: Electron Beam welding machine working principle[50]

when heated by the filament. The discharged electrons are accelerated by voltage and converged by an electromagnetic coil. The electrons produce big heat energy when they hit the base material. This heat is used by EBW for welding. The figure 2-7 validates this description.

2.2.2.2 Electrostatic Precipitator(ESP)

It is referred to as a filtration device used to eliminate fine particles such as smoke and fine dust from the flowing gas e.g air[9]. It is commonly known in air filtration and pollution control[33]. These devices frequently used in steel and thermal energy plants. The ESP working principle is based on the electrostatic properties. It is made

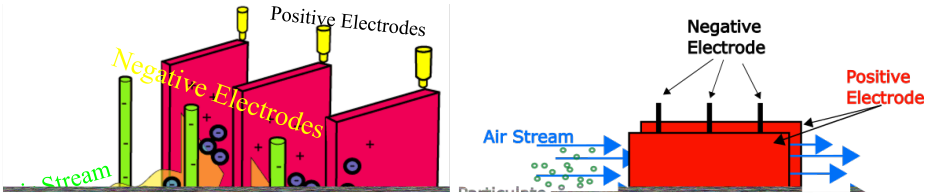

Figure 2-8: Electrostatic Precipitator working principle[33, 9]

of dual electrode sets. i.e positive and negative. The positive electrodes are in the shape of plates, whereas the negative electrodes are a wire mesh. These electrodes are arranged alternately and vertically as illustrated in the figure 2-8. The indicated electrodes are connected to a High Voltage DC source. The negative and positive terminals of the high voltage DC source are utilised to link the negative electrodes and the positive plates, respectively[33]. Maintaining a certain distance between the positive, negative electrode and the DC source causes a strong voltage gradient, which is used to ionise the medium between the negative and the positive electrode. Air serves as the medium in between the two electrodes. Since negative charges have a high degree of negativity, there may be corona discharge surrounding the electrode

rods or wire mesh. An entrance for flue gases and an exit for filtered gases are located on opposite sides of a metallic enclosure that houses the complete system. The ionisation of the electrodes releases a large number of free electrons, which interact with the dust particles in the gas to produce a negative charge on them. These particles migrate in the direction of positive electrodes before falling off owing to gravity. After passing through the electrostatic precipitator and being released into the atmosphere through the chimney, the flue gas is free of dust particles. Following the description in [9], the ESP can classified in four types. i.e. Plate recipitator, Dry Electrostatic Precipitator, Wet Electrostatic Precipitator and Tubular Precipitator

2.2.2.3 Traveling-wave tube(TWT)

The travelling wave tube, a type of thermionic valve or tube, is still utilized in high power microwave amplifier designs[8]. Although there are many different types of semiconductor microwave devices, TWTs are still employed because they may offer performance levels in some areas that semiconductor devices cannot yet match[26, 37]. In wide-band RF amplifier designs, the traveling wave tube may be employed, and even today, it outperforms equipment that uses more modern technology. The TWTs are commonly known in applications like broadcasting, radar and in satellite transponders. They are still considered in use dispite the drastic development of semi-conductor technology. Compared to many other designs, the travelling wave tube (TWT) has a high bandwidth and can operate over bands of up to an octave, while it is also feasible to use narrow band designs when the applications require for it. Its working principle is illustrated on the figure 2-9. The TWT is enclosed in glass vacuum tube, to maintain the vacuum necessary for the TWT operation. Inside the TWT, the electron gun comprising of a heated cathode and grids is observed. This is to produce and accelerate a beam of electrons that travel along the length of the tube. The DC is required to facilitate in the generation and acceleration of electrons long the tube. The cathode and grids are connected to High Voltage DC negative and positive terminals respectively. Due to the presence of High Voltage DC, the cathode (of high resistance) heats up and emits electrons. The last are accelerated

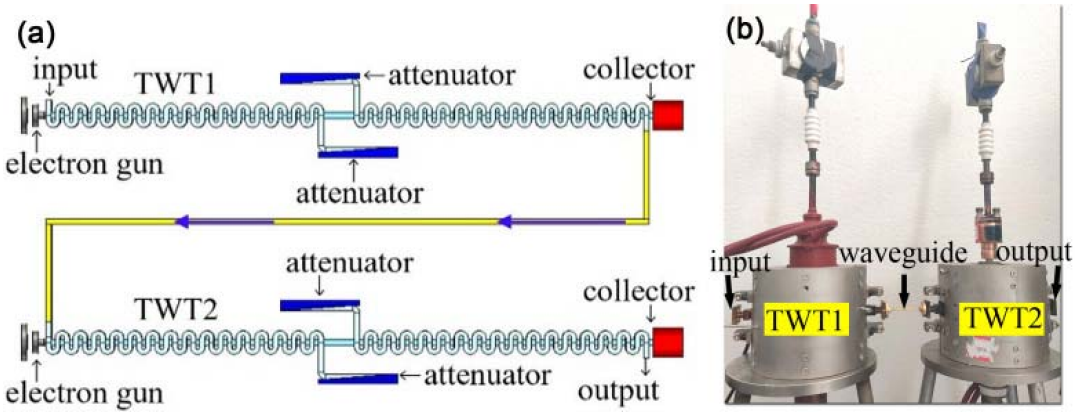

Figure 2-9: Traveling-Wave working principle[56]

towards the collector. The TWT is made of the following major elements: Vacuum tube, Electron gun, Magnet and focussing structure, RF input, Helix, and Collector.

2.3 High Voltage DC Conversion Sytems

The aforementioned applications indicated that high voltage DC is crucial for free electrons generation. The free electrons are on base of X-ray production as well as EBW functionality. In addition, with the development of High voltage DC transmission (HVDC), and the fact of making flexible and low loss power transmission system, the voltage in range kilovolts is capital. Various power conversion techniques have been suggested for decades, as a way for supplying high voltage DC[1, 91, 15, 32, 10, 58, 2, 107]. However, the structure of the conversion system; which is: power stage (usually full bridge), a high voltage transformer, and an output rectifier and a filter pose some hindrance. In order to minimize the size and weight the DC-DC converters, it is a common to increase somehow the frequency, in such a way that the size of reactive elements as capacitors and inductors (which are the most bulky elements) be reduced. The typical scheme used in low voltage converters consists on a PWM signal which is applied to a transformer in order to modify its levels; then the signal is rectified and filtered as indicated in figure 2-10. If the duty cycle of the signal is modified, it is possible to modify power transferred to the secondary side as well.

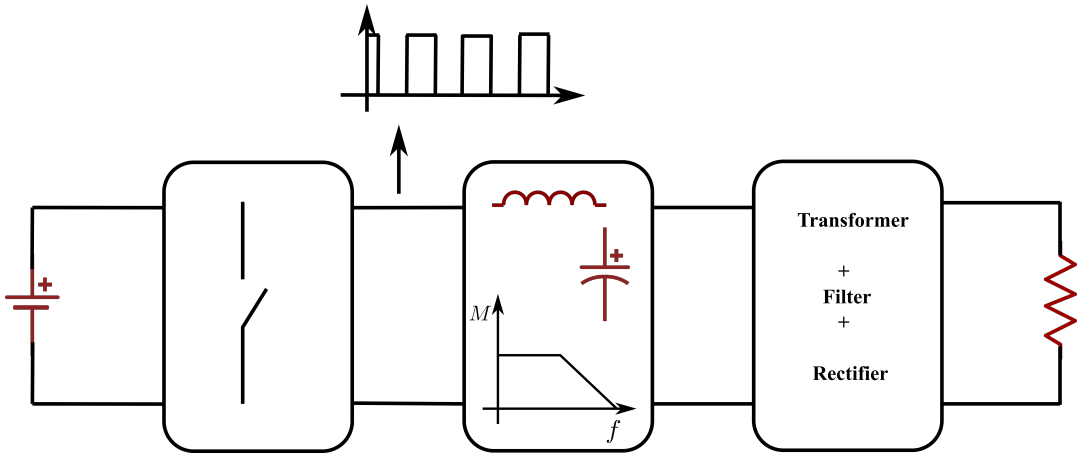

Figure 2-10: Illustration HV DC conversion and energy transfer process

As it is well known, these converters operate under the principle of if the switch operates only in ON and OFF state, there will be no losses in them. As it is obvious, this is not completely true, there are losses in ON state due to the ON resistor basically. There is another possibility to modify the power transferred, and it is adding resonant elements (inductors and capacitors) and operate the converter at variable frequency; doing so, the resonant tank modifies the power transmission to the output, provided it acts as a HF filter (or band-pass/LF). Finally, at the output filter, the waveform will be sinusoidal, with an amplitude that depends somehow with the frequency. Whatever the method used to modulate the power transference, if the frequency increases (as it is desired in order to reduce size and weight), the switching losses increases significantly, and they can limit the value of the frequency. There are several solutions, such as the use of snubbers[71, 109, 112, 117], selecting different switches (MOSFET, SiC, etc), soft-switching, etc, that can cope with these losses or modifying the topology in such a way that the transitions are carried out in a "soft way", it means, trying that voltage and current don´t be present at the same time (see figure 2-11), obtaining either Zero Voltage Switching (ZVS) or Zero Current Switching (ZCS); in both cases, the switching losses are reduced to zero, since one of the magnitudes is zero.

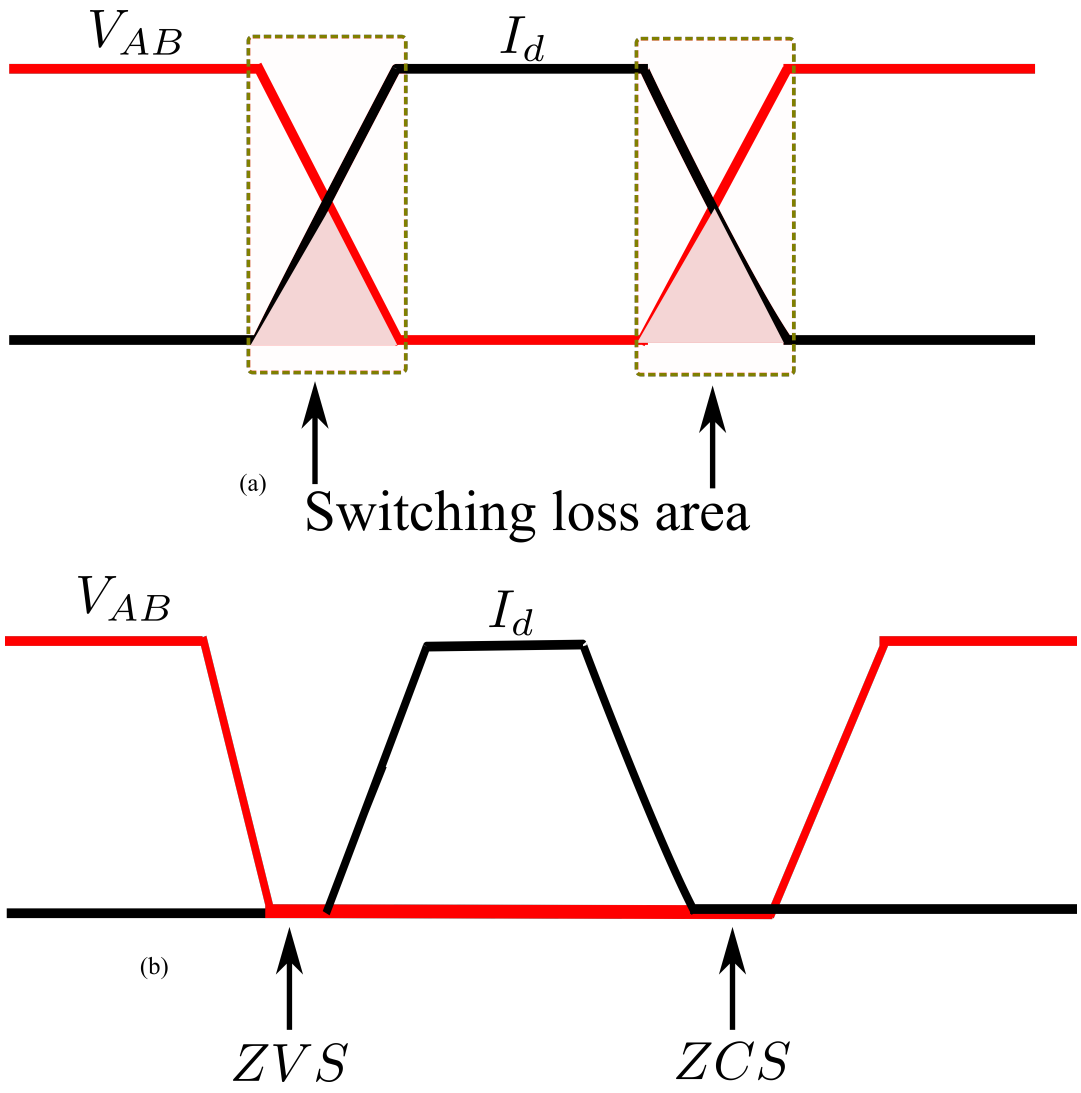

Figure 2-11: Illustration of (a) hard switching and (b) soft switching, with ZVS and ZCS shown.

The figure 2-11 shows the difference between hard-switching (figure 2-11 (a)) and soft-switching (figure 2-11 (b)). In this way, resonant converter topologies include reactive elements, in such a way sinusoidal waveforms are obtained. The goal is try to operate these topologies so that present the aforementioned waveforms; obviously, the control stage is needs to consider this in addition, making it more difficult. In HV converters, the high-ratio transformer exhibits parasitic elements that are impossible to avoid; one of the possible solutions to overcome the effects, consists in including these parasitics in the topology. Hence, the PWM application in this case is possible. The resonant

structure were proven the best suit. They allow the high voltage transformer parasitics inclusion in the conversion structure is some topologies. The resonant converters have drastically gained the use in various applications due to high efficiency and power density. Therefore, high voltage transformer is needed to ensure a large turn ratio. The complete conversion process is shwon in the figure 2-12.

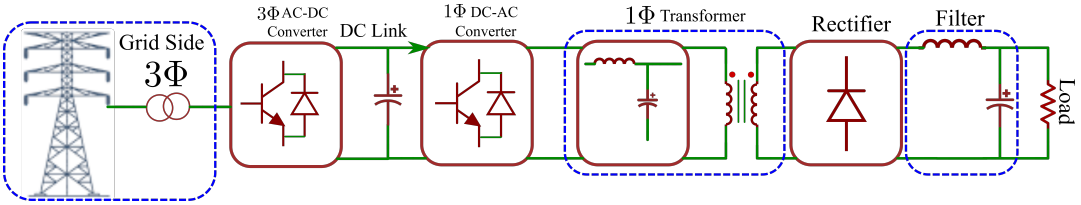

Figure 2-12: Illustration of the complete power conversion stream

2.3.1 DC-DC Resonant Conversion Systems

As previously stated, resonant converters have risen to prominence in high voltage DC applications, excelling all other DC-DC converter types due to high efficiency and power density. As a result, many studies in various types of use and domains have been done. This chapter will provide an overview of the resonant converters

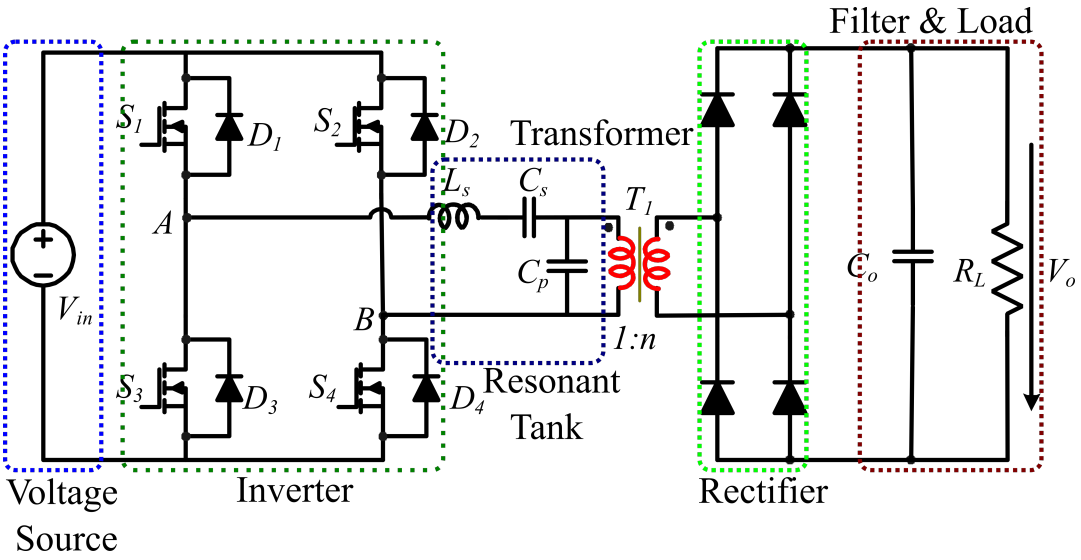

Figure 2-13: Illustration of the resonant converter

literature. They're known as electrical converters, and they're made up of a network of inductors and capacitors. This network is referred to as a "resonant tank," as it

is set to a specific frequency[102]. The figure 2-13 illustrate the resonant converter, broke-down in the following components:

- **DC voltage source**; it is the voltage supply source to the converter and plays a role of the base for the voltage normalization purpose. Any change in the input voltage affects the output of the converter. Which is usually obtained from mains (single phase or three phase) and then it is rectified and filtered.

- **Inverter**: active front-end made of IGBTs; it is the stage that converters the input DC voltage to Square waveform, of a given frequency. This waveform can be as simple as an $+V_{cc}$ and $-V_{cc}$ or much more complex, such as in matrix converters. The desired waveform defines somehow the switches as well as the power topology.

- **Resonant tank**, it is a network configuration made of reactive elements i.e. inductor and capacitor. They can take various configurations depending on the application in place. They play a capital role in power transfer following the conditions of switching in place. Basically, the resonant tank filters the output square waveform generated by the power stage and outputs the first harmonic.

- **High voltage transformer**; it is important in stepping up the resonant tank voltage level, in order to track the level of voltage necessary at the converter output. These kind of transformers, since they have to cope with isolation distances, etc, present important parasitic elements.

- **Rectifier**; it converts the AC voltage and current from the transformer back to DC at the output of the convert.

- **Output filter**; eliminates the ripples to the necessary level and provides clean output DC voltage.

Various studies were carried out on the switching mode DC-DC converters to guarantee that they respond to the most critical criteria for power electronics application i.e reduction of switching and conduction losses in switch-mode while commutating

on high frequency. A number of switching topologies can achieve high-power transfer, however the challenge reside on the power switches (transistors, MOSFEs, IGBTs and diodes) and energy storage passive elements (capacitors and inductors). They take part in the the design of the power converter and affect the efficiency. Alternatively, the resonant converter can minimize the converter size and the switching loss, thereby providing higher efficiency[73, 18, 89]. For high power applications where isolation is required, high power transformer is always necessary.

2.3.1.1 Resonant Tank Topology

It consists inductor and capacitor circuitry (reactive elements) in various configurations.i.e LLC, LCC and etc. They store oscillating energy with the frequency of the resonant circuitry. The resonant tank can be tuned to a certain resonant frequency through the adjustment of reactive element data. Hence, the resonant tank is a crucial part of the resonant network. They can be in several categories three of which are the following:

1. The first classification depends on the reactive components configurations. Different topologies appear; in this work, two of them will be the objective of study i.e. series resonant converter (SRC) and parallel resonant converters (PRC).

2. The second classification is based on the number of the reactive components in the resonant tank (determines the transfer function order).

3. The third classification covers the elements and multi-elements resonant tank[86]. The number of the reactive components in the tank determine the tank transfer function; hence the power transfer.

Therefore, the control should adapt to the tank configuration too. The figure 2-14 illustrates the commonly known classification of the resonant tanks. The power transformer makes a key component of the DC-DC resonant converter introduced previously.

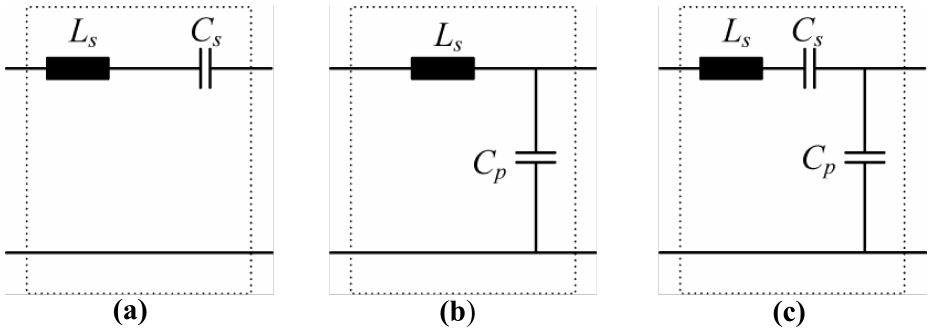

Figure 2-14: Resonant Tank: (a) Series Resonant; (b) Parallel Resonant; (c) Series-Parallel Resonant.

2.3.1.2 Power Transformer

Referring to the topology in the figure 2-13, the power transformer is crucial. It reflects two important particularities:

1. ***Large Turn Ratio***: due to the high voltage required at the output of the converter, the transformer with a typically large turn ration is necessary. Usually the input voltage is smaller, mostly from a three phase line of 400 V, it means that the maximum can reach 700 V. So, to generate the output voltage in the range on kilo-volts, a transformer with a larger turn ratio is capital. This implies the big number of turns at the transformer's secondary winding, and therefore, a significant capacitance in it. The same capacitance is reflected to the primary as a product of the squared transformer turn ratio. It is commonly several hundreds of nano that can be achieved from the primary. This capacitance is illustrated as C_P as indicated in figure 2-15.

2. ***High Isolation Distance***: the large isolation distance between primary and secondary winding of the transformer and in the secondary itself result in large leakage inductance. This inductance is illustrated as L_S. The leakage inductance L_S and the parasitic capacitance C_P are the transformer's major non-idealities that cannot be neglected. As a result, the commonly used resonant topologies try to include those transformer non-idealities in the resonant tank[83, 97, 113, 104].

After having discussed the resonant converter mentioned in the figure 2-13 and outlin-

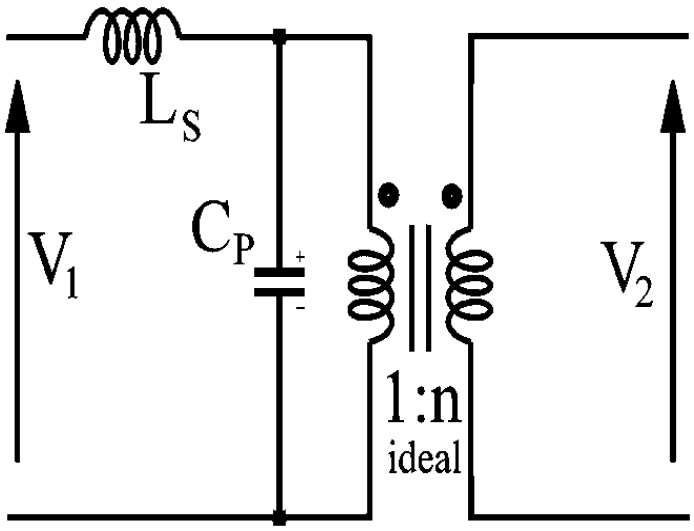

Figure 2-15: Illustration of equivalent topology to the step-up transformer

ing various components that make it. It was shown that the resonant tank; in various configurations plays a capital role in power transfer. The figure 2-15 illustrates the power transformer, on which the transformer parasitics are indicated. They can be included in the topology depending on the application whether it is SRC or PRC. In case of SRC, for applications such as WPT, the large leakage inductance L_s is experienced, while the parallel capacitance C_p is neglectable. For the case of PRC in HV application, the large leakage inductance L_s and the large parallel capacitance C_p are experienced. Therefore, the next subsections will elaborate more on the Parallel resonant converter (PRC) and Series Resonant converter (SRC) configurations. The last two resonant structures have very different applications, they are flexible and they will serve as an example to demonstrate the whole process: polynomial model and its implementation in different digital controllers.

2.3.2 Parallel Resonant Converter

The PRC particularly seems to be a better fit for resonant topologies; as its structure allows both step up and step down of the DC voltage applied to it. The PRC is structurally shown as in figure 2-14(b). It is an advantage that PRC can produce the output voltage higher than the input voltage. In PRC topology the transformer parasitics can be considered as part of the resonant tank. They have a particularity

of exhibiting a current-source characteristics near the resonance[28]. However, it very challenging to control it if the load and the input voltage vary widely[97]. The figure 2-16 represents the parallel resonant connect to full-bridge converter. A serial capacitor is also included in the PRC, but it serves as a DC level remover rather than a resonant element (it is not taken into account in the calculations). The primary purpose of its inclusion is to eliminate the aforementioned DC level; it has no impact on the resonant tank. The voltage conversion ratio of PRC is obtained in terms

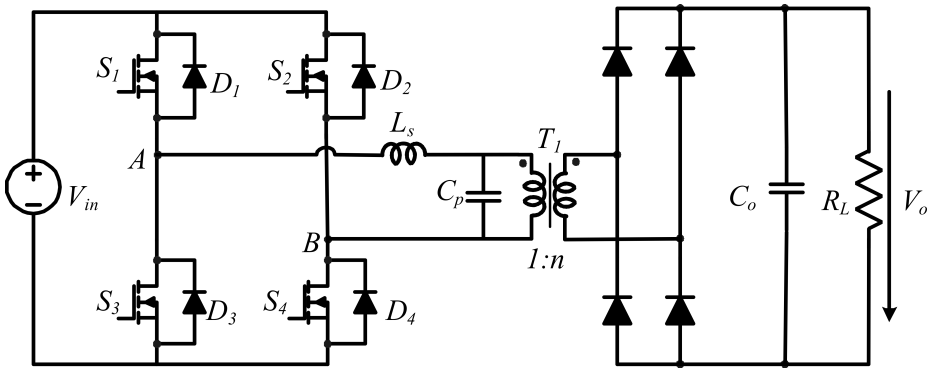

Figure 2-16: Parallel resonant DC-DC converter applied at full with output capacitive filter

of an equation in normalizd values through the First Harmonic Approach using the approximation shown in [43] and it is shown in the equation 2.1.

$$\frac{V_0}{nV_{in}} = \frac{4}{\pi}.\frac{k_{21}}{k_v} \tag{2.1}$$

where

$$k_{21} = \frac{1}{\sqrt{\left[\left(1-\hat{f}^2\right).\left(1+\frac{\tan\left(|\beta|\right)}{\omega C_p R_e}\right)\right]^2 + \left[\hat{f}^2.\frac{1}{\omega C_p R_e}\right]^2}} \tag{2.2}$$

$$k_v = 1 + 0.27.\sin\left(\frac{\vartheta}{2}\right) \tag{2.3}$$

1. ϑ: output rectifier conduction angle (proportional to the load), more details are given in [43]),
2. β and $\omega C_p R_e$: the details for those are given in [43],
3. n: transformer turns ratio,

4. $\hat{f} = \frac{f_s}{f_0}$:normalized switching frequency,

5. f_s:switching frequency, and

6. $f_0 = \frac{1}{2\pi\sqrt{L_s C_s}}$: parallel resonant frequency

The equations 2.1, 2.2 and 2.3 together with the figure 2-17 illustrate the voltage conversion ratio of the parallel resonant converter. Contrary to the series resonant converter, the PRC can regulate the output voltage at no-load condition when it operates above resonance. Note that at resonance, the output voltage is proportional to the load, hence it hikes up to very high value at no load. The PRC is structurally protected from short-circuit. This fact is proved by applying the short circuit across the resonant capacitor. In this case the voltage applied by the inverter is the same voltage accross the inductor and the inductor impedance limits the current[10]. Thus, the parallel resonant converter is exceptionally preferable for applications with critical short-circuit requirements. In this case, the PRC presents an advantage of being high current device and comparatively independent of the load. The operating frequency increases with the increase in the load resistance(load decreasing) to regulate the output voltage. In this case, the resonant tank current remains nearly constants. Consequently, the conduction losses in the power electronic switches and the reactive components will remain nearly fixed as the load reduces. Hence the converter efficiency declines at low load. Additionally, the circulating current rises with the increase in the converter input DC voltage.

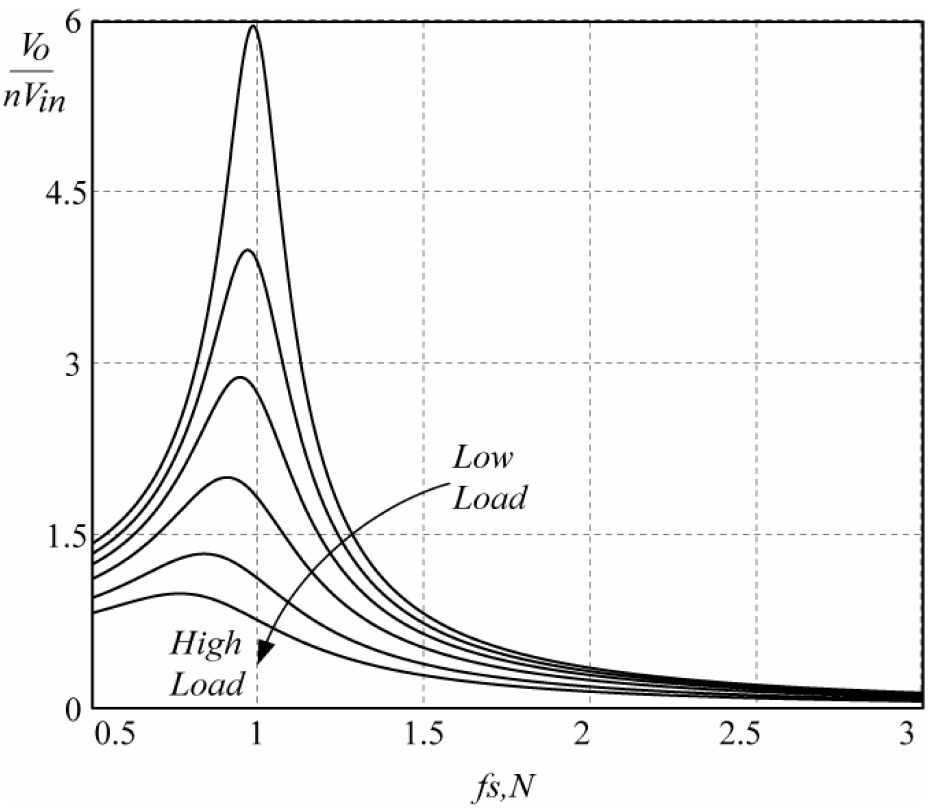

Figure 2-17: PRC voltage conversion characteristics, with respect to the load level and frequency

The PRC is approriate for applications which run from comparatively narrow input voltage range and that exhibit a nearly constant load closer to the maximum power[95]. The PRC are usually used in low output voltage application with an inductive output filter, with high current application. However, it can be used with high output voltage by omitting the inductor and use the capacitive filter, in case of low current applications. The indicated omission of the inductor alter the waveform of the resonant circuit but the converter performance remains unchanged[46].

2.3.3 Series Resonant Converter

The series resonant converter (SRC) is the commonly used resonant topology, as it can facilitate in its control if the load and the input voltage vary widely i.e. they have a better control characteristics[113, 104]. The SRC is structurally shown as in figure

2-14(a). The series capacitor is this structure serves both resonant element and the DC component suppressor of the converter output signal. Therefore the unbalance in switching times of the switches as well as the transformer saturation are avoided in full-bridge applications. The SRC is illustrated in figure 2-18, with an inductor omitted in the output filter. Hence, it is suitable for high-power applications.

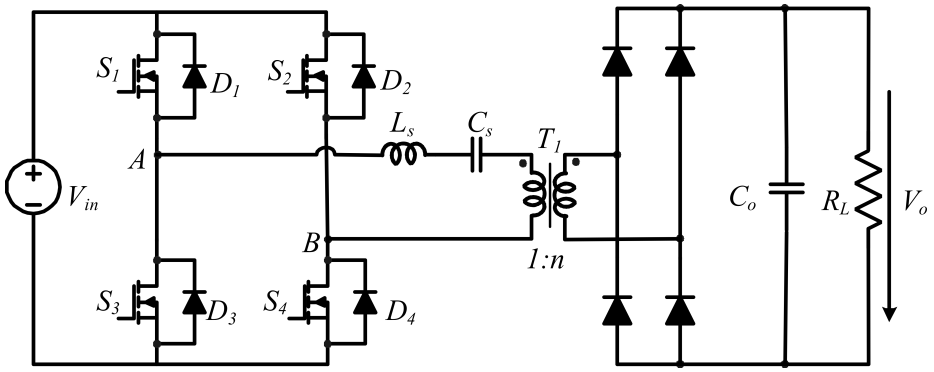

Figure 2-18: Series resonant DC-DC converter applied at full with output capacitive filter

The voltage conversion ration of a SRC is obtained in normalized values through the First Harmonic Approach using the approximation suggested by Steigerwald in[95] as given in equation 2.4.

$$\frac{V_0}{nV_{in}} = \frac{1}{1 + j\frac{\pi^2}{8}Q\left[\hat{f} - \frac{1}{\hat{f}}\right]} \tag{2.4}$$

Where,

1. $Q = \frac{Z}{R_0}$: the normalized load,
2. $Z = \sqrt{\frac{L_s}{C_s}}$: characteristic impedance of the resonant tank
3. n: transformer turns ratio,
4. $\hat{f} = \frac{f_s}{f_0}$:normalized switching frequency,
5. f_s:switching frequency, and
6. $f_0 = \frac{1}{2\pi\sqrt{L_s C_s}}$: series resonant frequency

However, it presents some more advantages including the reduction in current of the power switches which goes with the load drop. Hence less conduction losses as the load reduces. Therefore the high part of the load efficiency is maintained. The SRC is not drawback free as it has challenges in regulating the output voltage at no load conditions[65]. The last fact is demonstrated by the equation 2.4 and illustrated by the graphical representation in figure 2-19. Additionally, it does not cope with the transformer parasitics, and output voltage is always lower than the input voltage.

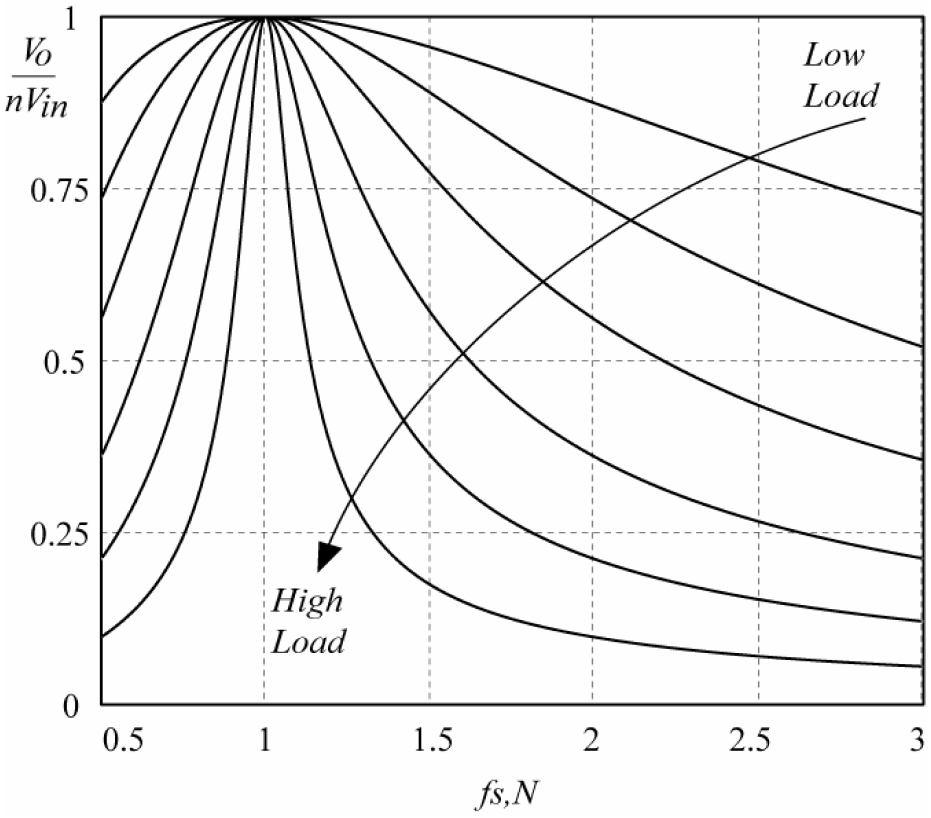

Figure 2-19: SRC voltage conversion characteristics, with respect to the load level and frequency

From the figure 2-19, the lower the load, the flatter the voltage conversion characteristic. It is an implication that the SRC is suitable for applications where no load regulation is not necessary.

For both SRC and PRC, the control topologies are key to be able to track the right and desired output. This work will consider the SRC and PRC in their various application, but focusing more on the control side. This helps in making easy, faster and

quick fixing algorithms. The goal is obtain a model valid for digital controllers. This work focuses on PRC and SRC, since they have different applications, so that it is demonstrated that the method is valid.

2.4 The Propositions and Contributions of the Project

As indicated previously, this project considers both SRC and PRC, and focus much on their respective control sides. It springs from their steady-state model illustrated in [25]. However, the steady-state model renders the control algorithm much complex in such a way that the use controllers with high computational capability is required. Therefore, the polynomial model was suggested and developed from the steady-state model, as a alternative solution. The last is a fast, quick fix and easily applicable option to various Digital Signal Controllers (DSC) and FPGA. The detailed polynomial models for both SRC and PRC will be illustrated in this work. Their respective control program will be built based on their respective polynomial model. Their implementation on the DSC and FPGA will be done. The closed loop control of PRC shall be proposed using the fuzzy control algorithm.

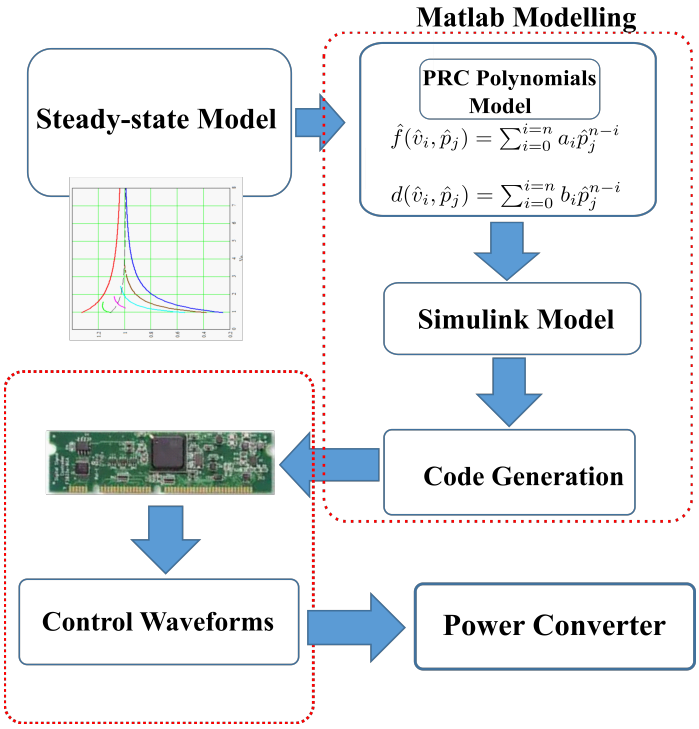

Figure 2-20: The process of generating a polynomial model from the PRC's steady state models is depicted in this illustration.

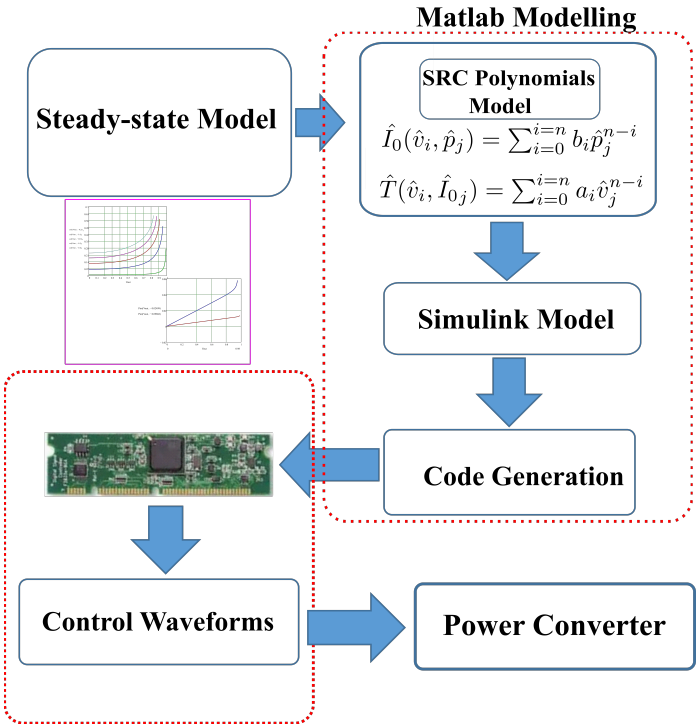

Figure 2-21: Illustration SRC of the Polynomial model construction from the steady state Model

The complete process of developing the polynomial models from the steady-state models is shown in figures 2-20 and 2-21. The steady-state models are created in MathCad, and the PRC model equations are published in [25]. Normalized data are used in the models to broaden the operational range of related prototypes. The parameters of steady-state models are graphically portrayed, and the same graphs are modified to produce a graphical representation of the polynomial model. To obtain the equivalent polynomial term for each graph, the Data Fitting and B-spline numerical analysis approach are employed. As a result, the general polynomial expressions can be found. The general equation are used to generate programming codes that can be fed into a DCS or FPGA for the production of control waveforms. The power electronics switches are activated by the same waveforms. As a result, the polynomial models are easy to run on any DSC or FPGA; they are faster and quick fix. The closed loop control for the PRC will be done in this work using fuzzy control algorithm.

2.5 The review of the cutting-edge solutions for the implementation of resonant converter control in the programmable circuits

The use of programmable circuits is not new in the research about the control of resonant converters. This section give a look back in the literature and highlights various cutting solutions in implementing the control of the resonant converters in programmable circuit. Various control techniques for the Series Resonant converter were run for comparison purposes in [72]. Different controls topologies and algorithms were developed and executed using the 16-bit DSPIC33FJ16GS502 digital signal controller (DSC). It generates control signal and digitize the feedback. The DSPIC33FJ16GS502 is found among the Microchip technology solutions. The controls for soft start-up of pulse-density-modulated series resonant converter for induction heating were discussed in [40]. The control system is based on the STM32H743ZIT6 microcontroller (MC), which an STMicroelectronics product. The control of LCC resonant converter to generate X-ray with optimal trajectory start-up was implemented in [120]. The control algorithms were build and executed on both FPGA and DSP28335 (TI product) for speed comparison purposes. The real-time hardware-in-loop implementation of LLC resonant converter at worst operating point based on time domain analysis was discussed in [34]. In this, the control algorithm is built OPAL-RT and FPGA. The control of PV micro-converter based on CLL resonant conversion was discussed with a power control scheme using resonant circuit voltage control loops in [49]. The control algorithm in this case, was built in TMS320F28335 DSP board, which is a TI product. Apart from those instance mentioned, there alot of solutions where the programmable circuit involve in various controls.

2.6 Conclusions

This chapter elaborated more on the High Voltage DC equipment. The use of high voltage DC in medical and industrial application was tackled. The commonly used switch mode power supply systems were highlighted, with strong emphasis on resonant converters. In those, the series and parallel configurations were taken into consideration. In this case, the resonant converter parallel configuration suites the high voltage DC application. Due to the needs of high voltage DC, the power transformer was found necessary in these topologies; therefore the power transformer nonidealities and their inclusion in the resonant tank structure was discussed. On the other hand, the resonant converter series configuration fits the low voltage applications i.e. Wireless Power Transformer (WPT). In this chapter the method of implementing the control in digital controllers and their application to the two indicated converters were introduced. Finally, the steady-state model of both SRC and PRC was indicated and the development of polynomial model for both SRC and PRC and the process required were mentioned in this chapter.

Chapter 3

Overview of PRC and SRC Steady State Models

Contents

3.1 Introduction 74

3.2 Steady State Model of the Series Resonant Converter 75

3.2.1 Analytical study of SRC Steady State Model 77

3.2.2 Graphical Represention of SRC Steady State Model 80

3.3 Steady State Model of the Parallel Resonant Converter 82

3.3.1 Analytical study of PRC Steady State Model 83

3.3.2 Base and Normalized values 84

3.3.3 PRC Operating Modes 85

3.3.4 Graphical Represention of PRC Steady State Model 90

3.4 Conclusions 93

3.1 Introduction

Nowadays, in modern technologies, high voltage is applied in various domains; the high voltage levels (teens of kV) is required in a wide range of applications: medical, industrial, environmental, measurements, etc[75, 79, 3]. Due to high efficiency and power density, the resonant converters have drastically gained the use in plenty of applications[76, 70, 48, 87, 54]. Various power conversions systems have been suggested for decades, as ways of supplying high voltage[32, 58, 10, 2, 107]. In this way, switching mode power converters are commonly used to achieve high power densities. High-frequency operation is mostly preferred to minimize the size of the topology. However, it could be the cause of a significant increase in switching losses. As a result, resonant converters were introduced as a possible solution. Resonant converters can perform at very high switching frequencies while maintaining high efficiency since they can operate with soft-switching and, consequently, low switching losses. Hence, it found place into a wide range of applications. The resonant converter involves different issues as far as control is concerned; one of which is determining how to control the switching pattern to maintain soft switching under a variety of input voltage and load values. The converter's parameters (component specifications, switching pattern) can only be optimized at a specified operating point (a given output voltage and power). The converter will drift away from its optimal functioning point when the working conditions change, and the soft switching function might be lost, since soft-switching operation mode is achieved under given conditions(input voltage, power and load). The only control freedom left is the switching pattern of the switches, as component specifications cannot normally be modified once the converter has been developed. The wide frequency variation required to sustain soft switching functioning is one of the major drawbacks of this technology. The switching frequency for Zero Voltage Switching (ZVS) could range from one to more than double the resonant frequency[6]. The resonant converter topology determines whether the application uses variable switching frequency or both variable switching frequency and variable duty cycle. The chapter 2, introduced the resonant converters and articulated on two topologies

i.e. Parallel Resonant Converters(PRC) specifically for HV applications and Series Resonant Converters(SRC), for any other application that doesn't involve high Voltage. The ZVS and Zero Current Switching (ZCS) are achieved when both variable switching frequency and duty are applied to a Parallel Resonant converter(PRC). The variable switching frequency can be used in Series Resonant Converters (SRC) to achieve ZVS only. The optimal mode of operation is achieved by combining the ZVS and ZCS, which is typical in PRC applications; and by controlling the switching frequency and duty cycle in such a way that the target output voltage and power are tracked. The optimal mode is further detailed later in 3.3, illustrated in the figure 3-4 and given deep focus in 3.3.3.3. The normalized values are utilized to increase the converter operational span. This chapter will present the steady state model control for PRC a shown [25] and the steady state model control for SRC.

3.2 Steady State Model of the Series Resonant Converter

The converter's output voltage and power depend not only on the input voltage and output load but also strongly on the resonant tank component, switching frequency and the switching pattern. The SRC has a resonant tank that consists of capacitor and inductor in series configurations as it was exposed previously. The resonant tank components strongly react to changes in the switching frequency; the power transfer is affected. Hence, the output voltage and power gets affected too. This is a setback as far as control is concerned. Most of researchers avoid it by only analyzing SRC on first harmonic approach. To ease the analysis of the SRC parameters at larger span, the normalized values are utilized. The steady state model only for the SRC can be studied under time domain, and this section of the work will exclusively be limited to steady state model of the SRC. The analytical expressions will be illustrated and validated graphically. The last representation will show the various operating points to consider while drawing the control philosophy. The Figure 3-1 shows different

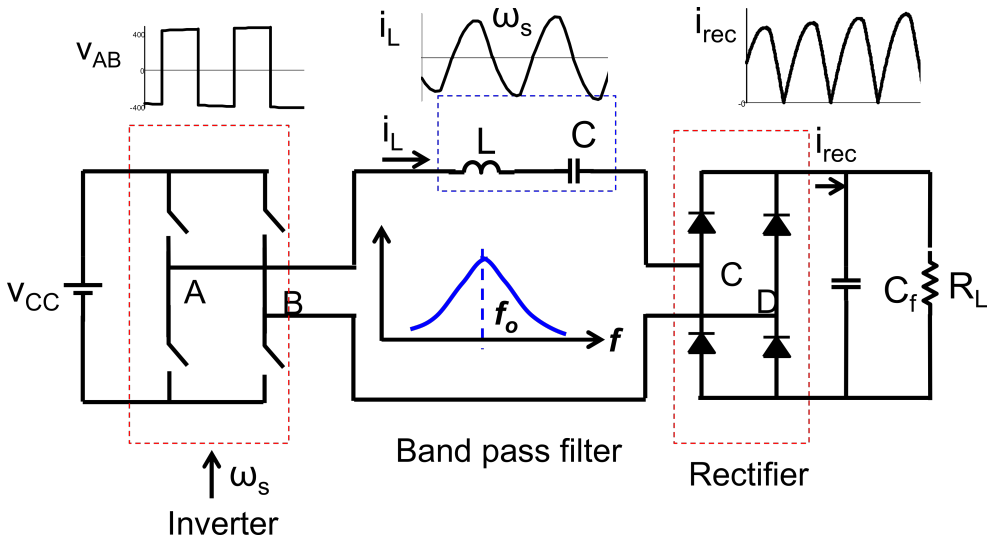

Figure 3-1: SRC block with major related waveforms[100]

output waveforms respective to each step of the converter. The series resonant tank act as band bass filter; it maximizes the power transfer at resonance. The control scheme for SRC is slightly sophisticated, and controllers with computational capabilities (modern digital controllers, Micro-controllers, Digital Signal Processors, Digital Signal Controllers, etc) are quite ideal for this task. Regarding their cost, it seems to think that it should be a drawback; by contrast, the cost of digital control circuits have been decreasing during last years. Micro-controllers (MCUs) are a good solution for implementing complex algorithms in low power systems, such as electronic ballasts: in [5], the use of an MCU enables to control the power converter with two different feed-back loops: resonant tank inductance current and switching frequency. Without a MCU, the implemented control scheme would be problematic to realize. For high-power systems, once again the use of digital controllers is also common; in [17], a Digital Signal Processor is used to control a resonant converter at low frequencies. On the other hand, the software tools available for designers enable fast development prototyping. High-level synthesis tools, such as Hardware in the Loop (HIL), reduce the development times and ease the test and verification of complex algorithms, as well as testing the system reliability and reducing development times[45]. The digital controllers development has been driven by power control requirements as well. In this way, Digital Signal Controllers (DSC) implement in hardware Multiply-

Accumulate instructions, in only one cycle (to obtain Fast Fourier Transform) and incorporate high-speed PWM dedicated outputs, for instance. These devices are applied to different power systems [84]. On the other hand, resonant converters are being widely used, in many different applications; as far as SRC is concerned, the power topology is frequently used in Wireless Power Transmission systems[119, 51], since the ineluctable transformer leakage inductance is included in the resonant tank. In this way, this work is framed within this line i.e. power systems (resonant converters, SRC in this case) controlled by DSCs. In order to implement a valid control algorithms for these converters, first it is necessary to obtain a suitable model. Using the SRC as an example, the steady state model, its equivalent expressions and graphical representations shall be illustrated in this chapter. As mentioned in 2.3.1, SRC is used in applications such as WPT, hence the power transfer and the output voltage are the key controllable parameters. The controllers force the output voltage and power to tack and follow the required reference values. it means that the output voltage and power are controlled with the change in initial resonant current and the switching frequency.

3.2.1 Analytical study of SRC Steady State Model

The operation mode selected for the converter is fixed duty cycle, variable frequency and some assumptions are made:

- The components are ideal: no losses and delays are caused by them.
- The output ripple is considered negligible and the output voltage can be considered constant, specially during a switching-period.
- No temperature effects are considered.
- Input voltage is kept constant.
- The converter will operate above resonant frequency.
- The converter will operate in continuous mode.

There are many models of resonant converters, using different methods, such as Laplace [23, 22] , First-Harmonic approach [95, 99],state-plane diagram [55],time-domain [30] and etc. In this chapter, the last option has been selected, and the SRC fixed-duty, variable frequency is modeled in time-domain, based on its equivalent circuits. The process is summarized in figure 3-2, which shows the equivalent circuits according to the waveforms presented. The converter will operate above resonance, so the current will have a positive lag to the input voltage. It is possible to distinguish two different equivalent circuits, according to the time; in figure 3-2, are labeled as 1 and 2. The first one takes place at the beginning of the cycle, and as long as the current is negative, D2 and D3 are in ON state, so the output voltage is reflected to the primary side as negative; as soon as the current cross zero and becomes positive, diodes D1 and D4 are now in ON state, reflecting the output as a positive voltage. Figure 3-2 shows also the value of the initial and final magnitudes for each equivalent circuit, as well as the times at which they are valid. As it can be seen, it is only necessary to analyze half-period, since the circuit is operating with duty cycle 0.5 and in steady-state as shown in equations 3.3, 3.4, 3.8. Things being so, the converter operation is summarized by expressions from equation 3.1 to equation 3.10.

$$\frac{(-\mathrm{Vco}+\mathrm{V1})+\mathrm{V2})}{\mathrm{L}\cdot\mathrm{w}}\sin(\mathrm{w}\cdot\mathrm{t1})+\mathrm{I_o}\cdot\cos(\mathrm{w}\cdot\mathrm{t1})=0 \tag{3.1}$$

$$\begin{aligned}&(\mathrm{Vco}+\frac{-\mathrm{Vco}+\mathrm{V1}+\mathrm{V2}}{\mathrm{L}\cdot\mathrm{C}\cdot\mathrm{w}^2})\cdot(1-\cos(\mathrm{w}\cdot\mathrm{t1}))+\\&+\frac{\mathrm{I_o}}{\mathrm{C}\cdot\mathrm{w}}\cdot\sin(\mathrm{w}\cdot\mathrm{t1})=\mathrm{Vc1}\end{aligned} \tag{3.2}$$

$$-\mathrm{I_o}=\frac{\mathrm{V_1}-\mathrm{V_{c1}}-\mathrm{V_2}}{\mathrm{L}\cdot\mathrm{w}}\cdot\sin(\mathrm{w}\cdot(0.5\cdot\mathrm{T}-\mathrm{t1})) \tag{3.3}$$

$$-\mathrm{Vco}=\mathrm{Vc1}+\frac{\mathrm{V1}-\mathrm{Vc1}-\mathrm{V2}}{\mathrm{L}\cdot\mathrm{C}\cdot\mathrm{w}^2}\cdot(1-\cos(0.5\cdot\mathrm{T}-\mathrm{t1})) \tag{3.4}$$

The next step is obtain the normalized expressions of the aforementioned equations;

the following base terms will be used:

$$V_B = V1;\ \ Z_B = \sqrt{\frac{L}{C}};\ \ I_B = \frac{V_B}{Z_B} = \frac{V1}{\sqrt{\frac{L}{C}}} \tag{3.5}$$

This base values give raise to the next set of normalized equations:

$$(-\hat{v}_{co} + 1) + \hat{v}_2) \cdot \sin(2 \cdot \pi \cdot \hat{t}_1) + \hat{I}_o \cdot \cos(2 \cdot \pi \cdot \hat{t}_1) = 0 \tag{3.6}$$

$$\hat{v}_{c1} = \left(\hat{v}_{co} + (1 + \hat{v}_2 - \hat{v}_{co}) \cdot \left(1 - \cos\left(2 \cdot \pi \cdot \hat{t}_1\right)\right) + \hat{I}_o \cdot \sin\left(2 \cdot \pi \cdot \hat{t}_1\right)\right. \tag{3.7}$$

$$(1 - \hat{v}_{c1} - \hat{v}_2) \cdot \sin(2 \cdot \pi \cdot (0.5 \cdot \hat{T} - \hat{t}_1)) = -\hat{I}_o \tag{3.8}$$

$$(\hat{v}_{c1} + (1 - \hat{v}_{c1} - \hat{v}_2)) \cdot (1 - \cos(\pi \cdot \hat{T} - \hat{t}_1)) = -\hat{v}_{co} \tag{3.9}$$

$$0.5 \cdot \hat{T} > \hat{t}_1;\ \ \hat{t}_1 > 0;\ \ \hat{v}_2 < 1;\ \ \hat{T} < 1 \tag{3.10}$$

Where $\hat{T}$ is the normalized period, while $\hat{t}_1$ is the normalized time. In the same way, $\hat{v}_{co}$, $\hat{v}_{c1}$, $\hat{v}_1$ and $\hat{v}_2$ are normalized values, respective to their values in equations 3.1, 3.2, 3.3 and 3.4. In order to solve completely the converter, it is necessary to include the output power values. the figure 3-2 shows that during step 1, the power flows from the output to the input, and during step 2, the process is the opposite. This means that it is necessary to consider a proper balance between both stages (reactive/active power). Once the different values (period, Vc1, etc) are known, it is possible to calculate the delivered power to the output. The previous non-linear equation system does not have an easy solution, and the best option is to obtain some plots, that help in the converter design process.

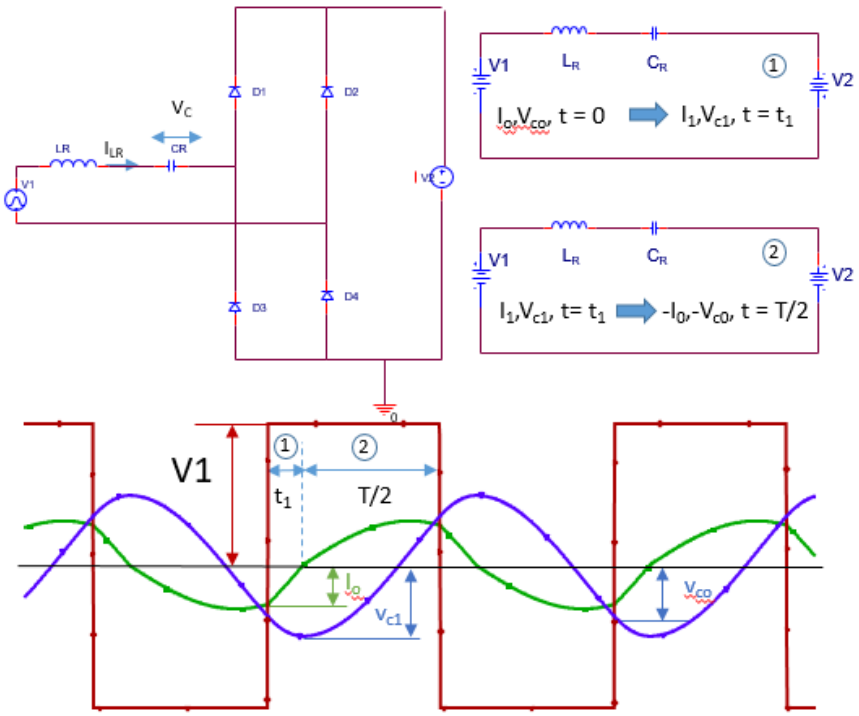

Figure 3-2: SRC main waveforms and its equivalent circuits.

3.2.2 Graphical Represention of SRC Steady State Model

Figure 3-3 shows in horizontal axis the output voltage in normalized values, it means, the voltage gain vs the period (at the top) and vs output power (bottom). Every curve is plotted for a given value of the initial resonant current. As it was mentioned, this value is negative, since the converter is operating above resonance. With this set of plots, it is possible to design a SRC converter. In the next chapter, the polynomial model attainment procedure is shown. The SRC steady-state model is illustrated by the equations 3.6, 3.7, 3.8, 3.9 and 3.10. Since these equations do not have easy solution, the graphical representation is a capital tool to ease the converter design process. The graphical representation is indicated in figure 3-3. On the same figure, the top illustrates the normalized period $\hat{T}$ versus output normalized voltage $\hat{v}$ in presence of normalized initial resonant current $\hat{I}_o$. While, the bottom part of the figure shows the normalized output power $\hat{p}$ versus the normalized output voltage $\hat{v}$ in presence of normalized initial resonant current $\hat{I}_o$. Both figures can be summerized

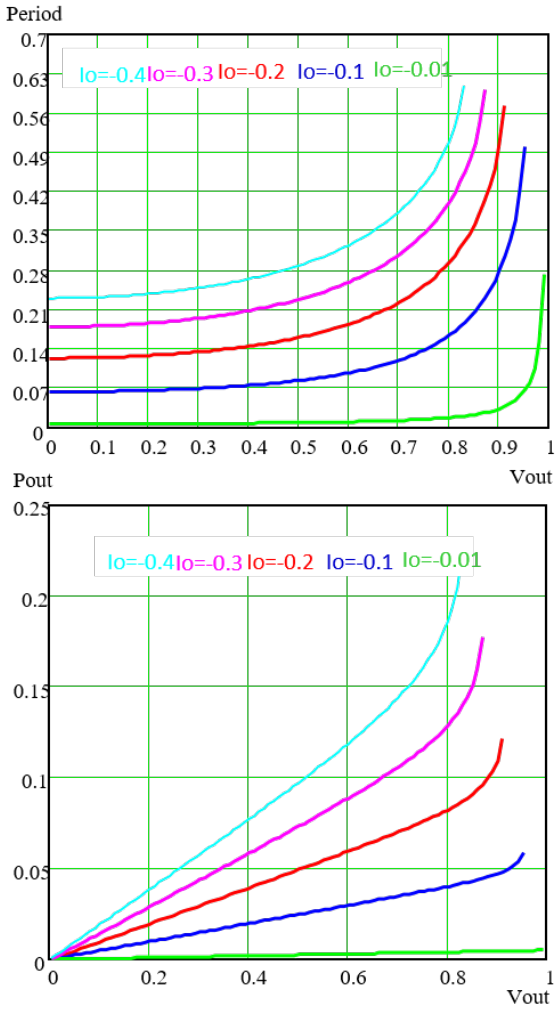

Figure 3-3: Voltage gain vs. period (top) and output power vs. voltage gain, every curve is plotted for initial current different values. All the magnitudes are normalized.

into the expression shown in equation 3.11.

$$\hat{T} = F\left(\hat{I}_o, \hat{v}\right) \quad \text{and} \quad \hat{p} = F\left(\hat{I}_o, \hat{v}\right) \tag{3.11}$$

The equations 3.11 show the period as a parameter depending on the normalized output voltage and normalized initial current of the converter. It is the same case on the normalized output power. Therefore, the power and period are interdependent. As longer as the output power is the posed parameter, it can be packed. The normalized period, therefore, becomes an unknown parameter on which depends the power transfer. So, the normalized period i.e the normalized frequency is considered

as capital for this work and expressed in the equation 3.12.

$$\hat{T} = F\left(\hat{I}_o, \hat{v}\right)) \quad \text{and} \quad \hat{f} = \frac{1}{\hat{T}} \tag{3.12}$$

From the graphical representation 3-3, beyond the normalized output voltage $\hat{v} = 0.8$, the converter voltage attains its cut-off for various levels of initial current I_0, and the output power increases sharply. It affects the switching frequency behavior. Therefore, the SRC design will not go beyond $\hat{v} = 0.8$, to avoid the drastic increase in power and decrease in switching frequency. Hence, the SRC design considers the equations 3.12 as important, and assumes this equation as a polynomial expression. It leads to a polynomial expression of n_{th} order. The last is simple and make the control philosophy of SRC.

3.3 Steady State Model of the Parallel Resonant Converter

The PRC and PRC-LCC are the most common topologies in high voltage application, since with the inclusion of the high voltage transformer they implicate the parasitics as part of the resonant tank[47] as shown in figure 3-4. By applying the phase-shifted PWM, it is easier to operate the converter in optimum mode[25] as illustrated in Figure 3-5 and detailed later in 3.3.3.3. As it is well known, in order to operate the converter[25, 65, 66], the frequency and duty are modified, in such a way that the output voltage and power requirements are achieved. As the duty and frequency are variables, a couple of combinations of power and voltage at the output of the converter are produced and keep the converter operating in the optimum mode. However, at every desired value of output voltage and power, the corresponding frequency and duty have to be pre-calculated[65, 66, 114, 97, 90]. The last is a complex process; it renders the implementation mores sophisticated. Hence, any algorithm computing it in any type of Digital Signal Processor (DSC) is of capital interest.

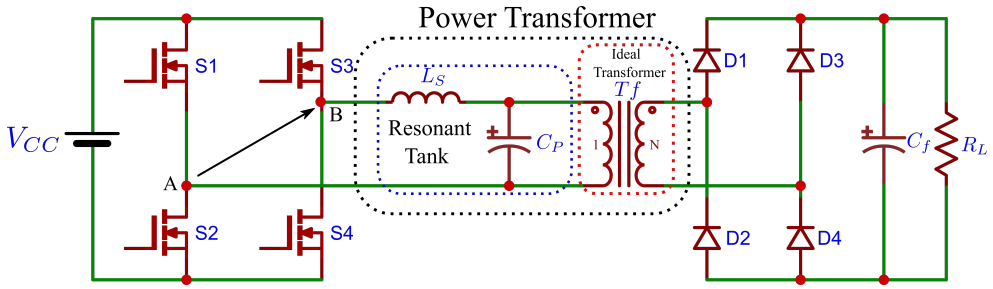

Figure 3-4: The PRC with the resonant tank components embedded in the Power Transformer.

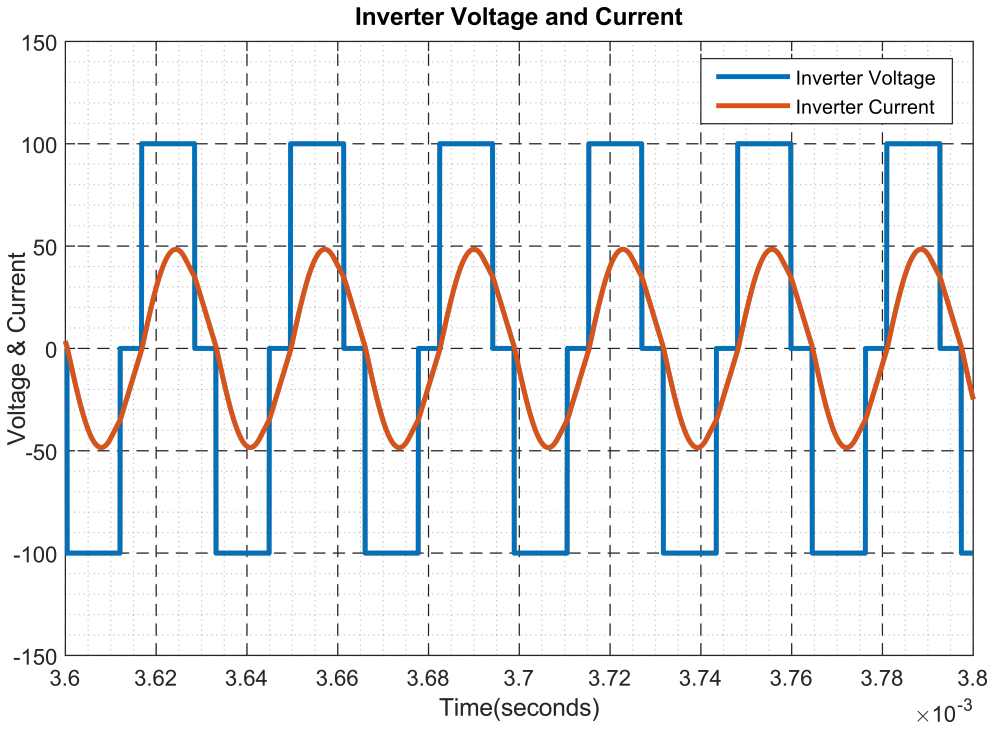

Figure 3-5: Output of PRC in terms of voltage and current in optimum mode of operation

3.3.1 Analytical study of PRC Steady State Model

In 2.3.2, the Figure 2-16 shows the parallel resonant converter (PRC). In this case the output filter is capacitor based; it omits the inductor to avoid a bigger choke size in high voltage applications[25, 65, 78, 67, 59, 118]. The resonant tank in parallel configuration can either be made of discrete components or be included in the parasitics of the high voltage transformer. If the last option is considered, the design of high

voltage transformer keeps the necessary distance between the windings for insulation improvement; it results into a high leakage inductance L_s. While, due to the large number of windings at the secondary side of the transformer; the bigger number of turns result into a very big capacitor. The last is referred to as a parasitic capacitor C_p. The mentioned parasitic elements make part of the resonant tank components. Considering the active front-end inverter in Figure 2-16 and 3-4, the voltage square waveform is generated with fours switches. It will be filtered by the resonant tank, thus the quasi-sidusoidal voltage waveform is obtained at the secondary. The analysis is done under time domain to process the topology calculus[113]. Apart from the SRC and some other configuration of the same components presented in [104], where the series capacitor C_s plays both the role of resonant tank element and DC component suppressor. The series capacitor C_s plays only the role of DC component filter, and it does not resonate with the resonant converter. Therefore, the line-commutated-converter-type (PRC)/ (PRC-LCC) is obtained [95, 64, 43]. However, the C_s is not considered in modeling and calculations. As the serial capacitor is only for DC level suppression in the DC signal, there is no need of particular specifications for it. The PRC efficiency improves when the output power decreases[25]. The PRC with resonant tank components included in high voltage transformer will be analyzed in this section. Therefore, the number of external components is reduced, unless, the transformer parasitics are not big enough.

3.3.2 Base and Normalized values

For the ease of application and on a wide range, the normalized parameters are used. Hence the equations 3.13 and 3.14 illustrate the respective base and normalized parameters for the indicated PRC. In which, $\hat{f}$, $\hat{v}$, $\hat{\Omega}$ and $\hat{p}$ are normalized frequency,

normalized output voltage, normalized load and normalized power respectively.

$$V_{Base} = V_{CC} \quad Z_{Base} = \sqrt{\frac{L_S}{C_P}} \quad P_{Base} = \frac{V_{CC}^2}{Z_{Base}}$$
$$f_{Base} = \frac{1}{2.\pi\sqrt{L_s.C_P}} \qquad \omega_{Base} = \frac{1}{\sqrt{L_S.C_P}} \tag{3.13}$$

Based on the equation 3.13, the normalized parameters are illustrated as follows:

$$\hat{v} = \frac{V_{out}}{V_{CC}} \quad \hat{p} = \frac{P_{out}}{\frac{V_{CC}^2}{Z_{Base}}} \quad \hat{\Omega} = \frac{R_L}{Z_{Base}} \quad \hat{f} = \frac{f}{f_{Base}} \tag{3.14}$$

3.3.3 PRC Operating Modes

The PRC will generate waveform identical to that illustrated in Figure 3-5. The four power electronic switches will allow to implement various controls. This work shall tackle and limit itself to variation of frequency and duty. The operation of the converter targets to generate the resonant inductor lagging the voltage (inductive mode). Therefore, at least one of the legs is zero voltage switching (ZVS). The analysis of the converter will be carried out by its various stages, with each of the equivalent circuits that these stages produce being studied. The currents and voltages at the resonant components, which in our instance are the serial inductor and parallel capacitor, must be considered. The ideal transformer is considered for translating all the magnitudes to the primary side, and the parallel capacitor clamps to the output full bridge rectifier. The voltage waveform in parallel capacitor reflect that this voltage is clamped to the output voltage on positive and negative polarity, when it reaches this value. This "time to clamp" help to differentiate two modes as indicated in Figure 3-6. The normalized values will be to carry out the complete analysis of the converter. The related equations are illustrated in equations 3.13 and 3.14.

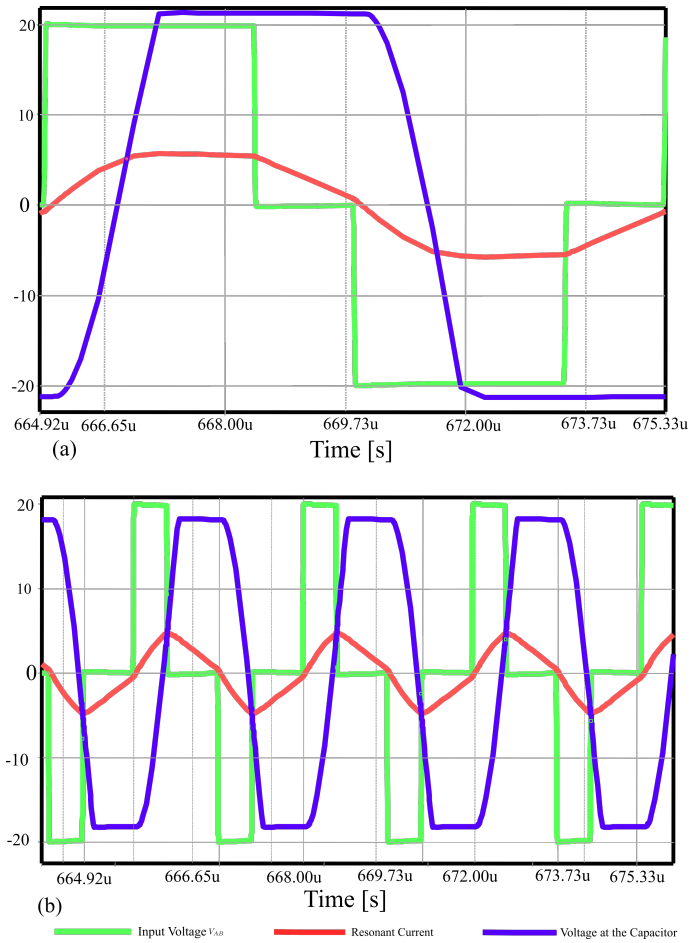

Figure 3-6: Mode I: at (a), Capacitor (C_p) voltage clamps before DT. Mode II: at (b) the capacitor (C_p) voltage clamp is produced after DT. Both the figures (a) and (b) illustrate Mode I and Mode II in Optimum mode[25]

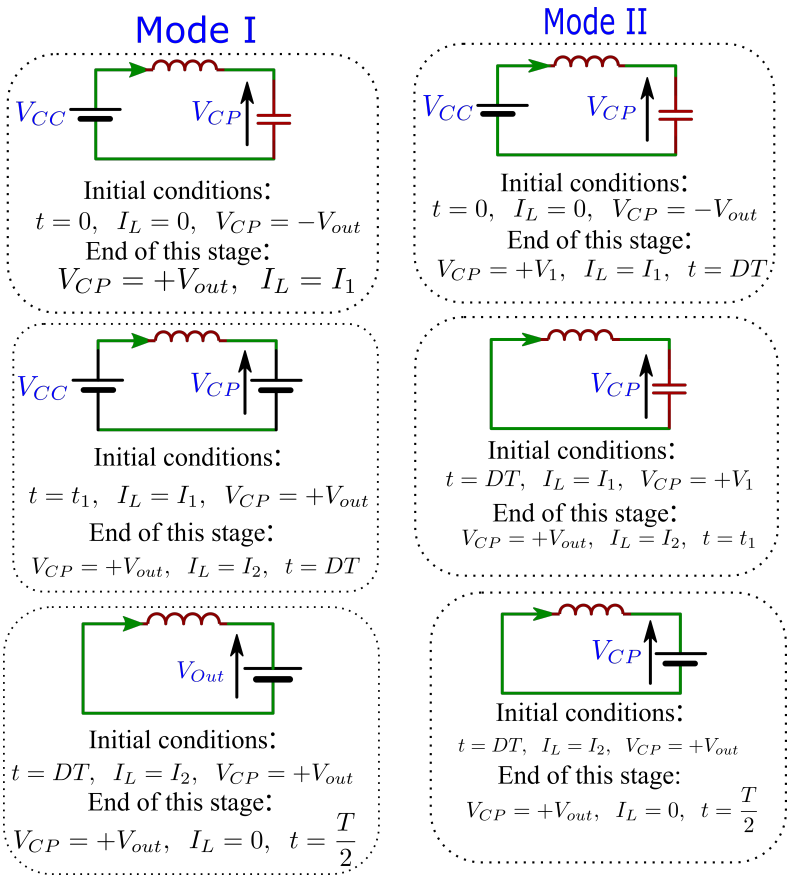

Figure 3-7: The illustration of Mode I and Mode II in their respective circuitry and expression, both in their Optimum Mode.

3.3.3.1 Mode I

From the Figure 3-6 and 3-7 , considering that the output voltage is maintained constant all along the switching period T once the voltage in the parallel capacitor reaches V_{out} it will stop to charge since the output filter capacitor acts as voltage source placed in parallel with this capacitor. Once the resonant current falls to zero and becomes negative, the parallel capacitor will starts to decrease and the current accross the diodes will be zero. The voltage at the parallel capacitor is clamped as long as V_{AB} is positive and equation to V_{CC}. The condition of operation are illustrated in equation 3.15.

$$t_L \geq 0 \qquad t_L + t_C \leq d.T \tag{3.15}$$

The mode I is typically of high duty-cycle as the parallel capacitor has enough clamping time. This mode is defined by the following limits: $t_L = 0$ and $t_L + t_C = dT$. Once the duty-cycle get fixed; the complete equation that computes different current, voltage, and time is obtained.

3.3.3.2 Mode II

The mode II is illustrated in figure 3-6. In this mode, $t_L \geq 0$ and $t_C + t_L \geq dT$; hence the parallel capacitor clamps to the output voltage after that input voltage reaches zero. The limit to define this mode of operation are: $t_C + t_L = 0.5T$, since this is the cut-off for capacitor charging. This mode happens when the duty cycle is not high. Depending on the frequency and voltage gain; however, the same duty can be used to operate the converter in both modes. In both modes soft switching can be realized.

3.3.3.3 Optimum Mode

Let us refer to the cases in which $t_L = 0$, in this case the product of input voltage (V_{AB}) and the input current(resonant current) is always positive. It means that the power is positive and no energy is sent back to from the secondary side. The current is zero at any switching. It is a particular operation mode and it is included in the previous one. The Figure 3-4 illustrates the PRC with the transformer parasitics making the resonat tank. It is made of a power transformer, which has the ideal part and the parasitics. They make the resonant converters and they are the reason of the converter performance. The Figure 3-7 shows various steps of the resonant tank performance and the respective characteristics. The same figure highlights the basic equations on which are based the steady state modeling of the PRC. Hence, the Figure 3-7 results into the Equations 3.16, 3.17, 3.18, 3.19 and 3.20 [25]; respective to mode I as indicated in the Figure 3-7. The same equations are graphically represented in Figure 3-8(c). Here $\hat{T}$,$\hat{v}$, $\hat{t}$ and d are the the normalized period, normalized output voltage, normalized time and duty respectively.

$$\hat{v} = \frac{(1+\hat{v})}{2}.\left[1 - \cos\left(2\pi\hat{t}_1\right)\right] \tag{3.16}$$

$$I_1 = (1 + \hat{v}) \,.\, \sin\left(2\pi\hat{t}_1\right) \tag{3.17}$$

$$I_2 = (1 - \hat{v}) \,.2\pi.\, \left(d.\hat{T} - d.\hat{t}_1\right) + I_1 \tag{3.18}$$

$$\hat{T} > 0 \quad \hat{t}_1 \leq d.\hat{T} \tag{3.19}$$

$$0 = I_2 - 2\pi\hat{v}.\,(0.5 - d)\,.\hat{T} \tag{3.20}$$

For the optimum mode, the system of equations is illustrated in equations 3.21 and its graphically illustrated in the Figure 3-8(c).

$$I_2 = -\hat{v}_1 \sin\left[2\pi\left(\hat{t}_2 - d.\hat{T}\right)\right] + I_1 \cos\left[2\pi\left(\hat{t}_2 - d.\hat{T}\right)\right] \tag{3.21}$$

The Mode II indicated in Figure 3-7 result into the equations 3.22,3.23,3.24 and 3.25[25].

$$I_1 = (1 + \hat{v}) \,.\, \sin\left(2\pi d\hat{T}\right) \tag{3.22}$$

$$\hat{v}_1 + \hat{v} = (1 + \hat{v}) \,.\, \left(1 - \cos\left(2\pi d\hat{T}\right)\right) \tag{3.23}$$

$$\hat{v} = \hat{v}_1 \left[\cos\left(\pi.\hat{t}_2 - d\hat{T}\,\right) - 1\right] + I_1 \sin\left(2.\pi.\,\left(\hat{t}_2 - d\hat{T}\right)\right) + \hat{v}_1 \tag{3.24}$$

$$I_2 = 2.\pi.\hat{v}\left(0.5.\hat{T} - \hat{t}_2\right) \tag{3.25}$$

The same equations result into the graphical representation of the model as indicated in the Figure 3-8.

3.3.4 Graphical Represention of PRC Steady State Model

The steady state model normalized equations for PRC are detailed3.3.3[25], and represented graphically in Figures 3-8 to illustrate its behaviors. The Figure 3-8(a) and (b) show the normalized output voltage of the model with respect to the change in normalized switching frequency, and in presence of the suitable value of the duty. While, the Figure 3-8(c) illustrates the normalized power as a function of normalized output voltage in presence of respective duty values. The mentioned graphs highlight the process to establish the necessary duty and switching frequency for achieving the targeted output voltage and power. It is a long and complex process that humps the implementation mostly on low-cost DSC. That complexity imposes a requirement to use a micro-controller with reliable computational capability. Hence, the use of DSC is crucial, and converting the steady-state model into the algorithm that the DSC can handle is the goal. For simplification of the task, the steady state model graphical representation in Figures 3-8 (a), (b) and (c) give the approach of the PRC steady state mode behavior. However, they structured in such a way to easily generate duty and switching frequency once the power and output voltage are provided. Hence, the new form of graphical representation indicated in Figure 3-9 is obtained. In the last, the switching frequency and duty are functions of output voltage and power. The Figure 3-9 (a) indicates the normalized frequency as a function of normalized output power, in presence of the normalized output voltage. Hence, the normalized frequency is a function of both normalized output voltage and normalized output power. On the Figure 3-9 (b), the duty as a function of normalized power, in presence of normalized voltage is illustrated. It implies that the duty is a function of both normalized output voltage and normalized power.

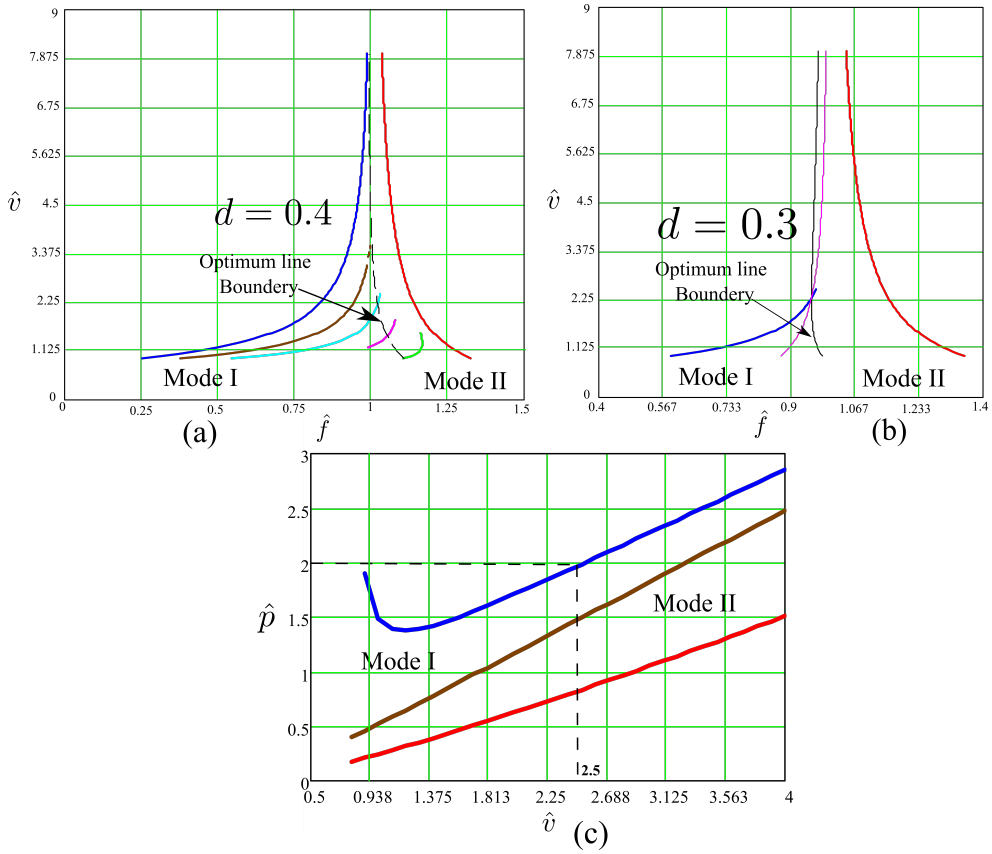

Figure 3-8: Normalized output voltage vs normalized frequency for two values of duty cycles[25]

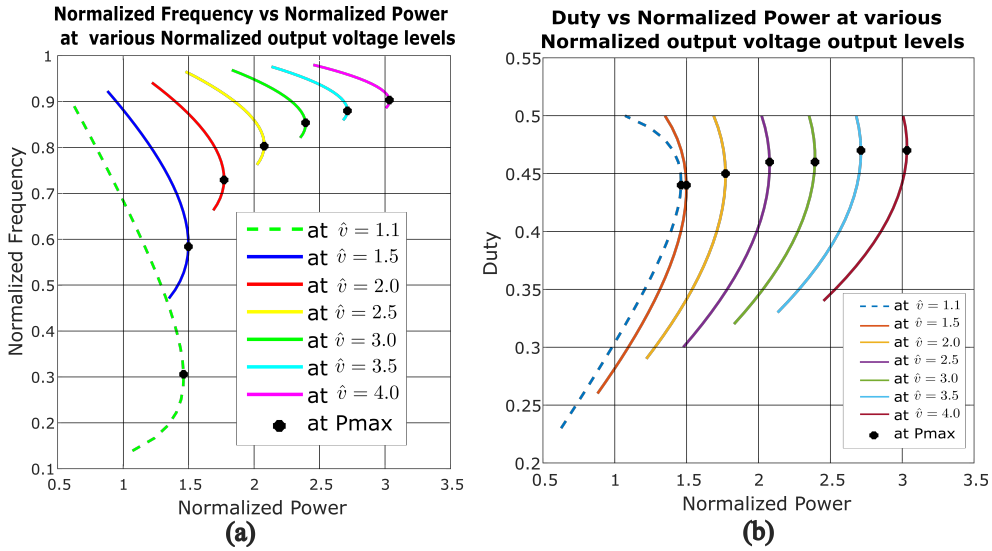

Figure 3-9: Normalized frequency vs normalized power and duty vs normalized power in presence of normalized voltage

The illustration in the Figure 3-9 consider and limits itself on the optimum mode of the PRC. Hence, all of the descriptions above together with the representations in Figures 3-8 and 3-9 are combined in the mathematical expression shown in the equation 3.26.

$$\hat{f} = F(\hat{v}, \hat{p}) \quad d = F(\hat{v}, \hat{p}) \tag{3.26}$$

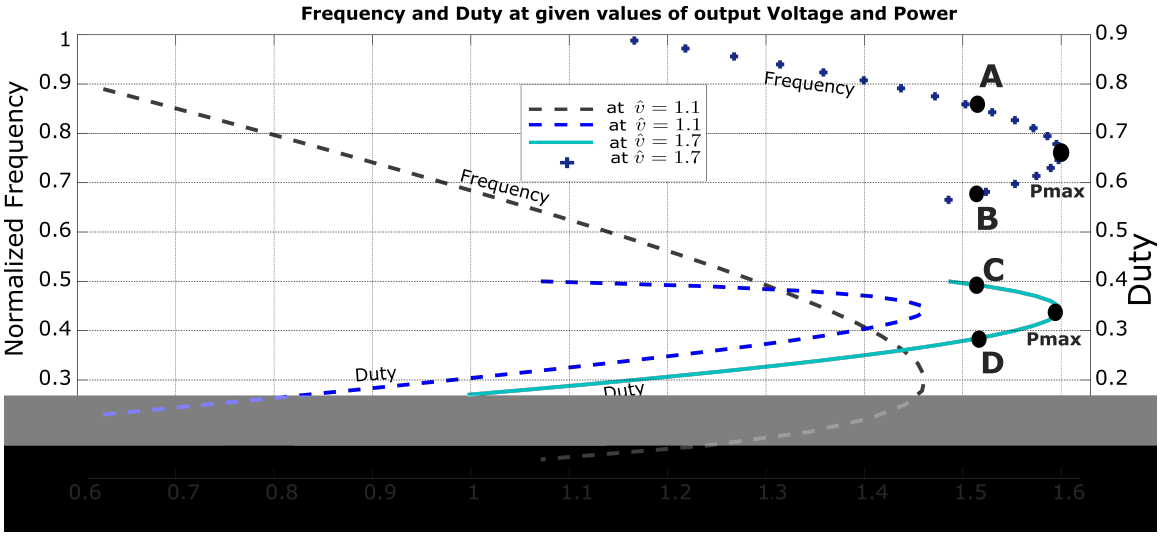

Figure 3-10: Illustration of normalized frequency vs normalized power and duty vs normalized power in presence of normalized voltage with the related behaviors

Figures 3-9 show that the power reaches its peak at each voltage level, with a given frequency or duty, and then begins to diminish. The power as a function of frequency and duty cycle is shown in Figure 3-10. The value of the power at point **A** is equal to the value of the power at point **B**. On the other hand, point **B** occurs after the maximum power point **Pmax**. Similarly, the power value at point **C** is the same as the power value at point **D**. The point **D** is reached after reaching the maximum power point **Pmax**. The design in place for power maximization at each frequency, duty, and voltage level ignores power over the maximum level **Pmax**. Assuming that the equation 3.26 is made of two polynomials for switching frequency and duty respectively; the next step is to find their respective coefficients. This process will result is a set of polynomials of n_{th} order. The last have to be simple and make the control philosophy to run the control topology in Figure 3-4 on DSC and in optimum

expression to the plot on which it is applied. In this case various fitting were tried and cubic resulted in accurate fitting. Therefore, the equivalent polynomial expression is of third order.

Table 4.6: The table illustrates various coefficients of different fittings on frequency plots, at specific levels of voltage. a_i: coefficients for frequency fitting.

$\hat{v}$	a_0	a_1	a_2	a_3
1.0	0	0	-0.61102	1.222
1.1	-0.70602	1.9259	-2.2687	1.7354
1.2	-1.288	3.6637	-3.9182	2.2918
1.3	-1.3247	3.9212	-4.2784	2.4819
1.4	-1.5175	4.6649	-5.1259	2.8205
.	.	.	.	.
.	.	.	.	.
.	.	.	.	.
3.6	-0.59499	4.2475	-10.184	9.1596
3.7	-0.74666	5.5661	-13.909	12.606
3.8	-0.65556	4.9904	-12.737	11.858
3.9	-0.57735	4.486	-11.689	11.175
4.0	-0.51036	4.0457	-10.758	10.559

Table 4.7: The table illustrates various coefficients of different fittings on duty plots, at specific levels of voltage. b_i: coefficients for duty fitting.

$\hat{v}$	b_0	b_1	b_2	b_3
1.0	0	0	0.19449	0.11102
1.1	0.25389	-0.69256	0.81585	-0.07406
1.2	0.51726	-1.4713	1.5735	-0.32038
1.3	0.58838	-1.7417	1.9003	-0.45238
1.4	0.74316	-2.2865	2.5136	-0.68055
.	.	.	.	.
.	.	.	.	.
.	.	.	.	.
3.6	0.89738	-6.408	15.368	-12.018
3.7	1.1575	-8.6289	21.562	-17.693
3.8	1.048	-7.9784	20.364	-17.059
3.9	0.95176	-7.3958	19.273	-16.475
4.0	0.86674	-6.872	18.276	-15.935

The tables 4.6 and 4.7 contains the different coefficients of each polynomial per level of output voltage. The a_i are coefficients for frequency polynomial expression while b_i are those for duty polynomial expressions. The output voltage as a leading parameter was posed to run from 1.0 to 4.0 with a constant step of 0.1. Therefore the tables 4.6 and 4.7 are summarized, the full tables, for further references and studies, are detailed in Appendix A.

$$\hat{f}(\hat{v}, \hat{p}) = a_0\hat{p}^3 + a_1\hat{p}^2 + a_2\hat{p} + a_3 \tag{4.10}$$

for frequency and

$$d(\hat{v}, \hat{p}) = b_0\hat{p}^3 + b_1\hat{p}^2 + b_2\hat{p} + b_3 \tag{4.11}$$

for duty.

4.3.2 B-Spline Application

The coefficients a_i and b_i in table 4.6 and 4.7 are polynomials too and functions of normalized output voltage $\hat{v}$. They are in the form illustrated in the equation 4.12. Therefore, their respective coefficients are computed in turn. The data in tables 4.6 and 4.7 are graphically represented and Data fitting is applied as shown in Figure 4-5(a). However, Data fitting results into big outliers once applied to coefficients a_i and b_i as in Figure 4-5(a), and it was immediately ignored. Therefore, an alternative was to apply B-spline[115, 31, 14, 61]. The last is part of numerical analysis, which is mostly applied in curve-fitting and numerical differentiation of data. By applying B-spline on data in tables 4.6 and 4.7, the coefficients for polynomials a_i and b_i are retrieved. The obtained coefficients are piece-wise linear at each output voltage level as showed in Figure 4-5(b).

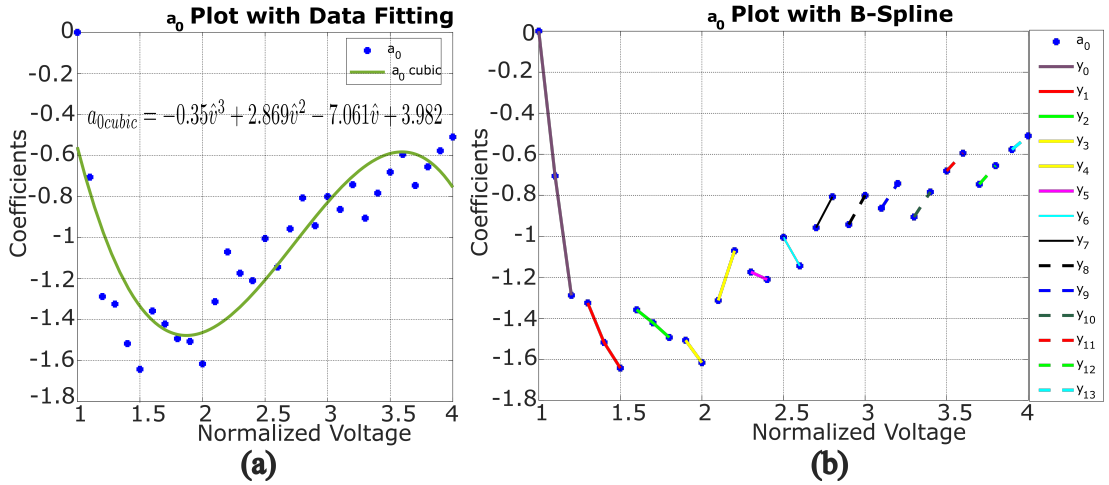

Figure 4-5: Illustration of a_0 plotting, Data fitting and B-Spline application.

Table 4.8: This table shows the specific coeffiecients retrieved from the coefficients in table 4.6 after B-spline.

$\hat{v}$	a_0		a_1		a_2		a_3	
	α_0	λ_0	α_1	λ_1	α_2	λ_2	α_3	λ_3
1.0 - 1.2	-6.44	6.4193	18.319	-18.287	-16.536	15.924	5.349	-4.1342
1.3 - 1.5	-1.59	0.73103	7.2865	-5.5462	-9.536	8.1538	4.222	-3.0346
1.6 - 1.8	-0.675	-0.27697	5.6585	-4.4915	-10.486	11.393	5.87	-6.306
1.9 - 2.0	-1.095	0.5737	8.328	-9.835	-16.523	23.247	10.022	-14.362
2.1 - 2.2	2.424	-6.4033	-9.185	24.994	11.445	-32.488	-4.495	14.611
2.3 - 2.4	-0.365	-0.3347	3.796	-3.17	-9.153	12.106	6.57	-9.3089
2.5 - 2.6	-1.393	2.4775	10.211	-20.46	-22.786	48.312	16.191	-34.545
2.7 - 2.8	1.5088	-5.0318	-7.101	24.405	10.879	-39.025	-5.261	21.15
2.9 - 3.0	1.4187	-5.0571	-7.191	26.411	11.834	-45.351	-6.159	26.178
3.1 - 3.2	1.2073	-4.606	-6.409	25.243	11	-45.349	-5.928	27.237
3.3 - 3.4	1.2193	-4.9297	-6.94	28.953	12.76	-55.668	-7.38	35.5
3.5 - 3.6	0.8654	-3.7104	-5.133	22.726	9.82	-45.536	-5.895	30.382
3.7 - 3.8	0.911	-4.1174	-5.757	26.867	11.72	-57.273	-7.48	40.282
3.9 - 4.0	0.6699	-3.19	-4.403	21.658	9.31	-47.998	-6.16	35.199

Table 4.9: This table shows the specific coeffiecients retrieved from the coefficients in table 4.7 after B-spline.

$\hat{v}$	b_0		b_1		b_2		b_3	
	β_0	φ_0	β_1	φ_1	β_2	φ_2	β_3	φ_3
1.0 - 1.2	2.5863	-2.5879	-7.3565	7.3709	6.8951	-6.7233	-2.157	2.2782
1.3 - 1.5	1.4197	-1.253	-5.573	5.5074	6.9235	-7.1266	-2.8196	3.231
1.6 - 1.8	1.0212	-0.84879	-5.669	6.4327	9.214	-11.632	-4.713	6.5631
1.9 - 2.0	1.48	-1.7409	-8.867	12.589	15.965	-24.54	-9.087	14.889
2.1 - 2.2	-1.4155	4.0245	4.987	-15.045	-5.526	18.38	1.776	-6.8231
2.3 - 2.4	0.916	-1.06	-6.297	9.5256	13.015	-21.959	-8.519	15.571
2.5 - 2.6	1.8546	-3.6424	-12.615	26.522	27.025	-58.994	-18.648	42
2.7 - 2.8	-1.2309	4.3582	5.429	-20.312	-7.493	30.662	3.007	-14.273
2.9 - 3.0	-1.2665	4.7769	6.027	-23.985	-8.97	38.931	3.906	-19.616
3.1 - 3.2	-1.1662	4.7107	5.796	-24.789	-8.93	41.962	3.946	-21.928
3.3 - 3.4	-1.271	5.4262	6.787	-30.625	-11.25	55.564	5.38	-31.26
3.5 - 3.6	-0.9676	4.3807	5.378	-25.769	-9.26	48.704	4.56	-28.434
3.7 - 3.8	-1.095	5.209	6.505	-32.697	-11.98	65.888	6.34	-41.151
3.9 - 4.0	-0.8502	4.2675	5.238	-27.824	-9.97	58.156	5.4	-37.535

The equations 3.26 results into two capital polynomial coefficients as follows, for frequency and duty respectively:

$$a_i(\hat{v}) = \alpha_i \hat{v} + \lambda_i \quad \text{and} \quad b_i(\hat{v}) = \beta_i \hat{v} + \varphi_i \tag{4.12}$$

The equations 4.10 and 4.11 provide the frequency and duty that are able to run the topology on Figure 3-4 in its optimum mode at a specified level of voltage, power and load. Combining the equations 4.10, 4.11, and 4.12, the general equations 4.13 for frequency and duty respectively are obtained. They can fit in any DSC and generate the suitable control signals.

$$\hat{f}(\hat{v}_i, \hat{p}_j) = \sum_{i=0}^{i=n} a_i \hat{p}_j^{n-i} \quad \text{and} \quad d(\hat{v}_i, \hat{p}_j) = \sum_{i=0}^{i=n} b_i \hat{p}_j^{n-i} \tag{4.13}$$

4.4 Conclusions

This chapter focused on the SRC and PRC, re-introduced their use in the respective applications and their popularity. The steady-state model for each was re-instated and their respective graphical representation were reminded. However, their respective control implementation was seen to have a possibility mostly on first harmonic approach. To mitigate that drawback, the polynomial model was suggested. Through the graphical representation of both topology, data fitting and B-spline numerical method; the polynomial models for both SRC and PRC were developed. Their respective expression were shown in this chapter. They facilitate to establish the right SRC and PRC controls in an easy and simple way.

Chapter 5

The Modeling and Simulations of SRC

Contents

5.1 Introduction 115
5.2 The Matlab Model of SRC 116
5.3 The simulation of SRC 117
5.4 The Simulink model: DSC implementation 118
5.4.1 DSC Configuration 119
5.5 Conclusions 122

5.1 Introduction

The polynomial model of SRC converter was developed and illustrated in details in 4.2. The related polynomial expressions are shown in equation 4.4, while, the general expression is illustrated in the equation 4.9. The goal is to implement the obtained polynomial model in a DSC; in order to do it, Matlab will be used. In this chapter, the mentioned polynomial expressions are model and simulated in Simulink. The

related models are shown in this chapter. The simulation results of the models are also illustrated in this chapter. In order to build the control prototype, the DSC with strong computational capability is needed. Therefore, the suitable DSC shall be shown and its configuration to Simulink for quick programming is illustrated in this chapter. The model-based programming is used to convert the Simulink model into DSC suitable codes; this is shown as well in this chapter.

5.2 The Matlab Model of SRC

The topology in figure 3-2 represents the SRC power topology and the polynomial expression in equation 4.9 represents the control side. Both control and power sides of the SRC are modeled in Simulink and simulated. The figure 5-1 shows the model, where the normalized power and normalized load help to determine the corresponding normalized voltage and normalized initial resonant current. The last, in turn are supplied to the polynomial block. The equation 4.8 and 4.8 are in detail scripted in the polynomial blocks, in a cascaded way. The two cascaded blocks are illustrated in figure 5-1, where first block (holding the script for the polynomial $\hat{I}_o$) receives the normalized values of power $\hat{p}$ and voltage $\hat{v}$ and produce the corresponding normalized initial resonant current $\hat{I}_o$. The last together with the normalized voltage $\hat{v}$ are fed to the second block (holding the script for the polynomial $\hat{T}$) and provide the suitable switching period. The last is obtained as a normalized value, and the normalized switching frequency is retrieved from it following the equation 4.9. The obtained switching period is hence supplied to the PWM generator block to give the suitable switching signal at the correct frequency. Therefore, the switching signals control the inverter and generated output is illustrated as in figure 5-2.

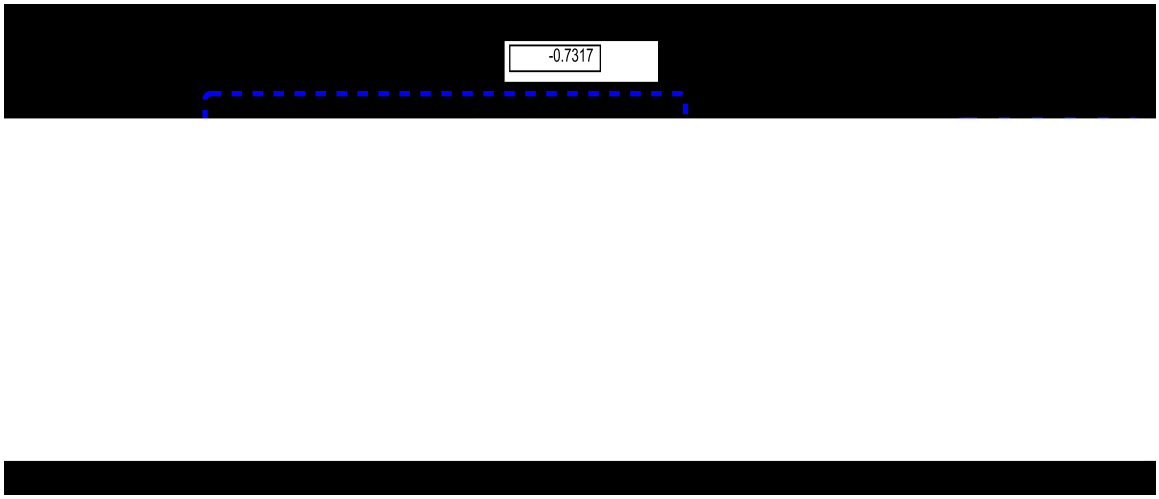

Figure 5-1: The illustration of the Simulink topology of the SRC polynomial model

The figure 5-1 illustrated the polynomial model control of the SRC. The parameter values in the table 5.1 are applied to the SRC as shown on the figure 2-18.

Table 5.1: The parameters used to simulate the SRC model in Simulink

Item	**value**	**unit**
V_{in}	100	V
L_s	34.232	uH
C_p	658.7	nF
C_f	30	uF
Z_{Base}	7.209	Ω
f_{Base}	33.527	kHz

5.3 The simulation of SRC

The Simulink model was built based on parameters in the table 5.1 in Simulink to run and validate the polynomial model on the simulation level. The control was done following the model in the figure 5-1 and the parameters were normalized following the equation 3.5. The SRC model is run in Simulink with the parameters shown in the table 5.1 , and control program based on the values in the table 4.8. Since the

obtained frequency value is above resonance, therefore the SRC polynomial model tracks the steady-state model. Similarly, the polynomial model graphs illustrated in figure 5-2 track the steady-state graphs shown in figure 3-2. The simulation results are tabulated in table 5.2 and graphically illustrated on the figure 5-2.

Table 5.2: Illustration of the SRC simulation results

Item	Value
$\hat{p}$	0.1000
$\hat{\Omega}$	0.8824
$\hat{v}$	0.2971
$\hat{I}_o$	-0.7317
$\hat{T}$	0.3858
$\hat{f}$	2.5920
f_{sw}	86 kHz

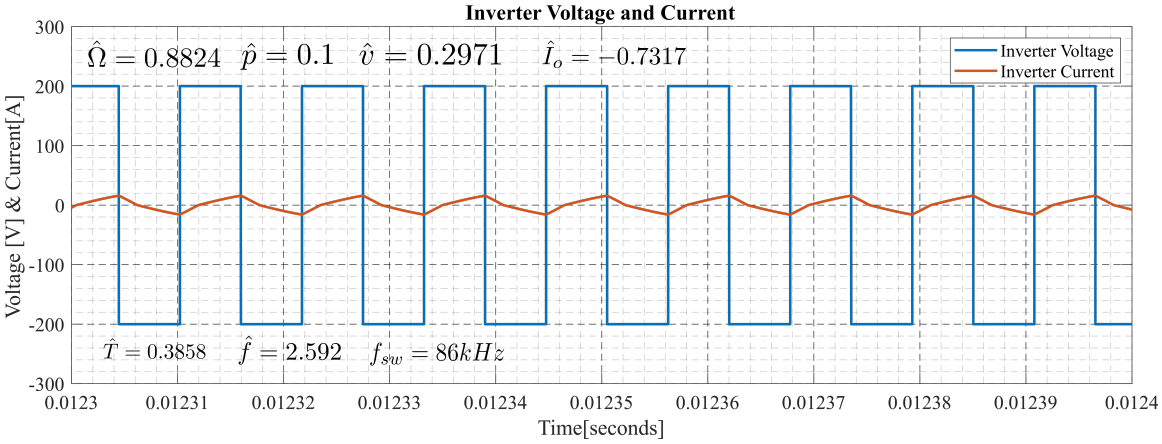

Figure 5-2: The SRC inverter output Voltage and Current

5.4 The Simulink model: DSC implementation

This section focuses on the SRC control implementation in DSC. It considers the polynomial model. The whole process was done in order to ease the control implementation and eradicate the steady-state complexities. The conversion of SRC

Simulink model into control program and fitting the same program into the DSC is the major outcome of this section.

5.4.1 DSC Configuration

This subsection deals with the selection of the DSC in use and its configuration. The Model-Based programming method as a quick fix and faster alternative is introduction, the use of Simulink as model-based IDE is shown and the conversion of model-based program into conventional program is elaborated.

5.4.1.1 The Use of TMS320F28335 DSC

Considering the complexity of the SRC conversion form Steady-state to polynomial model; higher computational capability is crucial. Therefore DSC is required; and this work takes the advantage of Texas Instrument (TI) TMS320F28335 DSC, which belongs to the family of C2000. It is characterised by its high-performance static CMOS technology, high-performance 32-bit CPU, fast interrupt response processing, on-chip memory and many more advantages[101]. The F28335 is shown on figure 5-3 for visual representation. The PWM signals that control the inverter power electronic switches are generated on TMS320F28335 Peripheral Explorer Kit through Matlab-Simulink . The F28335 is usually programmed through Code Composer Studio (CCS) development environment, which supports C or C++ language. Even though most control engineers are familiar with the stated languages, they are time intensive and prone to mistakes, making it difficult to code signals appropriately. Therefore, model-based programming in Matlab-Simulink is used as a quick and reliable alternative.

5.4.1.2 The Model-Based Programming

It is referred to as "Data Flow Diagram" or "Model-based design"[4, 27]. The model based programming is a mathematical and visual approach to solving issues in complicated control, signal processing, and communication systems design. It has a

Figure 5-3: Illustration of Texas Instrument (TI) TMS320F28335 DSC[101]

wide range of applications in motion control, industrial equipment, aerospace, and automotive[27]. Model-based programming is known as a quick technique for creating embedded softwares. It is quick fix and faster in building a control programs and not prone to mistakes. It uses models to mimmick the behaviors of the control systems envisaged. The model-based program is visual and sequential more than being logical and structural. This makes it different to conventional pragramming methods, where the projects get alot of delays dues to alot of time required in optimizing the program. There is alot of IDE developed that are suitable to Model-based programming; Simulink included. This method of programming is convertable to the conventional methods and the resulted program is able to fit the targeted micro-controller.

5.4.1.3 The TMS320F28335 Control Program

The entire control technique is written in Matlab-Simulink, and the PWM codes for the F28335 are created subsequently. Configuring a Peripheral Kit for Matlab-Simulink requires certain specific processes. Matlab-Simulink, as well as CCS, must be installed on the PC, along with other essential add-ons such as "Embedded Coder," "Simulink Coder," and "Matlab Coder." Matlab R2021a with the specified Add-on, as well as CCS 7.3.0, are installed on the PC in this situation. As a result, the target hardware (TI Delfino F2833x) has been set up. The PWM codes are created and downloaded to the TMS320F28335 Peripheral Explorer Kit using Simulink. CCS is

used to obtain backup or other analysis codes in project form. The F28335 model-

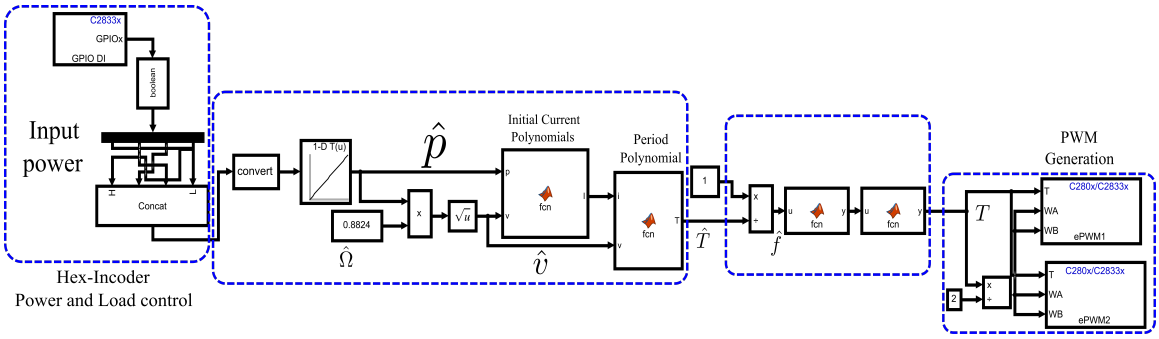

Figure 5-4: PWM code generation model in Simulink

based program considers the simulation control model in the figure 5-1 and modify it in such a way to generate the control code suitable for F28335. Then, the modified model is illustrated in the figure 5-4. The control model on the figure 5-1 shows that the model needs two inputs in which one is external i.e normalized power $\hat{p}$. In order to have a sequence of tests, a number of external inputs to F28335 is required. Then, the Hex-Encoder that can hold enough number of inputs is used. The Hex-Encoder serves as an input to the DSC and it accepts 16 different combinations i.e. it can enter 16 different inputs combinations on various steps. It is connected to four general purpose input-outputs (GPIOs). Those are GPIO15, GPIO14 GPIO13 and GPIO12 in order of most to least significant bit respectively. Using the look-up table block in Simulink, the Hex-Encoder inputs 16 different power values. With the help of the normalized load, the normalized voltage value is obtained. The normalized power and normalized output voltage are the two inputs to generate the normalized initial resonant current. The last is a polynomial expression as it is illustrated on the equation 4.7. The normalized initial resonant current and the normalized output voltage become the two inputs to the polynomial expression in the equation 4.8. It is scripted in the polynomial block to generate the normalized switching period $\hat{T}$. The last is converted into the period T following the expression in the equation 5.1 and fed to both ePWM1 and ePWM2 at input "T" for PWM signal generation for both converter legs. A half of the period is fed to both ePWM1 and ePWM2 on inputs "WA" and "WB" to maintain 50% duty cycle for each switching signal. The PWM

switching signals are created at an appropriate frequency. The first leg's switching signal is output by the ePMW1A and ePWM1B, while the second leg's switching signal is output by the ePWM2A and ePWM2B.

$$T = \frac{f_{clk}}{2 * f_{sw}} \tag{5.1}$$

From the equation 5.1; T is the period, f_{clk} is the F28335 maximum DSC clock frequency and f_{sw} is the switching frequency.

5.5 Conclusions

This chapter springs from the previous chapters of this work. The SRC is considered in both the steady-state and polynomial models, as a process towards the reliable, quick and easy control of serial resonant converters. The SRC was simulated in Simulink and results were illustrated in this chapter. The model-based programming as quick fix, faster and not prone to mistake programming method was illustrated. The model was configured to fit F28335 DSC, the control program was built using Simulink models and the control codes were generated and loaded to the DSC appropriately. The PWM signal were generated from the DSC as it was expected.

Chapter 6

The Modeling and Simulations of PRC

Contents

6.1 Introduction 124
6.2 The Matlab Model of PRC 124
6.2.1 Two inputs model Simulations 125
6.2.2 One input model Simulations 127
6.3 The Simulink model: DSC implementation 129
6.3.1 DSC Configuration 129
6.4 The Resonant converter controls: FPGA implementation 132
6.4.1 Model-Based FPGA programming 133
6.4.2 FPGA configuration to Simulink 134
6.4.3 Implementation in FPGA of the direct calculation of the Frequency and Duty-Cycle 135
6.5 The Fuzzy closed loop control of PRC 140
6.5.1 Fuzzy Control overview 141
6.5.2 Fuzzy closed-loop control of PRC polynomial model 142

6.6 Conclusions 148

6.1 Introduction

As introduced in the section 2.4, the "ON" and "OFF" nature of power electronics switches require that the switching signals be digital. The flexibility and computational capability lead to the use of Digital Signal Controllers (DSC)[12]. For the prediction of system outcome in real sens, the modeling and simulation is key. Therefore, in this chapter, the PRC shall be modeled and simulated using Simulink. The PRC polynomial mode illustrated in 3.3 shall be modeled and simulated for a validation, and gateway for practical implementation. The simulation results shall be shown in this chapter. Using Simulink, the model shall be used to generate the control code for DSC i.e. F28335 micro-controller. The control of the PRC using FPGA shall be discussed in this chapter. The closed-loop control using Fuzzy logic shall be illustrated, and the respective simulation results shall be indicated.

6.2 The Matlab Model of PRC

In order to validate the polynomials shown in equation 4.13. The model in Figure.3-4 was built in Matlab-Simulink R2021a. The polynomials were applied to the mentioned model to confirm the optimum mode of operation. The model validation considers output voltage and power as independent variables, while the switching frequency and duty are dependent. The last is illustrated in the equation 4.13. Each level of output voltage and power corresponds not only frequency and duty but also the load. Hence the load is dynamic in this case and governed by the equation 6.1, which is a polynomial in turn. The control model was build in Matlab-Simulink as well. It is made of Matlab function block to hold the equation 4.13. This block accepts two inputs (normalized output voltage and normalized power) and generate two outputs (normalized frequency and duty). The two last outputs are used to obtain the required

period and phase shift that run the PWM generator. The last in turn, generates the switching signals that runs the IGBTs on the model in the Figure 3-4. The control model is illustrated in both Figures 6-1 and 6-2. Both the power and control model are run in Matlab-Simulink for validation of the polynomials, before going for practical implementation.

$$\hat{\Omega} = F(\hat{v}_i, \hat{p}_j) \tag{6.1}$$

Practically, the load is not always variable; it is fixed in most of the case. Therefore, the simulation will be done in two ways: Two inputs model simulation and One input model simulation.

6.2.1 Two inputs model Simulations

The normalized output voltage and normalized output power are the capital. They make the independent variables to the polynomials in equation 4.13. Hence, they are the two inputs to the model in figure 6-1. They are fed to the polynomials' block. The last holds the equations 4.13; they are written in the form of control codes with the necessary protection and generate from them the necessary duty and frequency. The frequency is converted into equivalent period and it is feed to PWM generator for PWM signal generation. The duty is used to calculate the shifting time, this is fed to phase shift block and help to generate the phase-shifted PWM signals.

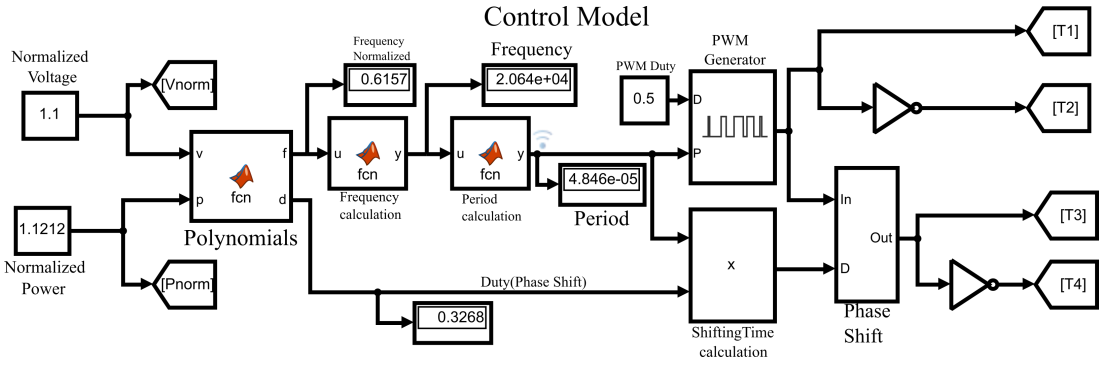

Figure 6-1: Illustration of Simulink model with normalized voltage and normalized power as inputs

$$\hat{\Omega} = \frac{\hat{v}^2}{\hat{p}} \tag{6.2}$$

The normalized load at each level of voltage and power is given by the equation 6.2. The simulation component values used in the simulation are from the prototype components values. They are indicated in the table 6.1.

Table 6.1: The parameters used to simulate the model in figure 6-1 with variable load

Item	**value**	**unit**
V_{in}	100	V
L_s	34.232	uH
C_p	658.7	nF
C_f	30	uF
Z_{Base}	7.209	Ω
f_{Base}	33.527	kHz

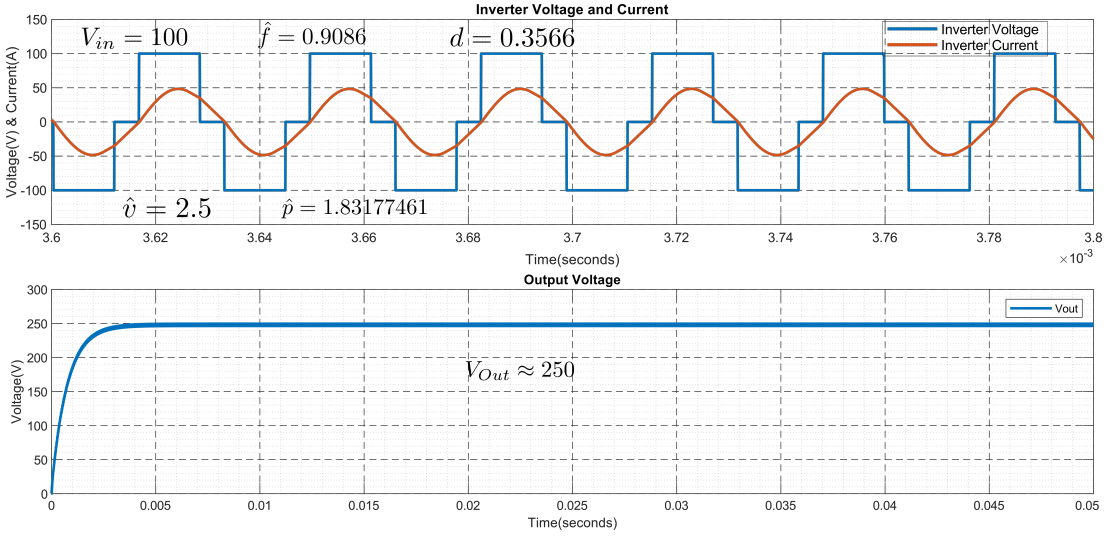

Figure 6-2: The voltage and current output of the converter with Normalized output voltage and normalized power as inputs

The equations 4.10 and 4.11 were simulated in Simulink. The parameters in table 6.1 were used.

Table 6.2: Simulation parameters and results of the PRC in two inputs case

Parameters		**Results**	
Item	Value	Item	Value
V_{in}	100V	$\hat{f}$	0.9086
V_{out}	250V	d	0.3566
$\hat{v}$	2.5	$\hat{\Omega}$	3.412
$\hat{p}$	1.831775		

If the parameters in the table 6.2 are considered, then the required frequency and duty are obtained by applying the equations 4.10 and 4.11 on the model in figure 7-1. The frequency $\hat{f} = 0.9086$ and the duty $d = 0.3566$ were obtained and applied in Simulink model. The load value is given by the equation 6.2 and the value $\hat{\Omega} = 3.412$. The results of the simulation are shown in the figure 6-2 and in the table 6.2. In this case, the optimum mode is fulfilled along the domain of the functions in equation 4.13.

6.2.2 One input model Simulations

In this case, the load is constant. Any change in the output power results in a different level of output voltage. The power is the only input to the control model, the corresponding voltage is illustrated with respect to the fixed load. Except having one input, the rest of the model component fit model description in subsection 6.2.1

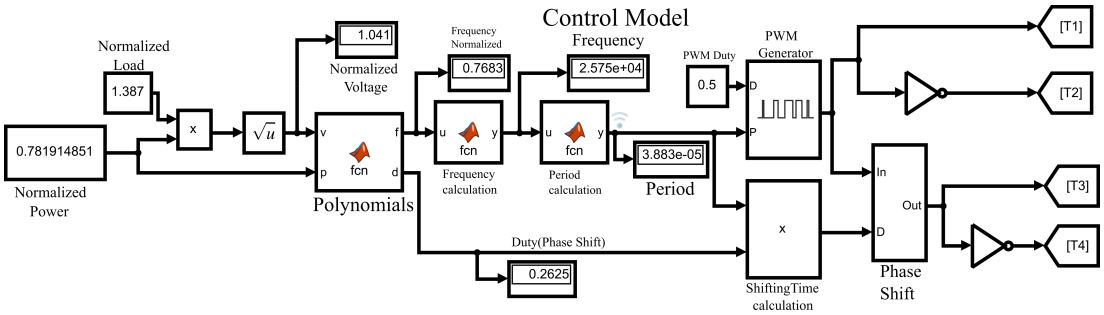

Figure 6-3: One input Simulink control model

Therefore, having the load as fixed parameter and the power as an input, the corresponding voltage is given by the equation 6.3.

$$\hat{\mathrm{v}} = \sqrt{\hat{\mathrm{p}} * \hat{\Omega}} \tag{6.3}$$

And the simulation parameters are given in the table 6.1.

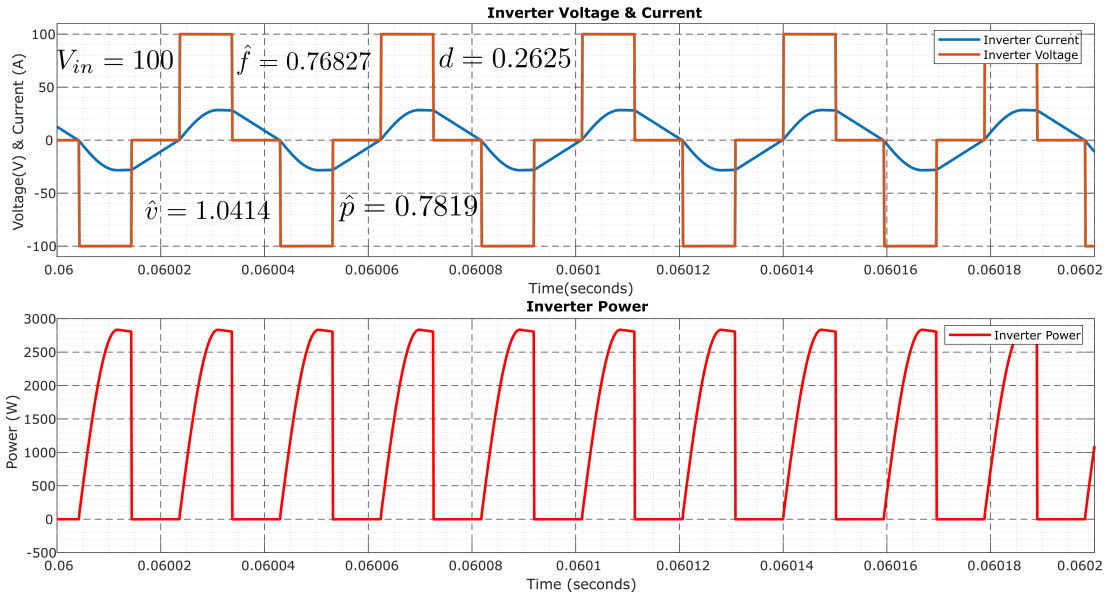

Figure 6-4: Inverter voltage, Current and power at fixed load

The power and the load are $\hat{\mathrm{p}} = 0.7819$ and $\hat{\Omega} = 1.387$ respectively; hence, the voltage is $\hat{\mathrm{v}} = 1.0414$. In this case the frequency and duty are $\hat{\mathrm{f}} = 0.76827$ and $\mathrm{d} = 0.2625$ respectively as shown in the table 6.3.

Table 6.3: Simulation parameters and results of the PRC in single input case

Parameters		**Results**	
Item	Value	Item	Value
$\mathrm{V_{in}}$	100V	$\hat{\mathrm{f}}$	0.76827
$\hat{\Omega}$	1.387	d	0.2625
$\hat{\mathrm{v}}$	1.0414	$\mathrm{V_{out}}$	104V
$\hat{\mathrm{p}}$	0.7819		

The Figure 6-4 displays the simulation results. In case of fixed load, the optimum mode is fulfilled at a fixed range of voltage. Hence, $\hat{\Omega} = 1.387$ runs from $\hat{v} = 1.00664$ to $\hat{v} = 1.441706$.

6.3 The Simulink model: DSC implementation

This section illustrates the implementation of the PRC control on the DSC using Simulink as an IDE. The PRC polynomial model built in Simulink is shown in this section. The same model holds the control of the PRC and will be used to generate the control program that fits the DSC of choice. Therefore, the configuration of the DSC to Simulink will be done in this section. The complete conversion of Simulink model into DSC C/C++ codes will be indicated and various inputs and outputs on DSC hardware will be shown.

6.3.1 DSC Configuration

Due to aforementioned operations, the indicated controls can not be easily implemented. The DCS is key, as it is has the computational capability; this work will take the advantage of Texas Instrument (TI) DSC. The last is a TMS320F28335 Peripheral Explorer Kit with high-performance static CMOS technology, high-performance 32-bit CPU, fast inturrupt response processing, on-chip memory and many more advantages[89]. The shifted Pulse Width Modulation (PWM) switching signals were generated on TMS320F28335 Peripheral Explorer Kit using Matlab-Simulink. In fact, the TMS320F28335 is a Texas Instrument Micro-controller, programmed through Code Composer Studio development environment (CCS). The CCS supports C or C++ language. Even if it is common to most of control engineers, the mentioned languages are time consuming and subjected to several errors; hence it is tiresome to code the signals accurately. However, those challenges are responded to by using model based programming through Matlab-Simulink. The complete control algorithm is done in Matlab-Simulink and later on, the PWM codes for the F28335 are generated. Some necessary steps are crucial to configure a Peripheral Kit to Matlab-

Simulink. Matlab-Simulink with some necessary adds-on like : "Embedded Coder", "Simulink Coder" and "Matlab Coder" together with CCS have to be installed on the PC. In this case, Matlab R2021a with the mentioned Adds-on, together with CCS 7.3.0 are installed on the PC. Hence, the target hardware (TI Delfino F2833x) is configured. The model is built in Simulink through which the PWM codes are generated and downloaded to TMS320F28335 Peripheral Explorer Kit. The last is visually illustrated on the figure 5-3, and the model for the code generation is shown on the figure 6-5. The last is based on single input configuration as shown in section 6.2.2 and on figure 6-3. In this case, the single input is the normalized power $\hat{p}$, which is the only external input. and the normalized load $\hat{\Omega}$, which is internal. The in order to test a sequence o scenarios, the Hex-Enc (hex-encoder), with its capability to input 16 values is used. The complete process of the Hex-Enc use in shown in the section 5.4.1.3. The look-up table from simulink help to hold the 16 power values. The last are fed to the PRC polynomial script block. The computed normalized output voltage is fed to the same block too. Therefore, the suitable normalized frequency $\hat{f}$ and duty d are obtained. From the normalized frequency, the switching period is obtained. The duty together with the switching period are fed to the PWM generator in order to generate the suitable switching signal. The complete block shown on the figure 6-5 is used as the model that generates the codes for F28335. The codes for back-up or any other analysis are retrieved in project form through CCS. The equations 4.13 is programmed in the F28335 using Matlab function block. They are quick and fast response polynomials. In the same coding is included the protection of the system, in case of mistake in entering values.

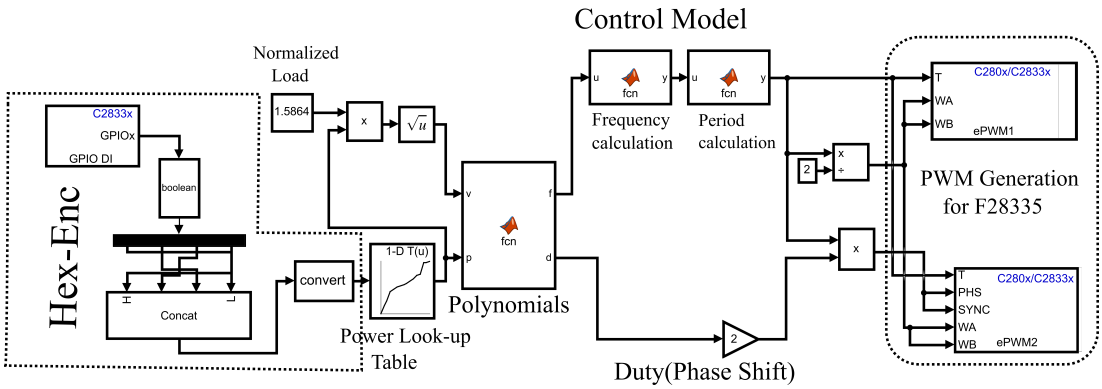

Figure 6-5: PWM Generation Model in Simulink

The Figure 6-5 mentions the model-based program to generate PWM for control purpose. The Hex-Encoder on the F28335 serves as input, as it accepts 16 inputs at different input steps. The Hex-Encoder is linked to four general purpose input-outputs (GPIO). The last are GPIO15, GPIO14 GPIO13 and GPIO12 in order of most to least significant bit respectively. They input 16 different values of power with the help of lookup table. Taking into consideration the fixed load, the equation6.3 gives the voltage. Both voltage and power are fed to polynomial block. The last hosts the equation 4.13 related codes. They generate in turn the corresponding frequency and duty. The frequency is converted to the corresponding period according to the equation 6.4. The period is fed to both ePWM1 and ePWM2 at input "T" for PWM signal generation for both converter legs. A half of the period is fed to both ePWM1 and ePWM2 on inputs "WA" and "WB" to maintain 50% duty cycle for each switching signal. The product of period and duty gives the adequate time-shift between the converter legs and it is fed to ePWM2 on input "PHS". The PWM switching signals at adequate frequency with the necessary duty shifting are generated. The ePMW1A and ePWM1B output the switching signal for the first leg while ePWM2A and ePWM2B give the shifted switching signal for the second leg.

$$T = \frac{f_{clk}}{2 * f_{sw}} \tag{6.4}$$

From the equation 6.4; T is the period, f_{clk} is the F28335 maximum clock frequency

and f_{sw} is the switching frequency.

6.4 The Resonant converter controls: FPGA implementation

Switching-frequency resolution and computational speed are limited in conventional digital controllers. In high frequency resonant converters, this produces in a huge output voltage ripple and poor dynamic performance with small control bandwidth[77]. For the switching -frequency resolution and dynamic performance improvement, the Field Programmable Gate Array (FPGA) is the best alternative for resonant converter controls. A variety of industrial fields today demand high power density and high power quality Power Converters in order to minimize size without sacrificing performance[39, 110, 52, 42]. The power density of the switch mode power supply can be improved by operations on high frequency. The Digital Signal Controller (DSC) has been playing a drastic role in converter controls, in various fields of applications. Since, the DSC is resistant to noise, it is able to implement complex algorithms and less affected by the environmental conditions. The high switching frequency improves the dynamic response in increasing the crossover frequency of the loop gain[77]. However, DSC is limited on switching frequency resolution and causes ripples in the output voltage and disturbances in current[81]. Additionally the DSC is limited on computational speed; it causes the delay in high frequency switching, which hinders the dynamic performance of the converter[74, 11, 7]. Various research activities were carried out to lift the DSC switching resolution limitations; however it was in vain for dynamic performance due to limited computational speed of the controller[77]. Different control methods were proposed to the dynamic performance and stability. The delay effect was taken into account while analyzing the dynamic response. As a result, the control algorithm was developed to boost dynamic performance. This approach, however, was unable to maintain the needed switching frequency resolution. It indicates that the two proposed solutions could not simul-

taneously overcome the switching frequency resolution limitation and the dynamic response. Compared to the conventional DSP, the FPGA controller is capable of improving both switching frequency resolution and dynamic performance. The FPGA controller uses its fast computation and intrinsic parallelism[77]. The FPGA is flexible in terms of bit width to optimize the digital computations. Hence, it is the major reason of using the FPGA controller to generate the switching PWM signals for PRC in this section.

6.4.1 Model-Based FPGA programming

The polynomial mode tackled in 4.3 is concluded in the equation 4.13. The same equation is scripted in Matlab, and used to generate the program suitable to a conroller in use. For this case the FPGA is used as a controller. The control program seems sophisticated so that it is time consumming and tiresome to complete the task. Programming complex embedded systems entails deducing complex system interactions via routes that connect input, outputs and control processors. It is a process that consumes time and error-prone. Hence, the resulting program lacks modularity and robustness. The *Model-based programming* overcomes these drawbacks by allowing engineers to program by defining high-level control techniques and putting together common-sense models of the system hardware and software. Model-based executives reason about the models "on the fly" to track system state, diagnose defects, and undertake re-configurations in order to implement a control plan[108]. Simulink is the integrated development environment (IDE) of choice for this work. The model-based program is built up of Simulink blocks that control the program's logic flow. The same blocks are compartible with both FPGA verilog and VHDL scripts. As a result, they may be easily converted to verilog or VHDL. The equation 4.13 is modeled in Simulink in this section, and the FPGA is configured on it. The model is then translated to VHDL and fed into the FPGA to generate the PRC power switch control signals.

6.4.2 FPGA configuration to Simulink

The "Arrow DECA Max 10" FPGA is used in this work. It is an Intel FPGA board, appears in the package that is supported by HDL coded add-on of Simulink.

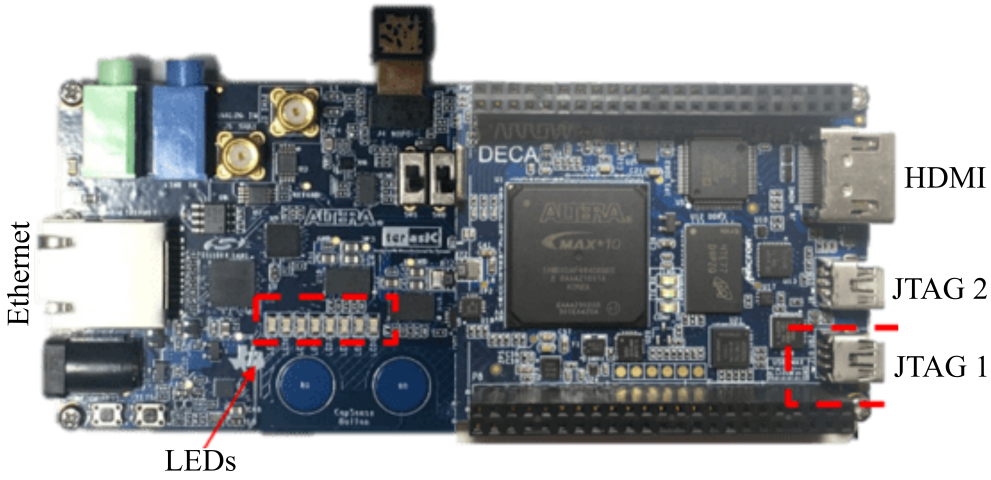

Figure 6-6: The Arrow DECA Max 10 FPGA

The figure 6-6 illustrates the Arrow DECA Max 10 FPGA Evaluation Kit. It is an Intel FPGA, with ALtera as an IDE. It is an "IP Core Generation Hardware", with "Altera Quartus II"(Altera Quartus II refers to the synthesis tool Intel Quartus Prime). Matlab-Simulink with "HDL coder" must be installed since the model-based programming language of Simulink will be utilized to code the FPGA. The "Altera Quartus II" must also be installed on the computer. The following are the key prerequisites for configuring the "Arrow DECA MAX 10 FPGA" Evaluation Kit on Matlab-Simulink[68]:

1. Intel Quartus Prime
2. Arrow DECA MAX 10 FPGA evaluation kit
3. HDL Coder Support Package for Intel FPGA Boards
4. HDL Verifier Support Package for Intel FPGA Boards (Optional)
5. HDL Coder Support Package for Intel SoC Devices (Optional: To integrate the IP core into your own custom reference design.)

Hence, Simulink is ready to generate code for FPGA. In the same breath, the Simulink model is built and verified for compatibility through "HDL Verifier". Once the hardware controller is connected, the "IP Core Workflow" is run and go through the verifications process illustrated in the figure 6-7 (a), (b) and (c). If all of the process have passed, the program is created and loaded to the FPGA. The same program can be retrieved from the link shown on figure 6-7 (c).

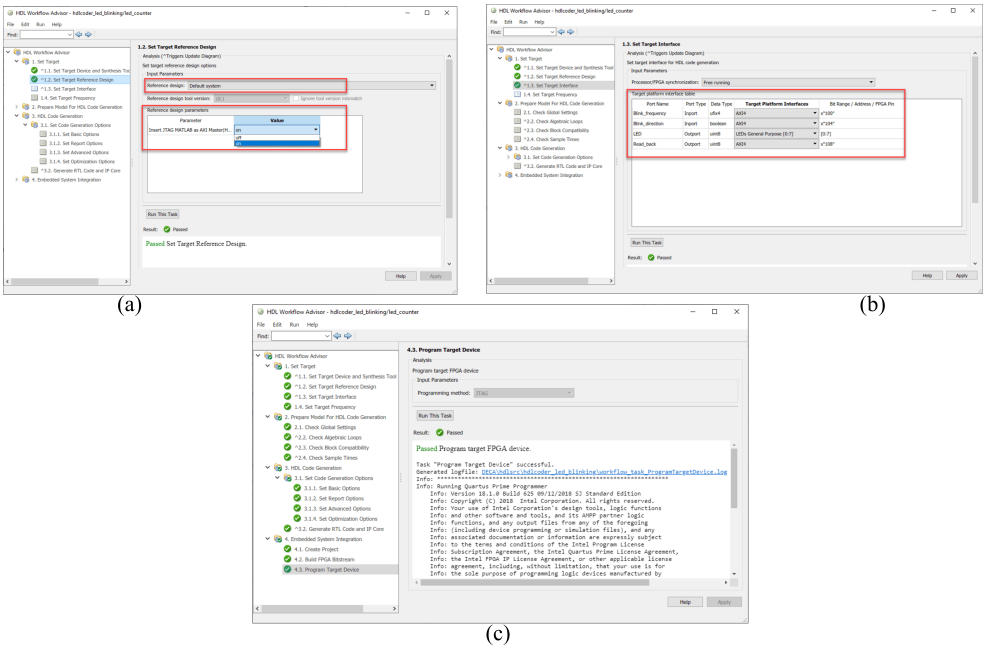

Figure 6-7: Illustration of the steps to generated the FPGA program from the Simulink Model[68]

6.4.3 Implementation in FPGA of the direct calculation of the Frequency and Duty-Cycle

Based on the polynomials obtained from the PRC (and SRC) equations, a VHDL program has been developed for an FPGA that calculates these parameters, in floating point and without the use of a processor. It is necessary to remember that it is possible to implement a micro-controller in an FPGA (NIOS II in the case of ALTERA/INTEL) with which the calculations of the polynomials would be immediate, since the said calculation are implemented in C language and executed by a CPU. It

is the same as if those calculations are implemented directly from Matlab. i.e. they are implemented in microprocessor, which does not differ so much from the previous method. Even if it is possible, but in order to take an advantage of FPGAs, is much better implement the algorithm directly in hardware. In the case at hand, it is decided to calculate these parameters by lowering the level and considering the operations in floating point and adjusting so that it does not overflow. Let's see the procedure for obtaining the frequency (duty is exactly the same), but before that, it is better to first understand how the numbers are stored. Fixed-comma:

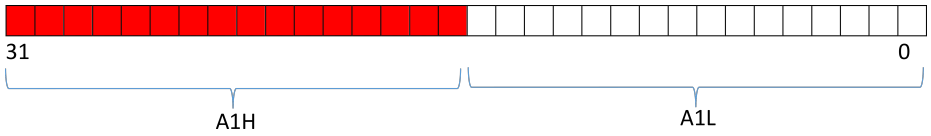

Figure 6-8: Illustration of how numbers are stored in memory.

The complete memory on the figure 6-8 is 32 bits, 16 bits for the integer part, 16 for the decimal. For instance:

```
1 6,44= 000670A3_{H}
2 -6,44 => FFFF FFFF_{H} - 000670A3_{H}=FFF9 8F5C_{H}
```

A1 complement for negative numbers

```
1 000670A3_{H}= 6*16^0 +7*16^-1+0*16^-2+3*16^-3 = 6.438_{d}
```

$FFF98F5C_H$ it is negative so $FFFFFFFF_H - FFF98F5C_H = 000670A3_H$ this last is the module. Therefore, the procedure for obtaining the frequency on constant duty is as follows:

- Selection of the A_{ij} coefficients.

  These coefficients depend on the voltage and power to be handled by the converter. Each coefficient Aij will be stored in a memory, in 32-bit fixed point format, with four hexadecimal digits for the integer part and four for the decimal part.

```
Function[f,d]=fcn(v,p)
if(v≥1)&&(v≤1.2)\&\&(0.560354057≤p&&p ≤1.948584073)
a1=6.44*v+6.4193
```

These coefficients Aij are the coefficients that allow obtaining the A_i

- Calculation of A_i:

  In this part, the calculations are made in floating point and a proprietary algorithm is developed, which anticipates overflows, and adjusts the value obtained to the range we have. For example, let's see how the product -6.44 * V is obtained. The digits are separated into their integer part and decimal part, A1H and A1L for the coef. A11, (which in this case is -6.44 and VH and VL for the voltage V:

```
A1H:= (A11/65536);
A1L:= (A11-A1H*65536);
VH:=(volt/65536);
VL:=(volt-VH*65536);
```

Once the values have been obtained, the operation is performed by adjusting the weight of each operand, conveniently shifting to be able to perform the addition and pre-adjusting the values of VL and A1L so that the result of the multiplication does not overflow:

```
h1:=((A1H*65536)*VH+(A1L*VH)+(A1H*VL)+(((A1L/2)*(VL/2))/16384))+A12
```

To the previous result, the term A12 is added, (in our case, it would be 6.4193) and we obtain the result of the coefficient A1. The following operations are implemented in a block whose output is, as has been said, the coefficients Ai. The error obtained is always less than 0.4. The graph on the figure 6-9 shows the simulation for voltage values of 1.15, 1.11, 1.18. The coefficients Ai are represented by hi.

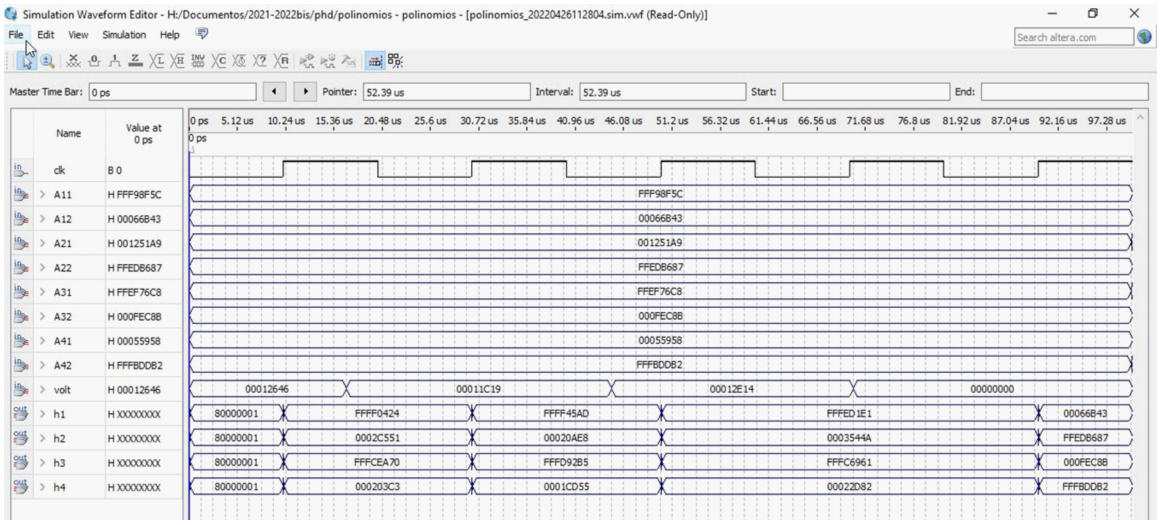

Figure 6-9: The illustration of results for $\hat{v}$=1.15, 1.11 and 1.18

The next step is to obtain the squared and cubed values for the power; Analogously to the previous case, the square and cube blocks are implemented:

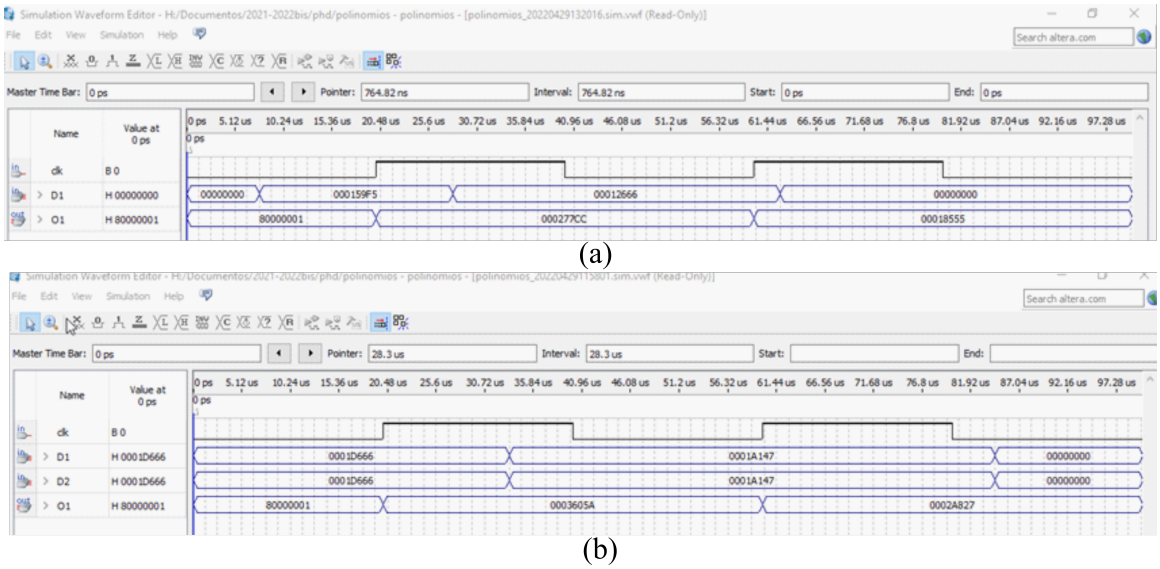

Figure 6-10: Illustration of results: (a) cubic block and (b) Square block

The next step is to obtain the different terms of the final polynomial of the frequency:

```
1       f =a1*(p*p*p)+a2*(p*p)+a3*p+a4;
```

To do this, once the cube, the square and the Ai coefficients have been obtained, it is

necessary to multiply two terms (A1 ∗ P3, for example), and finally, the sum of all of them. These processes must be carried out in sequence, that is, the final sum cannot be carried out without having previously obtained the different coefficients. To do this, it is necessary to implement a clock signal generator, which allows the different blocks to be activated synchronously from a single pattern:

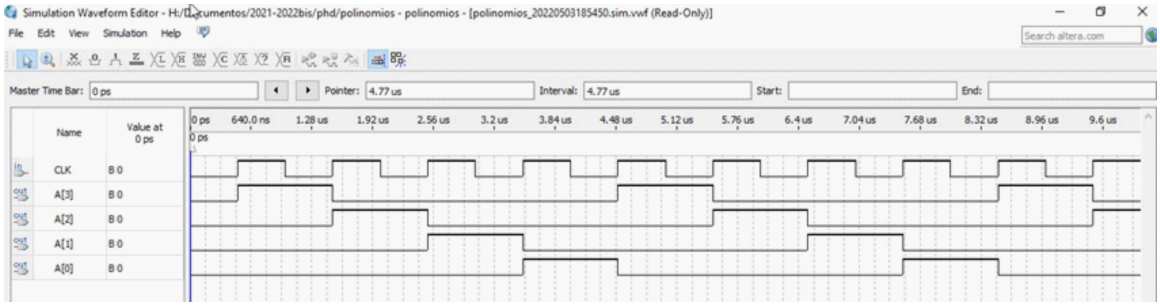

Figure 6-11: Illustration of precise clock signals generation

Generation of the precise clock signals. Note: It is possible to reduce the number of steps, since square and cube can be simultaneously with the Ai. The following figure shows the general scheme:

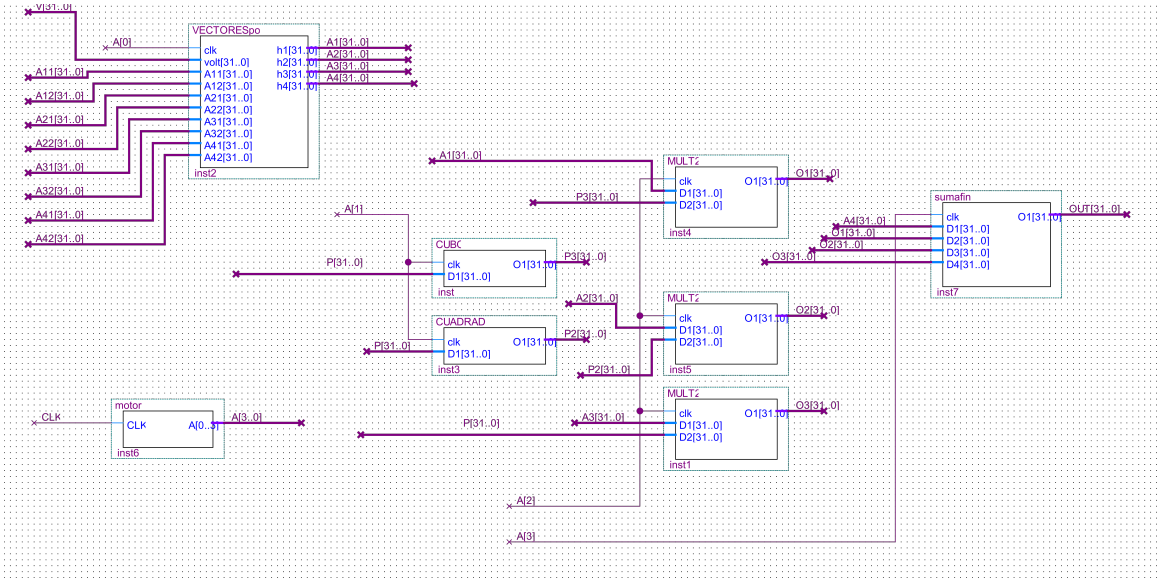

Figure 6-12: Illustration of FPGA complete model in Altera. The codes for various blocks shown in this figure are detailed in Appendix D

Calculation in this way has many advantages: Only three clock cycles are necessary,

which if we start from a 50 MHz clock allows us to work at very high frequencies, more than necessary. If this calculation is implemented with a micro-controller, we would not be able to reach very high frequencies. On the other hand, the area of the FPGA is reduced and it is possible to use said FPGA for other tasks, such as including a micro-controller for user interface, etc.

6.5 The Fuzzy closed loop control of PRC

Since there are many different types of resonant converters, each with its own set of benefits such as high frequency range power switches and low switching losses[111], the PRC-LCC resonant converter, which combines the benefits of both series and parallel resonant converters, is gaining a lot of attention in DC–DC converter applications[25, 65, 60]. In order to maximize the operating windows, the modeling of the resonant converter is done through normalized value[25, 67]. The PRC-LC configuration maximizes the efficiency through varying the switching frequency and the duty cycle[25, 65, 78, 67]. In this case the Power transfer is controlled by two dependent parameter i.e. frequency and duty cycle. Steady state and dynamic model were discussed in various research works[111, 88, 102]. Most of the resonant converter controls are open loop, only few research works show the closed loop cases[60]. And those works which are closed-loop, mostly consider one parameter; either frequency or Duty to predict the output voltage and power. For instance, the closed-loop power control of the resonant converter power transfer is detailed in [16], taking care of frequency only. In this case the frequency is a function of power and current. This work tackles the closed-loop control on the PRC polynomial model. As the Polynomial model described in this work considers two control parameters i.e. frequency and duty cycle, the Fuzzy closed-loop control is the best option. Therefore, this section details the Fuzzy closed-loop control of the PRC polynomial model. Reminding that the polynomial model indicated in this work considers only the optimum mode as shown in 3.3.3.3. The Fuzzy closed-loop control model of the PRC is built in Simulink and it is limited to simulations with the aim to show that this option is possible and feasible

for implementation.

6.5.1 Fuzzy Control overview

In contrast to classical or digital logic, which operates on discrete values of 1 or 0, a fuzzy control system analyzes analog input data in terms of logical variables that take on continuous values between 0 and 1. (false or true, respectively)[57, 98]. Fuzzy logic is widely used in machine control. The word "fuzzy" alludes to the fact that the logic involved may deal with ideas that are "partially true" rather than "true" or "false." Fuzzy controllers are conceptually quite simple. They are made up of three stages: input, processing, and output. Sensor or other inputs, such as switches, thumb-wheels, and so on, are mapped to the proper membership functions and truth values at the input stage. In a fuzzy control system, the input variables are often mapped by sets of membership functions that are similar to this, referred to as "fuzzy sets." Fuzzification is the process of transforming a crisp input value to a fuzzy one. Two fuzzy systems, one for incorrect heading angle and the other for velocity control, were designed using the fuzzy logic technique. The processing step calls each relevant rule and generates a result for each, before combining the results. Finally, at the output step, the combined result is converted back into a specified control output value.

6.5.1.1 Membership function

The indicator function for classical sets is an extension of the membership function for fuzzy sets. It reflects the degree of truth as an extension of valuation in fuzzy logic. Although they are conceptually similar, degrees of truth and probabilities are sometimes misconstrued because fuzzy truth refers to membership in ill-defined sets rather than the possibility of a certain occurrence or situation[116, 35]. There are various types of membership functions namely: Singleton, triangular, trapezoidal, gaussian and generalized bell shaped membership function[19].

6.5.2 Fuzzy closed-loop control of PRC polynomial model

As indicated in section 3.3 PRC is complex systems as far as control is concerned. To design the suitable control is a sophisticated process. Hence, fuzzy control methods and algorithms are the saving-grace alternative[53]. Fuzzy controls are particularly designed for non-linear dynamic systems with many inputs and outputs .i.e. significant level of complexity. The exact mathematical model in this case is almost impossible. The number and form of fuzzy sets used for dividing the computational domain of input and output signals, the operators for realizing fuzzy operations such as sum, product, and negation, the conclusion algorithm, and the function for computing numerical values of output signals are all characteristics of fuzzy controllers[80]. The polynomial model indicated in 4 and illustrated in equations 4.13 has two inputs ($\hat{v}$ and $\hat{p}$) and two outputs ($\hat{f}$ and d). The two outputs are polynomically expressed. Hence, the fuzzy controller is suitable for this scenario as it accepts both more inputs and outputs. For simplification purposes, the model will be simulated in Simulink.

6.5.2.1 Structure of the Fuzzy Logic Controller (FLC)

The fuzzy logic controller (FLC) consists of two inputs and two outputs. The inputs are input voltage error $e(n)$ and the rate of change of error $\Delta e(n)$ at n^{th} instant as illustrated in equations 6.5 and 6.6. The outputs are $\hat{f}$ and d, which are normalized switching frequency and duty respectively.

$$e(n) = \hat{v}_{ref} - \hat{v} \tag{6.5}$$

$$\Delta e(n) = e(n) - e(n-1) \tag{6.6}$$

With, $\hat{v}$, $\hat{v}_{ref}$ and $e(n-1)$ are normalized output voltage, reference normalized output voltage and voltage error at $(n-1)^{th}$ instant respectively.

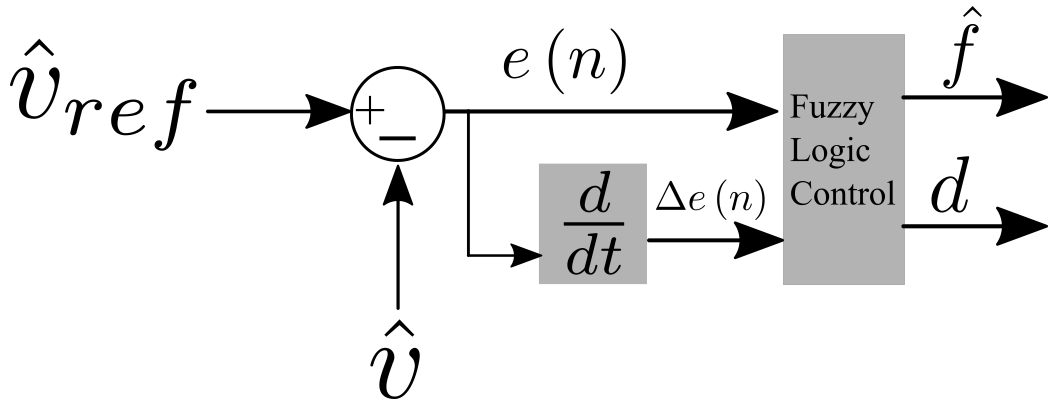

Figure 6-13: The illustration of fuzzy controller structure

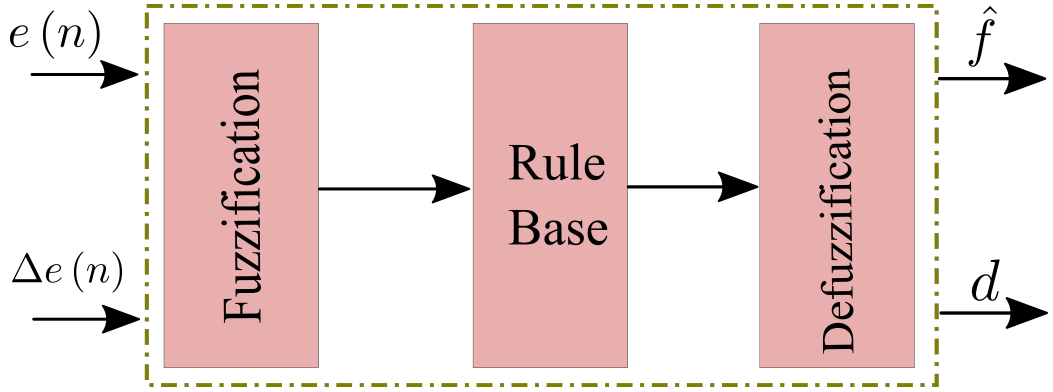

Figure 6-14: The illustration of fuzzification and defuzzification process

6.5.2.2 Control Setting

It is a closed loop control that regulate the output voltage at a given level of command i.e. the output voltage is automatically regulated to a desired level regardless of the changes in the input voltage. As the load in mostly constant in several cases, then fixing the value of the voltage at a certain number induces the power transfer to be constant. Therefore the switching frequency and the duty cycle are constant too. The change in power transfer will occur only when there is a change in output voltage command. On the other hand, at a given level of the load, there is a maximum power transfer limit, this imposes the limit on the change in the output voltage. The fuzzy control in this case follows the change in error between the command and the actual output voltage level, as well as the rate at which the error changes to produce the

adequate switching frequency and duty cycle. Therefore, the fuzzy controller has two input(the error and the rate of change of error) and two outputs (switching frequency and duty cycle). The ranges for both input and output values of the fuzzy controller are presented in the table 6.4.

Table 6.4: Illustration of ranges for the error and delta error, normalized frequency $\hat{f}$, the normalized output voltage $\hat{v}$, the normalized output power $\hat{p}$ and duty cycle.

Item	ranges
e (n)	-0.50 to 0.50
Δe (n)	-0.50 to 0.50
$\hat{f}$	0.30 to 0.97
d	0.22 to 0.45
$\hat{v}$	1.00 to 4.00
$\hat{p}$	0.50 to 3.50

The membership function is triangular with the ranges as presented in the table 6.5:

The acronyms used in the membership function are:

Table 6.5: This table shows the range of various membership functions respective to the variable i.e. input or output

e (n	Range
NB	-0.5 to -0.1
NS	-0.2 to 0.0
ZE	-0.1 to 0.1
PS	0.0 to 0.3
PB	0.2 to 0.5

Δe (n)	Range
NB	-0.5 to -0.1
NS	-0.2 to 0.0
ZE	-0.1 to 0.1
PS	0.0 to 0.3
PB	0.2 to 0.5

$\hat{f}$	Range
PS	0.3 to 0.5
PM	0.45 to 0.75
PB	0.73 to 1.0

d	Range
DS	0.22 to 0.28
DM	0.27 to 0.37
DB	0.35 to 0.47

1. For Error and Rate of change of error: **NB**: Negative Big, **NS**: Negative Small,

ZE: Zero Error, **PS**: Positive Small, **PB**: Positive Big.

2. For Normalized frequency, it represents how big is the power transfer. Therefore **PS**: Power Small, **PM**: Power Medium, **PB**: Power Big.

3. For the duty, **DS**: Duty Small, **DM**: Duty Medium, **DB**: Duty Big

Table 6.6: The illustation of Fuzzy rule base defining the relation between the input and the output

	Rate of change of Error($\Delta e\,(n)$)									
	NB		NS		ZE		PS		PB	
Error $(e\,(n))$	$\hat{f}$	d	$\hat{f}$	d	$\hat{f}$	d	$\hat{f}$	d	$\hat{f}$	d
NB	PB	DS	PB	DS	PB	DS	PB	DS	PB	DS
NS	PB	DM	PB	DM	PS	DM	PB	DM	PB	DM
ZE	PB	DB	-	-	PB	DB	PB	DB	PB	DB
PS	PM	DM	PM	DM	PM	DM	PM	DM	PM	DM
PB	PS	DB	PS	DB	PS	DB	PS	DB	PS	DB

The change in error and the rate at which the error changes, determine the frequency and duty cycle required to track the command i.e. the required output voltage, and determine the power transfer range at a given value of the of the load.

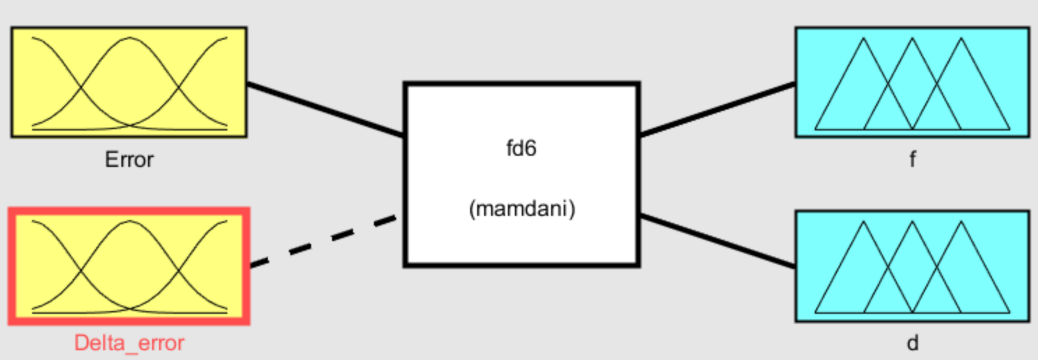

Figure 6-15: The illustration of fuzzy control design

The targeted output power and voltage are also shown in the table 6.4.

6.5.2.3 Simulink model of Fuzzy controller

The control model is built in Simulink, where the fuzzy control is based on Mamdani Fuzzy Inference Systems[62] as illustrated in the figure 6-15. The control mode is illustrated in figure 6-16.

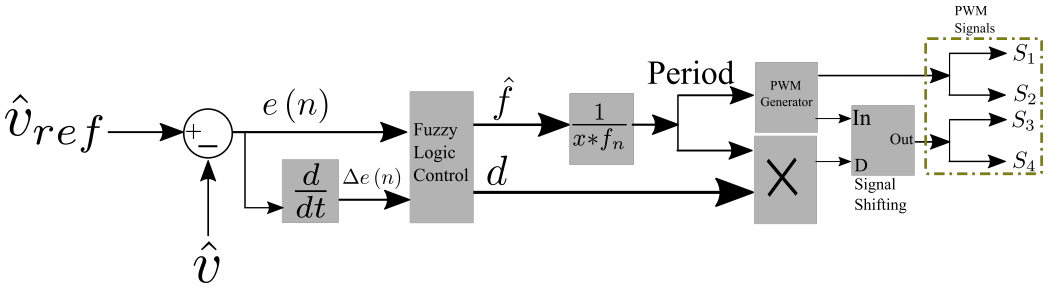

Figure 6-16: The illustration of fuzzy controller structure

It is made of the refernce voltage with the necessary steps and the feedback. Both generate the error, and the rate of change of error that are fed to the fuzzy controller. The last gives the normalized frequency and the duty. The normalized frequency is turned into normal frequency and later on into period through Matlab function blocks. The period is fed to the PWM generator and give the PWM signals, while the duty cycle value is used to obtain the right signal shifting. The simulation was run in Simulink, on the model shown on the figure 3-4 with the parameters indicated in the table 5.1.

6.5.2.4 Simulation results

The PRC is simulated in Simulink following the data illustrated in the table 6.4. It is a closed-loop model based on fuzzy logic. The normalized parameters are used in order to have the larger operating span.

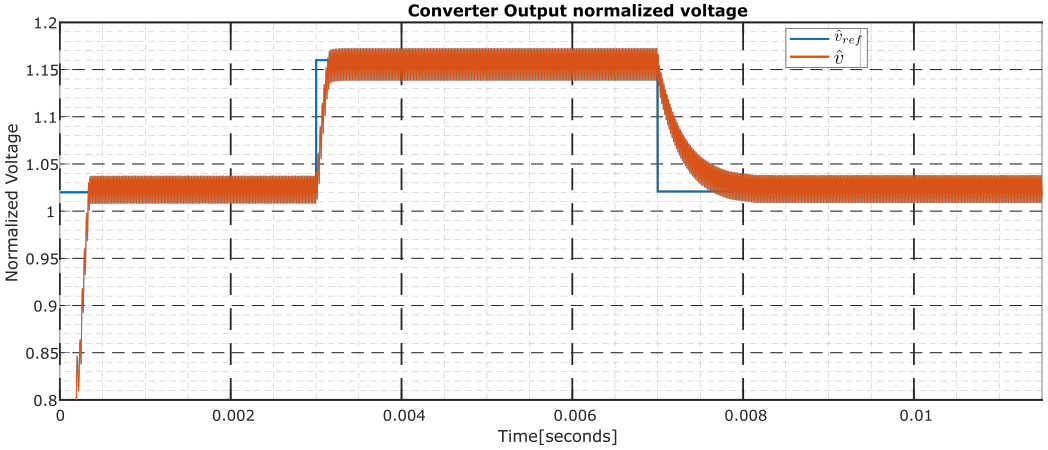

Figure 6-17: The illustration of fuzzy controller performance

The figure 6-17 shown the performance of the fuzzy controller. The output normalized voltage track the command as required. The results illustrated in the figure 6-17

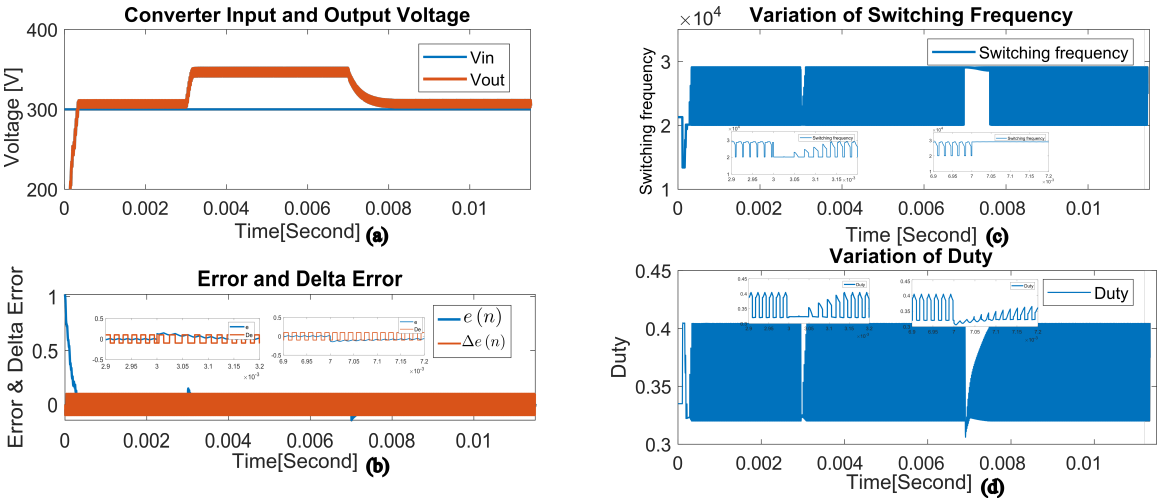

Figure 6-18: The illustration of fuzzy controller performance

spring from the process indicated in the table 6.6 and the results shown in the figures 6-18. The input voltage is kept constant, and the output voltage of the converter is controller, therefore the figure 6-18 (a) shows the variations in the output voltage, while the input is constant. The control depends strongly on the error and the rate at which it changes in time, the figure 6-18 (b) illustrates it. During the control process, the controller takes time to track the reference. In that process the switching frequency and duty vary continuously as indicated in the figure 6-18 (c) and (d).

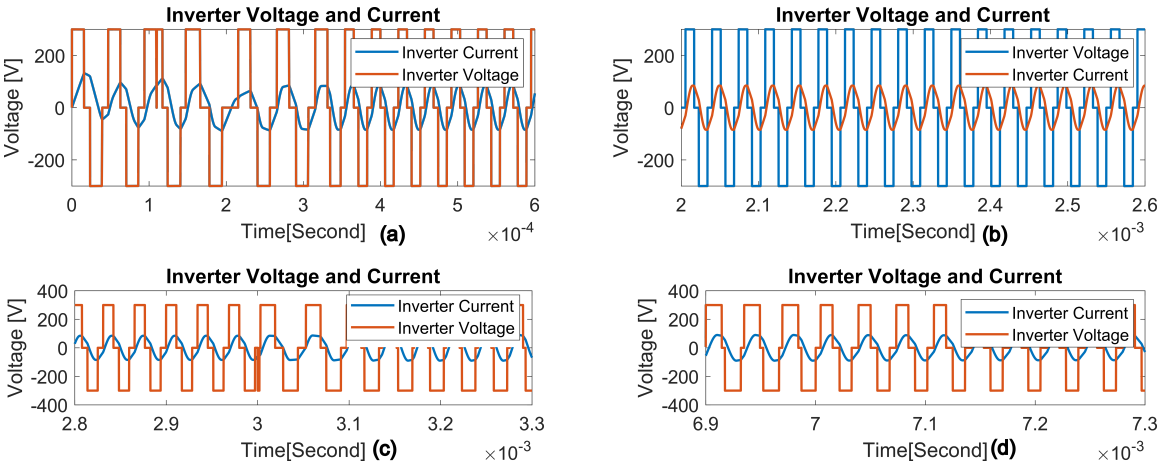

Figure 6-19: The illustration of inverter current and voltage

The variation of the switching frequency and duty have strong impact on the inverter

voltage and current and determine the level of energy transfer. Both figures 6-19 and 6-20 illustrate it.

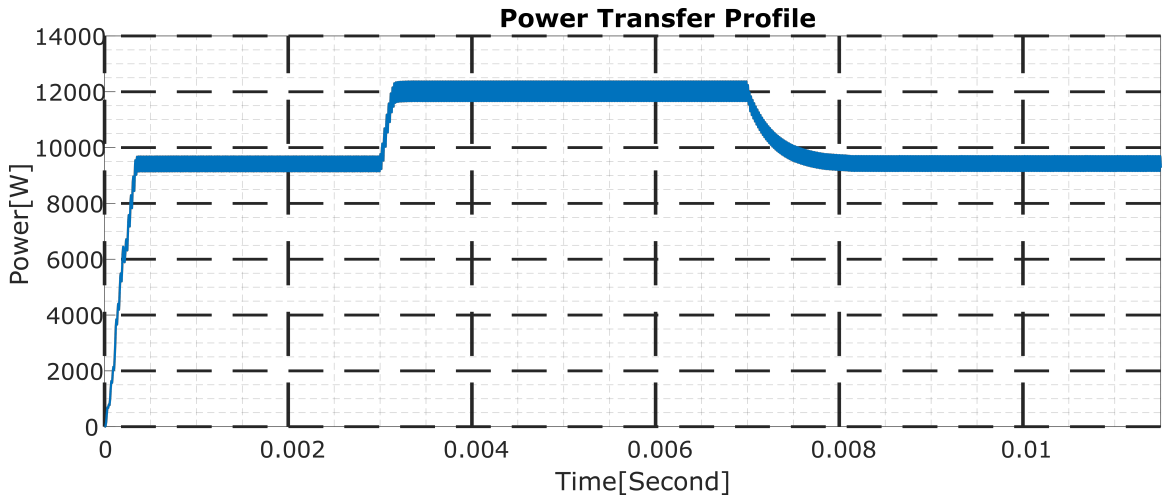

Figure 6-20: The illustration of power transfer profile

6.6 Conclusions

In this chapter the PRC was modeled and their topologies were built and simulated in Simulink for the validation. Using model based programming language, the F28335 TI micro-controller and Arrow Deca Max 10 FPGA were programmed for the generation of PWM switching signals. The closed loop control of PRC is proposed using Fuzzy controllers. The control model was built and validated in Simulink. At each section of this chapter, results were obtained as expected.

Chapter 7

The Experimental Prototyping and Results

Contents

7.1 Introduction 150

7.2 The Experimental Consideration 150

7.3 The Digital Control and Discretization 151

7.4 The Experimental Set-up 151

7.4.1 Gate Drivers Board 152

7.4.2 Power stage 152

7.5 The Outline of the experimental Results 154

7.5.1 Series Resonant Converter 154

7.5.2 Parallel Resonant Converter 158

7.6 Conclusions 167

7.1 Introduction

This chapter intends to experimentally confirm the theoretical results, preliminary supported by of the simulations presented, specified, examined, and confirmed in earlier chapters. It is all about building the laboratory prototypes' power experimental set-up parameters. The Model based DSC program in Simulink is highlighted. All the items needed (DSC, FPGA, PCB board) have been defined, designed and built for the experimental results obtention. It describes the complete components of the prototype. Finally, this chapter will describe the results of experiments conducted under the same settings as the prior simulations, allowing for easy comparison of the findings and validation of the suggested models reported in previous chapters.

7.2 The Experimental Consideration

The essential parameters of the laboratory set-up necessary to offer a platform for experimental verification of proposals are described in this section. It also takes into account considerations from a safety standpoint. Various component arrangements make suitable prototypes described in this work. Here to cite few:

- The figure 7-1 shows the schematic of the prototype components arrangement. With this schematic, the configuration of the power topology can be easily modified in order to act as many topologies described in this work.

- The control topology is made of resonant converter polynomial model, developed in Matlab, built and simulated in Simulink. It generates the control program that fits the programmable circuit (DSC or FPGA).

- The power topology in terms of a prototype is built in the laboratory, tested and the results are presented in this work.

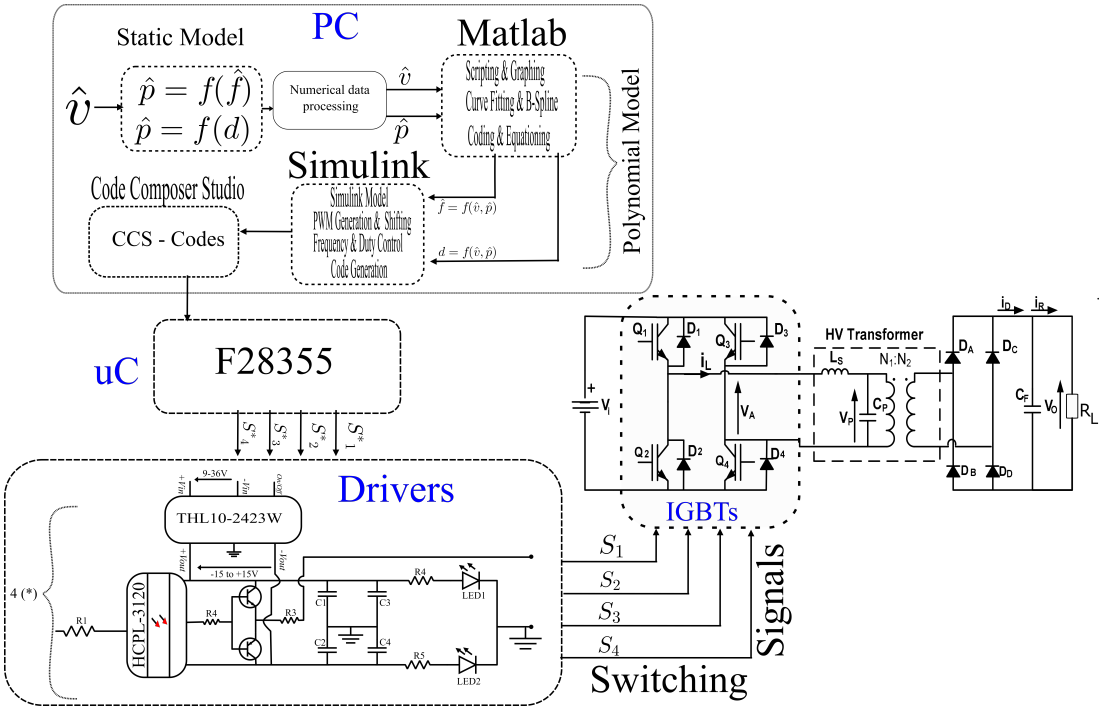

Figure 7-1: Illustration of the complete model of the practical implementation.

7.3 The Digital Control and Discretization

The control schemes are implemented in a DSC, "TMS320F28335" in particular and FPGA, "Arrow Deca Max 10" in particular. The programming of the programmable circuits is done in Simulink, using Model-Based option. The control is open-loop, there is no feedback to close the loop expected. Therefore, regulation, signal routing filtering and discretization are not applicable. The control program is generated and loaded to the programmable circuit through Simulink. The programmable circuit is hardwired linked to driver.

7.4 The Experimental Set-up

This section describes the experimental power setup as well as the PCBs that were built and used to achieve the desired results.

7.4.1 Gate Drivers Board

The gate driver is an interfacing board between the controller and the power stage. The PWM signals are sent from the DSC/FPGA dedicated module to the gate driver board. This connection is made through short hard-wires in order to minimize noise in the connections. The PWM signals of the DSC/FPGA are from 0 V to 3.3 V. Then, the driver board receives the PWM signals, after the opto-coupling stage, ranging from 0 V to 5 V. Therefore, the driver board adapts these signals and isolates the gating references between the upper IGBT and lower one. The opto-coupler used is HCPL-3120 from AVAGO Technologies with the power supply voltage ranging from 15 V to 30 V and the input current $I_{F(ON)} = 7mA$. The power is supplied by THL10-2423W general purpose converter from TRACO POWER. The input Voltage ranges in 9 V and 36 V while the output voltage ranges in -15 V and 15 V with the total power rating of 10 W. The embedded IGBTs switches F4-150R12KS4 are turned on and off with gate-to-source voltage (V_{GE}) value of 15 V and -15 V, respectively.

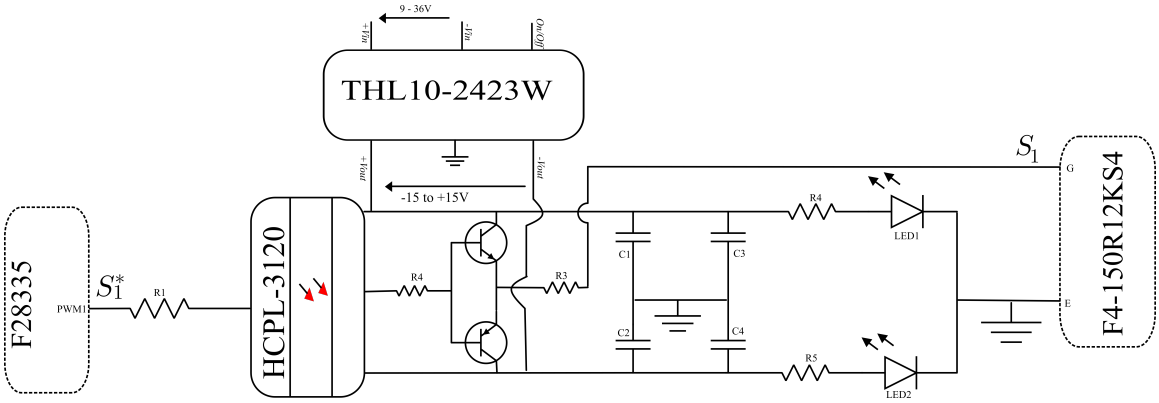

Figure 7-2: Driver Board Schematic

7.4.2 Power stage

The power stage starts with the DC voltage link; this is to generate the input DC voltage V_{in}. It supplies the DC voltage to the controlled front-end inverter. The last is an embedded system made of four IGBTs. It is an F4-150R12KS4 compact from Infineon. The F4-150R12KS4 embedded IGBTs is illustrated on the figure 7-4, while

its structure is shown on the figure 7-3.

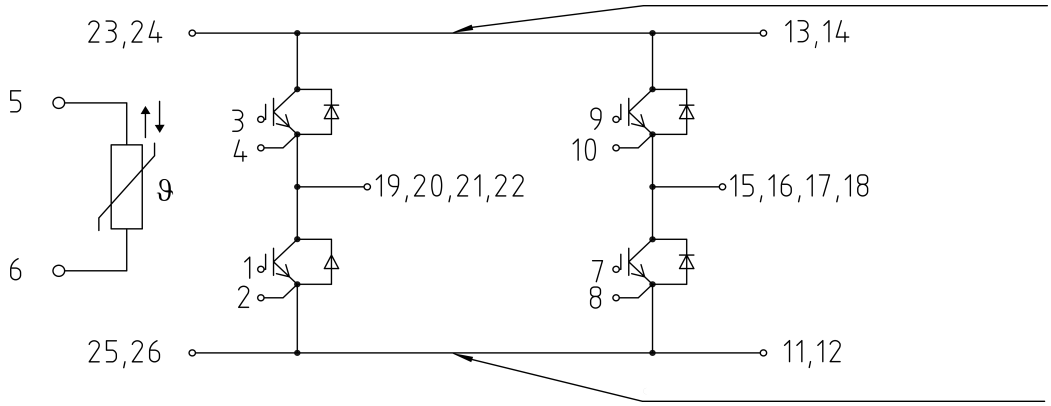

Figure 7-3: The F4-150R12KS4 IGBTs embedded structure

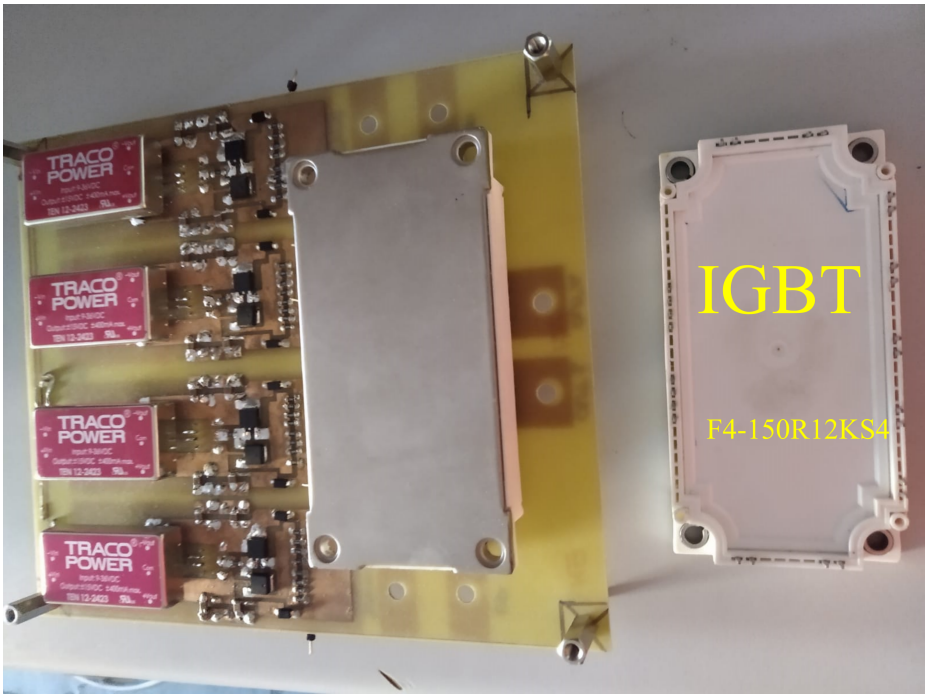

Figure 7-4: Illustration of embedded F4-150R12KS4 IGBTs

The resonant tank is connected next to the converter, with either series or parallel configuration depending on each of the topologies. The series inductance is L_s = 34.232 μH and the parallel capacitor is C_p = 658.7 nF. The uncontrolled rectifier links the resonant tank to the filter capacitor and the load of 30 μF, and 10 Ω respectively. The complete prototype is shown later in section 7.5.2.1 on the figure 7-9.

7.5 The Outline of the experimental Results

This section outlines various experiments done and the results achieved. It details all of the experiments conducted, the processes used, the target and the obtained results.

7.5.1 Series Resonant Converter

The Series Resonant Converter control model and topology is experimentally illustrated in this part. The practical vlidation of SRC is indicated in two ways i.e. the DSC configuration and PWM tests, and Experimental Prototyping, with results illustrations.

7.5.1.1 DSC Configuration and PWM tests

The prototype to validate control part of the simulated results of the SRC was built following the topology in the figure 3-1. The model in figure 7-1 is modified in such a way to meet the SRC topology. Based on the tables 4.1 and 4.1 , the polynomial equations 4.7 and 4.9 are respectively obtained, and used in the model program shown in figure 5-4. Therefore the level of normalized output power $\hat{p}$ results in the targeted initial resonant current and frequency as show in the table 7.1.

The equation 4.9 shows the frequeny as dependent variable, which varies with respect to the changes in initial converter current and output voltage. While the initial resonant current, shown in the equation 4.7 becomes dependent variable with respect to the changes in output voltage and power. Hence, the output power and output voltage are the independent variables of the model. The power transfer strongly depends on the switching frequency and initial resonant current. Therefore, at each level of targeted output power corresponds the switching frequency and initial resonant current. That is what detailed in the table 7.1. Practically, the normalized power of $\hat{p} = 0.10$ that corresponds to normalized voltage $\hat{v} = 0.2971$ and normalized initial converter current $\hat{I}_0 = -0.7317$, the resulted switching frequency f = 86.87kHz. It is illustrated in the figure 7-5, as the PWM signal reflect the mentioned switching

Table 7.1: Illustration of the experimental validation of the SRC polynomial model as indicated in figure 5-4

$\hat{p}$	$\hat{v}$	$\hat{I}_o$	$\hat{T}$	$\hat{f}$	f[kHz]	
					Simulated	Experimental
0.01	0.09394	-0.2214	0.1429	6.998	234.5	234.3
0.015	0.115	-0.2755	0.1739	5.749	192.7	192.76
0.02	0.1328	-0.3163	0.1971	5.074	170.1	170.07
0.025	0.1485	-0.3606	0.2216	4.513	151.3	151.15
0.03	0.1627	-0.3894	0.2376	4.208	141	140.92
.	.	.	.	.	.	.
.	.	.	.	.	.	.
.	.	.	.	.	.	.
0.06	0.2301	-0.565	0.3224	3.102	104	103.99
0.065	0.2395	-0.5882	0.332	3.012	101	100.93
0.07	0.2485	-0.6085	0.3384	2.955	99.05	99.05
0.075	0.2573	-0.6261	0.3483	2.871	96.23	96.23
0.08	0.2657	-0.6393	0.3509	2.85	95.53	95.53
0.085	0.2739	-0.6645	0.3601	2.777	93.09	93.04
0.1	0.2971	-0.7317	0.3858	2.592	86	86.87

frequency.

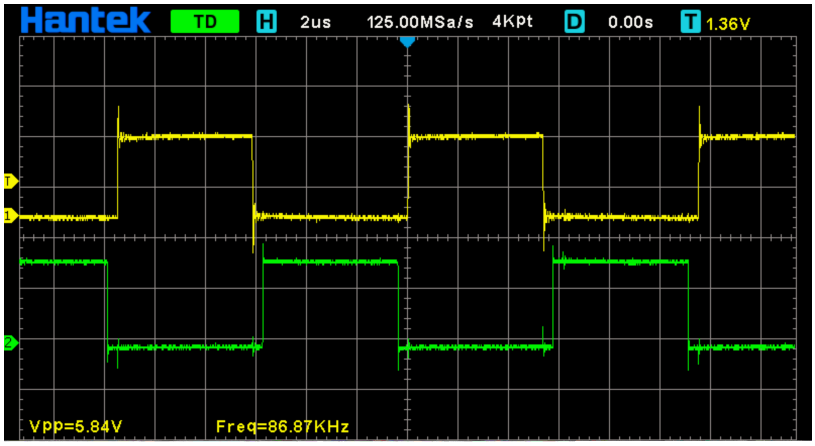

Figure 7-5: Illustration of the PWM generated at the normalized power $\hat{p} = 0.10$ and generate a frequency f = 86.87kHz.

Several tests were conducted as illustrated in the table 7.1 and more results were captured. Only the results on the figure 7-5 were indicated for the presentation purposes. The table 7.1 illustrates the practical results of the initial current and switching frequency polynomials. The initial resonant current is an input to the

Table 7.2: Illustration of polynomial model expermental testing and comparative study to various other models of SRC.

Parameter	L_s = 173uH, C = 447nF, R = 44Ω, V_{in} = 125V			
Test Type	SRC model	Simulated	Polynom	Experimental
Operation point 1				
f_{sw} [kHz]	73	74	71.4	74
V_{out} [V]	50	50	47.2	50
t_1 [µs]	2.38	2.4	2.263	2.3
I_1 [A]	2.38	2.4	2.276	2.3
Operation point 2				
f_{sw} [kHz]	39.86	40.6	39.9	40.6
V_{out} [V]	50	50	49.6	80
t_1 [µs]	2.59	2.53	2.572	2.6
I_1 [A]	3.4	3.19	3.36	3.25
Operation point 3				
f_{sw} [kHz]	30	30	29.54	29.92
V_{out} [V]	100	100	99.5	100
t_1 [µs]	2.2	2.53	2.479	2.6
I_1 [A]	3.2	3.6	3.675	3.5

parameters indicated in the table 7.2.

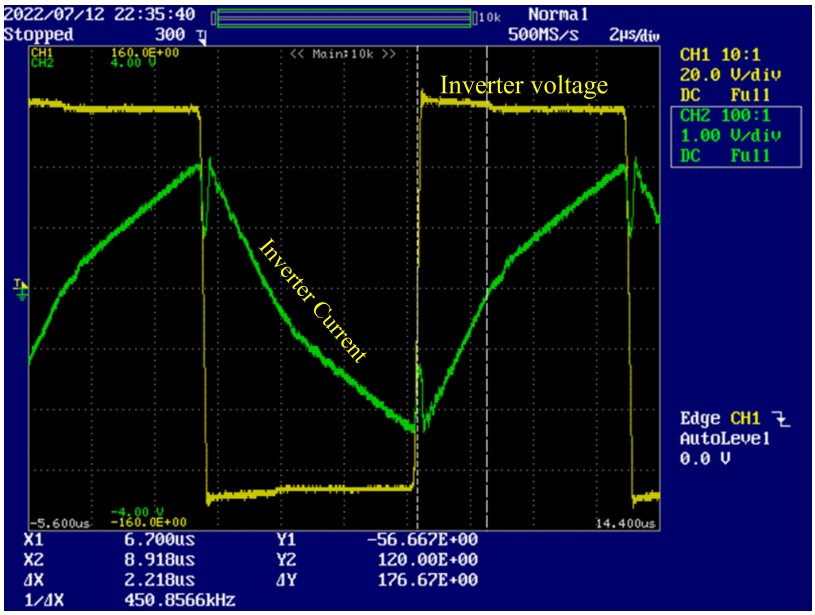

Figure 7-7: The illustration of the inverter current and voltage, based on the operation point 1 in the table 7.2

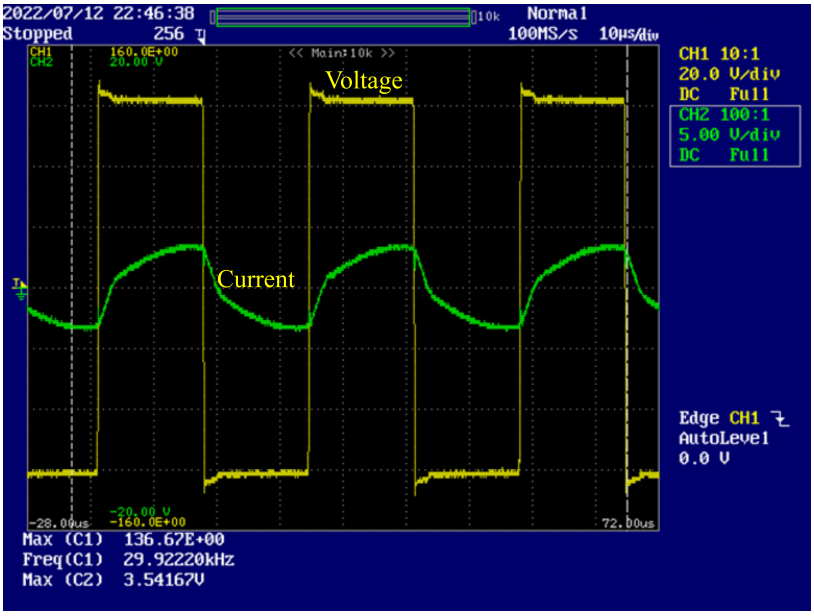

Figure 7-8: The illustration of the inverter current and voltage, based on the operation point 3 in the table 7.2

Several tests were made, and their respective results were captured, only few were illustrated in the table 7.2 and shown on the figures 7-7 and 7-8 for presentation purposes.

7.5.2 Parallel Resonant Converter

The topology shown in Figure 2-20 was used to build the prototype for practical experimentations, with the target of obtaining the model illustrated in Figure 7-1 and to practically prove the polynomial model. The model and the program script were obtained using Matlab-Simulink. The F28335 micro-controller is used for hosting the control program and to generate the corresponding switching signals, S^*_1, S^*_2, S^*_3, and S^*_4. The drivers are connected to the output of the controller and strengthen the switching signals to a suitable level of S_1, S_2, S_3, or S_4 for firing the IGBTs. The embedded IGBTs are used and provide an adequate commutation for the proper output of the prototype. The IGBTs form a converter and link the input voltage to the resonant tank. The last is made of leakage inductance and parallel capacitance connected in parallel. Both these components can be part of the power transformer

as parasitics. The diode rectifier and the filter capacitor output the DC voltage with proper smoothness. Figure 7-1 presents the steps and components of the prototype. The prototype can have different behaviors based on the components of the resonant tank. Two scenarios are tested in this work. The first scenario is the low-voltage prototype, where the resonant tank is made of an independent capacitor and inductor without a power transformer. This is the low-voltage case. The second option considers the resonant tank with an independent inductor together with the power transformer and its parasitics. This is a high-voltage case.

7.5.2.1 Low-Voltage Test

The prototype was made up of an F28335 TI micro-controller for shifted PWM signals, a driver to strengthen the PWM signals to a required switching level, an F4-150R12KS4-embedded IGBT converter, a resonant tank of $L_s = 34.232$ μH and $C_p = 658.7$ nF, an uncontrolled rectifier, a filter capacitor of 30 μF, and a 10 Ω load. The prototype was tested on a fixed load of 10Ω by applying Equation (6.3) on the program model in Figure 6-5. The power values in Table 7.3 were applied. Table 7.3 shows the data retrieved on the prototype in Figure 7-9. The same prototype was run from $\hat{v} = 1.00664$ to $\hat{v} = 1.441706$ and from $\hat{p} = 0.730587$ to $\hat{p} = 1.498569$. The resonant frequency of the prototype was $f_r = 33.517$ kHz. The behavior of the prototype at the fixed load is illustrated in Figure 7-10. As the output voltage increased, the power transfer increased as well. Hence, the switching frequency goes further below resonance, while the duty increases drastically. Figure 7-12 shows the behaviors of the prototype in Figure 7-9 in optimum mode. It was obtained through running the topology in Figure 7-9 in optimum mode and on the following data: power: $\hat{p} = 0.781915$; normalized load: $\hat{\Omega} = 1.387$. Hence, the voltage becomes $\hat{v} = 1.0414$. At the input voltage $V_{in} = 39.6$ V, the output voltage becomes $V_{out} = 41.24$. Therefore, the obtained frequency and duty are $\hat{f} = 0.76826685 \approx f = 25.75$ kHz and $d = 0.2625$, respectively.

Table 7.3: This table shows different operating points in the design operating window of the prototype in Figure 7-9 with the load of $10\Omega \approx \hat{\Omega}=1.387$

$\hat{v}$	$\hat{p}$	$\hat{f}$	d
1.00664	0.730587	0.780201	0.2535
1.041401	0.781915	0.768267	0.2625
1.074677	0.832682	0.757526	0.2716
1.120123	0.904597	0.74589	0.2842
1.150194	0.953819	0.74052	0.2925
1.172152	0.990585	0.737835	0.2985
1.30065	1.219677	0.695766	0.3417
1.316569	1.249714	0.685622	0.3488
1.332491	1.280124	0.673986	0.3567
1.348824	1.311699	0.661157	0.3656
1.359014	1.331593	0.652206	0.3716
1.372422	1.357997	0.639675	0.3801
1.389738	1.392481	0.621476	0.3924
1.403329	1.419851	0.605663	0.4032
1.412658	1.438791	0.593729	0.4112
1.441706	1.498569	0.550467	0.4404

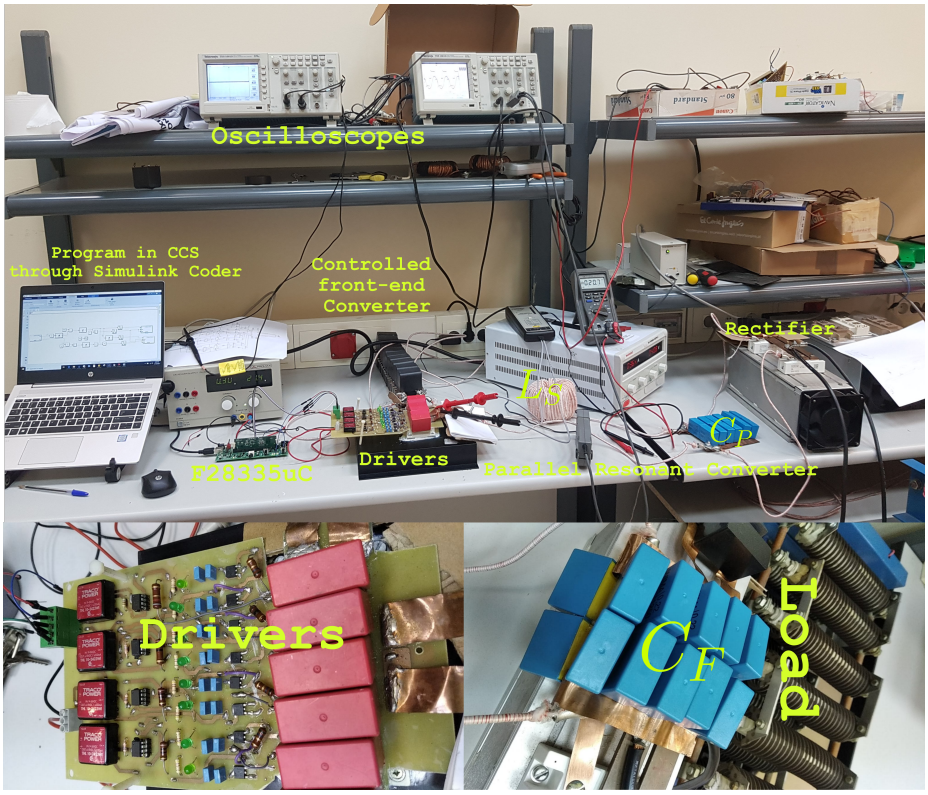

Figure 7-9: Illustration of the low-voltage prototype

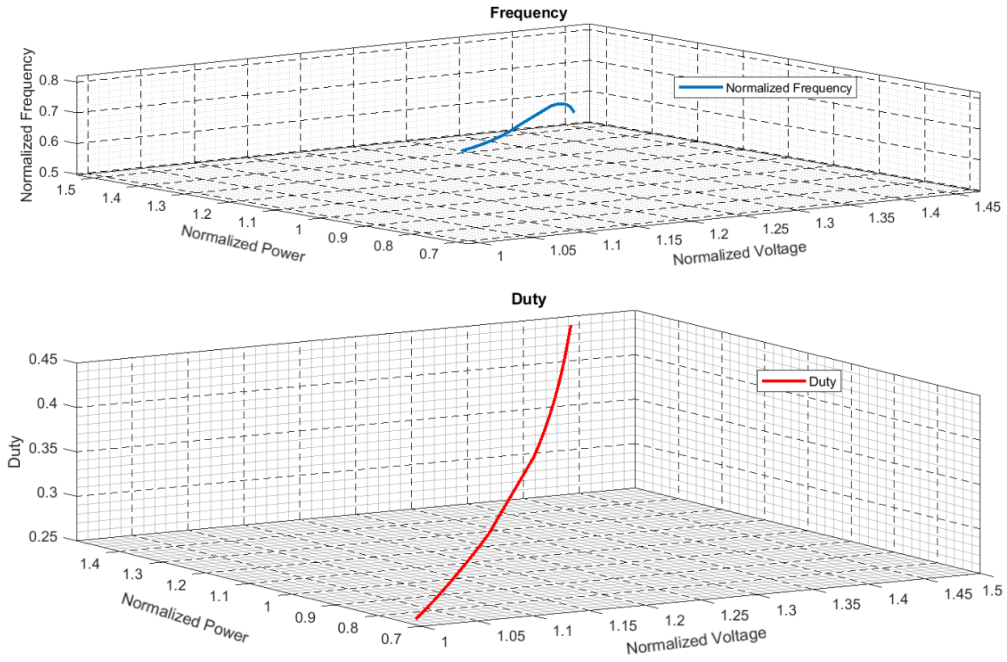

Figure 7-10: Illustration of normalized frequency and duty at a fixed load of $\hat{\Omega} = 1.387$, corresponding to 10 Ω.

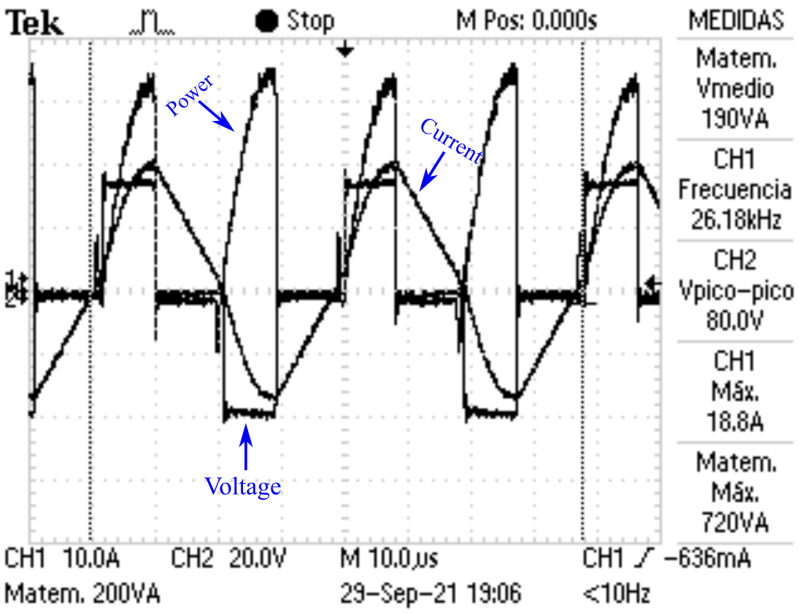

Figure 7-11: Illustration of the prototype output results as illustrated in table 7.4, Operational point 1

Table 7.4: Illustration of low voltage polynomial model experimental testing for PRC with f_r= 33.517 kHz and $\hat{\Omega}$=1.387

Parameter	L_s = 34.232uH, C_p = 658.7nF, R = 10Ω, V_{in} = 39.6V			
Test Type	PRC Model	Simulated	Polynom	Experimental
Operational Point 1				
$\hat{p}$	0.7306	0.7299	0.730	0.73
$\hat{v}$	1.0066	1.0064	1.0066	1.007
V_{out}	39.86	39.85	39.86	39.877
f_{sw}[kHz]	26.15	26.15	26.16	26.18
d	0.2535	0.2533	0.2535	0.254
Operational Point 2				
$\hat{p}$	0.7819	0.7819	0.7821	0.7817
$\hat{v}$	1.0414	1.0414	1.0416	1.042
V_{out}	41.239	41.239	41.247	41.246
f_{sw}[kHz]	25.75	25.77	25.80	25.84
d	0.2625	0.2623	0.262	0.2626
Operational Point 3				
$\hat{p}$	1.3117	1.3115	1.3113	1.310
$\hat{v}$	1.3488	1.3501	1.3491	1.3495
V_{out}	53.41	53.46	53.42	53.44
f_{sw}[kHz]	22.16	22.18	22.20	22.20
d	0.3656	0.3655	0.3659	0.366

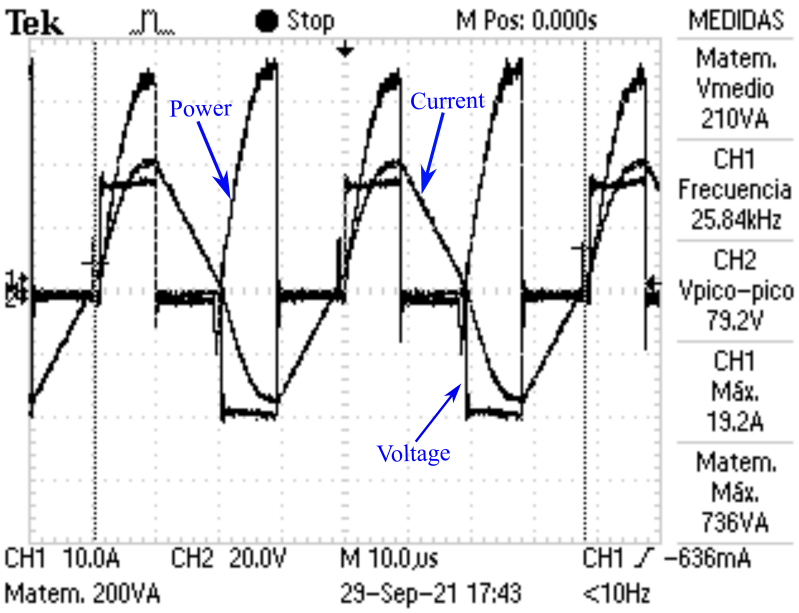

Figure 7-12: Illustration of the prototype output results as illustrated in table 7.4, Operational point 2

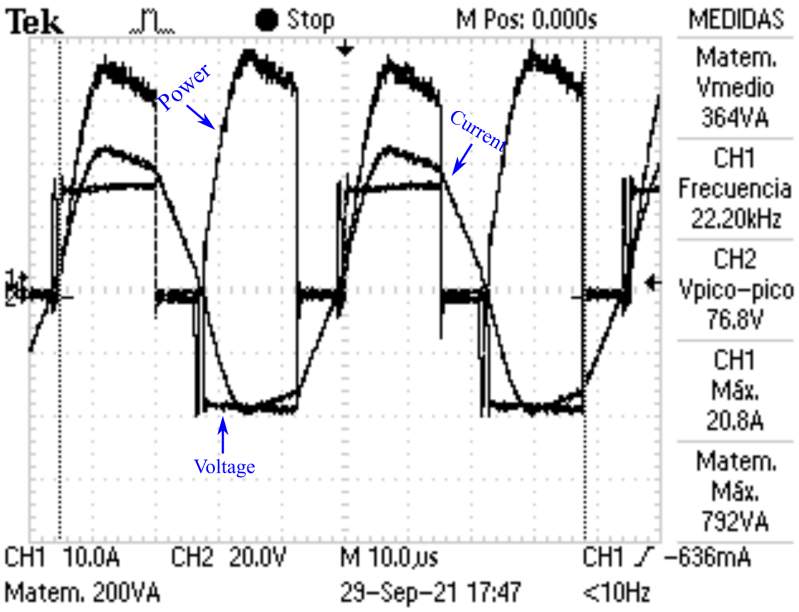

Figure 7-13: Illustration of the prototype output results as illustrated in table 7.4, Operational point 3

Several tests were made, and their respective results were captured, only few were illustrated in the table 7.4 and shown on the figures 7-12 and 7-13 for presentation purposes.

7.5.2.2 High-Voltage Test

The high-voltage prototype was built as illustrated in Figure 7-14. It uses the same components as the low-voltage prototype, with the exception of the high-voltage transformer; this was added for a higher transformation ratio. The inductor $L_S = 110.34$ µH (with 22.4 µH of transformer leakage inductance) and the parasitic capacitor $C_P = 43$ nF, the load is 57.575 Ω, the resonant frequency of $f_r = 73.067$ kHz, $Z_{base} = 50.6561$ Ω, and $n = 400/14$ is the transformer turn ratio. Transformer oil was used to insulate the transformer and the load for safe runs under high-voltage outputs. The maximum output voltage reached was 4 kV. Figure 7-14 shows the high-voltage transformer and the load immersed in transformer oil for high-voltage insulation. The converter selected in this case is the one used in the E-beam welding machine, one of the HV converters needed. The prototype in Figure 7-14 was

run at a fixed normalized load of $\hat{\Omega} = 1.1366$. The model-based program illustrated in Figure 6-5 runs on various power levels, in a range between $\hat{p} = 0.882826$ and $\hat{p} = 1.498569$. Figure 7-15 shows the output of the high-voltage test, where the input voltage is $V_{in} = 94$, the input current $I_{in} = 1$ A, the normalized power $\hat{p} = 0.882826$, the normalized frequency $\hat{f} = 0.6862$, the duty $d = 0.283$, and the output voltage $V_{out} = 2$ kV. The optimum mode is realized.

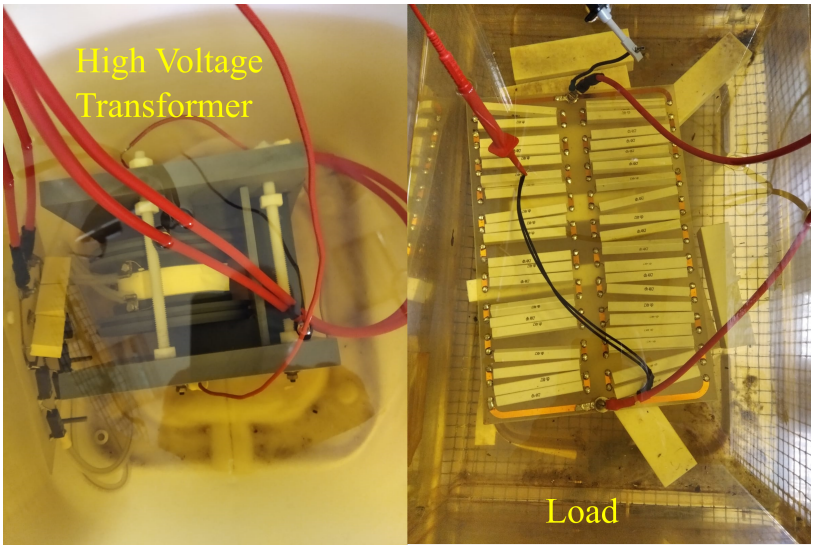

Figure 7-14: Illustration of the high-voltage prototype.

Table 7.5: Illustration of PRC polynomial model tests on High Voltage scenarios

Scenario 1				
Parameters	L_s = 110.34uH, C_p = 43nF, R = 57.5750Ω, f_r = 73.067kHz			
Test Type	PRC Model	Simulated	Polynom	Experimental
Operational Point 1				
$\hat{p}$	0.8828	0.8797	0.8815	0.89
V_{in} [V]	94	94	94	94
V_{out} [kV]	2.0	1.99	2.0	2.00
$\hat{f}$	0.6862	0.6865	0.6859	0.6860
d	0.2830		0.2828	0.2850
f_{sw}[kHz]	50.14		50.50	50.776
Operational Point 2				
$\hat{p}$	1.1429	1.143	1.143	1.1432
V_{in} [V]	95.1	94	94	95.1
V_{out} [kV]	2.51	2.49	2.49	2.50
$\hat{f}$	0.6331	0.6331	0.6329	0.6330
d	0.3305	0.3305	0.3305	0.3280
f_{sw}[kHz]	46.15	46.2	46.26	46.006

Scenario 2				
Parameters	L_s = 56.635uH, C_p = 43nF, R = 57.5750Ω, f_r = 101.99kHz			
Test Type	PRC Model	Simulated	Polynom	Experimental
Operational Point 1				
$\hat{p}$	1.4085	1.4082	1.4086	1.408
V_{in} [V]	117	117	117	117
V_{out} [kV]	4.0	3.999	4.00	4.00
$\hat{f}$	0.6903	0.6901	0.6899	0.6904
d	0.3834			
f_{sw}[kHz]	70.41	70.389	70.394	70.4

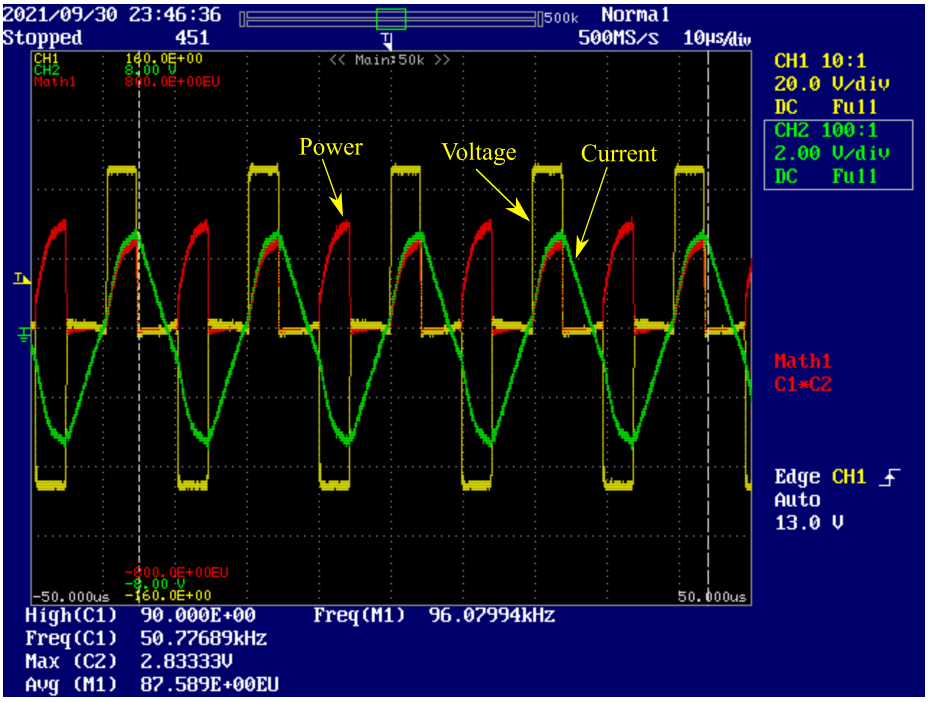

Figure 7-15: Illustration of converter output at 2 kV output voltage, following the data on scenario 1, operational point 1 in the table 7.5

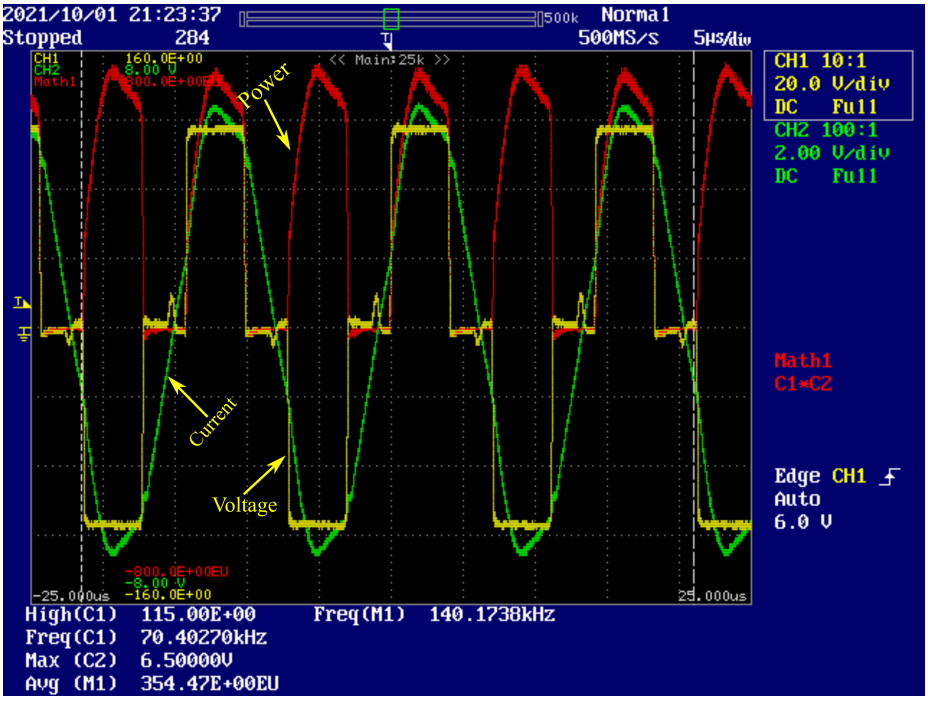

Figure 7-16: Illustration of converter output at 4 kV output voltage, following the data on scenario 2, operational point 1 in the table 7.5

Several tests were made, and their respective results were captured, only few were illustrated in the table 7.5 and shown on the figures 7-15 and 7-16 for presentation purposes.

7.5.2.3 Frequency change

The abrupt change in the switching frequency and duty were made 51.387kHz to 26.144kHz and 0.25 to 0.28 respectively through the Hex-Enc (hexa-decimal encoder) input of the F28335 micro-controller. It suddenly increases the power transfer. Such change in frequency is realized after a transition of one and a half period of time. The figure 7-17 illustrates the indicated changes.

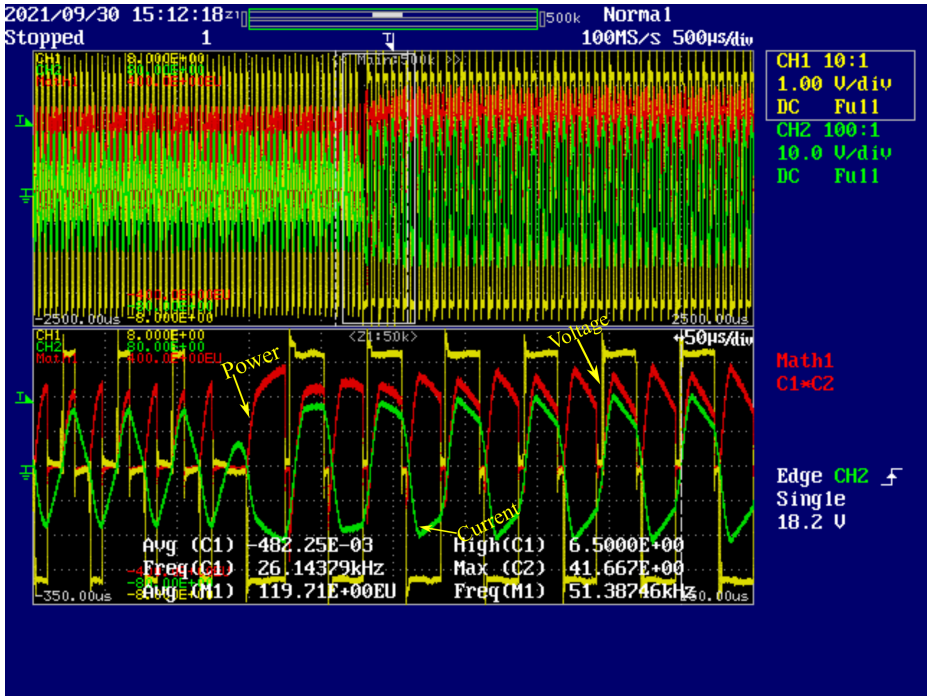

Figure 7-17: Frequency change from 51.387 kHZ to 26.144 kHz

7.6 Conclusions

In practically validating the model illustrated and simulated in the previous chapters; the experimental prototype were built in this chapter. Those are made of: personal computer to host the control program, the controller i.e. DSC or FPGA to generate

the control PWM signals, the driver for control signal strengthening and adaptation, the power topology. The last is made of the DC power supply, the controller front-end inverter (embedded IGBTs), resonant tank (with series of parallel configuration), the rectifier, the capacitive filter and the load. Here described prototype was run through the conditions indicated in the previous chapters, and considering the same parameters indicated in the simulations, for validation purposes. The results of the practical experimentations are shown in this chapter and confirm the model design and simulation outputs.

Chapter 8

The Conclusion and Future Development

Contents

8.1 Conclusions 169
8.2 The Publications 170
8.3 The Future Development 171

8.1 Conclusions

A proposal for implementing resonant converters control in digital devices have been presented. The steady state models for PRC and SRC were introduced and their difficulties in DSC implementation were highlighted. From the steady-state models, the polynomial models for both PRC and SRC converters have been obtained and implemented in a DSC, using MathLab-Simulink. The complete process was verified with the expermental results illustrated in this work. later on, the use of FPGA was introduced. The simple algorithms in VHDL to carry out the polynomials for PRC was proposed and verified by simulations in Altera. The results are indicated in this

work. The polynomial model implementation for PRC using Fuzzy logic controller was proposed and simulated in Simulink. The control rule base data and control simulation results were illustrated in this work. At last, the closed loop control of the PRC was as well attempted, using fuzzy logic control; the simulation results are promising and are indicated in this work. All of the simulated and practical results of the models mentioned and illustrated in this work; confirm and track the hypothesis of the project.

8.2 The Publications

The publications related to this work:

1. Conference proceedings:

    1. Evode, R. W. A. M. U. R. A. N. G. W. A. (2019, August). High Voltage DC Measurement Through Low-pass Filter Ripples Detection in Parallel Resonant Converters With no-Inductor at Output. In 2019 IEEE PES/IAS PowerAfrica (pp. 379-384). IEEE.

2. Journals:

    1. Rwamurangwa, E., and Mugisha, P. O. (2017). Approach on High Electric Fields for remedying the Micro-organisms attack on Crops. Agricultural Research and Technology, 10 (3).

    2. Rwamurangwa, E., González, J. D., Villegas Saiz, P. J., Martín-Ramos, J. A., and Pernía, A. M. (2022). A Parallel Resonant Converter Polynomial Model Implemented in a Digital Signal Controller. Electronics, 11(7), 1085.

The Publications not related to this work:

1. Conference proceedings:

1. Evode, R. (2021, October). Modeling of Electric Grid Behaviors having Electric Vehicle charging stations with G2V and V2G Possibilities. In 2021 International Conference on Electrical, Computer, Communications and Mechatronics Engineering (ICECCME) (pp. 1-5). IEEE.

8.3 The Future Development

The resonant converters and their use in high voltage DC application are illustrated in this work; with the major focus on PRC and SRC. The respective models i.e. steady-state and polynomial model were elaborated as well in this work. The simulation, programming of controllers and practical tests were done through Matlab-Simulink and built prototype respectively. All of this above constitute the reason of future orientations, applications, implementations as well as improvements of the models in place. Therefore, among the future activities related to this project; here are cited few:

. The implementation of the PRC polynomial model in FPGA was modeled. The simple algorithms in VHDL to carry out the polynomials for PRC was developed and verified by simulations and experimentally in Altera. The results are promising. Various various simulations were done in Simulink, and reflected a very good progress. The next step is to implement FPGA coding using model-based option in Simulink and building the prototype for experimental verification.

. The polynomial model for SRC was developed and implemented in DSC. The option of its implementation in FPGA was modeled. The preliminary simulations and experiments were done and the results are on the right stage. The next step is to complete the simulations, configure the Simulink model to FPGA, run the Simulation on the FPGA, built the prototype and experimental verification.

. The closed loop control of the parallel resonant converter, using fuzzy logic controls was proposed. The closed loop control is based on the polynomial model

concept. The fuzzy logic controller was set and the rule base data were obtained using Simulink. The simulations were done in Simulink and the results are promising. The next step is the implementation in DSC, building the prototype and experimental verification.

. The polynomial model closed loop control of Parallel Resonant converter implemention using neural network is proposed. This is an option to smoothen the PRC polynomial model control. The Neural Network base rules and simulations are done. The results are promising and the next step is to finalize with the simulations, implementations in the DSC, prototype building and experimental verification.

. The polynomial models (PRC and SRC) use in control of the battery charging in EV and drones application was done on a basic level with some models built in Simulink and some simulations. The next step shall is to finalize the simulations, implementation in DSC or FPGA and experimental verification.

Some more future works related to this project are being optimized, mostly focusing on wireless charging. The target is the charging stations of drones and other flying equipment.

Capítulo 8

Conclusiones y Futuros trabajos

Contents

8.1 Conclusiones 173
8.2 Publicaciones 174
8.3 Futuros trabajos 175

8.1 Conclusiones

Se ha presentado un método para implementar el control de convertidores resonantes en dispositivos programables. Se ha presentado el modelo en régimen permanente para los convertidores SRC y PRC y su implementación en un DSC. A partir de las ecuaciones en el dominio del tiempo, se han obtenido las ecuaciones en formato polinomio, y posteriormente, se implementan en un DSC, utilizando las herramientas de MathLab-Simulink, validando los resultados mediante simulación. El proceso se ha probado de forma experimental en un prototipo de laboratorio. Posteriormente, se implementan dichos polinomios en una FPGA. Se han implementado en lenguaje

VHDL y se ha verificado con el software de Altera, simulaciones para el convertidor PRC y de forma experimental para el convertidor SRC. Por otro lado, se basándose en los polinomios obtenidos, se explora el controlbasado en lógica difusa o fuzzy logic: se ha simulado el control en lazo cerrado para el convertidor PRC utilizando lógica difusa, mediante Simulink. Los resultados de simulación obtenidos son prometedores y constituyen una base para futuros trabajos. Todos los resultados anteriormente expuestos han sido validados por simulacionesmediante MathLab-SimuLink, simuladores eléctricos (ORCAD) y experimentales en prototipo de laboratorio.

8.2 Publicaciones

Directamente relacionadas con este trabajo:

1. Congresos:

    1. Evode, R. W. A. M. U. R. A. N. G. W. A. (2019, August). High Voltage DC Measurement Through Low-pass Filter Ripples Detection in Parallel Resonant Converters With no-Inductor at Output. In 2019 IEEE PES/IAS PowerAfrica (pp. 379-384). IEEE.

2. Revistas:

    1. Rwamurangwa, E., and Mugisha, P. O. (2017). Approach on High Electric Fields for remedying the Micro-organisms attack on Crops. Agricultural Research and Technology, 10 (3).

    2. Rwamurangwa, E., González, J. D., Villegas Saiz, P. J., Martín-Ramos, J. A., and Pernía, A. M. (2022). A Parallel Resonant Converter Polynomial Model Implemented in a Digital Signal Controller. Electronics, 11(7), 1085.

Indirectamente relacionadas con este trabajo::

1. Congresos:

1. Evode, R. (2021, October). Modeling of Electric Grid Behaviors having Electric Vehicle charging stations with G2V and V2G Possibilities. In 2021 International Conference on Electrical, Computer, Communications and Mechatronics Engineering (ICECCME) (pp. 1-5). IEEE.

8.3 Futuros trabajos

Se han presentado en este trabajo distintas aplicaciones de alta tensión de salida de los convertidores resonantes, prestando especial atención a los convertidores PRC y SRC. Se han elaborado los modelos en régimen permanente en el dominio del tiempo y en ecuaciones polinómicas. Las simulaciones y posterior implementación en el DSC se han realizado mediante MathLab y se ha implementado un prototipo para validar de forma experimental los resultados obtenidos. Estos trabajos previos abren la posibilidad de futuras ampliaciones y mejoras de lo realizado hasta ahora. Entre otras, citaremos las siguientes:

. La implementación de los polinomios para el convertidor SRC se ha realizado de forma directa en lenguaje VHDL, sin utilizar las herramientas de síntesis de Simulink. Un trabajo futuro puede basarse en la implementación de los modelos obtenidos de forma directa, y comparar los resultados obtenidos con los aquí presentados.

. Se propone la implementación de los modelos desarrollados para el PRC en la FPGA, de forma análoga al SRC, de forma directa mediante las herramientas de síntesis de MatLab.

. El estudio del lazo cerrado utilizando fuzzy logic es otra de las propuestas que se derivan de esta tesis. Se han obtenido los pasos previos, tales como el controlador fuzzy y las reglas, mediante simulink.

. Se propone la aplicación de redes neuronales para el lazo cerrado del convertidor PRC. Es una propuesta para facilitar el control mediante el modelo polinomial.

Se han establecido las reglas básicas y se han realizado las simulaciones básicas. Los resultados son prometedores y el siguiente paso consiste en avanzar con las simulaciones y su posterior implementación en DSC, y validación en prototipo.

. Evaluar la validez de los modelos polinomiales (PRC y SRC) en diferentes aplicaciones de carga de vehículos eléctricos, tales como drones. Se han realizado algunas simulaciones previas, y los resultados son prometedores. Los siguientes pasos consisten en finalizar con la implementación en DSC y FPGA y validar de forma experimental.

Se están optimizando algunos trabajos futuros más relacionados con este proyecto, centrándose principalmente en la carga inalámbrica. El objetivo son las estaciones de carga de drones y otros equipos voladores.

Appendix A

Tables of Parallel Resonant converter Data

Contents

A.1 Introduction 177
A.2 Tables 178
B.1 Introduction 193
C.1 PRC Polynomial Codes 243
C.2 SRC Polynomial Codes 248
C.2.1 Initial resonant current polynomial 248
C.2.2 Frequency polynomial 252

A.1 Introduction

This appendix shows in details the data used to convert the PRC steady-state model into graphical representation. The normalized frequency$\hat{f}$ and duty d are illustrated graphically with respect to the normalized power $\hat{p}$ in presence of the normalized output voltage $\hat{v}$. The same data were used through numerical analysis .i.e. Data

fitting and B-spline to obtain the equivalent polynomial model. The last is expressed in two polynomials .i.e normalize frequency and duty; both are functions of nornalized power and normalized output voltage. The complete process is detailed in the tables illustrated in this appendix.

A.2 Tables

Table A.1: Frequency vs Power at the Normalized voltage $\hat{v}$ varying from 1.0 to 1.4

$\hat{v}$									
1.0		1.1		1.2		1.3		1.4	
Power	Frequency	Power	Frequency	Power	Frequency	Power	Frequency	Power	Frequency
0.560354	0.879646	0.626457	0.8898668	0.697533	0.896439	0.773109	0.900546549	0.797236	0.92302039
0.61177	0.84823	0.678752	0.8620584	0.750651	0.871538	0.82691	0.878032885	0.852748	0.90295416
0.663186	0.816814	0.730587	0.8342501	0.80292	0.846637	0.879517	0.855519221	0.907039	0.88243247
0.714602	0.785398	0.781915	0.8064418	0.854265	0.821736	0.930834	0.833005558	0.95982	0.86191079
0.766018	0.753982	0.832682	0.7786334	0.904597	0.796835	0.980753	0.810491894	1.010979	0.8413891
0.817434	0.722566	0.882826	0.7508251	0.953819	0.771934	1.029155	0.78797823	1.060397	0.82086741
0.86885	0.69115	0.932274	0.7230168	1.00182	0.747033	1.075906	0.765464566	1.107937	0.80034573
0.920266	0.659734	0.980943	0.6952084	1.048475	0.722132	1.120855	0.742950903	1.153453	0.77982404
0.971681	0.628319	1.028736	0.6674001	1.093637	0.697231	1.163833	0.720437239	1.196781	0.75930236
1.023097	0.596903	1.075538	0.6395917	1.137142	0.67233	1.20465	0.697923575	1.237737	0.73878067
1.074513	0.565487	1.121215	0.6117834	1.178799	0.647429	1.24309	0.675409912	1.276119	0.71825899
1.125929	0.534071	1.165605	0.5839751	1.218385	0.622527	1.278907	0.652896248	1.311699	0.6977373
1.177345	0.502655	1.208516	0.5561667	1.255642	0.597626	1.31182	0.630382584	1.344223	0.67721562
1.228761	0.471239	1.249714	0.5283584	1.290267	0.572725	1.341505	0.60786892	1.373404	0.65669393
1.280177	0.439823	1.288914	0.5005501	1.321899	0.547824	1.367591	0.585355257	1.398919	0.63617225
1.331593	0.408407	1.325762	0.4727417	1.350112	0.522923	1.389646	0.562841593	1.420401	0.61565056
1.383009	0.376991	1.359818	0.4449334	1.374392	0.498022	1.407166	0.540327929	1.437432	0.59512888
1.434425	0.345575	1.390524	0.417125	1.394119	0.473121	1.41956	0.517814265	1.449537	0.57460719
1.485841	0.314159	1.417161	0.3893167	1.408534	0.44822	1.426127	0.495300602	1.456168	0.5540855
1.537257	0.282743	1.438791	0.3615084	1.4167	0.423319	1.426037	0.472786938	1.456692	0.53356382
1.588673	0.251327	1.454162	0.3337	1.417444	0.398418	1.41829	0.450273274	1.450378	0.51304213
1.640089	0.219911	1.461568	0.3058917	1.409283	0.373516	1.401677	0.427759611	1.43637	0.49252045
1.691504	0.188496	1.458617	0.2780834	1.390307	0.348615	1.374722	0.405245947	1.413665	0.47199876
1.74292	0.15708	1.441858	0.250275	1.358022	0.323714	1.335597	0.382732283	1.381077	0.45147708
1.794336	0.125664	1.406114	0.2224667	1.3091	0.298813	1.282023	0.360218619	1.337194	0.43095539
1.845752	0.094248	1.343247	0.1946584	1.239005	0.273912	1.211108	0.337704956	1.280322	0.41043371
1.897168	0.062832	1.239696	0.16685	1.141382	0.249011				
1.948584	0.031416	1.071052	0.1390417						

Table A.2: Frequency vs Power at the Normalized voltage $\hat{v}$ varying from 1.5 to 1.9

$\hat{v}$									
1.5		1.6		1.7		1.8		1.9	
Power	Frequency	Power	Frequency	Power	Frequency	Power	Frequency	Power	Frequency
0.879792	0.922985	0.907866	0.93874764	0.996743	0.9364478	1.088704	0.93380546	1.122564	0.94488393
0.936032	0.904173	0.96601	0.92194602	1.055333	0.9204791	1.147348	0.91874408	1.183327	0.93094119
0.990585	0.885336	1.022546	0.90455081	1.111877	0.9043303	1.20361	0.9036827	1.241644	0.91683602
1.04333	0.866499	1.077108	0.8871556	1.166179	0.8881816	1.257368	0.88862132	1.297326	0.90273085
1.094146	0.847662	1.129579	0.86976039	1.218114	0.8720328	1.308493	0.87355994	1.350247	0.88862568
1.142903	0.828825	1.179829	0.85236518	1.26755	0.855884	1.356846	0.85849856	1.400273	0.87452051
1.189455	0.809988	1.22772	0.83496998	1.314341	0.8397353	1.402278	0.84343719	1.447262	0.86041534
1.233647	0.791151	1.273103	0.81757477	1.358332	0.8235865	1.444632	0.82837581	1.491063	0.84631017
1.275305	0.772314	1.315811	0.80017956	1.399355	0.8074378	1.483734	0.81331443	1.531512	0.832205
1.314238	0.753477	1.355669	0.78278435	1.437228	0.791289	1.519402	0.79825305	1.568436	0.81809983
1.350239	0.73464	1.392481	0.76538914	1.471755	0.7751403	1.551437	0.78319167	1.601651	0.80399466
1.383074	0.715803	1.426035	0.74799394	1.502722	0.7589915	1.579625	0.76813029	1.630957	0.78988949
1.412487	0.696967	1.456098	0.73059873	1.529896	0.7428428	1.603736	0.75306892	1.656141	0.77578432
1.438194	0.67813	1.482414	0.71320352	1.553025	0.726694	1.62352	0.73800754	1.676974	0.76167915
1.459876	0.659293	1.504703	0.69580831	1.571833	0.7105452	1.638706	0.72294616	1.69321	0.74757398
1.477178	0.640456	1.522655	0.67841311	1.586018	0.6943965	1.649002	0.70788478	1.704583	0.73346881
1.489703	0.621619	1.535928	0.6610179	1.595251	0.6782477	1.654088	0.6928234	1.710809	0.71936365
1.497002	0.602782	1.544141	0.64362269	1.599169	0.662099	1.653617	0.67776202	1.711577	0.70525848
1.498569	0.583945	1.546874	0.62622748	1.597374	0.6459502	1.64721	0.66270065	1.706553	0.69115331
1.493831	0.565108	1.543657	0.60883227	1.589425	0.6298015	1.634452	0.64763927	1.695376	0.67704814
1.482137	0.546271	1.533964	0.59143707	1.574837	0.6136527	1.614891	0.63257789	1.677653	0.66294297
1.462741	0.527434	1.517207	0.57404186	1.553072	0.597504	1.588028	0.61751651	1.652957	0.6488378
1.434787	0.508597	1.492724	0.55664665	1.523531	0.5813552	1.553316	0.60245513	1.620823	0.63473263
1.397287	0.48976	1.459767	0.53925144	1.485549	0.5652064				
1.349096	0.470923	1.417489	0.52185624						

Table A.3: Frequency vs Power at the Normalized voltage $\hat{v}$ varying from 2.0 to 2.4

$\hat{v}$									
2.0		2.1		2.2		2.3		2.4	
Power	Frequency	Power	Frequency	Power	Frequency	Power	Frequency	Power	Frequency
1.219677	0.9413388	1.219677	0.941338837	1.293245	0.957708	1.397247	0.95342993	1.436698	0.959684
1.280124	0.9280805	1.280124	0.928080543	1.357997	0.946136	1.461249	0.94221311	1.502823	0.949146
1.337807	0.9148222	1.337807	0.91482225	1.419851	0.934309	1.522001	0.93099629	1.565635	0.938482
1.392605	0.901564	1.392605	0.901563956	1.478575	0.922483	1.579384	0.91977946	1.624961	0.927817
1.444387	0.8883057	1.444387	0.888305663	1.534048	0.910656	1.633274	0.90856264	1.680678	0.917153
1.493017	0.8750474	1.493017	0.875047369	1.586141	0.898829	1.683538	0.89734582	1.732661	0.906488
1.53835	0.8617891	1.53835	0.861789076	1.634719	0.887003	1.73004	0.886129	1.780775	0.895823
1.580231	0.8485308	1.580231	0.848530783	1.679638	0.875176	1.772634	0.87491217	1.82488	0.885159
1.618495	0.8352725	1.618495	0.835272489	1.72075	0.863349	1.811169	0.86369535	1.86483	0.874494
1.652968	0.8220142	1.652968	0.822014196	1.757896	0.851523	1.845485	0.85247853	1.900471	0.86383
1.683463	0.8087559	1.683463	0.808755902	1.790907	0.839696	1.875412	0.84126171	1.931642	0.853165
1.709781	0.7954976	1.709781	0.795497609	1.819606	0.827869	1.900772	0.83004488	1.958172	0.842501
1.731709	0.7822393	1.731709	0.782239315	1.843807	0.816042	1.921379	0.81882806	1.979883	0.831836
1.749022	0.768981	1.749022	0.768981022	1.86331	0.804216	1.937033	0.80761124	1.996588	0.821171
1.761475	0.7557227	1.761475	0.755722728	1.877905	0.792389	1.947526	0.79639441	2.008088	0.810507
1.768809	0.7424644	1.768809	0.742464435	1.88737	0.780562	1.952637	0.78517759	2.014176	0.799842
1.770743	0.7292061	1.770743	0.729206141	1.891467	0.768736	1.95213	0.77396077	2.014632	0.789178
1.76698	0.7159478	1.76698	0.715947848	1.889945	0.756909	1.94576	0.76274395	2.009225	0.778513
1.757194	0.7026896	1.757194	0.702689554	1.882536	0.745082	1.933262	0.75152712	1.99771	0.767849
1.741041	0.6894313	1.741041	0.689431261	1.868956	0.733256	1.914359	0.7403103	1.97983	0.757184
1.718143	0.676173	1.718143	0.676172967	1.8489	0.721429	1.888755	0.72909348	1.955311	0.74652
1.688098	0.6629147	1.688098	0.662914674	1.822045	0.709602				

Table A.4: Frequency vs Power at the Normalized voltage $\hat{v}$ varying from 2.5 to 2.9

$\hat{v}$									
2.5		2.6		2.7		2.8		2.9	
Power	Frequency	Power	Frequency	Power	Frequency	Power	Frequency	Power	Frequency
1.476245	0.9651931	1.58635	0.9606497	1.62828	0.9653685	1.670263	0.96958561	1.78563	0.9650385
1.544532	0.9552561	1.653352	0.95095925	1.697373	0.9561828	1.741471	0.96085163	1.854995	0.95649833
1.60943	0.9450938	1.716639	0.94125558	1.76267	0.9468995	1.808796	0.95195485	1.920175	0.94795817
1.670725	0.9349315	1.776089	0.93155191	1.824016	0.9376162	1.872052	0.94305808	1.981057	0.93941801
1.728298	0.9247692	1.83158	0.92184825	1.88129	0.9283329	1.931123	0.9341613	2.037523	0.93087784
1.782024	0.9146069	1.882987	0.91214458	1.934369	0.9190495	1.98589	0.92526453	2.089449	0.92233768
1.831775	0.9044446	1.930177	0.90244092	1.983126	0.9097662	2.036226	0.91636776	2.136709	0.91379751
1.877413	0.8942823	1.973013	0.89273725	2.027427	0.9004829	2.082002	0.90747098	2.17917	0.90525735
1.918798	0.88412	2.011352	0.88303358	2.067132	0.8911995	2.123081	0.89857421	2.216695	0.89671719
1.955782	0.8739577	2.045043	0.87332992	2.102096	0.8819162	2.159324	0.88967743	2.249142	0.88817702
1.988208	0.8637954	2.073931	0.86362625	2.132167	0.8726329	2.190582	0.88078066	2.276363	0.87963686
2.015914	0.8536331	2.09785	0.85392259	2.157189	0.8633496	2.216704	0.87188388	2.298205	0.8710967
2.03873	0.8434708	2.116631	0.84421892	2.176996	0.8540662	2.237532	0.86298711	2.314506	0.86255653
2.056477	0.8333085	2.130093	0.83451526	2.191417	0.8447829	2.252898	0.85409034	2.325102	0.85401637
2.068966	0.8231462	2.138049	0.82481159	2.200271	0.8354996	2.262632	0.84519356	2.32982	0.84547621
2.076001	0.8129839	2.140302	0.81510792	2.203372	0.8262162	2.266553	0.83629679	2.328478	0.83693604
2.077375	0.8028216	2.136646	0.80540426	2.200523	0.8169329	2.264474	0.82740001	2.320891	0.82839588
2.072869	0.7926593	2.126866	0.79570059	2.191519	0.8076496	2.256199	0.81850324	2.306863	0.81985571
2.062255	0.782497	2.110733	0.78599693	2.176145	0.7983663	2.241523	0.80960646	2.28619	0.81131555
2.045292	0.7723347	2.08801	0.77629326	2.154177	0.7890829	2.220234	0.80070969		
2.021725	0.7621724								

Table A.5: Frequency vs Power at the Normalized voltage $\hat{v}$ varying from 3.0 to 3.4

$\hat{v}$									
3.0		3.1		3.2		3.3		3.4	
Power	Frequency	Power	Frequency	Power	Frequency	Power	Frequency	Power	Frequency
1.82985536	0.9687559	1.874116	0.97210624	1.9184	0.97514204	2.040264	0.9707096	2.086666	0.9734557
1.90125255	0.9605946	1.947556	0.96429858	1.993896	0.96765691	2.113244	0.9633558	2.161602	0.9663854
1.96836907	0.9523844	2.016619	0.9563945	2.064914	0.96003757	2.181464	0.9560019	2.231676	0.9592797
2.03107266	0.9441742	2.081154	0.94849041	2.131288	0.95241822	2.244814	0.9486481	2.296763	0.9521739
2.0892472	0.935964	2.141046	0.94058632	2.192905	0.94479888	2.303179	0.9412942	2.356753	0.9450681
2.14277244	0.9277538	2.196178	0.93268224	2.249651	0.93717953	2.356441	0.9339403	2.411528	0.9379623
2.19152386	0.9195436	2.246428	0.92477815	2.301404	0.92956018	2.40448	0.9265865	2.46097	0.9308566
2.23537242	0.9113334	2.291669	0.91687406	2.348042	0.92194084	2.447168	0.9192326	2.504955	0.9237508
2.27418442	0.9031232	2.331771	0.90896998	2.389436	0.91432149	2.484378	0.9118788	2.543357	0.916645
2.30782124	0.8949129	2.366598	0.90106589	2.425455	0.90670215	2.515976	0.9045249	2.576044	0.9095392
2.33613911	0.8867027	2.396011	0.8931618	2.455961	0.8990828	2.541823	0.897171	2.602882	0.9024335
2.35898892	0.8784925	2.419864	0.88525772	2.480813	0.89146346	2.561777	0.8898172	2.623732	0.8953277
2.3762159	0.8702823	2.438008	0.87735363	2.499866	0.88384411	2.575691	0.8824633	2.638449	0.8882219
2.3876594	0.8620721	2.450286	0.86944954	2.512966	0.87622476	2.583412	0.8751095	2.646886	0.8811161
2.39315259	0.8538619	2.456537	0.86154546	2.519959	0.86860542	2.584783	0.8677556	2.648889	0.8740104
2.39252216	0.8456517	2.456593	0.85364137	2.520682	0.86098607	2.579641	0.8604017	2.644299	0.8669046
2.385588	0.8374415	2.450282	0.84573728	2.514967	0.85336673	2.567817	0.8530479	2.632954	0.8597988
2.37216288	0.8292313	2.437422	0.8378332	2.50264	0.84574738	2.549138	0.845694	2.614685	0.852693
2.35205206	0.8210211	2.417827	0.82992911	2.483521	0.83812803				

Table A.6: Frequency vs Power at the Normalized voltage $\hat{v}$ varying from 3.5 to 4.0

$\hat{v}$											
3.5		3.6		3.7		3.8		3.9		4.0	
Power	Frequency	Power	Frequency	Power	Frequency	Power	Frequency	Power	Frequency	Power	Frequency
2.133081	0.9759653	2.179505	0.97826478	2.306786	0.97403694	2.355205	0.9761797	2.403634	0.97814169	2.452064	0.979956
2.209982	0.9691579	2.258378	0.9717005	2.382451	0.96758636	2.43274	0.9699304	2.483038	0.97209641	2.533343	0.974101
2.281914	0.9622845	2.332174	0.96504502	2.452781	0.96113578	2.504826	0.9636728	2.556884	0.9660208	2.608951	0.968198
2.348745	0.955411	2.400753	0.95838954	2.517669	0.95468521	2.571354	0.9574152	2.625055	0.9599452	2.678767	0.962294
2.410363	0.9485375	2.464004	0.95173406	2.577004	0.94823463	2.632215	0.9511576	2.687443	0.9538696	2.742686	0.95639
2.466655	0.9416641	2.521816	0.94507857	2.630672	0.94178406	2.687295	0.9448999	2.743937	0.947794	2.800596	0.950487
2.517503	0.9347906	2.574073	0.93842309	2.678554	0.93533348	2.736479	0.9386423	2.794424	0.94171839	2.852385	0.944583
2.562786	0.9279172	2.620655	0.93176761	2.720532	0.92888291	2.779648	0.9323847	2.838785	0.93564279	2.897938	0.938679
2.60238	0.9210437	2.661441	0.92511212	2.75648	0.92243233	2.816681	0.9261271	2.876901	0.92956719	2.937136	0.932776
2.636156	0.9141702	2.696304	0.91845664	2.786272	0.91598175	2.847452	0.9198695	2.908649	0.92349159	2.969859	0.926872
2.663982	0.9072968	2.725114	0.91180116	2.809777	0.90953118	2.871833	0.9136119	2.933902	0.91741598	2.99598	0.920969
2.685721	0.9004233	2.747738	0.90514568	2.826859	0.9030806	2.889691	0.9073542	2.95253	0.91134038	3.015373	0.915065
2.701234	0.8935499	2.764039	0.89849019	2.837381	0.89663003	2.90089	0.9010966	2.964399	0.90526478	3.027907	0.909161
2.710375	0.8866764	2.773875	0.89183471	2.841199	0.89017945	2.905291	0.894839	2.969374	0.89918918	3.033446	0.903258
2.712995	0.8798029	2.7771	0.88517923	2.838167	0.88372888	2.90275	0.8885814	2.967312	0.89311357	3.031853	0.897354
2.708941	0.8729295	2.773564	0.87852374	2.828133	0.8772783	2.893119	0.8823238	2.95807	0.88703797	3.022987	0.89145
2.698052	0.866056	2.763111	0.87186826	2.810943	0.87082772	2.876247	0.8760662	2.941499	0.88096237	3.006701	0.885547
2.680166	0.8591826	2.745584	0.86521278								

Table A.7: Maximum Power, Maximum Frequency and Maximum expected load at each level of Normalize voltage $\hat{v}$.

$\hat{v}$	Max. Power	Max. Frequency	Max. Load
1.0	1.948584073	0.031415927	0.513193151
1.1	1.461567576	0.305891703	0.827878245
1.2	1.417443975	0.398417548	1.015913168
1.3	1.426127436	0.495300602	1.185027339
1.4	1.456692076	0.533563819	1.345514287
1.5	1.498568802	0.583944955	1.501432565
1.6	1.546873979	0.626227482	1.654950587
1.7	1.599169246	0.662098982	1.80718833
1.8	1.654088175	0.692823402	1.958783122
1.9	1.711576638	0.705258476	2.109166437
2.0	1.770743457	0.729206141	2.258938179
2.1	1.83078292	0.750206148	2.408805518
2.2	1.891467209	0.768735653	2.558860115
2.3	1.952636505	0.785177592	2.709157586
2.4	2.014631983	0.789177802	2.859082973
2.5	2.077374547	0.802821587	3.008605266
2.6	2.140302049	0.815107924	3.158432709
2.7	2.203372318	0.826216241	3.308564758
2.8	2.266553158	0.836296787	3.458996747
2.9	2.32981971	0.845476205	3.609721373
3.0	2.393152588	0.853861896	3.760729694
3.1	2.456593171	0.853641369	3.911921645
3.2	2.52068241	0.860986072	4.062391977
3.3	2.584782734	0.867755591	4.213120065
3.4	2.648888527	0.874010362	4.364094555
3.5	2.712995366	0.879802941	4.515304431
3.6	2.777099761	0.885179226	4.666739085
3.7	2.841198962	0.890179452	4.818388358
3.8	2.905290807	0.894839017	4.970242554
3.9	2.969373604	0.899189177	5.122292453
4.0	3.033446039	0.903257615	5.274529296

Table A.8: Duty vs Power at the Normalized voltage $\hat{v}$ varying from 1.0 to 1.4

$\hat{v}$									
1.0		1.1		1.2		1.3		1.4	
Power	Duty	Power	Duty	Power	Duty	Power	Duty	Power	Duty
0.560354	0.22	0.626457	0.23	0.697533	0.24	0.773109	0.25	0.797236	0.25
0.61177	0.23	0.678752	0.24	0.750651	0.25	0.82691	0.26	0.852748	0.26
0.663186	0.24	0.730587	0.25	0.80292	0.26	0.879517	0.27	0.907039	0.27
0.714602	0.25	0.781915	0.26	0.854265	0.27	0.930834	0.28	0.95982	0.28
0.766018	0.26	0.832682	0.27	0.904597	0.28	0.980753	0.29	1.010979	0.29
0.817434	0.27	0.882826	0.28	0.953819	0.29	1.029155	0.3	1.060397	0.3
0.86885	0.28	0.932274	0.29	1.00182	0.3	1.075906	0.31	1.107937	0.31
0.920266	0.29	0.980943	0.3	1.048475	0.31	1.120855	0.32	1.153453	0.32
0.971681	0.3	1.028736	0.31	1.093637	0.32	1.163833	0.33	1.196781	0.33
1.023097	0.31	1.075538	0.32	1.137142	0.33	1.20465	0.34	1.237737	0.34
1.074513	0.32	1.121215	0.33	1.178799	0.34	1.24309	0.35	1.276119	0.35
1.125929	0.33	1.165605	0.34	1.218385	0.35	1.278907	0.36	1.311699	0.36
1.177345	0.34	1.208516	0.35	1.255642	0.36	1.31182	0.37	1.344223	0.37
1.228761	0.35	1.249714	0.36	1.290267	0.37	1.341505	0.38	1.373404	0.38
1.280177	0.36	1.288914	0.37	1.321899	0.38	1.367591	0.39	1.398919	0.39
1.331593	0.37	1.325762	0.38	1.350112	0.39	1.389646	0.4	1.420401	0.4
1.383009	0.38	1.359818	0.39	1.374392	0.4	1.407166	0.41	1.437432	0.41
1.434425	0.39	1.390524	0.4	1.394119	0.41	1.41956	0.42	1.449537	0.42
1.485841	0.4	1.417161	0.41	1.408534	0.42	1.426127	0.43	1.456168	0.43
1.537257	0.41	1.438791	0.42	1.4167	0.43	1.426037	0.44	1.456692	0.44
1.588673	0.42	1.454162	0.43	1.417444	0.44	1.41829	0.45	1.450378	0.45
1.640089	0.43	1.461568	0.44	1.409283	0.45	1.401677	0.46	1.43637	0.46
1.691504	0.44	1.458617	0.45	1.390307	0.46	1.374722	0.47	1.413665	0.47
1.74292	0.45	1.441858	0.46	1.358022	0.47	1.335597	0.48	1.381077	0.48
1.794336	0.46	1.406114	0.47	1.3091	0.48	1.282023	0.49	1.337194	0.49
1.845752	0.47	1.343247	0.48	1.239005	0.49	1.211108	0.5	1.280322	0.5
1.897168	0.48	1.239696	0.49	1.141382	0.5				
1.948584	0.49	1.071052	0.5						

Table A.9: Duty vs Power at the Normalized voltage $\hat{v}$ varying from 1.5 to 1.9

$\hat{v}$									
1.5		1.6		1.7		1.8		1.9	
Power	Duty	Power	Duty	Power	Duty	Power	Duty	Power	Duty
0.879792	0.26	0.907866	0.26	0.996743	0.27	1.088704	0.28	1.122564	0.28
0.936032	0.27	0.96601	0.27	1.055333	0.28	1.147348	0.29	1.183327	0.29
0.990585	0.28	1.022546	0.28	1.111877	0.29	1.20361	0.3	1.241644	0.3
1.04333	0.29	1.077108	0.29	1.166179	0.3	1.257368	0.31	1.297326	0.31
1.094146	0.3	1.129579	0.3	1.218114	0.31	1.308493	0.32	1.350247	0.32
1.142903	0.31	1.179829	0.31	1.26755	0.32	1.356846	0.33	1.400273	0.33
1.189455	0.32	1.22772	0.32	1.314341	0.33	1.402278	0.34	1.447262	0.34
1.233647	0.33	1.273103	0.33	1.358332	0.34	1.444632	0.35	1.491063	0.35
1.275305	0.34	1.315811	0.34	1.399355	0.35	1.483734	0.36	1.531512	0.36
1.314238	0.35	1.355669	0.35	1.437228	0.36	1.519402	0.37	1.568436	0.37
1.350239	0.36	1.392481	0.36	1.471755	0.37	1.551437	0.38	1.601651	0.38
1.383074	0.37	1.426035	0.37	1.502722	0.38	1.579625	0.39	1.630957	0.39
1.412487	0.38	1.456098	0.38	1.529896	0.39	1.603736	0.4	1.656141	0.4
1.438194	0.39	1.482414	0.39	1.553025	0.4	1.62352	0.41	1.676974	0.41
1.459876	0.4	1.504703	0.4	1.571833	0.41	1.638706	0.42	1.69321	0.42
1.477178	0.41	1.522655	0.41	1.586018	0.42	1.649002	0.43	1.704583	0.43
1.489703	0.42	1.535928	0.42	1.595251	0.43	1.654088	0.44	1.710809	0.44
1.497002	0.43	1.544141	0.43	1.599169	0.44	1.653617	0.45	1.711577	0.45
1.498569	0.44	1.546874	0.44	1.597374	0.45	1.64721	0.46	1.706553	0.46
1.493831	0.45	1.543657	0.45	1.589425	0.46	1.634452	0.47	1.695376	0.47
1.482137	0.46	1.533964	0.46	1.574837	0.47	1.614891	0.48	1.677653	0.48
1.462741	0.47	1.517207	0.47	1.553072	0.48	1.588028	0.49	1.652957	0.49
1.434787	0.48	1.492724	0.48	1.523531	0.49	1.553316	0.5	1.620823	0.5
1.397287	0.49	1.459767	0.49	1.485549	0.5				
1.349096	0.5	1.417489	0.5						

Table A.10: Duty vs Power at the Normalized voltage $\hat{v}$ varying from 2.0 to 2.4

$\hat{v}$									
2.0		2.1		2.2		2.3		2.4	
Power	Duty	Power	Duty	Power	Duty	Power	Duty	Power	Duty
1.219677	0.29	1.25634	0.29	1.293245	0.29	1.397247	0.3	1.436698	0.3
1.280124	0.3	1.318935	0.3	1.357997	0.3	1.461249	0.31	1.502823	0.31
1.337807	0.31	1.37868	0.31	1.419851	0.31	1.522001	0.32	1.565635	0.32
1.392605	0.32	1.435417	0.32	1.478575	0.32	1.579384	0.33	1.624961	0.33
1.444387	0.33	1.489019	0.33	1.534048	0.33	1.633274	0.34	1.680678	0.34
1.493017	0.34	1.539356	0.34	1.586141	0.34	1.683538	0.35	1.732661	0.35
1.53835	0.35	1.586286	0.35	1.634719	0.35	1.73004	0.36	1.780775	0.36
1.580231	0.36	1.629662	0.36	1.679638	0.36	1.772634	0.37	1.82488	0.37
1.618495	0.37	1.669327	0.37	1.72075	0.37	1.811169	0.38	1.86483	0.38
1.652968	0.38	1.705115	0.38	1.757896	0.38	1.845485	0.39	1.900471	0.39
1.683463	0.39	1.736849	0.39	1.790907	0.39	1.875412	0.4	1.931642	0.4
1.709781	0.4	1.764343	0.4	1.819606	0.4	1.900772	0.41	1.958172	0.41
1.731709	0.41	1.787397	0.41	1.843807	0.41	1.921379	0.42	1.979883	0.42
1.749022	0.42	1.805801	0.42	1.86331	0.42	1.937033	0.43	1.996588	0.43
1.761475	0.43	1.819329	0.43	1.877905	0.43	1.947526	0.44	2.008088	0.44
1.768809	0.44	1.827742	0.44	1.88737	0.44	1.952637	0.45	2.014176	0.45
1.770743	0.45	1.830783	0.45	1.891467	0.45	1.95213	0.46	2.014632	0.46
1.76698	0.46	1.82818	0.46	1.889945	0.46	1.94576	0.47	2.009225	0.47
1.757194	0.47	1.81964	0.47	1.882536	0.47	1.933262	0.48	1.99771	0.48
1.741041	0.48	1.804852	0.48	1.868956	0.48	1.914359	0.49	1.97983	0.49
1.718143	0.49	1.78348	0.49	1.8489	0.49	1.888755	0.5	1.955311	0.5
1.688098	0.5	1.755166	0.5	1.822045	0.5				

Table A.11: Duty vs Power at the Normalized voltage $\hat{v}$ varying from 2.5 to 2.9

$\hat{v}$									
2.5		2.6		2.7		2.8		2.9	
Power	Duty	Power	Duty	Power	Duty	Power	Duty	Power	Duty
1.476245	0.3	1.58635	0.31	1.62828	0.31	1.670263	0.31	1.78563	0.32
1.544532	0.31	1.653352	0.32	1.697373	0.32	1.741471	0.32	1.854995	0.33
1.60943	0.32	1.716639	0.33	1.76267	0.33	1.808796	0.33	1.920175	0.34
1.670725	0.33	1.776089	0.34	1.824016	0.34	1.872052	0.34	1.981057	0.35
1.728298	0.34	1.83158	0.35	1.88129	0.35	1.931123	0.35	2.037523	0.36
1.782024	0.35	1.882987	0.36	1.934369	0.36	1.98589	0.36	2.089449	0.37
1.831775	0.36	1.930177	0.37	1.983126	0.37	2.036226	0.37	2.136709	0.38
1.877413	0.37	1.973013	0.38	2.027427	0.38	2.082002	0.38	2.17917	0.39
1.918798	0.38	2.011352	0.39	2.067132	0.39	2.123081	0.39	2.216695	0.4
1.955782	0.39	2.045043	0.4	2.102096	0.4	2.159324	0.4	2.249142	0.41
1.988208	0.4	2.073931	0.41	2.132167	0.41	2.190582	0.41	2.276363	0.42
2.015914	0.41	2.09785	0.42	2.157189	0.42	2.216704	0.42	2.298205	0.43
2.03873	0.42	2.116631	0.43	2.176996	0.43	2.237532	0.43	2.314506	0.44
2.056477	0.43	2.130093	0.44	2.191417	0.44	2.252898	0.44	2.325102	0.45
2.068966	0.44	2.138049	0.45	2.200271	0.45	2.262632	0.45	2.32982	0.46
2.076001	0.45	2.140302	0.46	2.203372	0.46	2.266553	0.46	2.328478	0.47
2.077375	0.46	2.136646	0.47	2.200523	0.47	2.264474	0.47	2.320891	0.48
2.072869	0.47	2.126866	0.48	2.191519	0.48	2.256199	0.48	2.306863	0.49
2.062255	0.48	2.110733	0.49	2.176145	0.49	2.241523	0.49	2.28619	0.5
2.045292	0.49	2.08801	0.5	2.154177	0.5	2.220234	0.5		
2.021725	0.5								

Table A.12: Duty vs Power at the Normalized voltage $\hat{v}$ varying from 3.0 to 3.4

$\hat{v}$									
3.0		3.1		3.2		3.3		3.4	
Power	Duty	Power	Duty	Power	Duty	Power	Duty	Power	Duty
1.829855	0.32	1.874116	0.32	1.9184	0.32	2.040264	0.33	2.086666	0.33
1.901253	0.33	1.947556	0.33	1.993896	0.33	2.113244	0.34	2.161602	0.34
1.968369	0.34	2.016619	0.34	2.064914	0.34	2.181464	0.35	2.231676	0.35
2.031073	0.35	2.081154	0.35	2.131288	0.35	2.244814	0.36	2.296763	0.36
2.089247	0.36	2.141046	0.36	2.192905	0.36	2.303179	0.37	2.356753	0.37
2.142772	0.37	2.196178	0.37	2.249651	0.37	2.356441	0.38	2.411528	0.38
2.191524	0.38	2.246428	0.38	2.301404	0.38	2.40448	0.39	2.46097	0.39
2.235372	0.39	2.291669	0.39	2.348042	0.39	2.447168	0.4	2.504955	0.4
2.274184	0.4	2.331771	0.4	2.389436	0.4	2.484378	0.41	2.543357	0.41
2.307821	0.41	2.366598	0.41	2.425455	0.41	2.515976	0.42	2.576044	0.42
2.336139	0.42	2.396011	0.42	2.455961	0.42	2.541823	0.43	2.602882	0.43
2.358989	0.43	2.419864	0.43	2.480813	0.43	2.561777	0.44	2.623732	0.44
2.376216	0.44	2.438008	0.44	2.499866	0.44	2.575691	0.45	2.638449	0.45
2.387659	0.45	2.450286	0.45	2.512966	0.45	2.583412	0.46	2.646886	0.46
2.393153	0.46	2.456537	0.46	2.519959	0.46	2.584783	0.47	2.648889	0.47
2.392522	0.47	2.456593	0.47	2.520682	0.47	2.579641	0.48	2.644299	0.48
2.385588	0.48	2.450282	0.48	2.514967	0.48	2.567817	0.49	2.632954	0.49
2.372163	0.49	2.437422	0.49	2.50264	0.49	2.549138	0.5	2.614685	0.5
2.352052	0.5	2.417827	0.5	2.483521	0.5				

Table A.13: Duty vs Power at the Normalized voltage $\hat{v}$ varying from 3.5 to 4.0

$\hat{v}$											
3.5		3.6		3.7		3.8		3.9		4.0	
Power	Duty	Power	Duty	Power	Duty	Power	Duty	Power	Duty	Power	Duty
2.133081	0.33	2.179505	0.33	2.306786	0.34	2.355205	0.34	2.403634	0.34	2.452064	0.34
2.209982	0.34	2.258378	0.34	2.382451	0.35	2.43274	0.35	2.483038	0.35	2.533343	0.35
2.281914	0.35	2.332174	0.35	2.452781	0.36	2.504826	0.36	2.556884	0.36	2.608951	0.36
2.348745	0.36	2.400753	0.36	2.517669	0.37	2.571354	0.37	2.625055	0.37	2.678767	0.37
2.410363	0.37	2.464004	0.37	2.577004	0.38	2.632215	0.38	2.687443	0.38	2.742686	0.38
2.466655	0.38	2.521816	0.38	2.630672	0.39	2.687295	0.39	2.743937	0.39	2.800596	0.39
2.517503	0.39	2.574073	0.39	2.678554	0.4	2.736479	0.4	2.794424	0.4	2.852385	0.4
2.562786	0.4	2.620655	0.4	2.720532	0.41	2.779648	0.41	2.838785	0.41	2.897938	0.41
2.60238	0.41	2.661441	0.41	2.75648	0.42	2.816681	0.42	2.876901	0.42	2.937136	0.42
2.636156	0.42	2.696304	0.42	2.786272	0.43	2.847452	0.43	2.908649	0.43	2.969859	0.43
2.663982	0.43	2.725114	0.43	2.809777	0.44	2.871833	0.44	2.933902	0.44	2.99598	0.44
2.685721	0.44	2.747738	0.44	2.826859	0.45	2.889691	0.45	2.95253	0.45	3.015373	0.45
2.701234	0.45	2.764039	0.45	2.837381	0.46	2.90089	0.46	2.964399	0.46	3.027907	0.46
2.710375	0.46	2.773875	0.46	2.841199	0.47	2.905291	0.47	2.969374	0.47	3.033446	0.47
2.712995	0.47	2.7771	0.47	2.838167	0.48	2.90275	0.48	2.967312	0.48	3.031853	0.48
2.708941	0.48	2.773564	0.48	2.828133	0.49	2.893119	0.49	2.95807	0.49	3.022987	0.49
2.698052	0.49	2.763111	0.49	2.810943	0.5	2.876247	0.5	2.941499	0.5	3.006701	0.5
2.680166	0.5	2.745584	0.5								

Table A.14: Maximum Power and Maximum Duty at each level of Normalize voltage $\hat{v}$.

$\hat{v}$	Max.Power	Duty
1.0	1.948584073	0.49
1.1	1.461567576	0.44
1.2	1.417443975	0.44
1.3	1.426127436	0.43
1.4	1.456692076	0.44
1.5	1.498568802	0.44
1.6	1.546873979	0.44
1.7	1.599169246	0.44
1.8	1.654088175	0.44
1.9	1.711576638	0.45
2.0	1.770743457	0.45
2.1	1.83078292	0.45
2.2	1.891467209	0.45
2.3	1.952636505	0.45
2.4	2.014631983	0.46
2.5	2.077374547	0.46
2.6	2.140302049	0.46
2.7	2.203372318	0.46
2.8	2.266553158	0.46
2.9	2.32981971	0.46
3.0	2.393152588	0.46
3.1	2.456593171	0.47
3.2	2.52068241	0.47
3.3	2.584782734	0.47
3.4	2.648888527	0.47
3.5	2.712995366	0.47
3.6	2.777099761	0.47
3.7	2.841198962	0.47
3.8	2.905290807	0.47
3.9	2.969373604	0.47
4.0	3.033446039	0.47

Appendix B

Tables of Series Resonant Converter Data

B.1 Introduction

This appendix illustrates in detailed form the data retrieved from the steady-state model of the SRC. The same data were used to generate the polynomial model through numerical analysis i.e B-spline and Data fitting. The data shown in this appendix are the illustration of the switching period versus the converter output voltage $\hat{v}$, in presence of the initial resonant current $\hat{I_0}$. The data are in normalized values. As well as the normalized power $\hat{p}$ versus the initial resonant current $\hat{I_0}$, in the presence of normalized output voltage $\hat{v}$. The complete process is detailed in the tables illustrated in this appendix.

Table B.1: Period vs Normalized output voltage $\hat{v}$ from 0.00 to 0.39 in Presence of $\hat{I}_o$ from –0.01 to –0.09.

	$\hat{I}_0$								
	-0.01	-0.02	-0.03	-0.04	-0.05	-0.06	-0.07	-0.08	-0.09
$\hat{v}$	Period								
0.00	0.006366	0.019084	0.025431	0.031765	0.038083	0.044383	0.050662	0.056916	0.063143
0.01	0.006366	0.019086	0.025433	0.031768	0.038087	0.044388	0.050667	0.056921	0.063149
0.02	0.006368	0.019092	0.025441	0.031778	0.038099	0.044401	0.050682	0.056938	0.063168
0.03	0.006371	0.019101	0.025454	0.031794	0.038118	0.044423	0.050707	0.056966	0.063199
0.04	0.006376	0.019115	0.025472	0.031816	0.038144	0.044454	0.050742	0.057006	0.063242
0.05	0.006382	0.019132	0.025494	0.031844	0.038178	0.044493	0.050787	0.057056	0.063298
0.06	0.006389	0.019153	0.025523	0.031879	0.03822	0.044542	0.050842	0.057118	0.063366
0.07	0.006397	0.019178	0.025556	0.031921	0.03827	0.0446	0.050908	0.057191	0.063448
0.08	0.006407	0.019207	0.025594	0.031969	0.038327	0.044666	0.050984	0.057276	0.063541
0.09	0.006418	0.01924	0.025638	0.032023	0.038392	0.044742	0.05107	0.057373	0.063648
0.10	0.00643	0.019277	0.025687	0.032084	0.038465	0.044827	0.051167	0.057481	0.063768
0.11	0.006444	0.019318	0.025741	0.032152	0.038546	0.044921	0.051274	0.057601	0.0639
0.12	0.006459	0.019363	0.025801	0.032227	0.038636	0.045025	0.051392	0.057733	0.064046
0.13	0.006475	0.019412	0.025867	0.032308	0.038733	0.045138	0.051521	0.057878	0.064206
0.14	0.006493	0.019465	0.025938	0.032397	0.038839	0.045261	0.051661	0.058034	0.064379
0.15	0.006512	0.019523	0.026014	0.032492	0.038953	0.045394	0.051812	0.058203	0.064566
0.16	0.006533	0.019585	0.026097	0.032595	0.039076	0.045537	0.051974	0.058385	0.064767
0.17	0.006555	0.019651	0.026185	0.032705	0.039208	0.04569	0.052148	0.05858	0.064982
0.18	0.006579	0.019722	0.026279	0.032823	0.039348	0.045853	0.052334	0.058788	0.065212
0.19	0.006604	0.019798	0.02638	0.032948	0.039498	0.046027	0.052532	0.05901	0.065457
0.20	0.006631	0.019878	0.026487	0.033081	0.039657	0.046212	0.052743	0.059245	0.065717
0.21	0.006659	0.019963	0.0266	0.033222	0.039826	0.046408	0.052966	0.059494	0.065992
0.22	0.006689	0.020053	0.02672	0.033371	0.040004	0.046616	0.053201	0.059758	0.066284
0.23	0.006721	0.020148	0.026846	0.033529	0.040193	0.046835	0.05345	0.060037	0.066591
0.24	0.006755	0.020248	0.026979	0.033695	0.040392	0.047065	0.053713	0.060331	0.066916
0.25	0.00679	0.020354	0.02712	0.03387	0.040601	0.047308	0.053989	0.06064	0.067257
0.26	0.006827	0.020465	0.027268	0.034054	0.040821	0.047564	0.05428	0.060965	0.067616
0.27	0.006866	0.020582	0.027423	0.034248	0.041052	0.047833	0.054585	0.061307	0.067994
0.28	0.006907	0.020704	0.027586	0.034451	0.041295	0.048115	0.054906	0.061665	0.06839
0.29	0.00695	0.020833	0.027757	0.034664	0.04155	0.04841	0.055242	0.062041	0.068805
0.30	0.006995	0.020967	0.027936	0.034887	0.041817	0.04872	0.055594	0.062435	0.06924
0.31	0.007042	0.021109	0.028124	0.035121	0.042096	0.049045	0.055963	0.062848	0.069695
0.32	0.007092	0.021256	0.02832	0.035366	0.042389	0.049385	0.05635	0.06328	0.070172
0.33	0.007143	0.021411	0.028526	0.035622	0.042695	0.04974	0.056754	0.063732	0.07067
0.34	0.007198	0.021573	0.028741	0.03589	0.043015	0.050112	0.057176	0.064204	0.071191
0.35	0.007254	0.021742	0.028966	0.03617	0.04335	0.050501	0.057618	0.064698	0.071736
0.36	0.007313	0.021919	0.029201	0.036463	0.0437	0.050907	0.058079	0.065214	0.072305
0.37	0.007375	0.022104	0.029447	0.036769	0.044066	0.051331	0.058562	0.065753	0.0729
0.38	0.00744	0.022297	0.029704	0.037089	0.044448	0.051775	0.059065	0.066316	0.073521
0.39	0.007507	0.022499	0.029972	0.037423	0.044847	0.052238	0.059592	0.066904	0.074169

Table B.2: Period vs Normalized output voltage $\hat{v}$ from 0.40 to 0.79 in Presence of $\hat{I}_o$ from –0.01 to –0.09.

	$\hat{I}_0$								
	-0.01	-0.02	-0.03	-0.04	-0.05	-0.06	-0.07	-0.08	-0.09
$\hat{v}$	Period								
0.40	0.007578	0.02271	0.030253	0.037773	0.045264	0.052722	0.060141	0.067518	0.074847
0.41	0.007652	0.022931	0.030546	0.038138	0.0457	0.053228	0.060715	0.068159	0.075554
0.42	0.007729	0.023161	0.030852	0.038519	0.046155	0.053756	0.061315	0.068829	0.076292
0.43	0.007809	0.023402	0.031172	0.038917	0.046631	0.054307	0.061941	0.069528	0.077063
0.44	0.007893	0.023653	0.031507	0.039333	0.047128	0.054884	0.062596	0.070259	0.077868
0.45	0.007982	0.023917	0.031856	0.039769	0.047647	0.055486	0.063279	0.071022	0.078708
0.46	0.008074	0.024192	0.032222	0.040224	0.04819	0.056116	0.063994	0.071819	0.079587
0.47	0.00817	0.02448	0.032604	0.040699	0.048758	0.056774	0.06474	0.072652	0.080505
0.48	0.008271	0.024781	0.033004	0.041197	0.049352	0.057462	0.065521	0.073524	0.081464
0.49	0.008376	0.025096	0.033423	0.041718	0.049973	0.058182	0.066338	0.074434	0.082467
0.50	0.008487	0.025426	0.033861	0.042263	0.050624	0.058936	0.067192	0.075387	0.083515
0.51	0.008603	0.025772	0.034321	0.042834	0.051305	0.059725	0.068087	0.076385	0.084613
0.52	0.008724	0.026134	0.034802	0.043433	0.052018	0.060551	0.069023	0.077429	0.085761
0.53	0.008851	0.026514	0.035306	0.04406	0.052766	0.061417	0.070005	0.078522	0.086964
0.54	0.008985	0.026913	0.035836	0.044718	0.053551	0.062325	0.071033	0.079669	0.088224
0.55	0.009125	0.027332	0.036392	0.045409	0.054374	0.063278	0.072112	0.08087	0.089545
0.56	0.009273	0.027772	0.036976	0.046135	0.055238	0.064278	0.073245	0.082131	0.090931
0.57	0.009428	0.028235	0.03759	0.046897	0.056147	0.065329	0.074435	0.083456	0.092385
0.58	0.009591	0.028722	0.038236	0.0477	0.057103	0.066434	0.075685	0.084847	0.093913
0.59	0.009763	0.029235	0.038916	0.048545	0.058108	0.067597	0.077	0.08631	0.095519
0.60	0.009945	0.029776	0.039633	0.049435	0.059168	0.068821	0.078384	0.087849	0.097208
0.61	0.010136	0.030346	0.04039	0.050374	0.060285	0.070112	0.079843	0.089471	0.098986
0.62	0.010339	0.030949	0.041189	0.051366	0.061465	0.071474	0.081382	0.09118	0.10086
0.63	0.010553	0.031587	0.042035	0.052414	0.062711	0.072912	0.083007	0.092984	0.102837
0.64	0.01078	0.032263	0.042929	0.053523	0.064029	0.074434	0.084724	0.09489	0.104924
0.65	0.01102	0.032979	0.043878	0.054699	0.065426	0.076044	0.086541	0.096906	0.107131
0.66	0.011276	0.033739	0.044885	0.055946	0.066907	0.077751	0.088466	0.09904	0.109466
0.67	0.011548	0.034548	0.045955	0.057272	0.06848	0.079563	0.090508	0.101303	0.11194
0.68	0.011838	0.035409	0.047094	0.058682	0.070153	0.08149	0.092678	0.103706	0.114565
0.69	0.012147	0.036328	0.04831	0.060185	0.071935	0.08354	0.094986	0.10626	0.117354
0.70	0.012478	0.03731	0.049608	0.061791	0.073837	0.085727	0.097446	0.108981	0.120323
0.71	0.012832	0.038362	0.050997	0.063508	0.07587	0.088063	0.100071	0.111882	0.123486
0.72	0.013213	0.039491	0.052488	0.065349	0.078048	0.090563	0.102879	0.114982	0.126864
0.73	0.013622	0.040705	0.05409	0.067326	0.080385	0.093245	0.105888	0.118301	0.130476
0.74	0.014064	0.042014	0.055816	0.069455	0.082899	0.096126	0.109118	0.121861	0.134348
0.75	0.014543	0.04343	0.057681	0.071752	0.08561	0.09923	0.112594	0.125688	0.138507
0.76	0.015062	0.044964	0.059702	0.074239	0.088541	0.102582	0.116343	0.129812	0.142984
0.77	0.015627	0.046633	0.061897	0.076937	0.091718	0.106211	0.120398	0.134268	0.147816
0.78	0.016245	0.048453	0.064289	0.079876	0.095173	0.110153	0.124796	0.139094	0.153044
0.79	0.016922	0.050447	0.066906	0.083085	0.098942	0.114446	0.129581	0.144338	0.158718

Table B.3: Period vs Normalized output voltage $\hat{v}$ from 0.79 to 0.99 in Presence of $\hat{I}_o$ from –0.01 to –0.09.

	$\hat{I}_0$								
	-0.01	-0.02	-0.03	-0.04	-0.05	-0.06	-0.07	-0.08	-0.09
$\hat{v}$	Period								
0.80	0.017668	0.052639	0.06978	0.086605	0.103068	0.11914	0.134803	0.150054	0.164896
0.81	0.018494	0.055061	0.072949	0.09048	0.107603	0.124289	0.140525	0.156308	0.171647
0.82	0.019412	0.057748	0.076461	0.094764	0.112608	0.129963	0.146818	0.163177	0.179054
0.83	0.020439	0.060745	0.080371	0.099526	0.118158	0.136242	0.15377	0.170754	0.187215
0.84	0.021595	0.06411	0.08475	0.104846	0.124345	0.143226	0.16149	0.179155	0.196252
0.85	0.022906	0.067912	0.089685	0.110826	0.131282	0.151039	0.170109	0.188521	0.206319
0.86	0.024405	0.07224	0.095286	0.117592	0.13911	0.159835	0.179793	0.199031	0.217604
0.87	0.026134	0.077209	0.101696	0.125309	0.148009	0.169808	0.190755	0.210912	0.230357
0.88	0.028152	0.08297	0.109096	0.134184	0.15821	0.181214	0.203268	0.224465	0.244901
0.89	0.030535	0.089724	0.117732	0.144495	0.170022	0.194387	0.217701	0.24009	0.261681
0.90	0.033393	0.097745	0.127931	0.156617	0.183858	0.209784	0.234558	0.258349	0.281324
0.91	0.036881	0.107419	0.140152	0.171066	0.200296	0.228051	0.254562	0.280059	0.304761
0.92	0.04123	0.1193	0.155052	0.188592	0.22018	0.250141	0.278804	0.306484	0.333481
0.93	0.046804	0.134227	0.173615	0.210321	0.244804	0.277558	0.309057	0.339754	0.370105
0.94	0.054196	0.153516	0.1974	0.238075	0.276321	0.312898	0.348535	0.383985	0.420146
0.95	0.064457	0.179397	0.229082	0.275092	0.318757	0.361353	0.404274	0.449456	0.500718
0.96	0.079623	0.216035	0.273873	0.328132	0.38137	0.436736	0.500468	0.631583	
0.97	0.104208	0.272663	0.344534	0.416614	0.500269				
0.98	0.150528	0.378793	0.500122						
0.99	0.270268	0.500031							

Table B.4: Period vs Normalized output voltage $\hat{v}$ from 0.00 to 0.39 in Presence of $\hat{I}_o$ from –0.10 to –0.18.

	$\hat{I}_0$								
	-0.10	-0.11	-0.12	-0.13	-0.14	-0.15	-0.16	-0.17	-0.18
$\hat{v}$	Period								
0.00	0.06934	0.075505	0.081636	0.08773	0.093785	0.0998	0.105771	0.111698	0.11758
0.01	0.069347	0.075513	0.081644	0.087739	0.093795	0.09981	0.105782	0.11171	0.117592
0.02	0.069367	0.075535	0.081668	0.087764	0.093822	0.099839	0.105813	0.111742	0.117626
0.03	0.069401	0.075572	0.081708	0.087807	0.093867	0.099887	0.105863	0.111796	0.117682
0.04	0.069449	0.075623	0.081763	0.087866	0.093931	0.099954	0.105934	0.11187	0.11776
0.05	0.06951	0.07569	0.081835	0.087943	0.094012	0.10004	0.106025	0.111966	0.11786
0.06	0.069585	0.075771	0.081922	0.088036	0.094111	0.100145	0.106136	0.112083	0.117983
0.07	0.069674	0.075867	0.082026	0.088147	0.094229	0.10027	0.106268	0.112221	0.118127
0.08	0.069776	0.075978	0.082145	0.088275	0.094365	0.100414	0.10642	0.11238	0.118295
0.09	0.069893	0.076105	0.082282	0.088421	0.09452	0.100578	0.106593	0.112562	0.118485
0.10	0.070024	0.076247	0.082434	0.088584	0.094694	0.100762	0.106786	0.112765	0.118697
0.11	0.070169	0.076404	0.082603	0.088765	0.094886	0.100966	0.107001	0.112991	0.118933
0.12	0.070328	0.076577	0.08279	0.088964	0.095098	0.10119	0.107237	0.113239	0.119193
0.13	0.070503	0.076766	0.082993	0.089181	0.095329	0.101434	0.107495	0.113509	0.119476
0.14	0.070692	0.076971	0.083214	0.089417	0.09558	0.1017	0.107775	0.113803	0.119783
0.15	0.070896	0.077193	0.083452	0.089672	0.095851	0.101986	0.108076	0.11412	0.120115
0.16	0.071116	0.077431	0.083708	0.089946	0.096142	0.102294	0.108401	0.11446	0.120471
0.17	0.071351	0.077686	0.083982	0.090239	0.096454	0.102624	0.108748	0.114825	0.120852
0.18	0.071603	0.077958	0.084275	0.090552	0.096787	0.102976	0.109119	0.115214	0.121259
0.19	0.07187	0.078248	0.084587	0.090886	0.097141	0.103351	0.109514	0.115628	0.121692
0.20	0.072155	0.078556	0.084918	0.091239	0.097517	0.103749	0.109933	0.116068	0.122152
0.21	0.072456	0.078882	0.085269	0.091614	0.097915	0.10417	0.110377	0.116534	0.122639
0.22	0.072774	0.079227	0.08564	0.092011	0.098337	0.104616	0.110846	0.117026	0.123154
0.23	0.07311	0.079592	0.086032	0.092429	0.098781	0.105086	0.111341	0.117545	0.123697
0.24	0.073465	0.079976	0.086445	0.092871	0.09925	0.105581	0.111863	0.118092	0.124269
0.25	0.073838	0.08038	0.08688	0.093335	0.099743	0.106103	0.112412	0.118668	0.124871
0.26	0.074231	0.080805	0.087336	0.093823	0.100262	0.106651	0.112989	0.119273	0.125503
0.27	0.074643	0.081251	0.087816	0.094335	0.100806	0.107226	0.113594	0.119908	0.126167
0.28	0.075075	0.08172	0.08832	0.094873	0.101377	0.10783	0.11423	0.120574	0.126862
0.29	0.075529	0.082211	0.088847	0.095436	0.101976	0.108462	0.114895	0.121272	0.127591
0.30	0.076004	0.082725	0.0894	0.096027	0.102602	0.109125	0.115592	0.122002	0.128355
0.31	0.076501	0.083263	0.089979	0.096644	0.103258	0.109818	0.116321	0.122767	0.129153
0.32	0.077022	0.083827	0.090584	0.097291	0.103944	0.110542	0.117083	0.123566	0.129987
0.33	0.077566	0.084416	0.091217	0.097966	0.104661	0.1113	0.11788	0.124401	0.130859
0.34	0.078135	0.085032	0.091878	0.098672	0.105411	0.112091	0.118713	0.125273	0.13177
0.35	0.07873	0.085675	0.09257	0.09941	0.106193	0.112918	0.119582	0.126183	0.132721
0.36	0.079351	0.086348	0.093291	0.10018	0.10701	0.113781	0.120489	0.127134	0.133713
0.37	0.08	0.08705	0.094045	0.100984	0.107864	0.114682	0.121436	0.128125	0.134748
0.38	0.080678	0.087783	0.094832	0.101823	0.108754	0.115621	0.122424	0.12916	0.135827
0.39	0.081385	0.088548	0.095653	0.102699	0.109683	0.116602	0.123454	0.130239	0.136953

Table B.5: Period vs Normalized output voltage $\hat{v}$ from 0.40 to 0.79 in Presence of $\hat{I}_o$ from –0.10 to –0.18.

	$\hat{I}_0$								
	-0.10	-0.11	-0.12	-0.13	-0.14	-0.15	-0.16	-0.17	-0.18
$\hat{v}$	Period								
0.40	0.082124	0.089346	0.096511	0.103613	0.110652	0.117625	0.124529	0.131364	0.138127
0.41	0.082895	0.09018	0.097405	0.104567	0.111663	0.118692	0.12565	0.132537	0.139351
0.42	0.0837	0.091051	0.098339	0.105562	0.112719	0.119805	0.126819	0.13376	0.140627
0.43	0.084541	0.091959	0.099313	0.106601	0.113819	0.120966	0.128038	0.135036	0.141957
0.44	0.085419	0.092907	0.10033	0.107685	0.114968	0.122177	0.12931	0.136366	0.143344
0.45	0.086335	0.093897	0.101392	0.108816	0.116166	0.12344	0.130636	0.137753	0.14479
0.46	0.087292	0.094931	0.1025	0.109996	0.117416	0.124758	0.13202	0.1392	0.146297
0.47	0.088292	0.096011	0.103658	0.111229	0.118721	0.126134	0.133463	0.140709	0.14787
0.48	0.089337	0.097139	0.104867	0.112516	0.120084	0.127569	0.134969	0.142283	0.14951
0.49	0.090429	0.098318	0.10613	0.11386	0.121507	0.129068	0.136542	0.143926	0.151221
0.50	0.091571	0.099551	0.107449	0.115265	0.122993	0.130633	0.138183	0.145641	0.153007
0.51	0.092766	0.100839	0.108829	0.116732	0.124546	0.132268	0.139897	0.147431	0.154871
0.52	0.094016	0.102187	0.110272	0.118267	0.12617	0.133977	0.141688	0.149302	0.156817
0.53	0.095324	0.103598	0.111782	0.119873	0.127867	0.135763	0.14356	0.151256	0.158851
0.54	0.096695	0.105076	0.113363	0.121553	0.129643	0.137632	0.145517	0.153298	0.160976
0.55	0.098131	0.106624	0.115018	0.123312	0.131502	0.139586	0.147564	0.155435	0.163197
0.56	0.099637	0.108246	0.116753	0.125154	0.133448	0.141633	0.149707	0.15767	0.165521
0.57	0.101218	0.109948	0.118572	0.127086	0.135488	0.143777	0.151951	0.16001	0.167954
0.58	0.102877	0.111734	0.12048	0.129111	0.137627	0.146024	0.154302	0.162461	0.170501
0.59	0.10462	0.11361	0.122483	0.131238	0.13987	0.14838	0.156767	0.16503	0.17317
0.60	0.106454	0.115582	0.124589	0.133471	0.142226	0.150854	0.159353	0.167725	0.175969
0.61	0.108383	0.117656	0.126802	0.135818	0.144701	0.153451	0.162069	0.170553	0.178906
0.62	0.110415	0.11984	0.129132	0.138287	0.147304	0.156182	0.164922	0.173524	0.18199
0.63	0.112558	0.122142	0.131586	0.140887	0.150043	0.159055	0.167923	0.176648	0.185232
0.64	0.114819	0.12457	0.134173	0.143626	0.152929	0.162081	0.171082	0.179936	0.188643
0.65	0.117208	0.127134	0.136904	0.146517	0.155972	0.165269	0.174411	0.183398	0.192234
0.66	0.119735	0.129844	0.139789	0.149569	0.159184	0.168634	0.177922	0.187049	0.19602
0.67	0.122411	0.132713	0.142842	0.152797	0.162579	0.172189	0.18163	0.190904	0.200015
0.68	0.125249	0.135753	0.146074	0.156214	0.166171	0.175949	0.185549	0.194977	0.204236
0.69	0.128262	0.138978	0.149503	0.159835	0.169977	0.17993	0.189699	0.199289	0.208703
0.70	0.131466	0.142407	0.153144	0.163679	0.174014	0.184153	0.194099	0.203858	0.213435
0.71	0.134878	0.146056	0.157018	0.167766	0.178305	0.188637	0.19877	0.208707	0.218457
0.72	0.138519	0.149946	0.161145	0.172118	0.182871	0.193409	0.203737	0.213864	0.223796
0.73	0.14241	0.1541	0.165549	0.176761	0.18774	0.198494	0.209029	0.219356	0.229481
0.74	0.146577	0.158546	0.170259	0.181722	0.192941	0.203923	0.214679	0.225217	0.235548
0.75	0.151048	0.163313	0.175307	0.187036	0.198508	0.209734	0.220723	0.231487	0.242036
0.76	0.155858	0.168437	0.180728	0.192739	0.204481	0.215966	0.227204	0.23821	0.248994
0.77	0.161043	0.173957	0.186564	0.198876	0.210906	0.222667	0.234172	0.245437	0.256474
0.78	0.166649	0.179919	0.192864	0.205498	0.217836	0.229893	0.241686	0.25323	0.264542
0.79	0.172728	0.186379	0.199686	0.212664	0.225333	0.237711	0.249814	0.261663	0.273274

Table B.6: Period vs Normalized output voltage $\hat{v}$ from 0.80 to 0.95 in Presence of $\hat{I}_o$ from –0.10 to –0.18.

	$\hat{I}_0$								
	-0.10	-0.11	-0.12	-0.13	-0.14	-0.15	-0.16	-0.17	-0.18
$\hat{v}$	Period								
0.80	0.17934	0.1934	0.207096	0.220447	0.233474	0.246198	0.258641	0.270823	0.282764
0.81	0.186558	0.20106	0.215176	0.228929	0.242346	0.25545	0.268265	0.280816	0.293125
0.82	0.19447	0.20945	0.224022	0.238216	0.25206	0.265583	0.278812	0.291775	0.304497
0.83	0.20318	0.218682	0.233754	0.248432	0.26275	0.27674	0.290435	0.303866	0.317061
0.84	0.212819	0.228894	0.24452	0.259737	0.274586	0.289105	0.303332	0.317302	0.331049
0.85	0.223548	0.24026	0.256505	0.27233	0.287785	0.302913	0.317759	0.332364	0.346769
0.86	0.235574	0.253002	0.269949	0.286474	0.302632	0.318477	0.334061	0.349435	0.36465
0.87	0.249164	0.267411	0.285172	0.302517	0.319513	0.336225	0.352719	0.369058	0.38531
0.88	0.264675	0.28388	0.302607	0.320943	0.338972	0.356775	0.374438	0.392048	0.409703
0.89	0.282597	0.302957	0.322873	0.342456	0.361814	0.381062	0.40032	0.419728	0.439452
0.90	0.303639	0.325448	0.346897	0.368137	0.389324	0.410635	0.432281	0.454537	0.477784
0.91	0.328878	0.352615	0.376183	0.399814	0.42378	0.448435	0.474286	0.502165	0.533712
0.92	0.360093	0.386636	0.413471	0.441066	0.4701	0.50174	0.538538	0.590078	
0.93	0.400615	0.431916	0.464937	0.501356	0.54535	0.64435			
0.94	0.458329	0.501014	0.555587						
0.95	0.573022								

Table B.7: Period vs Normalized output voltage $\hat{v}$ from 0.00 to 0.39 in Presence of $\hat{I}_o$ from –0.10 to –0.18.

	$\hat{I}_0$								
	-0.10	-0.11	-0.12	-0.13	-0.14	-0.15	-0.16	-0.17	-0.18
$\hat{v}$	Period								
0.00	0.06934	0.075505	0.081636	0.08773	0.093785	0.0998	0.105771	0.111698	0.11758
0.01	0.069347	0.075513	0.081644	0.087739	0.093795	0.09981	0.105782	0.11171	0.117592
0.02	0.069367	0.075535	0.081668	0.087764	0.093822	0.099839	0.105813	0.111742	0.117626
0.03	0.069401	0.075572	0.081708	0.087807	0.093867	0.099887	0.105863	0.111796	0.117682
0.04	0.069449	0.075623	0.081763	0.087866	0.093931	0.099954	0.105934	0.11187	0.11776
0.05	0.06951	0.07569	0.081835	0.087943	0.094012	0.10004	0.106025	0.111966	0.11786
0.06	0.069585	0.075771	0.081922	0.088036	0.094111	0.100145	0.106136	0.112083	0.117983
0.07	0.069674	0.075867	0.082026	0.088147	0.094229	0.10027	0.106268	0.112221	0.118127
0.08	0.069776	0.075978	0.082145	0.088275	0.094365	0.100414	0.10642	0.11238	0.118295
0.09	0.069893	0.076105	0.082282	0.088421	0.09452	0.100578	0.106593	0.112562	0.118485
0.10	0.070024	0.076247	0.082434	0.088584	0.094694	0.100762	0.106786	0.112765	0.118697
0.11	0.070169	0.076404	0.082603	0.088765	0.094886	0.100966	0.107001	0.112991	0.118933
0.12	0.070328	0.076577	0.08279	0.088964	0.095098	0.10119	0.107237	0.113239	0.119193
0.13	0.070503	0.076766	0.082993	0.089181	0.095329	0.101434	0.107495	0.113509	0.119476
0.14	0.070692	0.076971	0.083214	0.089417	0.09558	0.1017	0.107775	0.113803	0.119783
0.15	0.070896	0.077193	0.083452	0.089672	0.095851	0.101986	0.108076	0.11412	0.120115
0.16	0.071116	0.077431	0.083708	0.089946	0.096142	0.102294	0.108401	0.11446	0.120471
0.17	0.071351	0.077686	0.083982	0.090239	0.096454	0.102624	0.108748	0.114825	0.120852
0.18	0.071603	0.077958	0.084275	0.090552	0.096787	0.102976	0.109119	0.115214	0.121259
0.19	0.07187	0.078248	0.084587	0.090886	0.097141	0.103351	0.109514	0.115628	0.121692
0.20	0.072155	0.078556	0.084918	0.091239	0.097517	0.103749	0.109933	0.116068	0.122152
0.21	0.072456	0.078882	0.085269	0.091614	0.097915	0.10417	0.110377	0.116534	0.122639
0.22	0.072774	0.079227	0.08564	0.092011	0.098337	0.104616	0.110846	0.117026	0.123154
0.23	0.07311	0.079592	0.086032	0.092429	0.098781	0.105086	0.111341	0.117545	0.123697
0.24	0.073465	0.079976	0.086445	0.092871	0.09925	0.105581	0.111863	0.118092	0.124269
0.25	0.073838	0.08038	0.08688	0.093335	0.099743	0.106103	0.112412	0.118668	0.124871
0.26	0.074231	0.080805	0.087336	0.093823	0.100262	0.106651	0.112989	0.119273	0.125503
0.27	0.074643	0.081251	0.087816	0.094335	0.100806	0.107226	0.113594	0.119908	0.126167
0.28	0.075075	0.08172	0.08832	0.094873	0.101377	0.10783	0.11423	0.120574	0.126862
0.29	0.075529	0.082211	0.088847	0.095436	0.101976	0.108462	0.114895	0.121272	0.127591
0.30	0.076004	0.082725	0.0894	0.096027	0.102602	0.109125	0.115592	0.122002	0.128355
0.31	0.076501	0.083263	0.089979	0.096644	0.103258	0.109818	0.116321	0.122767	0.129153
0.32	0.077022	0.083827	0.090584	0.097291	0.103944	0.110542	0.117083	0.123566	0.129987
0.33	0.077566	0.084416	0.091217	0.097966	0.104661	0.1113	0.11788	0.124401	0.130859
0.34	0.078135	0.085032	0.091878	0.098672	0.105411	0.112091	0.118713	0.125273	0.13177
0.35	0.07873	0.085675	0.09257	0.09941	0.106193	0.112918	0.119582	0.126183	0.132721
0.36	0.079351	0.086348	0.093291	0.10018	0.10701	0.113781	0.120489	0.127134	0.133713
0.37	0.08	0.08705	0.094045	0.100984	0.107864	0.114682	0.121436	0.128125	0.134748
0.38	0.080678	0.087783	0.094832	0.101823	0.108754	0.115621	0.122424	0.12916	0.135827
0.39	0.081385	0.088548	0.095653	0.102699	0.109683	0.116602	0.123454	0.130239	0.136953

Table B.8: Period vs Normalized output voltage $\hat{v}$ from 0.40 to 0.79 in Presence of $\hat{I}_o$ from –0.10 to –0.18.

	$\hat{I}_0$								
	-0.10	-0.11	-0.12	-0.13	-0.14	-0.15	-0.16	-0.17	-0.18
$\hat{v}$	Period								
0.40	0.082124	0.089346	0.096511	0.103613	0.110652	0.117625	0.124529	0.131364	0.138127
0.41	0.082895	0.09018	0.097405	0.104567	0.111663	0.118692	0.12565	0.132537	0.139351
0.42	0.0837	0.091051	0.098339	0.105562	0.112719	0.119805	0.126819	0.13376	0.140627
0.43	0.084541	0.091959	0.099313	0.106601	0.113819	0.120966	0.128038	0.135036	0.141957
0.44	0.085419	0.092907	0.10033	0.107685	0.114968	0.122177	0.12931	0.136366	0.143344
0.45	0.086335	0.093897	0.101392	0.108816	0.116166	0.12344	0.130636	0.137753	0.14479
0.46	0.087292	0.094931	0.1025	0.109996	0.117416	0.124758	0.13202	0.1392	0.146297
0.47	0.088292	0.096011	0.103658	0.111229	0.118721	0.126134	0.133463	0.140709	0.14787
0.48	0.089337	0.097139	0.104867	0.112516	0.120084	0.127569	0.134969	0.142283	0.14951
0.49	0.090429	0.098318	0.10613	0.11386	0.121507	0.129068	0.136542	0.143926	0.151221
0.50	0.091571	0.099551	0.107449	0.115265	0.122993	0.130633	0.138183	0.145641	0.153007
0.51	0.092766	0.100839	0.108829	0.116732	0.124546	0.132268	0.139897	0.147431	0.154871
0.52	0.094016	0.102187	0.110272	0.118267	0.12617	0.133977	0.141688	0.149302	0.156817
0.53	0.095324	0.103598	0.111782	0.119873	0.127867	0.135763	0.14356	0.151256	0.158851
0.54	0.096695	0.105076	0.113363	0.121553	0.129643	0.137632	0.145517	0.153298	0.160976
0.55	0.098131	0.106624	0.115018	0.123312	0.131502	0.139586	0.147564	0.155435	0.163197
0.56	0.099637	0.108246	0.116753	0.125154	0.133448	0.141633	0.149707	0.15767	0.165521
0.57	0.101218	0.109948	0.118572	0.127086	0.135488	0.143777	0.151951	0.16001	0.167954
0.58	0.102877	0.111734	0.12048	0.129111	0.137627	0.146024	0.154302	0.162461	0.170501
0.59	0.10462	0.11361	0.122483	0.131238	0.13987	0.14838	0.156767	0.16503	0.17317
0.60	0.106454	0.115582	0.124589	0.133471	0.142226	0.150854	0.159353	0.167725	0.175969
0.61	0.108383	0.117656	0.126802	0.135818	0.144701	0.153451	0.162069	0.170553	0.178906
0.62	0.110415	0.11984	0.129132	0.138287	0.147304	0.156182	0.164922	0.173524	0.18199
0.63	0.112558	0.122142	0.131586	0.140887	0.150043	0.159055	0.167923	0.176648	0.185232
0.64	0.114819	0.12457	0.134173	0.143626	0.152929	0.162081	0.171082	0.179936	0.188643
0.65	0.117208	0.127134	0.136904	0.146517	0.155972	0.165269	0.174411	0.183398	0.192234
0.66	0.119735	0.129844	0.139789	0.149569	0.159184	0.168634	0.177922	0.187049	0.19602
0.67	0.122411	0.132713	0.142842	0.152797	0.162579	0.172189	0.18163	0.190904	0.200015
0.68	0.125249	0.135753	0.146074	0.156214	0.166171	0.175949	0.185549	0.194977	0.204236
0.69	0.128262	0.138978	0.149503	0.159835	0.169977	0.17993	0.189699	0.199289	0.208703
0.70	0.131466	0.142407	0.153144	0.163679	0.174014	0.184153	0.194099	0.203858	0.213435
0.71	0.134878	0.146056	0.157018	0.167766	0.178305	0.188637	0.19877	0.208707	0.218457
0.72	0.138519	0.149946	0.161145	0.172118	0.182871	0.193409	0.203737	0.213864	0.223796
0.73	0.14241	0.1541	0.165549	0.176761	0.18774	0.198494	0.209029	0.219356	0.229481
0.74	0.146577	0.158546	0.170259	0.181722	0.192941	0.203923	0.214679	0.225217	0.235548
0.75	0.151048	0.163313	0.175307	0.187036	0.198508	0.209734	0.220723	0.231487	0.242036
0.76	0.155858	0.168437	0.180728	0.192739	0.204481	0.215966	0.227204	0.23821	0.248994
0.77	0.161043	0.173957	0.186564	0.198876	0.210906	0.222667	0.234172	0.245437	0.256474
0.78	0.166649	0.179919	0.192864	0.205498	0.217836	0.229893	0.241686	0.25323	0.264542
0.79	0.172728	0.186379	0.199686	0.212664	0.225333	0.237711	0.249814	0.261663	0.273274

Table B.9: Period vs Normalized output voltage $\hat{v}$ from 0.80 to 0.95 in Presence of $\hat{I}_o$ from –0.10 to –0.18.

	$\hat{I}_0$								
	-0.10	-0.11	-0.12	-0.13	-0.14	-0.15	-0.16	-0.17	-0.18
$\hat{v}$	Period								
0.80	0.17934	0.1934	0.207096	0.220447	0.233474	0.246198	0.258641	0.270823	0.282764
0.81	0.186558	0.20106	0.215176	0.228929	0.242346	0.25545	0.268265	0.280816	0.293125
0.82	0.19447	0.20945	0.224022	0.238216	0.25206	0.265583	0.278812	0.291775	0.304497
0.83	0.20318	0.218682	0.233754	0.248432	0.26275	0.27674	0.290435	0.303866	0.317061
0.84	0.212819	0.228894	0.24452	0.259737	0.274586	0.289105	0.303332	0.317302	0.331049
0.85	0.223548	0.24026	0.256505	0.27233	0.287785	0.302913	0.317759	0.332364	0.346769
0.86	0.235574	0.253002	0.269949	0.286474	0.302632	0.318477	0.334061	0.349435	0.36465
0.87	0.249164	0.267411	0.285172	0.302517	0.319513	0.336225	0.352719	0.369058	0.38531
0.88	0.264675	0.28388	0.302607	0.320943	0.338972	0.356775	0.374438	0.392048	0.409703
0.89	0.282597	0.302957	0.322873	0.342456	0.361814	0.381062	0.40032	0.419728	0.439452
0.90	0.303639	0.325448	0.346897	0.368137	0.389324	0.410635	0.432281	0.454537	0.477784
0.91	0.328878	0.352615	0.376183	0.399814	0.42378	0.448435	0.474286	0.502165	0.533712
0.92	0.360093	0.386636	0.413471	0.441066	0.4701	0.50174	0.538538	0.590078	
0.93	0.400615	0.431916	0.464937	0.501356	0.54535	0.64435			
0.94	0.458329	0.501014	0.555587						
0.95	0.573022								

Table B.10: Period vs Normalized output voltage $\hat{v}$ from 0.00 to 0.39 in Presence of $\hat{I}_o$ from –0.19 to –0.27.

	$\hat{I}_0$								
	-0.19	-0.2	-0.21	-0.22	-0.23	-0.24	-0.25	-0.26	-0.27
$\hat{v}$	Period								
0.00	0.123413	0.129198	0.134933	0.140617	0.146249	0.151829	0.157354	0.162826	0.168243
0.01	0.123426	0.129212	0.134948	0.140633	0.146266	0.151846	0.157373	0.162846	0.168265
0.02	0.123462	0.12925	0.134987	0.140674	0.146309	0.151891	0.15742	0.162895	0.168315
0.03	0.123521	0.129311	0.135051	0.140741	0.146378	0.151963	0.157495	0.162972	0.168396
0.04	0.123602	0.129396	0.13514	0.140833	0.146474	0.152062	0.157597	0.163078	0.168505
0.05	0.123707	0.129505	0.135254	0.140951	0.146596	0.152189	0.157728	0.163213	0.168644
0.06	0.123835	0.129639	0.135392	0.141094	0.146745	0.152343	0.157887	0.163377	0.168813
0.07	0.123986	0.129796	0.135556	0.141264	0.14692	0.152524	0.158074	0.16357	0.169011
0.08	0.124161	0.129978	0.135745	0.14146	0.147123	0.152733	0.15829	0.163792	0.16924
0.09	0.124359	0.130184	0.135959	0.141682	0.147353	0.152971	0.158534	0.164044	0.169499
0.10	0.124581	0.130416	0.136199	0.141931	0.14761	0.153236	0.158808	0.164326	0.169788
0.11	0.124828	0.130672	0.136465	0.142207	0.147895	0.15353	0.159111	0.164637	0.170109
0.12	0.125098	0.130953	0.136757	0.142509	0.148208	0.153853	0.159444	0.16498	0.17046
0.13	0.125394	0.131261	0.137076	0.14284	0.14855	0.154205	0.159807	0.165353	0.170844
0.14	0.125714	0.131594	0.137422	0.143198	0.14892	0.154587	0.1602	0.165757	0.171259
0.15	0.12606	0.131954	0.137796	0.143584	0.149319	0.154999	0.160624	0.166193	0.171706
0.16	0.126431	0.13234	0.138196	0.143999	0.149748	0.155441	0.161079	0.166661	0.172187
0.17	0.126829	0.132754	0.138626	0.144444	0.150207	0.155915	0.161567	0.167162	0.172701
0.18	0.127253	0.133195	0.139083	0.144917	0.150696	0.156419	0.162086	0.167696	0.173249
0.19	0.127705	0.133665	0.139571	0.145422	0.151217	0.156956	0.162639	0.168264	0.173832
0.20	0.128184	0.134163	0.140087	0.145956	0.151769	0.157526	0.163225	0.168866	0.174449
0.21	0.128692	0.134691	0.140635	0.146523	0.152354	0.158128	0.163845	0.169503	0.175103
0.22	0.129228	0.135248	0.141213	0.147121	0.152972	0.158765	0.1645	0.170176	0.175794
0.23	0.129794	0.135837	0.141823	0.147752	0.153623	0.159436	0.165191	0.170886	0.176521
0.24	0.13039	0.136456	0.142465	0.148417	0.154309	0.160143	0.165918	0.171633	0.177288
0.25	0.131018	0.137108	0.143141	0.149115	0.155031	0.160887	0.166683	0.172418	0.178093
0.26	0.131676	0.137793	0.143851	0.149849	0.155789	0.161667	0.167485	0.173242	0.178938
0.27	0.132368	0.138511	0.144595	0.15062	0.156583	0.162486	0.168327	0.174107	0.179825
0.28	0.133093	0.139264	0.145376	0.151427	0.157416	0.163344	0.16921	0.175013	0.180754
0.29	0.133852	0.140053	0.146193	0.152272	0.158288	0.164242	0.170133	0.175961	0.181726
0.30	0.134647	0.140879	0.147049	0.153156	0.159201	0.165182	0.171099	0.176953	0.182742
0.31	0.135478	0.141742	0.147943	0.154081	0.160155	0.166164	0.172109	0.177989	0.183805
0.32	0.136347	0.142645	0.148878	0.155047	0.161152	0.167191	0.173164	0.179072	0.184914
0.33	0.137255	0.143587	0.149855	0.156056	0.162192	0.168262	0.174265	0.180202	0.186073
0.34	0.138203	0.144572	0.150874	0.15711	0.163279	0.16938	0.175415	0.181382	0.187281
0.35	0.139193	0.145599	0.151938	0.158209	0.164412	0.170547	0.176614	0.182612	0.188541
0.36	0.140225	0.146671	0.153047	0.159355	0.165594	0.171764	0.177863	0.183894	0.189855
0.37	0.141302	0.147788	0.154205	0.160551	0.166827	0.173032	0.179166	0.18523	0.191224
0.38	0.142426	0.148954	0.155411	0.161797	0.168111	0.174353	0.180524	0.186623	0.19265
0.39	0.143597	0.150169	0.156669	0.163096	0.16945	0.175731	0.181938	0.188073	0.194136

Table B.11: Period vs Normalized output voltage $\hat{v}$ from 0.40 to 0.79 in Presence of $\hat{I}_o$ from –0.19 to –0.27.

	$\hat{I}_0$								
	-0.19	-0.2	-0.21	-0.22	-0.23	-0.24	-0.25	-0.26	-0.27
$\hat{v}$	Period								
0.40	0.144818	0.151436	0.15798	0.164449	0.170845	0.177165	0.183412	0.189584	0.195683
0.41	0.146091	0.152756	0.159346	0.16586	0.172298	0.17866	0.184947	0.191158	0.197295
0.42	0.147418	0.154132	0.160769	0.167329	0.173811	0.180217	0.186545	0.192797	0.198972
0.43	0.1488	0.155566	0.162252	0.16886	0.175388	0.181838	0.188209	0.194503	0.200719
0.44	0.150242	0.15706	0.163798	0.170455	0.177031	0.183527	0.189943	0.19628	0.202538
0.45	0.151745	0.158618	0.165408	0.172116	0.178742	0.185286	0.191748	0.19813	0.204432
0.46	0.153311	0.160241	0.167087	0.173848	0.180525	0.187119	0.193629	0.200057	0.206404
0.47	0.154945	0.161934	0.168836	0.175652	0.182383	0.189028	0.195588	0.202064	0.208458
0.48	0.156648	0.163698	0.17066	0.177533	0.184319	0.191017	0.197629	0.204155	0.210597
0.49	0.158425	0.165539	0.172562	0.179494	0.186337	0.19309	0.199756	0.206334	0.212826
0.50	0.160279	0.167459	0.174545	0.181539	0.188441	0.195252	0.201973	0.208604	0.215149
0.51	0.162214	0.169462	0.176614	0.183672	0.190635	0.197506	0.204284	0.210972	0.21757
0.52	0.164234	0.171553	0.178774	0.185897	0.192925	0.199857	0.206695	0.21344	0.220094
0.53	0.166344	0.173736	0.181028	0.18822	0.195314	0.20231	0.20921	0.216015	0.222728
0.54	0.168548	0.176017	0.183383	0.190646	0.197808	0.20487	0.211835	0.218702	0.225475
0.55	0.170852	0.178401	0.185843	0.19318	0.200413	0.207545	0.214576	0.221508	0.228344
0.56	0.173262	0.180893	0.188414	0.195828	0.203136	0.210339	0.217439	0.224439	0.231341
0.57	0.175783	0.1835	0.191104	0.198597	0.205982	0.21326	0.220432	0.227502	0.234472
0.58	0.178423	0.186229	0.193919	0.201495	0.20896	0.216315	0.223563	0.230706	0.237747
0.59	0.181189	0.189087	0.196866	0.204529	0.212077	0.219513	0.226839	0.234058	0.241173
0.60	0.184088	0.192082	0.199955	0.207707	0.215342	0.222862	0.23027	0.237569	0.244761
0.61	0.187129	0.195224	0.203193	0.211039	0.218765	0.226373	0.233866	0.241248	0.248521
0.62	0.190322	0.198522	0.206592	0.214536	0.222356	0.230056	0.237638	0.245107	0.252465
0.63	0.193677	0.201986	0.210162	0.218208	0.226127	0.233923	0.241599	0.249158	0.256605
0.64	0.197206	0.205629	0.213915	0.222068	0.23009	0.237986	0.24576	0.253416	0.260956
0.65	0.200921	0.209464	0.217865	0.226129	0.23426	0.242262	0.250139	0.257895	0.265534
0.66	0.204837	0.213504	0.222026	0.230407	0.238652	0.246765	0.25475	0.262612	0.270355
0.67	0.208968	0.217766	0.226415	0.234919	0.243284	0.251513	0.259613	0.267587	0.275441
0.68	0.213332	0.222268	0.23105	0.239684	0.248174	0.256527	0.264748	0.272841	0.280812
0.69	0.217948	0.227029	0.235952	0.244722	0.253346	0.26183	0.270179	0.278398	0.286494
0.70	0.222838	0.232072	0.241143	0.250058	0.258824	0.267446	0.275932	0.284286	0.292515
0.71	0.228026	0.237422	0.24665	0.255719	0.264636	0.273406	0.282038	0.290536	0.298909
0.72	0.233541	0.243108	0.252504	0.261736	0.270813	0.279742	0.288531	0.297185	0.305713
0.73	0.239414	0.249163	0.258737	0.268144	0.277394	0.286493	0.295451	0.304274	0.31297
0.74	0.24568	0.255624	0.265389	0.274985	0.28442	0.293704	0.302846	0.311852	0.320733
0.75	0.252382	0.262535	0.272506	0.282305	0.291942	0.301427	0.310769	0.319977	0.32906
0.76	0.259569	0.269948	0.280141	0.290161	0.300018	0.309723	0.319287	0.328718	0.338026
0.77	0.267298	0.277922	0.288358	0.29862	0.308719	0.318668	0.328476	0.338156	0.347718
0.78	0.275636	0.286528	0.297231	0.30776	0.318128	0.328348	0.338433	0.348394	0.358243
0.79	0.284665	0.295853	0.306852	0.317679	0.328349	0.338876	0.349274	0.359556	0.369737

Table B.12: Period vs Normalized output voltage $\hat{v}$ from 0.80 to 0.91 in Presence of $\hat{I}_o$ from –0.19 to –0.27.

	$\hat{I}_0$								
	-0.19	-0.2	-0.21	-0.22	-0.23	-0.24	-0.25	-0.26	-0.27
$\hat{v}$	Period								
0.80	0.294484	0.306	0.317332	0.328496	0.339509	0.350387	0.361146	0.371802	0.382371
0.81	0.305212	0.317101	0.32881	0.340359	0.351768	0.363055	0.374239	0.385339	0.396373
0.82	0.317003	0.329317	0.341462	0.353461	0.365336	0.377109	0.388803	0.400441	0.412048
0.83	0.33005	0.34286	0.355519	0.368052	0.380488	0.392854	0.405179	0.417492	0.429828
0.84	0.344607	0.358008	0.371286	0.384475	0.397607	0.410721	0.423854	0.437052	0.450363
0.85	0.361015	0.375143	0.389194	0.403212	0.417244	0.431344	0.445572	0.459997	0.474709
0.86	0.379757	0.39481	0.409866	0.424989	0.440252	0.455742	0.471567	0.487868	0.504838
0.87	0.401544	0.417839	0.434284	0.450987	0.468082	0.485747	0.504235	0.523931	0.545494
0.88	0.427513	0.445612	0.464167	0.483407	0.503665	0.525475	0.549828	0.579052	0.623775
0.89	0.459705	0.480782	0.503129	0.527501	0.555445	0.591504	0.653259		
0.90	0.502628	0.530166	0.562952	0.612324					
0.91	0.573521	0.646949							

Table B.13: Period vs Normalized output voltage $\hat{v}$ from 0.00 to 0.39 in Presence of $\hat{I}_o$ from –0.28 to –0.36.

	$\hat{I}_0$								
	-0.28	-0.29	-0.30	-0.31	-0.32	-0.33	-0.34	-0.35	-0.36
$\hat{v}$	Period								
0.00	0.173605	0.178912	0.184164	0.18936	0.1945	0.199584	0.204613	0.209587	0.214505
0.01	0.173628	0.178937	0.18419	0.189387	0.194529	0.199616	0.204647	0.209623	0.214544
0.02	0.173681	0.178992	0.184247	0.189447	0.194592	0.199681	0.204714	0.209693	0.214616
0.03	0.173764	0.179078	0.184336	0.189539	0.194686	0.199778	0.204815	0.209797	0.214724
0.04	0.173877	0.179194	0.184456	0.189662	0.194813	0.199909	0.20495	0.209935	0.214866
0.05	0.17402	0.179341	0.184607	0.189818	0.194973	0.200073	0.205118	0.210108	0.215043
0.06	0.174194	0.17952	0.18479	0.190006	0.195166	0.200271	0.20532	0.210315	0.215255
0.07	0.174398	0.179729	0.185005	0.190226	0.195392	0.200502	0.205557	0.210557	0.215502
0.08	0.174633	0.17997	0.185253	0.190479	0.195651	0.200767	0.205828	0.210834	0.215785
0.09	0.174899	0.180243	0.185532	0.190766	0.195944	0.201066	0.206134	0.211146	0.216103
0.10	0.175196	0.180548	0.185844	0.191085	0.19627	0.2014	0.206474	0.211494	0.216458
0.11	0.175525	0.180885	0.186189	0.191438	0.196631	0.201769	0.206851	0.211877	0.216849
0.12	0.175885	0.181255	0.186568	0.191825	0.197027	0.202173	0.207263	0.212298	0.217277
0.13	0.176278	0.181657	0.18698	0.192247	0.197457	0.202612	0.207711	0.212755	0.217743
0.14	0.176704	0.182093	0.187426	0.192703	0.197924	0.203088	0.208196	0.213249	0.218246
0.15	0.177163	0.182564	0.187907	0.193195	0.198426	0.2036	0.208719	0.213781	0.218788
0.16	0.177656	0.183068	0.188424	0.193722	0.198964	0.204149	0.209279	0.214352	0.219369
0.17	0.178183	0.183608	0.188975	0.194286	0.19954	0.204737	0.209877	0.214961	0.219989
0.18	0.178745	0.184183	0.189563	0.194887	0.200153	0.205362	0.210514	0.21561	0.220649
0.19	0.179342	0.184794	0.190188	0.195525	0.200804	0.206026	0.211191	0.216299	0.221351
0.20	0.179975	0.185442	0.190851	0.196202	0.201495	0.20673	0.211908	0.217029	0.222094
0.21	0.180645	0.186127	0.191552	0.196918	0.202225	0.207475	0.212667	0.217801	0.222879
0.22	0.181352	0.186851	0.192292	0.197673	0.202996	0.208261	0.213467	0.218616	0.223707
0.23	0.182098	0.187614	0.193072	0.198469	0.203808	0.209088	0.21431	0.219474	0.22458
0.24	0.182882	0.188417	0.193892	0.199307	0.204663	0.209959	0.215197	0.220376	0.225497
0.25	0.183707	0.189261	0.194754	0.200188	0.205561	0.210874	0.216128	0.221324	0.226461
0.26	0.184573	0.190147	0.195659	0.201111	0.206503	0.211834	0.217106	0.222318	0.227472
0.27	0.185481	0.191075	0.196608	0.20208	0.20749	0.21284	0.21813	0.22336	0.228531
0.28	0.186432	0.192048	0.197602	0.203094	0.208524	0.213894	0.219202	0.224451	0.22964
0.29	0.187427	0.193066	0.198642	0.204155	0.209606	0.214996	0.220324	0.225592	0.2308
0.30	0.188468	0.19413	0.199729	0.205264	0.210737	0.216147	0.221496	0.226784	0.232012
0.31	0.189556	0.195242	0.200864	0.206423	0.211918	0.217351	0.222721	0.22803	0.233277
0.32	0.190691	0.196403	0.20205	0.207633	0.213151	0.218607	0.223999	0.229329	0.234598
0.33	0.191877	0.197615	0.203288	0.208895	0.214438	0.219917	0.225332	0.230685	0.235976
0.34	0.193113	0.198879	0.204578	0.210212	0.21578	0.221283	0.226723	0.232099	0.237412
0.35	0.194403	0.200197	0.205924	0.211584	0.217179	0.222707	0.228172	0.233572	0.238909
0.36	0.195747	0.201571	0.207326	0.213015	0.218636	0.224191	0.229681	0.235107	0.240469
0.37	0.197148	0.203002	0.208788	0.214505	0.220154	0.225737	0.231254	0.236705	0.242093
0.38	0.198607	0.204493	0.210309	0.216057	0.221735	0.227347	0.232891	0.23837	0.243783
0.39	0.200127	0.206046	0.211894	0.217672	0.223382	0.229022	0.234596	0.240102	0.245543

Table B.14: Period vs Normalized output voltage $\hat{v}$ from 0.40 to 0.79 in Presence of $\hat{I}_o$ from –0.28 to –0.36.

	$\hat{I}_0$								
	-0.28	-0.29	-0.30	-0.31	-0.32	-0.33	-0.34	-0.35	-0.36
$\hat{v}$	Period								
0.40	0.201709	0.207662	0.213544	0.219355	0.225095	0.230767	0.23637	0.241906	0.247375
0.41	0.203357	0.209346	0.215262	0.221106	0.226879	0.232582	0.238216	0.243782	0.249281
0.42	0.205072	0.211098	0.21705	0.222929	0.228736	0.234472	0.240138	0.245735	0.251265
0.43	0.206859	0.212922	0.218911	0.224826	0.230668	0.236438	0.242138	0.247768	0.253329
0.44	0.208718	0.214821	0.220848	0.226801	0.232679	0.238485	0.244219	0.249883	0.255477
0.45	0.210654	0.216798	0.222865	0.228856	0.234772	0.240615	0.246385	0.252083	0.257712
0.46	0.21267	0.218857	0.224965	0.230996	0.236951	0.242832	0.248639	0.254374	0.260038
0.47	0.214769	0.221	0.227151	0.233224	0.239219	0.245139	0.250985	0.256758	0.26246
0.48	0.216955	0.223232	0.229427	0.235543	0.241581	0.247542	0.253428	0.259241	0.264981
0.49	0.219233	0.225557	0.231798	0.237959	0.244041	0.250045	0.255973	0.261826	0.267606
0.50	0.221606	0.227979	0.234268	0.240476	0.246603	0.252652	0.258623	0.264519	0.27034
0.51	0.22408	0.230504	0.236843	0.243099	0.249273	0.255368	0.261384	0.267324	0.27319
0.52	0.226659	0.233136	0.239526	0.245833	0.252056	0.258199	0.264263	0.270249	0.27616
0.53	0.229349	0.235881	0.242325	0.248684	0.254959	0.261151	0.267264	0.273298	0.279257
0.54	0.232156	0.238745	0.245245	0.251658	0.257986	0.264231	0.270395	0.27648	0.282488
0.55	0.235086	0.241734	0.248293	0.254763	0.261147	0.267446	0.273664	0.279801	0.28586
0.56	0.238146	0.244857	0.251476	0.258005	0.264447	0.270803	0.277077	0.283269	0.289383
0.57	0.241344	0.248119	0.254802	0.261393	0.267895	0.274312	0.280644	0.286894	0.293065
0.58	0.244687	0.251531	0.258279	0.264935	0.271501	0.27798	0.284373	0.290684	0.296915
0.59	0.248186	0.2551	0.261918	0.268642	0.275274	0.281818	0.288277	0.294651	0.300945
0.60	0.25185	0.258838	0.265728	0.272523	0.279225	0.285839	0.292365	0.298807	0.305167
0.61	0.255689	0.262755	0.269721	0.27659	0.283367	0.290052	0.29665	0.303163	0.309594
0.62	0.259716	0.266863	0.273909	0.280857	0.287711	0.294473	0.301147	0.307736	0.314241
0.63	0.263943	0.271176	0.278306	0.285337	0.292273	0.299117	0.305871	0.312539	0.319125
0.64	0.268386	0.275709	0.282928	0.290047	0.29707	0.304	0.310839	0.317593	0.324263
0.65	0.273061	0.280479	0.287792	0.295004	0.302119	0.30914	0.316072	0.322916	0.329677
0.66	0.277985	0.285504	0.292917	0.300228	0.307442	0.314561	0.32159	0.328531	0.33539
0.67	0.283178	0.290805	0.298325	0.305742	0.31306	0.320285	0.327418	0.334465	0.341429
0.68	0.288665	0.296406	0.30404	0.31157	0.319002	0.326339	0.333586	0.340747	0.347825
0.69	0.294471	0.302335	0.310091	0.317743	0.325296	0.332756	0.340126	0.34741	0.354613
0.70	0.300625	0.308621	0.316509	0.324293	0.331979	0.339571	0.347075	0.354494	0.361834
0.71	0.307162	0.315301	0.323331	0.331258	0.339088	0.346826	0.354477	0.362046	0.369537
0.72	0.314121	0.322414	0.3306	0.338685	0.346673	0.354571	0.362385	0.370119	0.377779
0.73	0.321547	0.33001	0.338367	0.346624	0.354788	0.362864	0.370859	0.378779	0.386628
0.74	0.329494	0.338145	0.346691	0.35514	0.363499	0.371775	0.379974	0.388103	0.396168
0.75	0.338027	0.346885	0.355643	0.364307	0.372887	0.381389	0.389821	0.398189	0.406502
0.76	0.347222	0.356313	0.365309	0.374218	0.383049	0.39181	0.40051	0.409157	0.41776
0.77	0.357171	0.366527	0.375795	0.384985	0.394107	0.40317	0.412184	0.421161	0.430109
0.78	0.367992	0.377652	0.387236	0.396753	0.406216	0.415637	0.425028	0.434402	0.443772
0.79	0.379829	0.389845	0.399801	0.409708	0.419582	0.429437	0.439289	0.449155	0.459054

Table B.15: Period vs Normalized output voltage $\hat{v}$ from 0.80 to 0.87 in Presence of $\hat{I}_o$ from –0.28 to –0.36.

	$\hat{I}_0$								
	-0.28	-0.29	-0.30	-0.31	-0.32	-0.33	-0.34	-0.35	-0.36
$\hat{v}$	Period								
0.80	0.392869	0.403311	0.413715	0.424097	0.434476	0.444873	0.455309	0.465809	0.4764
0.81	0.407361	0.418324	0.429284	0.440263	0.451288	0.462388	0.473596	0.484951	0.4965
0.82	0.423648	0.43527	0.446945	0.458706	0.470595	0.482657	0.494952	0.507551	0.520549
0.83	0.442223	0.454717	0.46736	0.480209	0.493335	0.50683	0.520816	0.535464	0.551029
0.84	0.463846	0.477572	0.49163	0.506136	0.52125	0.537204	0.554363	0.573375	0.59562
0.85	0.489817	0.505472	0.521884	0.539374	0.558484	0.580276	0.607561	0.666085	
0.86	0.522759	0.542086	0.563649	0.589344	0.626719				
0.87	0.570267	0.602108	0.659668						

Table B.16: Period vs Normalized output voltage $\hat{v}$ from 0.00 to 0.39 in Presence of $\hat{I}_o$ from –0.37 to –0.45.

	$\hat{I}_0$								
	-0.37	-0.38	-0.39	-0.40	-0.41	-0.42	-0.43	-0.44	-0.45
$\hat{v}$	Period								
0.00	0.219369	0.224177	0.228932	0.233633	0.23828	0.242874	0.247415	0.251905	0.256342
0.01	0.219409	0.224221	0.228978	0.233682	0.238332	0.242929	0.247474	0.251966	0.256408
0.02	0.219485	0.2243	0.22906	0.233767	0.23842	0.243021	0.247569	0.252066	0.256511
0.03	0.219596	0.224414	0.229178	0.233888	0.238545	0.24315	0.247702	0.252203	0.256653
0.04	0.219742	0.224564	0.229332	0.234046	0.238708	0.243316	0.247873	0.252378	0.256832
0.05	0.219923	0.224749	0.229522	0.234241	0.238907	0.24352	0.248082	0.252592	0.257051
0.06	0.22014	0.224971	0.229748	0.234472	0.239143	0.243762	0.248329	0.252844	0.257308
0.07	0.220392	0.225229	0.230012	0.234741	0.239418	0.244042	0.248614	0.253134	0.257604
0.08	0.220681	0.225523	0.230312	0.235047	0.239729	0.244359	0.248937	0.253464	0.25794
0.09	0.221006	0.225855	0.23065	0.235391	0.24008	0.244716	0.2493	0.253833	0.258315
0.10	0.221368	0.226223	0.231025	0.235773	0.240468	0.245111	0.249702	0.254242	0.25873
0.11	0.221766	0.226629	0.231438	0.236193	0.240896	0.245546	0.250144	0.25469	0.259186
0.12	0.222202	0.227073	0.23189	0.236653	0.241363	0.24602	0.250626	0.25518	0.259683
0.13	0.222676	0.227555	0.23238	0.237151	0.24187	0.246535	0.251149	0.255711	0.260222
0.14	0.223189	0.228077	0.23291	0.23769	0.242417	0.247091	0.251713	0.256283	0.260803
0.15	0.22374	0.228637	0.23348	0.238269	0.243005	0.247688	0.252319	0.256898	0.261426
0.16	0.224331	0.229238	0.234091	0.238889	0.243635	0.248327	0.252967	0.257555	0.262093
0.17	0.224962	0.229879	0.234742	0.239551	0.244306	0.249009	0.253659	0.258257	0.262803
0.18	0.225633	0.230562	0.235436	0.240255	0.245021	0.249734	0.254394	0.259002	0.263559
0.19	0.226346	0.231287	0.236172	0.241003	0.245779	0.250503	0.255174	0.259793	0.26436
0.20	0.227102	0.232054	0.236951	0.241794	0.246582	0.251317	0.255999	0.260629	0.265207
0.21	0.2279	0.232865	0.237775	0.24263	0.24743	0.252177	0.256871	0.261512	0.266102
0.22	0.228742	0.23372	0.238643	0.243511	0.248324	0.253083	0.25779	0.262443	0.267045
0.23	0.229629	0.234621	0.239558	0.244439	0.249265	0.254038	0.258757	0.263423	0.268037
0.24	0.230561	0.235568	0.240519	0.245414	0.250255	0.255041	0.259773	0.264452	0.269079
0.25	0.231541	0.236563	0.241529	0.246439	0.251293	0.256093	0.260839	0.265532	0.270173
0.26	0.232568	0.237606	0.242587	0.247512	0.252382	0.257197	0.261957	0.266665	0.271319
0.27	0.233644	0.238699	0.243696	0.248637	0.253523	0.258353	0.263128	0.26785	0.272519
0.28	0.23477	0.239842	0.244857	0.249815	0.254716	0.259562	0.264353	0.269091	0.273775
0.29	0.235948	0.241038	0.24607	0.251045	0.255964	0.260826	0.265634	0.270387	0.275088
0.30	0.237179	0.242288	0.247338	0.252331	0.257267	0.262147	0.266972	0.271742	0.276458
0.31	0.238465	0.243593	0.248662	0.253674	0.258628	0.263526	0.268368	0.273155	0.277889
0.32	0.239806	0.244955	0.250044	0.255074	0.260047	0.264964	0.269824	0.27463	0.279381
0.33	0.241206	0.246375	0.251484	0.256535	0.261528	0.266464	0.271343	0.276168	0.280937
0.34	0.242664	0.247855	0.252986	0.258058	0.263071	0.268027	0.272926	0.27777	0.282559
0.35	0.244184	0.249398	0.254551	0.259644	0.264679	0.269655	0.274575	0.279439	0.284248
0.36	0.245767	0.251005	0.25618	0.261296	0.266353	0.271352	0.276293	0.281178	0.286007
0.37	0.247416	0.252678	0.257878	0.263017	0.268096	0.273117	0.278081	0.282987	0.287838
0.38	0.249133	0.25442	0.259644	0.264808	0.269911	0.274956	0.279942	0.284871	0.289745
0.39	0.25092	0.256233	0.261483	0.266672	0.2718	0.276869	0.281879	0.286832	0.291728

Table B.17: Period vs Normalized output voltage $\hat{v}$ from 0.40 to 0.79 in Presence of $\hat{I}_o$ from –0.37 to –0.45.

	$\hat{I}_0$								
	-0.37	-0.38	-0.39	-0.40	-0.41	-0.42	-0.43	-0.44	-0.45
$\hat{v}$	Period								
0.40	0.252779	0.25812	0.263397	0.268612	0.273765	0.278859	0.283895	0.288872	0.293793
0.41	0.254715	0.260083	0.265388	0.27063	0.275811	0.280931	0.285992	0.290995	0.29594
0.42	0.256728	0.262126	0.26746	0.27273	0.277938	0.283086	0.288174	0.293203	0.298175
0.43	0.258824	0.264252	0.269615	0.274915	0.280152	0.285328	0.290444	0.295501	0.3005
0.44	0.261004	0.266464	0.271858	0.277188	0.282456	0.287661	0.292806	0.297892	0.30292
0.45	0.263272	0.268765	0.274192	0.279554	0.284853	0.290089	0.295265	0.30038	0.305437
0.46	0.265634	0.271161	0.276621	0.282016	0.287348	0.292616	0.297823	0.30297	0.308058
0.47	0.268091	0.273654	0.27915	0.284579	0.289944	0.295246	0.300486	0.305666	0.310786
0.48	0.27065	0.27625	0.281782	0.287247	0.292648	0.297985	0.303259	0.308473	0.313627
0.49	0.273315	0.278953	0.284523	0.290026	0.295464	0.300837	0.306147	0.311397	0.316586
0.5	0.27609	0.281769	0.287379	0.292921	0.298397	0.303808	0.309156	0.314443	0.31967
0.51	0.278982	0.284703	0.290354	0.295937	0.301453	0.306905	0.312293	0.317619	0.322884
0.52	0.281996	0.287761	0.293456	0.299082	0.30464	0.310133	0.315563	0.32093	0.326236
0.53	0.28514	0.290951	0.296691	0.302361	0.307964	0.313501	0.318974	0.324385	0.329734
0.54	0.28842	0.294279	0.300066	0.305784	0.311433	0.317017	0.322535	0.327991	0.333386
0.55	0.291844	0.297753	0.30359	0.309357	0.315056	0.320688	0.326255	0.331759	0.337201
0.56	0.29542	0.301382	0.307272	0.313091	0.318841	0.324524	0.330142	0.335697	0.34119
0.57	0.299158	0.305176	0.311121	0.316995	0.322799	0.328537	0.334209	0.339817	0.345364
0.58	0.303068	0.309144	0.315148	0.321079	0.326941	0.332736	0.338465	0.344131	0.349735
0.59	0.30716	0.313299	0.319364	0.325357	0.33128	0.337136	0.342926	0.348652	0.354317
0.6	0.311448	0.317653	0.323783	0.329841	0.335829	0.34175	0.347605	0.353396	0.359126
0.61	0.315946	0.32222	0.328419	0.334547	0.340604	0.346594	0.352518	0.358379	0.364179
0.62	0.320667	0.327015	0.333289	0.33949	0.345621	0.351686	0.357684	0.363621	0.369496
0.63	0.325629	0.332057	0.33841	0.34469	0.350901	0.357045	0.363124	0.369141	0.375098
0.64	0.330852	0.337365	0.343802	0.350168	0.356464	0.362694	0.36886	0.374965	0.38101
0.65	0.336357	0.342961	0.34949	0.355947	0.362336	0.36866	0.37492	0.38112	0.387262
0.66	0.342168	0.34887	0.355498	0.362055	0.368545	0.374971	0.381334	0.387638	0.393886
0.67	0.348313	0.355122	0.361858	0.368524	0.375124	0.38166	0.388137	0.394557	0.400922
0.68	0.354825	0.361749	0.368603	0.375388	0.382109	0.388769	0.395371	0.401918	0.408414
0.69	0.361739	0.368791	0.375774	0.382691	0.389546	0.396343	0.403084	0.409774	0.416416
0.7	0.369099	0.376292	0.383419	0.390482	0.397487	0.404436	0.411335	0.418186	0.424993
0.71	0.376956	0.384306	0.391593	0.398821	0.405994	0.413116	0.420193	0.427227	0.434225
0.72	0.38537	0.392896	0.400364	0.407778	0.415142	0.422462	0.429744	0.436991	0.444209
0.73	0.394413	0.40214	0.409814	0.417441	0.425026	0.432575	0.440095	0.447591	0.455069
0.74	0.404176	0.412133	0.420045	0.427919	0.435762	0.443581	0.451383	0.459176	0.466967
0.75	0.414767	0.422992	0.431184	0.43935	0.4475	0.455643	0.463787	0.471942	0.48012
0.76	0.426328	0.434871	0.443396	0.451916	0.46044	0.46898	0.477549	0.48616	0.49483
0.77	0.439042	0.447969	0.456904	0.46586	0.474852	0.483897	0.493013	0.502221	0.511547
0.78	0.453153	0.46256	0.472012	0.481528	0.49113	0.500843	0.510699	0.520735	0.530994
0.79	0.469006	0.479035	0.489168	0.499435	0.509875	0.520533	0.531467	0.542751	0.554487

Table B.18: Period vs Normalized output voltage $\hat{v}$ from 0.80 to 0.84 in Presence of $\hat{I}_o$ from –0.37 to –0.45.

	$\hat{I}_0$								
	-0.37	-0.38	-0.39	-0.40	-0.41	-0.42	-0.43	-0.44	-0.45
$\hat{v}$	Period								
0.80	0.487114	0.49799	0.509075	0.520426	0.532117	0.544248	0.556956	0.570447	0.585043
0.81	0.5083	0.520426	0.532974	0.546077	0.55993	0.574835	0.591321	0.610479	0.635552
0.82	0.534074	0.548307	0.56353	0.580212	0.599277	0.623144	0.675636		
0.83	0.567927	0.586933	0.609864	0.644729					
0.84	0.625561								

Table B.19: Period vs Normalized output voltage $\hat{v}$ from 0.00 to 0.39 in Presence of $\hat{I}_o$ from –0.46 to –0.54.

	$\hat{I}_0$								
	-0.46	-0.47	-0.48	-0.49	-0.5	-0.51	-0.52	-0.53	-0.54
$\hat{v}$	Period								
0.00	0.260729	0.265066	0.269353	0.27359	0.277779	0.28192	0.286013	0.29006	0.294061
0.01	0.260798	0.265139	0.269429	0.273671	0.277864	0.282009	0.286107	0.290159	0.294164
0.02	0.260906	0.26525	0.269545	0.273791	0.277989	0.282139	0.286241	0.290297	0.294308
0.03	0.261052	0.2654	0.2697	0.27395	0.278153	0.282307	0.286415	0.290476	0.294492
0.04	0.261236	0.26559	0.269894	0.274149	0.278357	0.282516	0.286629	0.290696	0.294717
0.05	0.261459	0.265818	0.270127	0.274388	0.278601	0.282766	0.286884	0.290956	0.294982
0.06	0.261722	0.266086	0.2704	0.274667	0.278885	0.283055	0.287179	0.291257	0.29529
0.07	0.262023	0.266393	0.270714	0.274986	0.27921	0.283386	0.287516	0.2916	0.295638
0.08	0.262365	0.266741	0.271067	0.275345	0.279575	0.283758	0.287894	0.291985	0.296029
0.09	0.262747	0.267129	0.271462	0.275746	0.279983	0.284172	0.288315	0.292411	0.296463
0.1	0.263169	0.267557	0.271897	0.276188	0.280432	0.284628	0.288777	0.292881	0.296939
0.11	0.263632	0.268028	0.272374	0.276673	0.280923	0.285126	0.289283	0.293394	0.297459
0.12	0.264136	0.26854	0.272894	0.277199	0.281457	0.285668	0.289832	0.29395	0.298023
0.13	0.264683	0.269094	0.273456	0.277769	0.282035	0.286253	0.290425	0.294551	0.298632
0.14	0.265272	0.269691	0.274061	0.278383	0.282656	0.286883	0.291063	0.295197	0.299286
0.15	0.265904	0.270332	0.27471	0.27904	0.283323	0.287557	0.291746	0.295888	0.299985
0.16	0.266579	0.271016	0.275404	0.279743	0.284034	0.288278	0.292475	0.296626	0.300732
0.17	0.2673	0.271746	0.276143	0.280491	0.284791	0.289044	0.293251	0.297411	0.301526
0.18	0.268065	0.272521	0.276928	0.281286	0.285596	0.289858	0.294074	0.298244	0.302368
0.19	0.268876	0.273343	0.27776	0.282128	0.286448	0.29072	0.294946	0.299125	0.303259
0.2	0.269735	0.274212	0.278639	0.283018	0.287348	0.291631	0.295867	0.300056	0.304201
0.21	0.27064	0.275129	0.279567	0.283957	0.288298	0.292591	0.296838	0.301038	0.305193
0.22	0.271595	0.276095	0.280545	0.284946	0.289298	0.293603	0.297861	0.302072	0.306238
0.23	0.272599	0.277111	0.281573	0.285986	0.29035	0.294667	0.298936	0.303159	0.307336
0.24	0.273654	0.278179	0.282654	0.287079	0.291455	0.295784	0.300065	0.3043	0.308489
0.25	0.274762	0.279299	0.283787	0.288225	0.292614	0.296955	0.301249	0.305496	0.309697
0.26	0.275922	0.280473	0.284974	0.289425	0.293828	0.298182	0.302489	0.306748	0.310962
0.27	0.277136	0.281702	0.286217	0.290682	0.295098	0.299466	0.303786	0.308059	0.312287
0.28	0.278407	0.282987	0.287517	0.291997	0.296427	0.300809	0.305143	0.30943	0.313671
0.29	0.279735	0.284331	0.288876	0.29337	0.297815	0.302212	0.30656	0.310862	0.315117
0.3	0.281122	0.285734	0.290294	0.294804	0.299265	0.303676	0.30804	0.312357	0.316626
0.31	0.282569	0.287198	0.291775	0.296301	0.300777	0.305205	0.309584	0.313916	0.318201
0.32	0.284079	0.288725	0.293319	0.297862	0.302355	0.306799	0.311194	0.315542	0.319844
0.33	0.285653	0.290317	0.294928	0.299489	0.303999	0.30846	0.312873	0.317238	0.321556
0.34	0.287294	0.291976	0.296606	0.301184	0.305713	0.310191	0.314622	0.319004	0.323339
0.35	0.289003	0.293704	0.298353	0.30295	0.307497	0.311995	0.316443	0.320844	0.325197
0.36	0.290782	0.295503	0.300172	0.304789	0.309356	0.313872	0.31834	0.322759	0.327131
0.37	0.292635	0.297377	0.302066	0.306704	0.311291	0.315827	0.320314	0.324753	0.329145
0.38	0.294563	0.299327	0.304038	0.308697	0.313304	0.317861	0.322369	0.326829	0.331241
0.39	0.296569	0.301356	0.306089	0.31077	0.3154	0.319979	0.324508	0.328989	0.333422

Table B.20: Period vs Normalized output voltage $\hat{v}$ from 0.40 to 0.79 in Presence of $\hat{I}_o$ from –0.46 to –0.54.

	$\hat{I}_0$								
	-0.46	-0.47	-0.48	-0.49	-0.5	-0.51	-0.52	-0.53	-0.54
$\hat{v}$	Period								
0.40	0.298658	0.303468	0.308224	0.312928	0.31758	0.322182	0.326734	0.331237	0.335692
0.41	0.30083	0.305665	0.310446	0.315174	0.31985	0.324475	0.32905	0.333576	0.338054
0.42	0.303091	0.307951	0.312757	0.31751	0.322211	0.32686	0.33146	0.33601	0.340513
0.43	0.305443	0.31033	0.315162	0.319941	0.324668	0.329343	0.333968	0.338544	0.343071
0.44	0.30789	0.312805	0.317665	0.322471	0.327225	0.331927	0.336579	0.341181	0.345735
0.45	0.310437	0.315381	0.32027	0.325104	0.329886	0.334617	0.339296	0.343926	0.348508
0.46	0.313088	0.318062	0.322981	0.327846	0.332657	0.337417	0.342126	0.346785	0.351396
0.47	0.315849	0.320854	0.325804	0.3307	0.335543	0.340333	0.345073	0.349763	0.354404
0.48	0.318723	0.323762	0.328745	0.333673	0.338548	0.343371	0.348143	0.352865	0.357539
0.49	0.321717	0.326791	0.331808	0.336771	0.341681	0.346538	0.351343	0.356099	0.360806
0.5	0.324837	0.329947	0.335001	0.34	0.344946	0.349839	0.35468	0.359472	0.364215
0.51	0.32809	0.333239	0.338331	0.343368	0.348351	0.353282	0.358161	0.362991	0.367771
0.52	0.331483	0.336672	0.341804	0.346881	0.351904	0.356875	0.361795	0.366664	0.371484
0.53	0.335023	0.340255	0.34543	0.350549	0.355615	0.360628	0.36559	0.370501	0.375364
0.54	0.33872	0.343997	0.349217	0.354381	0.359491	0.364549	0.369556	0.374513	0.379421
0.55	0.342583	0.347907	0.353175	0.358387	0.363545	0.368651	0.373705	0.37871	0.383667
0.56	0.346623	0.351998	0.357315	0.362578	0.367787	0.372944	0.378049	0.383105	0.388114
0.57	0.35085	0.356279	0.361651	0.366967	0.37223	0.377441	0.382602	0.387713	0.392776
0.58	0.355279	0.360765	0.366194	0.371568	0.376889	0.382159	0.387378	0.392548	0.397671
0.59	0.359922	0.365469	0.37096	0.376396	0.38178	0.387112	0.392394	0.397629	0.402816
0.6	0.364797	0.37041	0.375967	0.381469	0.38692	0.39232	0.397671	0.402974	0.408232
0.61	0.36992	0.375604	0.381232	0.386807	0.39233	0.397804	0.403229	0.408608	0.413942
0.62	0.375313	0.381073	0.386778	0.392431	0.398034	0.403587	0.409093	0.414555	0.419972
0.63	0.380997	0.38684	0.39263	0.398368	0.404056	0.409697	0.415293	0.420845	0.426354
0.64	0.386999	0.392933	0.398814	0.404646	0.410429	0.416167	0.42186	0.427512	0.433124
0.65	0.393348	0.399382	0.405364	0.411299	0.417187	0.423031	0.428834	0.434598	0.440324
0.66	0.40008	0.406224	0.412318	0.418366	0.424371	0.430335	0.43626	0.442149	0.448004
0.67	0.407235	0.4135	0.41972	0.425896	0.432031	0.438129	0.444193	0.450224	0.456225
0.68	0.414861	0.421262	0.427622	0.433942	0.440225	0.446476	0.452697	0.458891	0.465061
0.69	0.423013	0.429569	0.436088	0.442572	0.449025	0.455451	0.461854	0.468237	0.474604
0.7	0.431761	0.438494	0.445195	0.451868	0.458518	0.465148	0.471764	0.47837	0.48497
0.71	0.44119	0.448126	0.45504	0.461934	0.468815	0.475688	0.482558	0.489431	0.496314
0.72	0.451403	0.45858	0.465744	0.472902	0.48006	0.487226	0.494406	0.501608	0.508841
0.73	0.462536	0.47	0.477467	0.484946	0.492444	0.499973	0.507541	0.515161	0.522845
0.74	0.474766	0.482581	0.490423	0.498302	0.506232	0.514226	0.5223	0.530472	0.538765
0.75	0.488331	0.49659	0.504911	0.513311	0.52181	0.53043	0.539198	0.548149	0.557323
0.76	0.503576	0.512418	0.521381	0.530493	0.539789	0.549311	0.559114	0.569271	0.579879
0.77	0.52102	0.530676	0.540559	0.550725	0.561248	0.572228	0.583808	0.596205	0.60978
0.78	0.541535	0.552433	0.563787	0.575742	0.588513	0.602457	0.618242	0.637467	0.667705
0.79	0.566816	0.579949	0.59423	0.61029	0.629578	0.657897			

Table B.21: Period vs Normalized output voltage $\hat{v}$ from 0.80 to 0.81 in Presence of $\hat{I}_o$ from –0.46 to –0.54

	$\hat{I}_0$								
	-0.46	-0.47	-0.48	-0.49	-0.5	-0.51	-0.52	-0.53	-0.54
$\hat{v}$	Period								
0.8	0.60133	0.620578	0.647139						
0.81	0.67885								

Table B.22: Period vs Normalized output voltage $\hat{v}$ from 0.00 to 0.39 in Presence of $\hat{I}_o$ from –0.55 to –0.63.

	$\hat{I}_0$								
	-0.55	-0.56	-0.57	-0.58	-0.59	-0.6	-0.61	-0.62	-0.63
$\hat{v}$	Period								
0	0.298016	0.301926	0.305792	0.309614	0.313394	0.317131	0.320826	0.32448	0.328093
0.01	0.298124	0.302039	0.30591	0.309738	0.313522	0.317265	0.320966	0.324625	0.328245
0.02	0.298273	0.302193	0.306069	0.309902	0.313692	0.317441	0.321147	0.324813	0.328438
0.03	0.298462	0.302388	0.30627	0.310108	0.313904	0.317658	0.32137	0.325042	0.328673
0.04	0.298692	0.302624	0.306511	0.310355	0.314157	0.317917	0.321635	0.325313	0.32895
0.05	0.298964	0.302901	0.306794	0.310644	0.314452	0.318218	0.321943	0.325626	0.32927
0.06	0.299277	0.30322	0.307119	0.310976	0.31479	0.318562	0.322293	0.325983	0.329633
0.07	0.299632	0.303581	0.307487	0.31135	0.31517	0.318949	0.322686	0.326383	0.33004
0.08	0.300029	0.303985	0.307897	0.311766	0.315593	0.319379	0.323123	0.326827	0.330491
0.09	0.300469	0.304432	0.308351	0.312227	0.316061	0.319853	0.323604	0.327315	0.330986
0.1	0.300953	0.304922	0.308848	0.312731	0.316572	0.320371	0.32413	0.327848	0.331526
0.11	0.30148	0.305456	0.30939	0.31328	0.317128	0.320935	0.324701	0.328426	0.332112
0.12	0.302051	0.306035	0.309976	0.313874	0.31773	0.321544	0.325318	0.329051	0.332744
0.13	0.302668	0.30666	0.310608	0.314514	0.318378	0.3222	0.325981	0.329722	0.333423
0.14	0.30333	0.30733	0.311286	0.3152	0.319072	0.322902	0.326692	0.330441	0.33415
0.15	0.304038	0.308046	0.312011	0.315933	0.319814	0.323652	0.32745	0.331208	0.334926
0.16	0.304793	0.30881	0.312784	0.316715	0.320603	0.324451	0.328257	0.332024	0.33575
0.17	0.305596	0.309622	0.313605	0.317545	0.321442	0.325299	0.329114	0.33289	0.336625
0.18	0.306447	0.310483	0.314475	0.318424	0.322331	0.326197	0.330022	0.333806	0.337551
0.19	0.307349	0.311394	0.315395	0.319354	0.323271	0.327146	0.330981	0.334775	0.338529
0.2	0.3083	0.312355	0.316367	0.320336	0.324263	0.328148	0.331992	0.335796	0.339561
0.21	0.309303	0.313369	0.317391	0.32137	0.325307	0.329203	0.333057	0.336872	0.340646
0.22	0.310359	0.314435	0.318468	0.322458	0.326406	0.330312	0.334177	0.338002	0.341788
0.23	0.311468	0.315556	0.3196	0.323601	0.32756	0.331477	0.335354	0.339189	0.342986
0.24	0.312632	0.316732	0.320788	0.3248	0.328771	0.332699	0.336587	0.340434	0.344242
0.25	0.313853	0.317964	0.322032	0.326057	0.330039	0.33398	0.337879	0.341738	0.345558
0.26	0.315131	0.319255	0.323335	0.327373	0.331367	0.33532	0.339232	0.343103	0.346935
0.27	0.316468	0.320605	0.324699	0.328749	0.332756	0.336722	0.340646	0.34453	0.348374
0.28	0.317866	0.322017	0.326124	0.330187	0.334208	0.338187	0.342124	0.346021	0.349878
0.29	0.319326	0.323491	0.327612	0.331689	0.335724	0.339716	0.343668	0.347578	0.351449
0.3	0.320851	0.32503	0.329165	0.333257	0.337306	0.341313	0.345278	0.349203	0.353088
0.31	0.322441	0.326636	0.330786	0.334892	0.338956	0.342978	0.346958	0.350898	0.354797
0.32	0.324099	0.32831	0.332475	0.336598	0.340677	0.344714	0.34871	0.352664	0.356579
0.33	0.325828	0.330054	0.334236	0.338375	0.34247	0.346523	0.350535	0.354506	0.358436
0.34	0.327628	0.331872	0.336071	0.340226	0.344338	0.348408	0.352436	0.356424	0.360371
0.35	0.329504	0.333765	0.337982	0.342155	0.346284	0.350371	0.354417	0.358421	0.362386
0.36	0.331457	0.335736	0.339972	0.344163	0.34831	0.352416	0.356479	0.360502	0.364484
0.37	0.33349	0.337789	0.342043	0.346253	0.35042	0.354544	0.358626	0.362667	0.366668
0.38	0.335606	0.339925	0.344199	0.348429	0.352615	0.356759	0.360861	0.364922	0.368943
0.39	0.337808	0.342148	0.346443	0.350694	0.354901	0.359065	0.363188	0.367269	0.37131

Table B.23: Period vs Normalized output voltage $\hat{v}$ from 0.40 to 0.77 in Presence of $\hat{I}_o$ from –0.55 to –0.63.

	$\hat{I}_0$								
	-0.55	-0.56	-0.57	-0.58	-0.59	-0.6	-0.61	-0.62	-0.63
$\hat{v}$	Period								
0.40	0.3401	0.344462	0.348779	0.353051	0.35728	0.361465	0.365609	0.369712	0.373775
0.41	0.342485	0.34687	0.351209	0.355504	0.359756	0.363964	0.36813	0.372256	0.37634
0.42	0.344968	0.349376	0.353739	0.358058	0.362333	0.366565	0.370755	0.374904	0.379012
0.43	0.347551	0.351985	0.356373	0.360717	0.365016	0.369273	0.373488	0.377661	0.381794
0.44	0.350241	0.354701	0.359115	0.363485	0.367811	0.372093	0.376334	0.380533	0.384692
0.45	0.353042	0.357529	0.361971	0.366368	0.370721	0.375031	0.379299	0.383526	0.387712
0.46	0.355959	0.360475	0.364945	0.369371	0.373753	0.378092	0.382389	0.386644	0.390859
0.47	0.358997	0.363544	0.368045	0.372501	0.376913	0.381282	0.385609	0.389895	0.394141
0.48	0.362164	0.366743	0.371275	0.375763	0.380208	0.384609	0.388968	0.393287	0.397565
0.49	0.365466	0.370078	0.374645	0.379167	0.383645	0.38808	0.392474	0.396826	0.401138
0.5	0.368909	0.373558	0.37816	0.382718	0.387232	0.391703	0.396133	0.400522	0.404871
0.51	0.372504	0.37719	0.38183	0.386426	0.390978	0.395488	0.399956	0.404384	0.408771
0.52	0.376257	0.380983	0.385664	0.3903	0.394893	0.399444	0.403953	0.408422	0.412851
0.53	0.38018	0.384949	0.389672	0.394352	0.398988	0.403582	0.408135	0.412648	0.417123
0.54	0.384282	0.389096	0.393866	0.398591	0.403274	0.407915	0.412515	0.417076	0.421598
0.55	0.388576	0.393439	0.398258	0.403033	0.407765	0.412457	0.417108	0.42172	0.426293
0.56	0.393075	0.39799	0.402862	0.40769	0.412476	0.417222	0.421927	0.426595	0.431225
0.57	0.397793	0.402765	0.407694	0.412579	0.417423	0.422228	0.426993	0.43172	0.436411
0.58	0.402749	0.407781	0.412771	0.417719	0.422626	0.427494	0.432324	0.437117	0.441874
0.59	0.407959	0.413058	0.418114	0.42313	0.428105	0.433043	0.437944	0.442808	0.447639
0.6	0.413445	0.418616	0.423745	0.428835	0.433886	0.4389	0.443878	0.448822	0.453734
0.61	0.419233	0.424482	0.429691	0.434862	0.439996	0.445094	0.450159	0.45519	0.460191
0.62	0.425348	0.430684	0.435981	0.441242	0.446468	0.45166	0.45682	0.46195	0.467051
0.63	0.431824	0.437256	0.442651	0.448012	0.45334	0.458637	0.463905	0.469145	0.474359
0.64	0.438699	0.444237	0.449742	0.455215	0.460658	0.466073	0.471463	0.476828	0.482172
0.65	0.446016	0.451674	0.457303	0.462903	0.468476	0.474026	0.479555	0.485064	0.490557
0.66	0.453828	0.459623	0.465392	0.471137	0.476861	0.482566	0.488256	0.493933	0.4996
0.67	0.4622	0.468152	0.474083	0.479995	0.485894	0.491781	0.49766	0.503534	0.509408
0.68	0.471211	0.477344	0.483464	0.489574	0.495678	0.501781	0.507886	0.513999	0.520124
0.69	0.480959	0.487306	0.49365	0.499996	0.506348	0.512713	0.519095	0.525501	0.531939
0.70	0.49157	0.498175	0.504792	0.511425	0.518083	0.524773	0.531504	0.538284	0.545124
0.71	0.503213	0.510135	0.51709	0.524086	0.531133	0.538243	0.545428	0.552705	0.560091
0.72	0.516116	0.523442	0.530833	0.538302	0.545865	0.553543	0.561358	0.569338	0.577518
0.73	0.53061	0.538471	0.546451	0.554573	0.562868	0.571372	0.580133	0.589212	0.598695
0.74	0.547205	0.555822	0.564657	0.57376	0.583197	0.593057	0.603469	0.614628	0.626858
0.75	0.566773	0.576568	0.586803	0.597614	0.609206	0.621925	0.636431	0.654376	0.685669
0.76	0.591079	0.603084	0.616252	0.631269	0.649852	0.682511			
0.77	0.625222	0.644226	0.676194						

Table B.24: Period vs Normalized output voltage $\hat{v}$ from 0.00 to 0.39 in Presence of $\hat{I}_o$ from –0.64 to –0.72.

	$\hat{I}_0$								
	-0.64	-0.65	-0.66	-0.67	-0.68	-0.69	-0.7	-0.71	-0.72
$\hat{v}$	Period								
0.00	0.331667	0.335202	0.338697	0.342155	0.345575	0.348958	0.352304	0.355615	0.35889
0.01	0.331824	0.335365	0.338866	0.34233	0.345756	0.349146	0.352499	0.355816	0.359098
0.02	0.332023	0.33557	0.339078	0.342548	0.34598	0.349376	0.352736	0.35606	0.359348
0.03	0.332265	0.335817	0.339331	0.342808	0.346247	0.349649	0.353015	0.356346	0.359641
0.04	0.332548	0.336107	0.339628	0.343111	0.346556	0.349965	0.353338	0.356676	0.359978
0.05	0.332875	0.33644	0.339967	0.343457	0.346909	0.350325	0.353705	0.357049	0.360358
0.06	0.333244	0.336816	0.34035	0.343847	0.347306	0.350729	0.354115	0.357467	0.360783
0.07	0.333658	0.337237	0.340777	0.344281	0.347747	0.351177	0.35457	0.357929	0.361253
0.08	0.334115	0.337701	0.341249	0.344759	0.348233	0.35167	0.355071	0.358436	0.361767
0.09	0.334618	0.338211	0.341766	0.345283	0.348764	0.352208	0.355617	0.35899	0.362328
0.1	0.335165	0.338766	0.342328	0.345853	0.349341	0.352793	0.356209	0.35959	0.362936
0.11	0.335759	0.339367	0.342937	0.346469	0.349965	0.353425	0.356848	0.360237	0.363591
0.12	0.336398	0.340014	0.343592	0.347133	0.350636	0.354104	0.357535	0.360932	0.364294
0.13	0.337086	0.340709	0.344295	0.347844	0.351356	0.354831	0.358271	0.361676	0.365046
0.14	0.337821	0.341453	0.345047	0.348604	0.352124	0.355608	0.359056	0.362469	0.365848
0.15	0.338605	0.342245	0.345848	0.349413	0.352941	0.356434	0.359891	0.363313	0.3667
0.16	0.339438	0.343087	0.346698	0.350273	0.35381	0.357311	0.360777	0.364207	0.367603
0.17	0.340322	0.34398	0.3476	0.351183	0.35473	0.35824	0.361715	0.365155	0.36856
0.18	0.341257	0.344925	0.348554	0.352147	0.355702	0.359222	0.362706	0.366155	0.36957
0.19	0.342245	0.345922	0.349561	0.353163	0.356728	0.360258	0.363751	0.36721	0.370634
0.20	0.343286	0.346973	0.350622	0.354234	0.357809	0.361348	0.364852	0.36832	0.371754
0.21	0.344382	0.348079	0.351738	0.355361	0.358946	0.362495	0.366009	0.369488	0.372932
0.22	0.345534	0.349241	0.352911	0.356544	0.36014	0.3637	0.367224	0.370713	0.374168
0.23	0.346743	0.350461	0.354142	0.357786	0.361392	0.364963	0.368498	0.371999	0.375464
0.24	0.34801	0.35174	0.355432	0.359087	0.362705	0.366287	0.369833	0.373345	0.376822
0.25	0.349338	0.353079	0.356783	0.36045	0.364079	0.367673	0.371231	0.374754	0.378243
0.26	0.350727	0.354481	0.358196	0.361875	0.365517	0.369122	0.372692	0.376228	0.379728
0.27	0.352179	0.355945	0.359674	0.363365	0.367019	0.370637	0.37422	0.377767	0.38128
0.28	0.353696	0.357476	0.361217	0.364921	0.368588	0.372219	0.375815	0.379375	0.382901
0.29	0.355281	0.359073	0.362828	0.366546	0.370226	0.373871	0.37748	0.381054	0.384593
0.30	0.356933	0.36074	0.364509	0.368241	0.371935	0.375594	0.379217	0.382804	0.386358
0.31	0.358657	0.362479	0.366262	0.370008	0.373717	0.37739	0.381028	0.38463	0.388198
0.32	0.360455	0.364291	0.36809	0.371851	0.375575	0.379263	0.382915	0.386533	0.390115
0.33	0.362327	0.36618	0.369994	0.373771	0.377511	0.381214	0.384882	0.388515	0.392114
0.34	0.364278	0.368147	0.371978	0.375771	0.379527	0.383247	0.386932	0.390581	0.394196
0.35	0.366311	0.370196	0.374044	0.377854	0.381628	0.385365	0.389066	0.392732	0.396364
0.36	0.368427	0.37233	0.376196	0.380024	0.383815	0.38757	0.391289	0.394973	0.398623
0.37	0.37063	0.374552	0.378436	0.382283	0.386093	0.389866	0.393604	0.397306	0.400975
0.38	0.372923	0.376865	0.380769	0.384635	0.388464	0.392257	0.396014	0.399736	0.403424
0.39	0.375311	0.379273	0.383197	0.387084	0.390933	0.394747	0.398524	0.402267	0.405975

Table B.25: Period vs Normalized output voltage $\hat{v}$ from 0.40 to 0.74 in Presence of $\hat{I}_o$ from –0.64 to –0.72.

	$\hat{I}_0$								
	-0.64	-0.65	-0.66	-0.67	-0.68	-0.69	-0.7	-0.71	-0.72
$\hat{v}$	Period								
0.40	0.377797	0.381781	0.385726	0.389634	0.393505	0.397339	0.401138	0.404903	0.408632
0.41	0.380385	0.384391	0.388359	0.392289	0.396183	0.40004	0.403861	0.407648	0.4114
0.42	0.38308	0.38711	0.391101	0.395055	0.398972	0.402853	0.406698	0.410508	0.414285
0.43	0.385887	0.389942	0.393958	0.397936	0.401878	0.405784	0.409654	0.413489	0.417291
0.44	0.388812	0.392892	0.396934	0.400939	0.404907	0.408839	0.412735	0.416597	0.420425
0.45	0.391859	0.395966	0.400036	0.404068	0.408064	0.412024	0.415948	0.419838	0.423694
0.46	0.395035	0.399172	0.403271	0.407332	0.411357	0.415346	0.4193	0.42322	0.427106
0.47	0.398347	0.402515	0.406645	0.410737	0.414793	0.418814	0.422799	0.426751	0.430668
0.48	0.401804	0.406004	0.410166	0.414291	0.418381	0.422434	0.426453	0.430438	0.43439
0.49	0.405412	0.409646	0.413844	0.418004	0.422128	0.426218	0.430272	0.434293	0.438281
0.5	0.409181	0.413452	0.417687	0.421884	0.426047	0.430174	0.434267	0.438326	0.442353
0.51	0.41312	0.417432	0.421706	0.425944	0.430146	0.434314	0.438448	0.442549	0.446618
0.52	0.417242	0.421596	0.425912	0.430193	0.434439	0.438651	0.442829	0.446975	0.451089
0.53	0.421558	0.425957	0.43032	0.434647	0.438939	0.443198	0.447424	0.451619	0.455782
0.54	0.426083	0.43053	0.434942	0.439319	0.443663	0.447973	0.452251	0.456497	0.460713
0.55	0.43083	0.435331	0.439796	0.444227	0.448626	0.452991	0.457326	0.46163	0.465904
0.56	0.435818	0.440376	0.4449	0.44939	0.453848	0.458275	0.462672	0.467038	0.471377
0.57	0.441066	0.445687	0.450275	0.45483	0.459354	0.463847	0.468312	0.472748	0.477157
0.58	0.446597	0.451287	0.455944	0.46057	0.465167	0.469734	0.474274	0.478787	0.483274
0.59	0.452436	0.457202	0.461936	0.466641	0.471318	0.475967	0.480591	0.48519	0.489765
0.60	0.458613	0.463462	0.468283	0.473076	0.477842	0.482584	0.487301	0.491997	0.496672
0.61	0.465163	0.470106	0.475022	0.479914	0.484781	0.489626	0.494451	0.499256	0.504044
0.62	0.472125	0.477174	0.482199	0.487202	0.492184	0.497148	0.502095	0.507026	0.511944
0.63	0.47955	0.484719	0.489868	0.494998	0.500113	0.505213	0.510301	0.515379	0.520449
0.64	0.487496	0.492803	0.498094	0.503373	0.50864	0.5139	0.519154	0.524405	0.529656
0.65	0.496036	0.501503	0.506961	0.512413	0.517862	0.523311	0.528763	0.534223	0.539693
0.66	0.50526	0.510916	0.516573	0.522233	0.5279	0.533578	0.539273	0.544989	0.550731
0.67	0.515285	0.52117	0.527067	0.53298	0.538916	0.544881	0.55088	0.556921	0.563013
0.68	0.526266	0.532432	0.538628	0.544861	0.551139	0.557472	0.563868	0.570341	0.576904
0.69	0.538415	0.544939	0.551521	0.558171	0.564903	0.571732	0.578676	0.585756	0.592999
0.70	0.552037	0.559037	0.566141	0.573367	0.58074	0.588288	0.59605	0.604071	0.612414
0.71	0.567608	0.575281	0.583142	0.591232	0.599603	0.608325	0.617497	0.627262	0.637849
0.72	0.585941	0.594665	0.603768	0.613358	0.623599	0.634753	0.6473	0.662316	0.683812
0.73	0.6087	0.619407	0.631112	0.644366	0.660472	0.68522			
0.74	0.640772	0.657875	0.686118						

Table B.26: Period vs Normalized output voltage $\hat{v}$ from 0.00 to 0.39 in Presence of $\hat{I}_o$ from –0.73 to –0.80.

	$\hat{I}_0$							
	-0.73	-0.74	-0.75	-0.76	-0.77	-0.78	-0.79	-0.8
$\hat{v}$	Period							
0.00	0.362131	0.365338	0.36851	0.37165	0.374757	0.377832	0.380875	0.380875
0.01	0.362345	0.365559	0.368738	0.371885	0.374999	0.37808	0.38113	0.38113
0.02	0.362602	0.365822	0.369009	0.372162	0.375283	0.378372	0.381429	0.381429
0.03	0.362902	0.366129	0.369323	0.372483	0.375611	0.378707	0.381772	0.381772
0.04	0.363246	0.36648	0.36968	0.372848	0.375983	0.379086	0.382158	0.382158
0.05	0.363633	0.366874	0.370082	0.373257	0.376399	0.37951	0.382589	0.382589
0.06	0.364065	0.367313	0.370528	0.37371	0.37686	0.379978	0.383065	0.383065
0.07	0.364542	0.367797	0.37102	0.374209	0.377366	0.380492	0.383586	0.383586
0.08	0.365064	0.368327	0.371557	0.374754	0.377919	0.381052	0.384154	0.384154
0.09	0.365633	0.368903	0.372141	0.375345	0.378518	0.381659	0.384769	0.384769
0.10	0.366248	0.369526	0.372772	0.375984	0.379165	0.382313	0.385431	0.385431
0.11	0.366911	0.370197	0.37345	0.376671	0.379859	0.383016	0.386142	0.386142
0.12	0.367622	0.370916	0.374178	0.377406	0.380603	0.383768	0.386902	0.386902
0.13	0.368382	0.371685	0.374954	0.378191	0.381396	0.38457	0.387712	0.387712
0.14	0.369192	0.372503	0.375781	0.379027	0.38224	0.385423	0.388574	0.388574
0.15	0.370053	0.373373	0.37666	0.379914	0.383136	0.386327	0.389487	0.389487
0.16	0.370966	0.374294	0.37759	0.380853	0.384085	0.387284	0.390453	0.390453
0.17	0.371931	0.375269	0.378574	0.381846	0.385087	0.388296	0.391474	0.391474
0.18	0.37295	0.376297	0.379612	0.382893	0.386143	0.389362	0.392549	0.392549
0.19	0.374024	0.377381	0.380705	0.383997	0.387256	0.390484	0.393682	0.393682
0.20	0.375155	0.378521	0.381855	0.385157	0.388426	0.391665	0.394872	0.394872
0.21	0.376342	0.379719	0.383064	0.386375	0.389655	0.392904	0.396121	0.396121
0.22	0.377589	0.380977	0.384331	0.387654	0.390944	0.394203	0.397431	0.397431
0.23	0.378896	0.382295	0.38566	0.388993	0.392295	0.395565	0.398804	0.398804
0.24	0.380265	0.383675	0.387052	0.390396	0.393709	0.39699	0.40024	0.40024
0.25	0.381697	0.385119	0.388507	0.391863	0.395188	0.398481	0.401743	0.401743
0.26	0.383195	0.386628	0.390029	0.393397	0.396733	0.400038	0.403312	0.403312
0.27	0.38476	0.388205	0.391618	0.394999	0.398348	0.401665	0.404952	0.404952
0.28	0.386393	0.389852	0.393278	0.396672	0.400033	0.403364	0.406663	0.406663
0.29	0.388099	0.391571	0.39501	0.398417	0.401792	0.405136	0.408449	0.408449
0.30	0.389877	0.393363	0.396816	0.400237	0.403626	0.406984	0.410311	0.410311
0.31	0.391731	0.395232	0.3987	0.402135	0.405539	0.408911	0.412252	0.412252
0.32	0.393664	0.39718	0.400663	0.404113	0.407532	0.410919	0.414276	0.414276
0.33	0.395678	0.39921	0.402708	0.406174	0.409609	0.413012	0.416384	0.416384
0.34	0.397777	0.401324	0.404839	0.408321	0.411772	0.415192	0.418581	0.418581
0.35	0.399962	0.403527	0.407059	0.410558	0.414026	0.417463	0.420869	0.420869
0.36	0.402239	0.405821	0.409371	0.412888	0.416374	0.419829	0.423253	0.423253
0.37	0.404609	0.40821	0.411779	0.415315	0.41882	0.422293	0.425736	0.425736
0.38	0.407078	0.410699	0.414287	0.417843	0.421367	0.42486	0.428323	0.428323
0.39	0.40965	0.413291	0.4169	0.420476	0.424021	0.427535	0.431019	0.431019

Table B.27: Period vs Normalized output voltage $\hat{v}$ from 0.40 to 0.70 in Presence of $\hat{I}_o$ from –0.73 to –0.80.

	$\hat{I}_0$							
	-0.73	-0.74	-0.75	-0.76	-0.77	-0.78	-0.79	-0.8
$\hat{v}$	Period							
0.40	0.412328	0.415991	0.419621	0.42322	0.426787	0.430322	0.433828	0.433828
0.41	0.415119	0.418805	0.422458	0.426079	0.429669	0.433228	0.436756	0.436756
0.42	0.418027	0.421737	0.425414	0.429059	0.432673	0.436257	0.43981	0.43981
0.43	0.421058	0.424793	0.428496	0.432167	0.435807	0.439416	0.442995	0.442995
0.44	0.42422	0.427981	0.431711	0.435409	0.439076	0.442712	0.446319	0.446319
0.45	0.427517	0.431307	0.435065	0.438792	0.442488	0.446154	0.44979	0.44979
0.46	0.430959	0.434779	0.438568	0.442325	0.446052	0.449749	0.453416	0.453416
0.47	0.434553	0.438406	0.442227	0.446017	0.449777	0.453507	0.457208	0.457208
0.48	0.438309	0.442196	0.446052	0.449877	0.453672	0.457438	0.461175	0.461175
0.49	0.442237	0.446161	0.450054	0.453917	0.45775	0.461554	0.465329	0.465329
0.50	0.446348	0.450312	0.454245	0.458148	0.462022	0.465867	0.469685	0.469685
0.51	0.450655	0.454661	0.458638	0.462585	0.466503	0.470393	0.474255	0.474255
0.52	0.455172	0.459224	0.463247	0.467242	0.471208	0.475147	0.479059	0.479059
0.53	0.459914	0.464017	0.468091	0.472137	0.476156	0.480148	0.484114	0.484114
0.54	0.4649	0.469058	0.473187	0.47729	0.481366	0.485416	0.489442	0.489442
0.55	0.47015	0.474368	0.478559	0.482723	0.486863	0.490978	0.495069	0.495069
0.56	0.475688	0.479972	0.48423	0.488463	0.492673	0.49686	0.501024	0.501024
0.57	0.481539	0.485897	0.49023	0.49454	0.498828	0.503095	0.507341	0.507341
0.58	0.487737	0.492177	0.496594	0.50099	0.505366	0.509723	0.514063	0.514063
0.59	0.494318	0.49885	0.503362	0.507856	0.512332	0.516792	0.521237	0.521237
0.60	0.501327	0.505963	0.510583	0.515188	0.519779	0.524357	0.528925	0.528925
0.61	0.508816	0.513573	0.518317	0.52305	0.527774	0.532491	0.537202	0.537202
0.62	0.516851	0.521748	0.526637	0.531521	0.536402	0.541282	0.546164	0.546164
0.63	0.525514	0.530576	0.535637	0.540701	0.545771	0.550849	0.555938	0.555938
0.64	0.53491	0.54017	0.54544	0.550723	0.556024	0.561346	0.566696	0.566696
0.65	0.545177	0.550681	0.55621	0.561767	0.567361	0.572996	0.578682	0.578682
0.66	0.556505	0.562318	0.568178	0.574092	0.580071	0.586125	0.592267	0.592267
0.67	0.569164	0.575386	0.581691	0.588092	0.594609	0.60126	0.608073	0.608073
0.68	0.583573	0.590367	0.59731	0.604432	0.611769	0.619369	0.627297	0.627297
0.69	0.600437	0.608113	0.616081	0.624418	0.633229	0.642677	0.653029	0.653029
0.70	0.621167	0.630453	0.640469	0.651544	0.664344	0.680669	0.714353	0.714353
0.71	0.649662	0.66356	0.682246	0.711202				

Table B.28: Coefficients of resulted equivalent polynomials by Data Fitting application.

$\hat{I}_0$	**a0**	**a1**	**a2**	**a3**
-0.01	0.04525	-0.02902	0.007814	0.006021
-0.02	0.1334	-0.08501	0.02295	0.01807
-0.03	0.1752	-0.1111	0.03006	0.02411
-0.04	0.215	-0.1355	0.03677	0.03015
-0.05	0.2526	-0.158	0.04302	0.03619
-0.06	0.2878	-0.1785	0.0488	0.04224
-0.07	0.3205	-0.1971	0.05412	0.04829
-0.08	0.3509	-0.2138	0.05899	0.05433
-0.09	0.3791	-0.2287	0.06345	0.06036
-0.1	0.4052	-0.2421	0.06753	0.06638
-0.11	0.4294	-0.2541	0.0713	0.07239
-0.12	0.452	-0.2649	0.07478	0.07837
-0.13	0.4731	-0.2747	0.07804	0.08432
-0.14	0.4929	-0.2838	0.08112	0.09025
-0.15	0.5118	-0.2923	0.08405	0.09613
-0.16	0.5298	-0.3003	0.08687	0.102
-0.17	0.5471	-0.3081	0.08963	0.1078
-0.18	0.5639	-0.3158	0.09235	0.1136
-0.19	0.5803	-0.3234	0.09507	0.1193
-0.2	0.5966	-0.3311	0.09779	0.1249
-0.21	0.6127	-0.3391	0.1006	0.1306
-0.22	0.6288	-0.3473	0.1034	0.1361
-0.23	0.6451	-0.3559	0.1063	0.1416
-0.24	0.6615	-0.365	0.1093	0.1471
-0.25	0.6783	-0.3745	0.1124	0.1525
-0.26	0.6955	-0.3847	0.1156	0.1578
-0.27	0.7131	-0.3955	0.119	0.163
-0.28	0.7313	-0.407	0.1226	0.1683
-0.29	0.7502	-0.4194	0.1263	0.1734
-0.3	0.7698	-0.4325	0.1302	0.1785
-0.31	0.7902	-0.4467	0.1344	0.1835
-0.32	0.8116	-0.4618	0.1388	0.1884
-0.33	0.834	-0.4781	0.1434	0.1933
-0.34	0.8575	-0.4956	0.1483	0.1981
-0.35	0.8823	-0.5144	0.1536	0.2029
-0.36	0.9085	-0.5347	0.1592	0.2075
-0.37	0.9363	-0.5566	0.1652	0.2121
-0.38	0.966	-0.5803	0.1716	0.2166
-0.39	0.9976	-0.6062	0.1786	0.2211
-0.4	1.032	-0.6344	0.1861	0.2254

Table B.29: Coefficients of resulted equivalent polynomials by Data Fitting application.

$\hat{I}_0$	a_0	a_1	a_2	a_3
-0.41	1.068	-0.6653	0.1944	0.2297
-0.42	1.108	-0.6994	0.2034	0.2339
-0.43	1.152	-0.7374	0.2134	0.238
-0.44	1.201	-0.7802	0.2246	0.2419
-0.45	1.256	-0.8291	0.2374	0.2458
-0.46	1.319	-0.8866	0.2523	0.2495
-0.47	1.395	-0.9572	0.2707	0.2529
-0.48	1.499	-1.056	0.2962	0.256
-0.49	1.335	-0.8806	0.2501	0.2626
-0.5	1.415	-0.954	0.2689	0.2659
-0.51	1.529	-1.062	0.2965	0.2687
-0.52	1.351	-0.8739	0.2476	0.2753
-0.53	1.434	-0.9497	0.2668	0.2785
-0.54	1.56	-1.067	0.2966	0.2811
-0.55	1.364	-0.8659	0.2448	0.2877
-0.56	1.45	-0.9434	0.2642	0.2907
-0.57	1.588	-1.071	0.2962	0.2931
-0.58	1.377	-0.8564	0.2417	0.2996
-0.59	1.464	-0.9347	0.2611	0.3025
-0.6	1.61	-1.069	0.2942	0.3047
-0.61	1.387	-0.845	0.2383	0.3112
-0.62	1.475	-0.9232	0.2573	0.314
-0.63	1.622	-1.056	0.2898	0.3161
-0.64	1.385	-0.8318	0.2344	0.3224
-0.65	1.483	-0.9086	0.2529	0.3251
-0.66	1.623	-1.033	0.283	0.3273
-0.67	1.4	-0.8165	0.2302	0.3333
-0.68	1.487	-0.891	0.2479	0.3359
-0.69	1.617	-1.005	0.275	0.3381
-0.7	1.403	-0.7992	0.2257	0.3438
-0.71	1.488	-0.8707	0.2425	0.3464
-0.72	1.607	-0.9737	0.2666	0.3487
-0.73	1.404	-0.7799	0.2208	0.354
-0.74	1.486	-0.8479	0.2366	0.3566
-0.75	1.596	-0.9408	0.2581	0.3589
-0.76	1.761	-1.084	0.2912	0.3606
-0.77	1.481	-0.823	0.2304	0.3665
-0.78	1.582	-0.9069	0.2496	0.3688
-0.79	1.777	-1.074	0.2878	0.3702
-0.8	1.777	-1.074	0.2878	0.3702

Table B.30: Simulation and Practical Test results of the SRC code Model.

Power	Frequency[kHz]		$\hat{v}$	$\hat{I}_0$
	Simimulated	Practical		
0.01	inf	inf	0.09394	-0.1065
0.02	323.63	323.42	0.1328	-0.1506
0.03	268.90	268.82	0.1627	-0.1844
0.04	235.30	235.16	0.1879	-0.2129
0.05	212.40	212.40	0.2100	-0.2380
0.06	195.20	195.31	0.2301	-0.2608
0.07	181.60	181.55	0.2485	-0.2817
0.08	inf	inf	0.2657	-0.3011
0.09	161.00	160.98	0.2818	-0.3194
0.10	153.10	153.08	0.2971	-0.3366
0.11	146.20	146.20	0.3116	-0.3531
0.12	140.10	140.13	0.3254	-0.3688
0.13	134.70	134.63	0.3387	-0.3838
0.14	129.80	129.74	0.3515	-0.3983
0.15	126.70	126.70	0.3638	-0.4123
0.16	122.70	122.73	0.3757	-0.4258
0.17	119.00	119.05	0.3873	-0.4389
0.18	115.50	115.53	0.3985	-0.4517
0.19	112.20	112.26	0.4095	-0.4640
0.20	109.20	109.17	0.4201	-0.4761
0.21	inf	inf	0.4305	-0.4878
0.22	104.00	103.99	0.4406	-0.4993
0.23	inf	inf	0.4505	-0.5105
0.24	99.190	99.210	0.4602	-0.5215
0.25	96.790	96.750	0.4697	-0.5323

Table B.31: Normalized Power $\hat{p}$ vs Normalized initial resonant current $\hat{I}_0$ in presence of normalized output voltage $\hat{v}$.

					$\hat{v}$				
	0.01	0.02	0.03	0.04	0.05	0.06	0.07	0.08	0.09
$\hat{I}_0$					$\hat{p}$				
-0.01	5E-05	1E-04	0.00015	0.0002	0.00025	0.0003	0.00035	0.0004	0.00045
-0.02	1E-04	0.0002	0.0003	0.0004	0.0005	0.000599	0.0007	0.0008	0.0009
-0.03	0.00015	0.0003	0.00045	0.0006	0.00075	0.000899	0.00105	0.0012	0.001349
-0.04	0.0002	0.0004	0.0006	0.000799	0.000999	0.001199	0.001399	0.001599	0.001799
-0.05	0.00025	0.000499	0.000749	0.000999	0.001249	0.001498	0.001748	0.001998	0.002248
-0.06	0.0003	0.000599	0.000899	0.001198	0.001498	0.001797	0.002097	0.002396	0.002696
-0.07	0.000349	0.000699	0.001048	0.001397	0.001746	0.002096	0.002445	0.002794	0.003144
-0.08	0.000399	0.000798	0.001197	0.001596	0.001995	0.002394	0.002793	0.003192	0.003591
-0.09	0.000449	0.000897	0.001346	0.001794	0.002243	0.002691	0.00314	0.003588	0.004037
-0.1	0.000498	0.000996	0.001494	0.001992	0.00249	0.002988	0.003486	0.003984	0.004482
-0.11	0.000547	0.001095	0.001642	0.002189	0.002737	0.003284	0.003831	0.004378	0.004926
-0.12	0.000597	0.001193	0.00179	0.002386	0.002983	0.003579	0.004176	0.004772	0.005369
-0.13	0.000646	0.001291	0.001937	0.002582	0.003228	0.003874	0.004519	0.005165	0.00581
-0.14	0.000695	0.001389	0.002084	0.002778	0.003473	0.004167	0.004862	0.005556	0.006251
-0.15	0.000743	0.001487	0.00223	0.002973	0.003717	0.00446	0.005203	0.005947	0.00669
-0.16	0.000792	0.001584	0.002376	0.003168	0.00396	0.004752	0.005544	0.006336	0.007128
-0.17	0.00084	0.001681	0.002521	0.003362	0.004202	0.005043	0.005883	0.006723	0.007564
-0.18	0.000889	0.001777	0.002666	0.003555	0.004444	0.005332	0.006221	0.00711	0.007999
-0.19	0.000937	0.001874	0.00281	0.003747	0.004684	0.005621	0.006558	0.007495	0.008432
-0.2	0.000985	0.001969	0.002954	0.003939	0.004924	0.005909	0.006894	0.007878	0.008863
-0.21	0.001032	0.002065	0.003097	0.00413	0.005163	0.006195	0.007228	0.00826	0.009293
-0.22	0.00108	0.00216	0.00324	0.00432	0.0054	0.006481	0.007561	0.007561	0.009721
-0.23	0.001127	0.002255	0.003382	0.00451	0.005637	0.006765	0.007892	0.00902	0.010148
-0.24	0.001174	0.002349	0.003524	0.004698	0.005873	0.007048	0.008223	0.009398	0.010573
-0.25	0.001221	0.002443	0.003664	0.004886	0.006108	0.00733	0.008552	0.009774	0.010996
-0.26	0.001268	0.002536	0.003805	0.005073	0.006342	0.00761	0.008879	0.010148	0.011417
-0.27	0.001315	0.002629	0.003944	0.005259	0.006575	0.00789	0.009205	0.010521	0.011836
-0.28	0.001361	0.002722	0.004083	0.005445	0.006806	0.008168	0.00953	0.010892	0.012254
-0.29	0.001407	0.002814	0.004222	0.005629	0.007037	0.008445	0.009853	0.011261	0.01267
-0.3	0.001453	0.002906	0.00436	0.005813	0.007267	0.008721	0.010175	0.011629	0.013084
-0.31	0.001499	0.002998	0.004497	0.005996	0.007496	0.008995	0.010495	0.011995	0.013496
-0.32	0.001544	0.003089	0.004633	0.006178	0.007723	0.009269	0.010814	0.01236	0.013906
-0.33	0.001589	0.003179	0.004769	0.006359	0.00795	0.009541	0.011132	0.012723	0.014315
-0.34	0.001635	0.003269	0.004904	0.00654	0.008176	0.009812	0.011448	0.013085	0.014722
-0.35	0.001679	0.003359	0.005039	0.006719	0.0084	0.010081	0.011763	0.013444	0.015127
-0.36	0.001724	0.003448	0.005173	0.006898	0.008624	0.01035	0.012076	0.013803	0.01553
-0.37	0.001768	0.003537	0.005307	0.007076	0.008846	0.010617	0.012388	0.01416	0.015932
-0.38	0.001813	0.003626	0.005439	0.007253	0.009068	0.010883	0.012699	0.014515	0.016331
-0.39	0.001857	0.003714	0.005572	0.00743	0.009289	0.011148	0.013008	0.014868	0.01673
-0.4	0.001901	0.003802	0.005703	0.007605	0.009727	0.011412	0.013316	0.015221	0.017126

Table B.32: Normalized Power $\hat{p}$ vs Normalized initial resonant current $\hat{I}_0$ in presence of normalized output voltage $\hat{v}$.

					$\hat{v}$				
	0.01	0.02	0.03	0.04	0.05	0.06	0.07	0.08	0.09
$\hat{I}_o$					$\hat{p}$				
-0.41	0.001944	0.003889	0.005834	0.00778	0.009727	0.011674	0.013622	0.015571	0.017521
-0.42	0.001988	0.003976	0.005965	0.007954	0.009945	0.011936	0.013928	0.01592	0.017914
-0.43	0.002031	0.004062	0.006095	0.008128	0.010162	0.012196	0.014232	0.016268	0.018305
-0.44	0.002074	0.004149	0.006224	0.0083	0.010377	0.012455	0.014534	0.016614	0.018695
-0.45	0.002117	0.004234	0.006353	0.008472	0.010592	0.012714	0.014836	0.016959	0.019084
-0.46	0.002159	0.00432	0.006481	0.008643	0.010806	0.012971	0.015136	0.017303	0.019471
-0.47	0.002202	0.004405	0.006609	0.008814	0.01102	0.013227	0.015435	0.017645	0.019856
-0.48	0.002244	0.004489	0.006736	0.008983	0.011232	0.013482	0.015733	0.017986	0.02024
-0.49	0.002286	0.004574	0.006862	0.009152	0.011443	0.013736	0.01603	0.018325	0.020622
-0.5	0.002328	0.004658	0.006988	0.00932	0.011654	0.013989	0.016325	0.018663	0.021003
-0.51	0.00237	0.004741	0.007114	0.009488	0.011864	0.014241	0.01662	0.019	0.021382
-0.52	0.002412	0.004824	0.007239	0.009655	0.012073	0.014492	0.016913	0.019336	0.021761
-0.53	0.002453	0.004907	0.007363	0.009821	0.012281	0.014742	0.017205	0.01967	0.022137
-0.54	0.002494	0.00499	0.007488	0.009987	0.012488	0.014991	0.017496	0.020003	0.022513
-0.55	0.002535	0.005072	0.007611	0.010152	0.012695	0.015239	0.017786	0.020335	0.022887
-0.56	0.002576	0.005154	0.007734	0.010316	0.0129	0.015487	0.018075	0.020666	0.02326
-0.57	0.002617	0.005236	0.007857	0.01048	0.013105	0.015733	0.018363	0.020996	0.023631
-0.58	0.002658	0.005317	0.007979	0.010643	0.01331	0.015979	0.01865	0.021324	0.024001
-0.59	0.002698	0.005398	0.008101	0.010806	0.013513	0.016223	0.018936	0.021652	0.024371
-0.6	0.002738	0.005479	0.008222	0.010968	0.013716	0.016467	0.019221	0.021978	0.024738
-0.61	0.002778	0.005559	0.008343	0.011129	0.013918	0.01671	0.019505	0.022304	0.025105
-0.62	0.002818	0.005639	0.008463	0.01129	0.01412	0.016953	0.019789	0.022628	0.025471
-0.63	0.002858	0.005719	0.008583	0.01145	0.014321	0.017194	0.020071	0.022951	0.025835
-0.64	0.002898	0.005799	0.008703	0.01161	0.014521	0.017435	0.020352	0.023274	0.026199
-0.65	0.002938	0.005878	0.008822	0.01177	0.01472	0.017675	0.020633	0.023595	0.026561
-0.66	0.002977	0.005957	0.008941	0.011928	0.014919	0.017914	0.020913	0.023915	0.026923
-0.67	0.003016	0.006036	0.00906	0.012087	0.015118	0.018152	0.021192	0.024235	0.027283
-0.68	0.003056	0.006115	0.009178	0.012244	0.015315	0.01839	0.02147	0.024554	0.027642
-0.69	0.003095	0.006193	0.009295	0.012402	0.015512	0.018627	0.021747	0.024871	0.028001
-0.7	0.003134	0.006271	0.009413	0.012559	0.015709	0.018864	0.022023	0.025188	0.028358
-0.71	0.003172	0.006349	0.00953	0.012715	0.015905	0.0191	0.022299	0.025504	0.028715
-0.72	0.003211	0.006426	0.009646	0.012871	0.0161	0.019335	0.022574	0.025819	0.02907
-0.73	0.00325	0.006504	0.009763	0.013026	0.016295	0.019569	0.022849	0.026134	0.029425
-0.74	0.003288	0.006581	0.009878	0.013181	0.016489	0.019803	0.023122	0.026447	0.029779
-0.75	0.003326	0.006658	0.009994	0.013336	0.016683	0.020036	0.023395	0.02676	0.030132
-0.76	0.003365	0.006734	0.010109	0.01349	0.016876	0.020269	0.023667	0.027072	0.030484
-0.77	0.003403	0.006811	0.010224	0.013644	0.017069	0.020501	0.023939	0.027384	0.030835
-0.78	0.003441	0.006887	0.010339	0.013797	0.017262	0.020732	0.02421	0.027694	0.031186
-0.79	0.003479	0.006963	0.010454	0.01395	0.017453	0.020963	0.02448	0.028004	0.031536
-0.8	0.003516	0.007039	0.010568	0.014103	0.017645	0.021194	0.02475	0.028313	0.031885

Table B.33: Normalized Power $\hat{p}$ vs Normalized initial resonant current $\hat{I}_0$ in presence of normalized output voltage $\hat{v}$.

					$\hat{v}$				
	0.11	0.12	0.13	0.14	0.15	0.16	0.17	0.18	0.19
$\hat{I}_o$					$\hat{p}$				
-0.01	0.00055	0.0006	0.00065	0.0007	0.00075	0.0008	0.00085	0.0009	0.00095
-0.02	0.0011	0.0012	0.0013	0.0014	0.0015	0.0016	0.0017	0.0018	0.0019
-0.03	0.001649	0.001799	0.001949	0.002099	0.002249	0.002399	0.002549	0.002699	0.002849
-0.04	0.002199	0.002398	0.002598	0.002798	0.002998	0.003198	0.003398	0.003598	0.003797
-0.05	0.002747	0.002997	0.003247	0.003496	0.003746	0.003996	0.004246	0.004495	0.004745
-0.06	0.003295	0.003579	0.003894	0.004194	0.004493	0.004793	0.005092	0.005392	0.006637
-0.07	0.003842	0.004176	0.004541	0.00489	0.005239	0.005589	0.005938	0.006287	0.006637
-0.08	0.004388	0.004787	0.005186	0.005585	0.005984	0.006383	0.006782	0.007181	0.00758
-0.09	0.004934	0.005382	0.005831	0.006279	0.006728	0.007176	0.007625	0.008073	0.008522
-0.1	0.005478	0.005976	0.006474	0.006972	0.007469	0.007967	0.008465	0.008963	0.009461
-0.11	0.00602	0.006568	0.007115	0.007662	0.00821	0.008757	0.009304	0.009852	0.010399
-0.12	0.006562	0.007158	0.007755	0.008351	0.008948	0.009544	0.010141	0.010737	0.011334
-0.13	0.007102	0.007747	0.008393	0.009039	0.009684	0.01033	0.010975	0.011621	0.012267
-0.14	0.00764	0.008335	0.009029	0.009724	0.010418	0.011113	0.011807	0.012502	0.013197
-0.15	0.008177	0.00892	0.009663	0.010407	0.01115	0.011894	0.012637	0.01338	0.01597
-0.16	0.008712	0.010085	0.010296	0.011088	0.01188	0.012672	0.013464	0.014256	0.01597
-0.17	0.009245	0.010085	0.010926	0.011767	0.012607	0.013448	0.014288	0.015129	0.01597
-0.18	0.009776	0.010665	0.011554	0.012443	0.013332	0.014221	0.01511	0.015999	0.016888
-0.19	0.010306	0.011243	0.01218	0.013117	0.014054	0.014991	0.015928	0.016865	0.017803
-0.2	0.010833	0.011818	0.012803	0.013788	0.014774	0.015759	0.016744	0.017729	0.018714
-0.21	0.011359	0.012392	0.013424	0.014457	0.01549	0.016523	0.017556	0.01859	0.019623
-0.22	0.011882	0.012963	0.014043	0.015124	0.016204	0.017285	0.018366	0.019447	0.020528
-0.23	0.012404	0.013532	0.01466	0.015788	0.016916	0.018044	0.019172	0.020301	0.021429
-0.24	0.012923	0.014098	0.015273	0.016449	0.017624	0.0188	0.019976	0.021151	0.022327
-0.25	0.01344	0.014662	0.015885	0.017107	0.01833	0.019553	0.020776	0.021999	0.023222
-0.26	0.013955	0.015224	0.016494	0.017763	0.019033	0.020303	0.021573	0.022843	0.024113
-0.27	0.014468	0.015784	0.0171	0.018416	0.019733	0.021049	0.022366	0.023683	0.025001
-0.28	0.014978	0.016341	0.017704	0.019067	0.02043	0.021793	0.023157	0.024521	0.025885
-0.29	0.015487	0.016896	0.018305	0.019714	0.021124	0.022534	0.023944	0.025354	0.026765
-0.3	0.015993	0.017448	0.018904	0.020359	0.021815	0.023272	0.024728	0.026185	0.027642
-0.31	0.016497	0.017998	0.0195	0.021002	0.022504	0.024006	0.025509	0.027012	0.028516
-0.32	0.016999	0.018546	0.020094	0.021641	0.023189	0.024738	0.026287	0.027836	0.029386
-0.33	0.017499	0.019092	0.020685	0.022278	0.023872	0.025467	0.027061	0.028657	0.030253
-0.34	0.017997	0.019635	0.021274	0.022913	0.024552	0.026192	0.027833	0.029474	0.031116
-0.35	0.018492	0.020176	0.02186	0.023544	0.02523	0.026915	0.028601	0.030288	0.031976
-0.36	0.018986	0.020715	0.022444	0.024174	0.025904	0.027635	0.029367	0.031099	0.032833
-0.37	0.019477	0.021251	0.023025	0.0248	0.026576	0.028352	0.030129	0.031907	0.033686
-0.38	0.019967	0.021785	0.023604	0.025424	0.027245	0.029066	0.030889	0.032712	0.034536
-0.39	0.020454	0.022317	0.024181	0.026046	0.027911	0.029778	0.031645	0.033514	0.035383
-0.4	0.020939	0.022847	0.024755	0.026665	0.028575	0.030487	0.032399	0.034312	0.036227

Table B.34: Normalized Power $\hat{p}$ vs Normalized initial resonant current $\hat{I}_0$ in presence of normalized output voltage $\hat{v}$.

					$\hat{v}$				
	0.11	0.12	0.13	0.14	0.15	0.16	0.17	0.18	0.19
$\hat{I}_o$					$\hat{p}$				
-0.41	0.021422	0.023374	0.025327	0.027281	0.029236	0.031193	0.03315	0.035108	0.037068
-0.42	0.021904	0.0239	0.025897	0.027896	0.029895	0.031896	0.033898	0.035901	0.037906
-0.43	0.022383	0.024423	0.026465	0.028508	0.030552	0.032597	0.034643	0.036691	0.038741
-0.44	0.022861	0.024945	0.02703	0.029117	0.031205	0.033295	0.035386	0.037479	0.039573
-0.45	0.023336	0.025464	0.027594	0.029725	0.031857	0.033991	0.036126	0.038263	0.040402
-0.46	0.02381	0.025982	0.028155	0.03033	0.032506	0.034684	0.036864	0.039045	0.041229
-0.47	0.024282	0.026497	0.028714	0.030933	0.033153	0.035375	0.037599	0.039825	0.042053
-0.48	0.024752	0.027011	0.029271	0.031533	0.033797	0.036063	0.038331	0.040602	0.042874
-0.49	0.025221	0.027523	0.029826	0.032132	0.03444	0.03675	0.039062	0.041376	0.043693
-0.5	0.025688	0.028033	0.03038	0.032729	0.03508	0.037433	0.039789	0.042148	0.044509
-0.51	0.026153	0.028541	0.030931	0.033323	0.035718	0.038115	0.040515	0.042917	0.045323
-0.52	0.026616	0.029047	0.03148	0.033916	0.036354	0.038795	0.041238	0.043685	0.046134
-0.53	0.027078	0.029552	0.032028	0.034507	0.036988	0.039472	0.041959	0.04445	0.046943
-0.54	0.027538	0.030055	0.032574	0.035095	0.03762	0.040148	0.042678	0.045973	0.04775
-0.55	0.027997	0.030556	0.033118	0.035682	0.03825	0.040821	0.043395	0.045973	0.048554
-0.56	0.028454	0.031056	0.03366	0.036268	0.038878	0.041492	0.04411	0.046731	0.049357
-0.57	0.02891	0.031554	0.034201	0.036851	0.039505	0.042162	0.044823	0.047488	0.050157
-0.58	0.029364	0.03205	0.03474	0.037433	0.040129	0.04283	0.045534	0.048243	0.050956
-0.59	0.029817	0.032545	0.035277	0.038013	0.040752	0.043495	0.046243	0.048995	0.051752
-0.6	0.030269	0.033039	0.035813	0.038591	0.041373	0.044159	0.04695	0.049746	0.052546
-0.61	0.030719	0.033531	0.036347	0.039168	0.041993	0.044822	0.047656	0.050495	0.053339
-0.62	0.031168	0.034022	0.03688	0.039743	0.04261	0.045482	0.04836	0.051242	0.05413
-0.63	0.031615	0.034511	0.037412	0.040317	0.043227	0.046141	0.049062	0.051987	0.054919
-0.64	0.032061	0.034999	0.037942	0.04146	0.043841	0.046799	0.049762	0.052731	0.055706
-0.65	0.032507	0.035486	0.03847	0.04146	0.044454	0.047455	0.050461	0.053473	0.056492
-0.66	0.03295	0.035971	0.038998	0.042029	0.045066	0.048109	0.051158	0.054214	0.057276
-0.67	0.033393	0.036456	0.039524	0.042597	0.045677	0.048762	0.051854	0.054953	0.058059
-0.68	0.033835	0.036939	0.040048	0.043164	0.046285	0.049414	0.052548	0.05569	0.05884
-0.69	0.034275	0.03742	0.040572	0.043729	0.046893	0.050064	0.053241	0.056427	0.059619
-0.7	0.034714	0.037901	0.041094	0.044293	0.047499	0.050713	0.053933	0.057161	0.060398
-0.71	0.035152	0.03838	0.041615	0.044856	0.048104	0.05136	0.054623	0.057895	0.061175
-0.72	0.03559	0.038859	0.042135	0.045418	0.048708	0.052006	0.055312	0.058627	0.06195
-0.73	0.036026	0.039336	0.042654	0.045978	0.049311	0.052651	0.056	0.059358	0.062725
-0.74	0.036461	0.039812	0.043171	0.046538	0.049912	0.053295	0.056687	0.060087	0.063498
-0.75	0.036895	0.040288	0.043688	0.047096	0.050512	0.053938	0.057372	0.060816	0.06427
-0.76	0.037328	0.040762	0.044203	0.047653	0.051112	0.054579	0.058056	0.061543	0.065041
-0.77	0.037761	0.041235	0.044718	0.048209	0.05171	0.05522	0.058739	0.06227	0.065811
-0.78	0.038192	0.041708	0.045232	0.048765	0.052307	0.055859	0.059422	0.062995	0.06658
-0.79	0.038623	0.042179	0.045744	0.049319	0.052903	0.056497	0.060103	0.063719	0.067347
-0.8	0.039053	0.04265	0.046256	0.049872	0.053498	0.057135	0.060783	0.064442	0.068114

Table B.35: Normalized Power $\hat{p}$ vs Normalized initial resonant current $\hat{I}_0$ in presence of normalized output voltage $\hat{v}$.

				$\hat{v}$					
	0.1	0.2	0.21	0.22	0.23	0.24	0.25	0.26	0.27
$\hat{I}_o$					$\hat{p}$				
-0.01	0.0005	0.001	0.00105	0.0011	0.00115	0.0012	0.00125	0.0013	0.00135
-0.02	0.001	0.002	0.0021	0.0022	0.0023	0.0024	0.0025	0.0026	0.0027
-0.03	0.001499	0.002999	0.003149	0.003299	0.003449	0.003599	0.003749	0.003899	0.004048
-0.04	0.001999	0.003997	0.004197	0.004397	0.004597	0.004797	0.004997	0.005197	0.005396
-0.05	0.002497	0.004995	0.005245	0.005494	0.005744	0.005994	0.006243	0.006493	0.006743
-0.06	0.002996	0.005991	0.006291	0.00659	0.00689	0.007189	0.007489	0.007788	0.008088
-0.07	0.003493	0.006986	0.007335	0.007684	0.008034	0.008383	0.008732	0.009082	0.009431
-0.08	0.003989	0.007979	0.008378	0.008777	0.009176	0.009575	0.009974	0.010373	0.010772
-0.09	0.004485	0.00897	0.009419	0.009867	0.010316	0.010764	0.011213	0.011661	0.01211
-0.1	0.00498	0.009959	0.010457	0.010955	0.011453	0.011951	0.012449	0.012947	0.013445
-0.11	0.005473	0.010946	0.011493	0.012041	0.012588	0.013135	0.013683	0.01423	0.014777
-0.12	0.005965	0.011931	0.012527	0.013124	0.01372	0.014317	0.014913	0.01551	0.016106
-0.13	0.006456	0.012912	0.013558	0.014204	0.014849	0.015495	0.016141	0.016786	0.017432
-0.14	0.006945	0.013891	0.014586	0.01528	0.015975	0.01667	0.017364	0.018059	0.018754
-0.15	0.007433	0.014867	0.015611	0.016354	0.017098	0.017841	0.018585	0.019328	0.020072
-0.16	0.00792	0.01584	0.016632	0.017425	0.018217	0.019009	0.019801	0.020594	0.021386
-0.17	0.008404	0.01681	0.017651	0.018492	0.019332	0.020173	0.021014	0.021855	0.022696
-0.18	0.008887	0.017777	0.018666	0.019555	0.020444	0.021333	0.022223	0.023112	0.024001
-0.19	0.009369	0.01874	0.019677	0.020615	0.021552	0.02249	0.023427	0.024365	0.025303
-0.2	0.009848	0.0197	0.020685	0.021671	0.022656	0.023642	0.024628	0.025614	0.0266
-0.21	0.010326	0.020656	0.021689	0.022723	0.023756	0.02479	0.025824	0.026858	0.027892
-0.22	0.010802	0.021609	0.02269	0.023771	0.024853	0.025934	0.027016	0.028098	0.02918
-0.23	0.011276	0.022558	0.023687	0.024816	0.025945	0.027074	0.028203	0.029333	0.030463
-0.24	0.011748	0.023504	0.02468	0.025856	0.027033	0.02821	0.029387	0.030564	0.031741
-0.25	0.012218	0.024445	0.025669	0.026893	0.028117	0.029341	0.030566	0.03179	0.033015
-0.26	0.012686	0.025384	0.025669	0.027925	0.029197	0.030468	0.03174	0.033012	0.034285
-0.27	0.013152	0.026318	0.027636	0.028954	0.030272	0.031591	0.03291	0.03423	0.03555
-0.28	0.013616	0.027249	0.028614	0.029979	0.031344	0.03271	0.034076	0.035443	0.03681
-0.29	0.014078	0.028176	0.029588	0.031	0.032412	0.033824	0.035238	0.036651	0.038066
-0.3	0.014538	0.0291	0.030558	0.032016	0.033475	0.034935	0.036395	0.037855	0.039317
-0.31	0.014996	0.03002	0.031524	0.033029	0.034535	0.036041	0.037548	0.039055	0.040564
-0.32	0.015453	0.030936	0.032487	0.034038	0.035591	0.037143	0.038697	0.040251	0.041806
-0.33	0.015907	0.031849	0.033446	0.035044	0.036642	0.038241	0.039841	0.041442	0.043044
-0.34	0.016359	0.032758	0.034401	0.036045	0.03769	0.039336	0.040982	0.042629	0.044278
-0.35	0.016809	0.033664	0.035353	0.037043	0.038734	0.040426	0.042119	0.043813	0.045508
-0.36	0.017258	0.034567	0.036302	0.038037	0.039774	0.041512	0.043251	0.044992	0.046733
-0.37	0.017704	0.035466	0.037246	0.039028	0.040811	0.042595	0.04438	0.046167	0.047955
-0.38	0.018149	0.036361	0.038188	0.040015	0.041844	0.043674	0.045505	0.047338	0.049173
-0.39	0.018591	0.037254	0.039126	0.040999	0.042873	0.044749	0.046627	0.048506	0.050387
-0.4	0.019032	0.038143	0.04006	0.041979	0.043899	0.045821	0.047744	0.04967	0.051597

Table B.36: Normalized Power $\hat{p}$ vs Normalized initial resonant current $\hat{I}_0$ in presence of normalized output voltage $\hat{v}$.

					$\hat{v}$				
	0.1	0.2	0.21	0.22	0.23	0.24	0.25	0.26	0.27
$\hat{I}_o$					$\hat{p}$				
-0.41	0.019471	0.039029	0.040992	0.042956	0.044922	0.046889	0.048859	0.05083	0.052803
-0.42	0.019908	0.039912	0.04192	0.04393	0.045941	0.047954	0.049969	0.051987	0.054006
-0.43	0.020344	0.040792	0.042845	0.0449	0.046957	0.049016	0.051077	0.05314	0.055206
-0.44	0.020777	0.041669	0.043767	0.045867	0.047969	0.050074	0.052181	0.05429	0.056402
-0.45	0.021209	0.042543	0.044686	0.046832	0.048979	0.051129	0.053282	0.055437	0.057595
-0.46	0.02164	0.043415	0.045603	0.047793	0.049986	0.052181	0.054379	0.056581	0.058785
-0.47	0.022068	0.044283	0.046516	0.048751	0.050989	0.05323	0.055474	0.057721	0.059972
-0.48	0.022495	0.045149	0.047427	0.049707	0.05199	0.054276	0.056566	0.058859	0.061156
-0.49	0.022921	0.046012	0.048335	0.05066	0.052988	0.05532	0.057655	0.059994	0.062337
-0.5	0.023344	0.046873	0.04924	0.05161	0.053983	0.05636	0.058741	0.061126	0.063515
-0.51	0.023767	0.047731	0.050143	0.052558	0.054976	0.057398	0.059825	0.062255	0.064691
-0.52	0.024187	0.048587	0.051043	0.053503	0.055966	0.058434	0.060906	0.063382	0.065864
-0.53	0.024607	0.04944	0.051941	0.054445	0.056954	0.059467	0.061984	0.064507	0.067034
-0.54	0.025024	0.050291	0.052836	0.055385	0.057939	0.060497	0.06306	0.065628	0.068202
-0.55	0.025441	0.05114	0.053729	0.056323	0.058922	0.061525	0.064134	0.066748	0.069368
-0.56	0.025856	0.051986	0.05462	0.057259	0.059902	0.062551	0.065205	0.067865	0.070532
-0.57	0.026269	0.052831	0.055509	0.058192	0.060881	0.063575	0.066275	0.068981	0.071693
-0.58	0.026681	0.053673	0.056396	0.059124	0.061857	0.064597	0.067342	0.070094	0.072853
-0.59	0.027092	0.054514	0.057281	0.060053	0.062832	0.065616	0.068407	0.071205	0.07401
-0.6	0.027502	0.055352	0.058163	0.060981	0.063804	0.066634	0.06947	0.072314	0.075166
-0.61	0.02791	0.056189	0.059044	0.061906	0.064774	0.067649	0.070532	0.073422	0.07632
-0.62	0.028317	0.057024	0.059923	0.06283	0.065743	0.068663	0.071591	0.074528	0.077472
-0.63	0.028723	0.057857	0.060801	0.063752	0.06671	0.069676	0.072649	0.075632	0.078623
-0.64	0.029128	0.058688	0.061676	0.064672	0.067675	0.070686	0.073706	0.076734	0.079772
-0.65	0.029532	0.059517	0.06255	0.06559	0.068638	0.071695	0.07476	0.077835	0.08092
-0.66	0.029934	0.060345	0.063422	0.066507	0.0696	0.072702	0.075814	0.078935	0.082066
-0.67	0.030336	0.061172	0.064293	0.067423	0.070561	0.073708	0.076866	0.080033	0.083212
-0.68	0.030736	0.061997	0.065162	0.068337	0.07152	0.074713	0.077916	0.08113	0.084355
-0.69	0.031135	0.062821	0.06603	0.069249	0.072478	0.075716	0.078965	0.082226	0.085498
-0.7	0.031533	0.063643	0.066897	0.07016	0.073434	0.076718	0.080013	0.08332	0.08664
-0.71	0.031931	0.064464	0.067762	0.07107	0.074389	0.077719	0.08106	0.084414	0.087781
-0.72	0.032327	0.065283	0.068626	0.071979	0.075343	0.078718	0.082106	0.085506	0.088921
-0.73	0.032722	0.066102	0.069489	0.072886	0.076296	0.079717	0.083151	P073'!B28	0.090059
-0.74	0.033116	0.066919	0.07035	0.073793	0.077247	0.080714	0.084194	0.087689	0.091198
-0.75	0.03351	0.067735	0.07121	0.074698	0.078198	0.081711	0.085237	0.088779	0.092335
-0.76	0.033903	0.068549	0.07207	0.075602	0.079147	0.082706	0.086279	0.089868	0.093472
-0.77	0.034294	0.069363	0.072928	0.076505	0.080096	0.083701	0.087321	0.090956	0.094608
-0.78	0.034685	0.070176	0.073785	0.077408	0.081044	0.084695	0.088361	0.092044	0.095744
-0.79	0.035075	0.070988	0.074642	0.078309	0.081991	0.085688	0.089401	0.093131	0.096879
-0.8	0.035464	0.071799	0.075497	0.07921	0.082937	0.08668	0.09044	0.094218	0.098014

Table B.37: Normalized Power $\hat{p}$ vs Normalized initial resonant current $\hat{I}_0$ in presence of normalized output voltage $\hat{v}$.

					$\hat{v}$				
	0.28	0.29	0.3	0.31	0.32	0.33	0.34	0.35	0.36
$\hat{I}_o$					$\hat{p}$				
-0.01	0.0014	0.00145	0.0015	0.00155	0.0016	0.00165	0.0017	0.00175	0.0018
-0.02	0.0028	0.0029	0.002999	0.003099	0.003199	0.003299	0.003399	0.003499	0.003599
-0.03	0.004198	0.004348	0.004498	0.004648	0.004798	0.004948	0.005098	0.005248	0.005398
-0.04	0.005596	0.005796	0.005996	0.006196	0.006396	0.006596	0.006795	0.006995	0.007195
-0.05	0.006993	0.007242	0.007492	0.007742	0.007992	0.008241	0.008491	0.008741	0.008991
-0.06	0.008387	0.008687	0.008987	0.009286	0.009586	0.009885	0.010185	0.010484	0.010784
-0.07	0.00978	0.010129	0.010479	0.010828	0.011177	0.011527	0.011876	0.012225	0.012575
-0.08	0.01117	0.011569	0.011968	0.012367	0.012766	0.013165	0.013564	0.013963	0.014362
-0.09	0.012558	0.013007	0.013455	0.013904	0.014352	0.014801	0.015249	0.015698	0.016147
-0.1	0.013943	0.014441	0.014939	0.015437	0.015935	0.016433	0.016931	0.017429	0.017927
-0.11	0.015325	0.015872	0.016419	0.016967	0.017514	0.018062	0.018609	0.019157	0.019704
-0.12	0.016703	0.0173	0.017896	0.018493	0.01909	0.019686	0.020283	0.02088	0.021477
-0.13	0.018078	0.018723	0.019369	0.020015	0.020661	0.021307	0.021953	0.022599	0.023245
-0.14	0.019449	0.020143	0.020838	0.021533	0.022228	0.022923	0.023618	0.024313	0.025008
-0.15	0.020815	0.021559	0.022303	0.023047	0.02379	0.024534	0.025278	0.026022	0.026766
-0.16	0.022178	0.022971	0.023763	0.024556	0.025348	0.026141	0.026934	0.027727	0.02852
-0.17	0.023537	0.024378	0.025219	0.02606	0.026902	0.027743	0.028585	0.029426	0.030268
-0.18	0.024891	0.025781	0.02667	0.02756	0.02845	0.02934	0.03023	0.031121	0.032011
-0.19	0.026241	0.027179	0.028117	0.029055	0.029993	0.030932	0.031871	0.03281	0.033749
-0.2	0.027586	0.028572	0.029558	0.030545	0.031532	0.032519	0.033506	0.034493	0.035481
-0.21	0.028926	0.02996	0.030995	0.03203	0.033065	0.0341	0.035136	0.036172	0.037208
-0.22	0.030262	0.031344	0.032427	0.03351	0.034593	0.035676	0.03676	0.037845	0.038929
-0.23	0.031593	0.032723	0.033854	0.034985	0.036116	0.037248	0.03838	0.039512	0.040645
-0.24	0.032919	0.034097	0.035276	0.036455	0.037634	0.038813	0.039994	0.041174	0.042355
-0.25	0.034241	0.035467	0.036693	0.037919	0.039147	0.040374	0.041602	0.042831	0.044061
-0.26	0.035558	0.036831	0.038105	0.039379	0.040654	0.04193	0.043206	0.044483	0.04576
-0.27	0.03687	0.038191	0.039512	0.040834	0.042157	0.04348	0.044804	0.046129	0.047455
-0.28	0.038177	0.039546	0.040915	0.042284	0.043654	0.045025	0.046397	0.04777	0.049144
-0.29	0.03948	0.040896	0.042312	0.043729	0.045147	0.046566	0.047986	0.049406	0.050828
-0.3	0.040779	0.042241	0.043705	0.045169	0.046635	0.048101	0.049569	0.051038	0.052508
-0.31	0.042073	0.043582	0.045093	0.046605	0.048118	0.049632	0.051147	0.052664	0.054182
-0.32	0.043362	0.044919	0.046477	0.048036	0.049596	0.051158	0.052721	0.054286	0.055852
-0.33	0.044647	0.046251	0.047856	0.049462	0.05107	0.052679	0.05429	0.055903	0.057517
-0.34	0.045928	0.047578	0.049231	0.050884	0.052539	0.054196	0.055855	0.057515	0.059178
-0.35	0.047204	0.048902	0.050601	0.052302	0.054004	0.055709	0.057415	0.059123	0.060834
-0.36	0.048476	0.050221	0.051967	0.053715	0.055465	0.057217	0.058971	0.060727	0.062486
-0.37	0.049745	0.051536	0.053329	0.055124	0.056921	0.058721	0.060523	0.062327	0.064134
-0.38	0.051009	0.052847	0.054687	0.056529	0.058374	0.060221	0.062071	0.063923	0.065779
-0.39	0.052269	0.054154	0.056041	0.057931	0.059822	0.061717	0.063615	0.065515	0.067419
-0.4	0.053526	0.055458	0.057392	0.059328	0.061267	0.063209	0.065155	0.067104	0.069056

Table B.38: Normalized Power $\hat{p}$ vs Normalized initial resonant current $\hat{I}_0$ in presence of normalized output voltage $\hat{v}$.

					$\hat{v}$				
	0.28	0.29	0.3	0.31	0.32	0.33	0.34	0.35	0.36
$\hat{I}_o$					$\hat{p}$				
-0.41	0.054779	0.056757	0.058738	0.060722	0.062708	0.064698	0.066691	0.068689	0.07069
-0.42	0.056029	0.058053	0.060081	0.062112	0.064146	0.066183	0.068225	0.07027	0.07232
-0.43	0.057275	0.059346	0.061421	0.063499	0.06558	0.067665	0.069755	0.071848	0.073947
-0.44	0.058517	0.060635	0.062757	0.064882	0.067011	0.069144	0.071281	0.073424	0.075571
-0.45	0.059757	0.061922	0.06409	0.066262	0.068439	0.07062	0.072805	0.074996	0.077192
-0.46	0.060993	0.063204	0.06542	0.067639	0.069863	0.072092	0.074326	0.076565	0.07881
-0.47	0.062226	0.064484	0.066747	0.069014	0.071285	0.073562	0.075844	0.078132	0.080426
-0.48	0.063456	0.065761	0.068071	0.070385	0.072704	0.075029	0.07736	0.079696	0.08204
-0.49	0.064684	0.067035	0.069392	0.071753	0.07412	0.076493	0.078873	0.081258	0.083651
-0.5	0.065909	0.068307	0.07071	0.073119	0.075534	0.077955	0.080383	0.082818	0.085261
-0.51	0.067131	0.069576	0.072026	0.074483	0.076946	0.079415	0.081892	0.084376	0.086868
-0.52	0.06835	0.070842	0.07334	0.075844	0.078355	0.080873	0.083398	0.085931	0.088474
-0.53	0.069567	0.072106	0.074651	0.077203	0.079762	0.082328	0.084902	0.087485	0.090078
-0.54	0.070782	0.073368	0.07596	0.078559	0.081166	0.083781	0.086405	0.089038	0.09168
-0.55	0.071994	0.074627	0.077267	0.079914	0.082569	0.085233	0.087906	0.090588	0.093281
-0.56	0.073205	0.075884	0.078572	0.081267	0.08397	0.086683	0.089405	0.092137	0.094881
-0.57	0.074413	0.07714	0.079874	0.082618	0.08537	0.088131	0.090903	0.093685	0.09648
-0.58	0.075619	0.078393	0.081175	0.083967	0.086767	0.089578	0.092399	0.095232	0.098077
-0.59	0.076823	0.079645	0.082475	0.085314	0.088164	0.091024	0.093895	0.096778	0.099674
-0.6	0.078026	0.080895	0.083773	0.08666	0.089558	0.092468	0.095389	0.098323	0.10127
-0.61	0.079227	0.082143	0.085069	0.088005	0.090952	0.093911	0.096882	0.099867	0.102866
-0.62	0.080426	0.08339	0.086363	0.089348	0.092344	0.095353	0.098375	0.10141	0.104461
-0.63	0.081624	0.084635	0.087657	0.09069	0.093736	0.096794	0.099866	0.102953	0.106056
-0.64	0.08282	0.085879	0.088949	0.092031	0.095126	0.098234	0.101357	0.104496	0.107651
-0.65	0.084015	0.087122	0.09024	0.093371	0.096515	0.099674	0.102848	0.106038	0.109245
-0.66	0.085209	0.088363	0.09153	0.09471	0.097904	0.101113	0.104338	0.10758	0.11084
-0.67	0.086402	0.089604	0.092819	0.096048	0.099292	0.102552	0.105828	0.109122	0.112435
-0.68	0.087593	0.090843	0.094107	0.097386	0.10068	0.10399	0.107317	0.110664	0.11403
-0.69	0.088783	0.092082	0.095395	0.098723	0.102067	0.105428	0.108807	0.112206	0.115625
-0.7	0.089973	0.09332	0.096681	0.100059	0.103453	0.106865	0.110296	0.113748	0.117221
-0.71	0.091161	0.094557	0.097967	0.101395	0.104839	0.108303	0.111786	0.115291	0.118818
-0.72	0.092349	0.095793	0.099253	0.10273	0.106225	0.10974	0.113276	0.116834	0.120415
-0.73	0.093536	0.097028	0.100538	0.104065	0.107611	0.111178	0.114766	0.118377	0.122013
-0.74	0.094722	0.098264	0.101822	0.1054	0.108997	0.112616	0.116257	0.119922	0.123612
-0.75	0.095908	0.099498	0.103107	0.106735	0.110383	0.114054	0.117748	0.121467	0.125212
-0.76	0.097093	0.100732	0.104391	0.108069	0.111769	0.115492	0.119239	0.123013	0.126814
-0.77	0.098278	0.101966	0.105675	0.109404	0.113156	0.116931	0.120732	0.124559	0.128416
-0.78	0.099462	0.1032	0.106959	0.110739	0.114542	0.11837	0.122225	0.126107	0.13002
-0.79	0.100646	0.104434	0.108242	0.112074	0.115929	0.11981	0.123719	0.127657	0.131625
-0.8	0.10183	0.105667	0.109526	0.113409	0.117317	0.121251	0.125214	0.129207	0.133232

Table B.39: Normalized Power $\hat{p}$ vs Normalized initial resonant current $\hat{I}_0$ in presence of normalized output voltage $\hat{v}$.

				$\hat{v}$					
	0.37	0.38	0.39	0.4	0.41	0.42	0.43	0.44	0.45
$\hat{I}_o$					$\hat{p}$				
-0.01	0.00185	0.0019	0.00195	0.002	0.00205	0.0021	0.00215	0.0022	0.00225
-0.02	0.003699	0.003799	0.003899	0.003999	0.004099	0.004199	0.004299	0.004399	0.004499
-0.03	0.005548	0.005698	0.005848	0.005998	0.006148	0.006298	0.006448	0.006598	0.006747
-0.04	0.007395	0.007595	0.007795	0.007995	0.008195	0.008394	0.008594	0.008794	0.008994
-0.05	0.00924	0.00949	0.00974	0.00999	0.010239	0.010489	0.010739	0.010989	0.011238
-0.06	0.011083	0.011383	0.011683	0.011982	0.012282	0.012581	0.012881	0.013181	0.01348
-0.07	0.012924	0.013273	0.013622	0.013972	0.014321	0.014671	0.01502	0.015369	0.015719
-0.08	0.014761	0.01516	0.015559	0.015958	0.016357	0.016756	0.017155	0.017555	0.017954
-0.09	0.016595	0.017044	0.017492	0.017941	0.01839	0.018838	0.019287	0.019736	0.020185
-0.1	0.018425	0.018923	0.019422	0.01992	0.020418	0.020916	0.021415	0.021913	0.022411
-0.11	0.020252	0.020799	0.021347	0.021894	0.022442	0.02299	P011'!B45	0.024086	0.024633
-0.12	0.022073	0.02267	0.023267	0.023864	0.024461	0.025058	0.025656	0.026253	0.026851
-0.13	0.023891	0.024537	0.025183	0.025829	0.026476	0.027122	0.027769	0.028416	0.029063
-0.14	0.025703	0.026398	0.027094	0.027789	0.028485	0.029181	0.029877	0.030573	0.031269
-0.15	0.027511	0.028255	0.028999	0.029744	0.030489	0.031234	0.031979	0.032724	0.03347
-0.16	0.029313	0.030106	0.0309	0.031694	0.032487	0.033282	0.034076	0.034871	0.035666
-0.17	0.03111	0.031952	0.032795	0.033637	0.03448	0.035324	0.036167	0.037011	0.037855
-0.18	0.032902	0.033793	0.034684	0.035576	0.036468	0.03736	0.038253	0.039146	0.040039
-0.19	0.034688	0.035628	0.036568	0.037509	0.038449	0.039391	0.040332	0.041275	0.042218
-0.2	0.036469	0.037458	0.038446	0.039436	0.040425	0.041416	0.042406	0.043398	0.04439
-0.21	0.038244	0.039281	0.040319	0.041357	0.042396	0.043435	0.044475	0.045515	0.046557
-0.22	0.040014	0.0411	0.042186	0.043273	0.04436	0.045448	0.046537	0.047627	0.048718
-0.23	0.041779	0.042913	0.044047	0.045183	0.046319	0.047456	0.048594	0.049734	0.050874
-0.24	0.043537	0.04472	0.045903	0.047087	0.048273	0.049459	0.050646	0.051834	0.053024
-0.25	0.045291	0.046522	0.047754	0.048987	0.050221	0.051456	0.052692	0.05393	0.05517
-0.26	0.047039	0.048318	0.049599	0.05088	0.052163	0.053447	0.054733	0.056021	0.05731
-0.27	0.048782	0.05011	0.051439	0.052769	0.054101	0.055434	0.056769	0.058106	0.059445
-0.28	0.050519	0.051896	0.053273	0.054652	0.056033	0.057416	0.0588	0.060186	0.061575
-0.29	0.052252	0.053677	0.055103	0.056531	0.057961	0.059392	0.060826	0.062262	0.063701
-0.3	0.053979	0.055453	0.056928	0.058404	0.059883	0.061364	0.062848	0.064334	0.065823
-0.31	0.055702	0.057224	0.058747	0.060273	0.061801	0.063332	0.064865	0.066401	0.06794
-0.32	0.05742	0.05899	0.060563	0.062137	0.063715	0.065295	0.066878	0.068464	0.070054
-0.33	0.059134	0.060752	0.062374	0.063997	0.065624	0.067254	0.068887	0.070523	0.072164
-0.34	0.060843	0.06251	0.06418	P030'!B42	0.067529	0.069209	0.070892	0.072579	0.074271
-0.35	0.062548	0.064264	0.065983	0.067705	0.06943	0.07116	0.072893	0.074631	0.076374
-0.36	0.064248	0.066013	0.067781	0.069553	0.071328	0.073107	0.074891	0.07668	0.078474
-0.37	0.065945	0.067758	0.069576	0.071397	0.073222	0.075052	0.076886	0.078726	0.080572
-0.38	0.067638	0.0695	0.071367	0.073237	0.075113	0.076993	0.078878	0.08077	0.082667
-0.39	0.069327	0.071238	0.073154	0.075075	0.077	0.078931	0.080867	0.08281	0.08476
-0.4	0.071013	0.072973	0.074939	0.076909	0.078885	0.080866	0.082854	0.084849	0.086851

Table B.40: Normalized Power $\hat{p}$ vs Normalized initial resonant current $\hat{I}_0$ in presence of normalized output voltage $\hat{v}$.

				$\hat{v}$					
	0.37	0.38	0.39	0.4	0.41	0.42	0.43	0.44	0.45
$\hat{I}_o$					$\hat{p}$				
-0.41	0.072695	0.074705	0.07672	0.07874	0.080766	0.082799	0.084838	0.086885	0.08894
-0.42	0.074374	0.076433	0.078498	0.080569	0.082646	0.084729	0.086821	0.08892	0.091027
-0.43	0.07605	0.078159	0.080274	0.082395	0.084522	0.086658	0.088801	0.090952	0.093113
-0.44	0.077723	0.079882	0.082047	0.084218	0.086397	0.088584	0.090779	0.092984	0.095199
-0.45	0.079394	0.081602	0.083817	0.08604	0.08827	0.090509	0.092756	0.095014	0.097283
-0.46	0.081062	P040'!B40	0.085586	0.087859	0.090141	0.092432	0.094732	0.097044	0.099366
-0.47	0.082728	0.08332	0.087352	0.089676	0.09201	0.094353	0.096707	0.099072	0.10145
-0.48	0.084391	0.08675	0.089116	0.091492	0.093878	0.096274	0.098681	0.1011	0.103533
-0.49	0.086052	0.088461	0.090879	0.093307	0.095744	0.098193	0.100654	0.103128	0.105616
-0.5	0.087712	0.090171	0.09264	0.09512	0.09761	0.100112	0.102627	0.105156	0.107699
-0.51	0.089369	0.09188	0.0944	0.096932	0.099475	0.10203	0.1046	0.107183	0.109783
-0.52	0.091025	0.093587	0.096159	0.098743	0.101339	0.103948	0.106572	0.109211	0.111867
-0.53	0.09268	0.095292	0.097917	0.100553	0.103202	0.105866	0.108545	0.11124	0.113953
-0.54	0.094333	0.096997	0.099673	0.102362	0.105066	0.107784	0.110518	0.113269	0.11604
-0.55	0.095985	0.098701	0.101429	0.104172	0.106929	0.109701	0.112491	0.115299	0.118128
-0.56	0.097636	0.100404	0.103185	0.10598	0.108792	0.11162	0.114465	0.117331	0.120217
-0.57	0.099286	0.102106	0.10494	0.107789	0.110655	0.113538	0.116441	0.119364	0.122309
-0.58	0.100935	0.103808	0.106695	0.109598	0.112518	0.115458	0.118417	0.121398	0.124402
-0.59	0.102584	0.105509	0.108449	0.111407	0.114383	0.117378	0.120394	0.123434	0.126498
-0.6	0.104232	0.10721	0.110204	0.113216	0.116247	0.119299	0.122373	0.125472	0.128596
-0.61	0.10588	0.108911	0.111959	0.115026	0.118113	0.121222	0.124354	0.127512	0.130696
-0.62	0.107528	0.110612	0.113714	0.116837	0.11998	0.123146	0.126337	0.129554	0.1328
-0.63	0.109176	0.112313	0.11547	0.118648	0.121848	0.125072	0.128321	0.131599	0.134906
-0.64	0.110823	0.114015	0.117227	0.12046	0.123717	0.126999	0.130308	0.133646	0.137016
-0.65	0.112471	0.115717	0.118984	0.122274	0.125588	0.128928	0.132297	0.135697	0.139129
-0.66	0.114119	0.117419	0.120742	0.124088	0.12746	0.13086	0.134289	0.13775	0.141246
-0.67	0.115768	0.119123	0.122501	0.125904	0.129334	0.132793	0.136283	0.139807	0.143367
-0.68	0.117417	0.120827	0.124261	0.127722	0.131211	0.134729	0.138281	0.141867	0.145491
-0.69	0.119067	0.122532	0.126023	0.129541	0.133089	0.136668	0.140281	0.143931	0.14762
-0.7	0.120717	0.124239	0.127786	0.131363	0.134969	0.138609	0.142285	0.145998	0.149754
-0.71	0.122369	0.125946	0.129551	0.133186	0.136852	0.140553	0.144292	0.14807	0.151892
-0.72	0.124021	0.127655	0.131317	0.135011	0.138738	0.142501	0.146302	0.150146	0.154035
-0.73	0.125675	0.129365	0.133086	0.136839	0.140626	0.144451	0.148317	0.152226	0.156182
-0.74	0.12733	0.131077	0.134856	0.138669	0.142517	0.146405	0.150335	0.154311	0.158335
-0.75	0.128986	0.132791	0.136629	0.140501	0.144411	0.148363	0.152358	0.1564	0.160494
-0.76	0.130644	0.134507	0.138403	0.142336	0.146309	0.150324	0.154384	0.158494	0.162658
-0.77	0.132304	0.136224	0.14018	0.144174	0.148209	0.152289	0.156415	0.160594	0.164828
-0.78	0.133965	0.137944	0.14196	0.146015	0.150113	0.154257	0.158451	0.162699	0.167004
-0.79	0.135628	0.139666	0.143742	0.147859	0.152021	0.156231	0.160492	0.164809	0.169186
-0.8	0.137292	0.14139	0.145527	0.149707	0.153932	0.158208	0.162537	0.166925	0.171375

Table B.41: Normalized Power $\hat{p}$ vs Normalized initial resonant current $\hat{I}_0$ in presence of normalized output voltage $\hat{v}$.

					$\hat{v}$				
	0.46	0.47	0.48	0.49	0.5	0.51	0.52	0.53	0.54
$\hat{I}_o$					$\hat{p}$				
-0.01	0.0023	0.00235	0.0024	0.00245	0.0025	0.00255	0.0026	0.00265	0.0027
-0.02	0.004599	0.004699	0.004799	0.004899	0.004999	0.005099	0.005199	0.005299	0.005399
-0.03	0.006897	0.007047	0.007197	0.007347	0.007497	0.007647	0.007797	0.007947	0.008097
-0.04	0.009194	0.009394	0.009594	0.009794	0.009994	0.010193	0.010393	0.010593	0.010793
-0.05	0.011488	0.011738	0.011988	0.012238	0.012487	0.012737	0.012987	0.013237	0.013487
-0.06	0.01378	0.014079	0.01378	0.014679	0.014979	0.015278	0.015578	0.015878	0.016178
-0.07	0.016068	0.016418	0.016767	0.017117	0.017466	0.017816	0.018165	0.018515	0.018865
-0.08	0.018353	0.018752	0.019151	0.019551	0.01995	0.02035	0.020749	0.021149	0.021548
-0.09	0.020634	0.021083	0.021532	0.021981	0.02243	0.022879	0.023328	0.023778	0.024227
-0.1	0.02291	0.023409	0.023907	0.024406	0.024905	0.025404	0.025903	0.026402	0.026902
-0.11	0.025182	0.02573	0.026278	0.026827	0.027375	0.027924	0.028473	0.029022	0.029022
-0.12	0.027448	0.028046	0.028644	0.029242	0.02984	0.030439	0.031038	0.031637	0.032236
-0.13	0.02971	0.030357	0.031004	0.031652	0.0323	0.032949	0.033597	0.034246	0.034896
-0.14	0.031966	0.032662	0.03336	0.034057	0.034755	0.035453	0.036151	0.036851	0.03755
-0.15	0.034216	0.034962	0.035709	0.036456	0.037204	0.037952	0.0387	0.039449	0.040199
-0.16	0.036461	0.037257	0.038053	0.03885	0.039647	0.040445	0.041243	0.042043	0.042843
-0.17	0.0387	0.039545	0.040391	0.041238	0.042085	0.042932	0.043781	0.044631	0.045482
-0.18	0.040933	0.041828	0.042724	0.04362	0.044517	0.045415	0.046314	0.047214	0.048115
-0.19	0.043161	0.044105	0.04505	0.045996	0.046943	0.047892	0.048841	0.049792	0.050744
-0.2	0.045383	0.046377	0.047372	0.048368	0.049365	0.050363	0.051363	0.052365	0.053368
-0.21	0.047599	0.048643	0.049688	0.050733	0.051781	0.05283	0.05388	0.054933	0.055988
-0.22	0.04981	0.050903	0.051998	0.053094	0.054192	0.055291	0.056393	0.057497	0.058603
-0.23	0.052016	0.053159	0.054303	0.05545	0.056598	0.057748	0.058901	0.060056	0.061214
-0.24	0.054216	0.055409	0.056603	0.0578	0.058999	0.060201	0.061405	0.062612	0.063822
-0.25	0.056411	0.057654	0.058899	0.060146	0.061396	0.062649	0.063905	0.065164	0.066427
-0.26	0.058601	0.059894	0.061189	0.062488	0.063789	0.065093	0.066401	0.067712	0.069028
-0.27	0.060786	0.06213	0.063476	0.064825	0.066177	0.067533	0.068893	0.070258	0.071627
-0.28	0.062967	0.064361	0.065758	0.067158	0.068562	0.06997	0.071383	0.0728	0.074223
-0.29	0.065143	0.066588	0.068036	0.069488	0.070944	0.072404	0.07387	0.075341	0.076818
-0.3	0.067315	0.068811	0.07031	0.071814	0.073322	0.074835	0.076354	0.077879	0.07941
-0.31	0.069483	0.07103	0.072581	0.074137	0.075698	0.077264	0.078836	0.080415	0.082002
-0.32	0.071648	0.073246	0.074849	0.076457	0.078071	0.07969	0.081317	0.082951	0.084593
-0.33	0.073809	0.075459	0.077114	0.078774	0.080441	0.082115	0.083796	0.085485	0.087183
-0.34	0.075967	0.077669	0.079376	0.081089	0.08281	0.084538	0.086273	0.088018	0.089773
-0.35	0.078122	0.079876	0.081636	0.083402	0.085177	0.086959	0.08875	0.090551	0.092363
-0.36	0.080274	0.08208	0.083893	0.085714	0.087542	0.08938	0.091227	0.093085	0.094954
-0.37	0.082424	0.084283	0.086149	0.088024	0.089907	0.0918	0.093703	0.095618	0.097546
-0.38	0.084572	0.086483	0.088403	0.090332	0.092271	0.094219	0.09618	0.098153	0.100139
-0.39	0.086717	0.088682	0.090656	0.09264	0.094634	0.096639	0.098657	0.100688	0.102735
-0.4	0.088861	0.09088	0.092908	0.094947	0.096997	0.099059	0.101135	0.103225	0.105332

Table B.42: Normalized Power $\hat{p}$ vs Normalized initial resonant current $\hat{I}_0$ in presence of normalized output voltage $\hat{v}$.

					$\hat{v}$				
	0.46	0.47	0.48	0.49	0.5	0.51	0.52	0.53	0.54
$\hat{I}_o$					$\hat{p}$				
-0.41	0.091003	0.093076	0.095159	0.097254	0.09936	0.10148	0.103614	0.105764	0.107932
-0.42	0.093144	0.095272	0.09741	0.09956	0.101724	0.103902	0.106095	0.108305	0.110534
-0.43	0.095285	0.097467	0.099661	0.101867	0.104088	0.106325	0.108578	0.110849	0.11314
-0.44	0.097424	0.099661	0.101911	0.104175	0.106454	0.108749	0.111063	0.113396	0.11575
-0.45	0.099563	0.101856	0.104162	0.106483	0.108821	0.111176	0.11355	0.115946	0.118364
-0.46	0.101702	0.10405	0.106414	0.108793	0.111189	0.113605	0.116041	0.118499	0.120982
-0.47	0.10384	0.106245	0.108666	0.111104	0.11356	0.116036	0.118534	0.121057	0.123605
-0.48	0.105979	0.108441	0.110919	0.113416	0.115932	0.11847	0.121032	0.123618	0.126233
-0.49	0.108118	0.110638	0.113174	0.115731	0.118308	0.120908	0.123533	0.126185	0.128867
-0.5	0.110258	0.112835	0.115431	0.118047	0.120686	0.123349	0.126038	0.128757	0.131507
-0.51	0.112399	0.115034	0.11769	0.120366	0.123067	0.125793	0.128548	0.131333	0.134153
-0.52	0.114542	0.117235	0.11995	0.122688	0.125452	0.128242	0.131063	0.133916	0.136805
-0.53	0.116685	0.119438	0.122213	0.125013	0.12784	0.130696	0.133583	0.136505	0.139465
-0.54	0.11883	0.121643	0.124479	0.127342	0.130232	0.133154	0.136109	0.1391	0.142133
-0.55	0.120977	0.12385	0.126748	0.129674	0.132629	0.135617	0.13864	0.141703	0.144808
-0.56	0.123126	0.12606	0.12902	0.132009	0.13503	0.138085	0.141178	0.144312	0.147491
-0.57	0.125278	0.128273	0.131296	0.134349	0.137436	0.140559	0.143722	0.146929	0.150183
-0.58	0.127431	0.130488	0.133575	0.136694	0.139847	0.14304	0.146274	0.149554	0.152884
-0.59	0.129588	0.132707	0.135858	0.139042	0.142264	0.145526	0.148832	0.152187	0.155595
-0.6	0.131748	0.13493	0.138145	0.141396	0.144686	0.148019	0.151398	0.154829	0.158315
-0.61	0.13391	0.137156	0.140437	0.143755	0.147115	0.150519	0.153972	0.157479	0.161046
-0.62	0.136077	0.139387	0.142734	0.14612	0.149549	0.153026	0.156554	0.160139	0.163787
-0.63	0.138246	0.141622	0.145035	0.14849	0.151991	0.155541	0.159145	0.162809	0.166539
-0.64	0.14042	0.143861	0.147342	0.150866	0.154439	0.158063	0.161745	0.165489	0.169303
-0.65	0.142598	0.146105	0.149654	0.153249	0.156894	0.160594	0.164354	0.16818	0.172079
-0.66	0.144779	0.148353	0.151972	0.155638	0.159357	0.163133	0.166973	0.170882	0.174867
-0.67	0.146966	0.150608	0.154296	0.158034	0.161828	0.165682	0.169602	0.173595	0.177668
-0.68	0.149157	0.152867	0.156626	0.160437	0.164306	0.168239	0.172241	0.176319	0.180482
-0.69	0.151353	0.155132	0.158962	0.162847	0.166793	0.170806	0.174891	0.179056	0.18331
-0.7	0.153554	0.157403	0.161305	0.165265	0.169289	0.173382	0.177552	0.181805	0.186153
-0.71	0.15576	0.15968	0.163655	0.167691	0.171794	0.175969	0.180224	0.184568	0.18901
-0.72	0.157972	0.161964	0.166013	0.170126	0.174308	0.178566	0.182908	0.187344	0.191882
-0.73	0.16019	0.164254	0.168378	0.172568	P073'!B45	0.181174	0.185605	0.190133	0.194769
-0.74	0.162414	0.16655	0.17075	0.17502	0.179365	0.183794	0.188314	0.192937	0.197673
-0.75	0.164644	0.168854	0.173131	0.17748	0.181909	0.186425	0.191037	0.195756	0.200594
-0.76	0.16688	0.171165	0.17552	0.17995	0.184463	0.189067	0.193773	0.19859	0.203532
-0.77	0.169123	0.173484	0.177917	0.182429	0.187028	0.191723	0.196523	0.20144	0.206488
-0.78	0.171373	0.175811	0.180323	0.184919	0.189605	0.194391	0.199287	0.204306	0.209462
-0.79	0.17363	0.178145	0.182739	0.187418	0.192193	0.197072	0.202066	0.207189	0.212456
-0.8	0.175894	0.180488	0.185163	0.189929	0.194793	0.199766	0.20486	0.210089	0.215468

Table B.43: Normalized Power $\hat{p}$ vs Normalized initial resonant current $\hat{I}_0$ in presence of normalized output voltage $\hat{v}$.

					$\hat{v}$				
	0.55	0.56	0.57	0.58	0.59	0.6	0.61	0.62	0.63
$\hat{I}_o$					$\hat{p}$				
-0.01	0.00275	0.0028	0.00285	0.0029	0.00295	0.003	0.00305	0.0031	0.00315
-0.02	0.005499	0.005599	0.005699	0.005799	0.005899	0.005999	0.006099	0.006199	0.006299
-0.03	0.008247	0.008397	0.008547	0.008697	0.008847	0.008997	0.009147	0.009297	0.009447
-0.04	0.010993	0.011193	0.011393	0.011593	0.011793	0.011993	0.012193	0.012393	0.012594
-0.05	0.013737	0.013987	0.014237	0.014487	0.014737	0.014987	0.015237	0.015487	0.015738
-0.06	0.016478	0.016777	0.017077	0.017378	0.017678	0.017978	0.018278	0.018578	0.018879
-0.07	0.019215	0.019565	0.019915	0.020265	0.020615	0.020965	0.021316	0.021666	0.022017
-0.08	0.021948	0.022348	0.022348	0.023148	0.023549	0.023949	0.02435	0.024751	0.025152
-0.09	0.024677	0.025127	0.025577	0.026028	0.026478	0.026929	0.02738	0.027832	0.028284
-0.1	0.027402	0.027902	0.028402	0.028902	0.029403	0.029905	0.030406	0.030909	0.031411
-0.11	0.030121	0.030672	0.031222	0.031773	0.032324	0.032876	0.033428	0.033982	0.034536
-0.12	0.032836	0.033436	0.034037	0.034639	0.03524	0.035843	0.036447	0.037051	0.037656
-0.13	0.035546	0.036196	0.036848	0.0375	0.038152	0.038806	0.03946	0.040116	0.040773
-0.14	0.03825	0.038951	0.039653	0.040356	0.04106	0.041764	0.042471	0.043178	0.043887
-0.15	0.04095	0.041701	0.042454	0.043208	0.043963	0.044719	0.045477	0.046237	0.046998
-0.16	0.043644	0.044447	0.04525	0.046055	0.046861	0.04767	0.04848	0.049292	0.050107
-0.17	0.046334	0.047187	0.048042	0.048898	0.049756	0.050617	0.051479	0.052345	0.053213
-0.18	0.049018	0.049923	0.050829	0.051737	0.052647	0.053561	0.054476	0.055395	0.056318
-0.19	0.051698	0.052654	0.053612	0.054572	0.055535	0.056501	0.057471	0.058444	0.059421
-0.2	0.054373	0.055381	0.056391	0.057404	0.05842	0.05944	0.060463	0.061491	0.062524
-0.21	0.057045	0.058104	0.059167	0.060233	0.061302	0.062376	0.063454	0.064537	0.065626
-0.22	0.059712	0.060824	0.061939	0.063059	0.064182	0.06531	0.066444	0.067583	0.068729
-0.23	0.062376	0.06354	0.064709	0.065882	0.06706	0.068244	0.069433	0.070629	0.071833
-0.24	0.065036	0.066254	0.067477	0.068704	0.069937	0.071176	0.072422	0.073676	0.074938
-0.25	0.067694	0.068965	0.070242	0.071524	0.072813	0.074108	0.075412	0.076724	0.078046
-0.26	0.070348	0.071674	0.073005	0.074343	0.075688	0.077041	0.078402	0.079774	0.081156
-0.27	0.073001	0.074381	0.075768	0.077162	0.078563	0.079974	0.081394	0.082826	0.084269
-0.28	0.075652	0.077087	0.078529	0.07998	0.081439	0.082908	0.084388	0.085881	0.087387
-0.29	0.078301	0.079792	0.08129	0.082798	0.084316	0.085844	0.087385	0.08894	0.090509
-0.3	0.080949	0.082496	0.084052	0.085617	0.087194	0.088783	0.090385	0.092003	0.093637
-0.31	0.083596	0.0852	0.086813	0.088438	0.090074	0.091724	0.093389	0.09507	0.09677
-0.32	0.086244	0.087904	0.089576	0.09126	0.092957	0.094669	0.096397	0.098144	0.099911
-0.33	0.088891	0.090609	0.09234	0.094084	0.095842	0.097617	0.09941	0.101223	0.103058
-0.34	0.091538	0.093316	0.095106	0.096911	0.098732	0.10057	0.102429	0.104309	0.106214
-0.35	0.094187	0.096023	0.097874	0.099741	0.101625	0.103528	0.105453	0.107402	0.109378
-0.36	0.096836	0.098733	0.100645	0.102574	0.104522	0.106492	0.108485	0.110503	0.112552
-0.37	0.099488	0.101445	0.103419	0.105412	0.107425	0.109461	0.111523	0.113613	0.115735
-0.38	0.102141	0.10416	0.106197	0.108254	0.110333	0.112438	0.11457	0.116732	0.11893
-0.39	0.104797	0.106878	0.108979	0.111101	0.113248	0.115421	0.117625	0.119862	0.122136
-0.4	0.107456	0.1096	0.111765	0.113954	0.116169	0.118413	0.120689	0.123001	0.125354

Table B.44: Normalized Power $\hat{p}$ vs Normalized initial resonant current $\hat{I}_0$ in presence of normalized output voltage $\hat{v}$.

					$\hat{v}$				
	0.55	0.56	0.57	0.58	0.59	0.6	0.61	0.62	0.63
$\hat{I}_o$					$\hat{p}$				
-0.41	0.110118	0.112326	0.114556	0.116812	0.119097	0.121412	0.123763	0.126152	0.128585
-0.42	0.112784	0.115056	0.117353	0.119678	0.122033	0.124421	0.126847	0.129315	0.131829
-0.43	0.115454	0.117792	0.120156	0.12255	0.124976	0.127439	0.129942	0.13249	0.135089
-0.44	0.118128	0.120533	0.122965	0.12543	0.127929	0.130467	0.133049	0.135679	0.138363
-0.45	0.120808	0.123279	0.125781	0.128318	0.130891	0.133506	0.136168	0.138882	0.141654
-0.46	0.123492	0.126032	0.128605	0.131214	0.133863	0.136557	0.1393	0.142099	0.144961
-0.47	0.126183	0.128792	0.131436	0.134119	0.136845	0.139619	0.142446	0.145332	0.148286
-0.48	0.128879	0.131559	0.134276	0.137034	0.139838	0.142693	0.145606	0.148581	0.151629
-0.49	0.131582	0.134333	0.137124	0.139959	0.142843	0.145781	0.14878	0.151848	0.154992
-0.5	0.134292	0.137115	0.139981	0.142894	0.14586	0.148883	0.151971	0.155132	0.158375
-0.51	0.137009	0.139906	0.142849	0.145841	0.148889	0.151999	0.155178	0.158434	0.161779
-0.52	0.139734	0.142706	0.145726	0.148799	0.151931	0.15513	0.158402	0.161756	0.165205
-0.53	0.142467	0.145515	0.148614	0.15177	0.154988	0.158276	0.161643	0.165099	0.168654
-0.54	0.145209	0.148334	0.151514	0.154753	0.158059	0.161439	0.164904	0.168462	0.172128
-0.55	0.14796	0.151163	0.154425	0.157749	0.161145	0.16462	0.168184	0.171848	0.175626
-0.56	0.15072	0.154003	0.157348	0.16076	0.164247	0.167818	0.171484	0.175257	0.179151
-0.57	0.15349	0.156855	0.160284	0.163784	0.167365	0.171034	0.174805	0.178689	0.182703
-0.58	0.15627	0.159718	0.163233	0.166824	0.1705	0.17427	0.178148	0.182147	0.186284
-0.59	0.159061	0.162593	0.166196	0.16988	0.173653	0.177527	0.181514	0.185631	0.189894
-0.6	0.161863	0.16548	0.169173	0.172951	0.176824	0.180804	0.184904	0.189141	0.193536
-0.61	0.164677	0.168381	0.172166	0.17604	0.180015	0.184102	0.188318	0.19268	0.19721
-0.62	0.167503	0.171296	0.175174	0.179146	0.183225	0.187424	0.191759	0.196249	0.200917
-0.63	0.170342	0.174225	0.178197	0.18227	0.186456	0.190769	0.195226	0.199848	0.20466
-0.64	0.173193	0.177168	0.181238	0.185414	0.189708	0.194138	0.19872	0.203479	0.20844
-0.65	0.176058	0.180127	0.184296	0.188576	0.192983	0.197532	0.202244	0.207143	0.212258
-0.66	0.178937	0.183102	0.187372	0.19176	0.196281	0.200953	0.205798	0.210842	0.216116
-0.67	0.181831	0.186093	0.190466	0.194964	0.199603	0.204401	0.209383	0.214577	0.220016
-0.68	0.184739	0.189101	0.19358	0.19819	0.202949	0.207878	0.213001	0.21835	0.22396
-0.69	0.187663	0.192127	0.196713	0.201439	0.206322	0.211384	0.216653	0.222162	0.22795
-0.7	0.190604	0.195171	0.199867	0.204711	0.209721	0.214921	0.220341	0.226015	0.231988
-0.71	0.19356	0.198233	0.203043	0.208008	0.213148	0.21849	0.224065	0.229911	0.236077
-0.72	0.196534	0.201315	0.206241	0.211329	0.216604	0.222092	0.227828	0.233852	0.240219
-0.73	0.199526	0.204418	0.209461	0.214677	0.22009	0.225729	0.23163	0.23784	0.244416
-0.74	0.202536	0.207541	0.212706	0.218052	0.223607	0.229401	0.235475	0.241877	0.248672
-0.75	0.205565	0.210685	P075'!B45	0.221455	0.227156	0.233111	0.239363	0.245966	0.25299
-0.76	0.208614	0.213852	0.219269	0.224888	0.230739	0.23686	0.243298	0.250109	0.257372
-0.77	0.211683	0.217042	0.222589	0.22835	0.234357	0.24065	0.247279	0.254309	0.261823
-0.78	0.214772	0.220256	0.225937	0.231844	0.238011	0.244482	0.251311	0.258569	0.266347
-0.79	0.217884	0.223495	0.229313	0.23537	0.241703	0.248359	0.255396	0.262891	0.270948
-0.8	0.221018	0.226759	0.232719	0.238931	0.245435	0.252281	0.259535	0.26728	0.27563

Table B.45: Normalized Power $\hat{p}$ vs Normalized initial resonant current $\hat{I}_0$ in presence of normalized output voltage $\hat{v}$.

					$\hat{v}$				
	0.64	0.65	0.66	0.67	0.68	0.69	0.7	0.71	0.72
$\hat{I}_o$					$\hat{p}$				
-0.01	0.0032	0.00325	0.0033	0.00335	0.0034	0.00345	0.0035	0.00355	0.0036
-0.02	0.006399	0.006499	0.006599	0.006699	0.006799	0.006899	0.006999	0.0071	0.0072
-0.03	0.009597	0.009747	0.009898	0.010048	0.010198	0.010348	0.010498	0.010649	0.010799
-0.04	0.012794	0.012994	0.013194	0.013395	0.013595	0.013795	0.013996	0.014197	0.014398
-0.05	P005'!B45	0.016238	0.016489	0.01674	0.01699	0.017241	0.01699	0.017744	0.017995
-0.06	0.01918	0.01948	0.019781	0.020083	0.020384	0.020686	0.020988	0.02129	0.021593
-0.07	0.022368	0.02272	0.023071	0.023423	0.023775	0.024128	0.024481	0.024835	0.02519
-0.08	0.025554	0.025956	0.026358	0.026761	0.027165	0.027569	0.027974	0.02838	0.028786
-0.09	0.028736	0.029189	0.029643	0.030097	0.030552	0.031008	0.031465	0.031924	0.032383
-0.1	0.031915	0.032419	0.032924	0.03343	0.033937	0.034446	0.034956	0.035468	0.035981
-0.11	0.03509	0.035646	0.036203	0.036761	0.037321	0.037883	0.038446	0.039012	0.039581
-0.12	0.038263	0.03887	0.03948	0.040091	0.040704	0.041319	0.041937	0.042558	0.043182
-0.13	0.041432	0.042092	0.042754	0.043419	0.044085	0.044755	0.045428	0.046105	0.046787
-0.14	0.044598	0.045312	0.046027	0.046746	0.047467	0.048192	0.048921	0.049656	0.050395
-0.15	0.047763	0.048529	0.049299	0.050072	0.050849	0.05163	0.052417	0.053209	0.054009
-0.16	0.050925	0.051745	0.05257	0.053399	0.054232	0.055071	0.055916	0.056768	0.057628
-0.17	0.054085	0.054961	0.055841	0.056726	0.057617	0.058514	0.059418	0.060331	0.061254
-0.18	0.057245	0.058176	0.059112	0.060055	0.061004	0.06196	0.062926	0.063901	0.064889
-0.19	0.060404	0.061391	0.062385	0.063385	0.064394	0.065411	0.066439	0.067479	0.068532
-0.2	0.063562	0.064607	0.065659	0.066719	0.067788	0.068868	0.06996	0.071065	0.072186
-0.21	0.066722	0.067825	0.068936	0.070056	0.071187	0.072331	0.073488	0.07466	0.075851
-0.22	0.069883	0.071045	0.072216	0.073398	0.074592	0.075801	0.077025	0.078267	0.07953
-0.23	0.073045	0.074267	0.0755	0.076745	0.078004	0.079278	0.080571	0.081885	0.083222
-0.24	0.07621	0.077493	0.078789	0.080098	0.081423	0.082766	0.084129	0.085516	0.086929
-0.25	0.079379	0.080724	0.082083	0.083457	0.08485	0.086263	0.087698	0.089161	0.090654
-0.26	0.082551	0.083959	0.085383	0.086825	0.088286	0.089771	0.091281	0.092821	0.094396
-0.27	0.085727	0.0872	0.08869	0.090201	0.091733	0.093291	0.094878	0.096498	0.098157
-0.28	0.088909	0.090447	0.092006	0.093586	0.095191	0.096824	0.09849	0.100193	0.101939
-0.29	0.092096	0.093702	0.09533	0.096981	0.098661	0.100372	0.102119	0.103907	0.105743
-0.3	0.09529	0.096965	0.098663	0.100388	0.102144	0.103935	0.105765	0.107642	0.109571
-0.31	0.098491	0.100236	0.102006	0.103807	0.105641	0.107514	0.109431	0.111398	0.113424
-0.32	0.101701	0.103516	0.105361	0.107239	0.109153	0.111111	0.113116	0.115178	0.117304
-0.33	0.104919	0.106807	0.108728	0.110684	0.112682	0.114726	0.116823	0.118982	0.121212
-0.34	0.108146	0.110109	0.112108	0.114145	0.116227	0.118361	0.120553	0.122812	0.125151
-0.35	0.111384	0.113423	0.115501	0.117622	0.119791	0.122017	0.124307	0.126671	0.129121
-0.36	0.114632	0.11675	0.118909	0.121115	0.123374	0.125695	0.128086	0.130558	0.133126
-0.37	0.117893	0.12009	0.122333	0.124626	0.126978	0.129397	0.131892	0.134477	0.137166
-0.38	0.121165	0.123444	0.125773	0.128156	0.130604	0.133124	0.135727	0.138429	0.141244
-0.39	0.124451	0.126814	0.12923	0.131707	0.134252	0.136877	0.139593	0.142415	0.145363
-0.4	0.127751	0.1302	0.132706	0.135278	0.137924	0.140657	0.143489	0.146438	0.149523

Table B.46: Normalized Power $\hat{p}$ vs Normalized initial resonant current $\hat{I}_0$ in presence of normalized output voltage $\hat{v}$.

					$\hat{v}$				
	0.64	0.65	0.66	0.67	0.68	0.69	0.7	0.71	0.72
$\hat{I}_o$					$\hat{p}$				
-0.41	0.131066	0.133603	0.136202	0.138871	0.141622	0.144467	0.14742	0.1505	0.153729
-0.42	0.134397	0.137023	0.139718	0.142488	0.145347	0.148307	0.151386	0.154602	0.157983
-0.43	0.137744	0.140463	0.143255	0.14613	0.1491	0.15218	0.155389	0.158748	0.162287
-0.44	0.141108	0.143922	0.146815	0.149797	0.152882	0.156087	0.159431	0.16294	0.166644
-0.45	0.144491	0.147403	0.150399	0.153492	0.156696	0.16003	0.163515	0.167179	0.171058
-0.46	0.147893	0.150905	0.154008	0.157215	0.160542	0.16401	0.167643	0.17147	0.175533
-0.47	0.151315	0.15443	0.157642	0.160968	0.164423	0.16803	0.171816	0.175815	0.180071
-0.48	0.154758	0.157979	0.161305	0.164752	0.16834	0.172092	0.176038	0.180217	0.184677
-0.49	0.158223	0.161553	0.164996	0.168569	0.172295	0.176198	0.180312	0.18468	0.189356
-0.5	0.158375	0.165153	0.168717	0.172421	0.176289	0.18035	0.18464	0.189207	0.194113
-0.51	0.165223	0.168781	0.172469	0.176309	0.180326	0.184551	0.189026	0.193803	0.198952
-0.52	0.16876	0.172438	0.176255	0.180235	0.184407	0.188804	0.193472	0.198471	0.203881
-0.53	0.172324	0.176124	0.180075	0.184201	0.188534	0.193111	0.197983	0.203218	0.208905
-0.54	0.175915	0.179842	0.183931	0.188209	0.192709	0.197475	0.202563	0.208047	0.214032
-0.55	0.179535	0.183594	0.187826	0.192261	0.196937	0.201901	0.207216	0.212966	0.219271
-0.56	0.183185	0.187379	0.19176	0.196359	0.201218	0.206391	0.211946	0.217981	0.22463
-0.57	0.186866	0.191201	0.195735	0.200506	0.205557	0.210949	0.21676	0.223098	0.230122
-0.58	0.19058	0.19506	0.199755	0.204704	0.209957	0.21558	0.221662	0.228327	0.235758
-0.59	0.194328	0.198959	0.20382	0.208956	0.214421	0.220289	0.22666	0.233677	0.241552
-0.6	0.198112	0.202899	0.207934	0.213264	0.218952	0.22508	0.23176	0.239158	0.247523
-0.61	0.201933	0.206882	0.212098	0.217633	0.223556	0.229959	0.236971	0.244783	0.253689
-0.62	0.205793	0.210911	0.216316	0.222065	0.228236	0.234932	0.242302	0.250565	0.260076
-0.63	0.209694	0.214987	0.220589	0.226565	0.232998	0.240008	0.247763	0.256522	0.266713
-0.64	0.213637	0.219113	0.224922	0.231135	0.237847	0.245192	0.253366	0.262673	0.273636
-0.65	0.217626	0.223292	0.229318	0.235781	0.24279	0.250495	0.259125	0.269042	0.280892
-0.66	0.221661	0.227527	0.23378	0.240508	0.247832	0.255927	0.265056	0.275658	0.288543
-0.67	0.225745	0.231819	0.238312	0.24532	0.252982	0.261498	0.271179	0.282555	0.296671
-0.68	0.229881	0.236173	0.242918	0.250224	0.258249	0.267222	0.277515	0.28978	0.305391
-0.69	0.234071	0.240592	0.247603	0.255226	0.263641	0.273116	0.284092	0.297389	0.314876
-0.7	0.238318	0.245079	0.252371	0.260334	0.26917	0.279196	0.290945	0.305463	0.325402
-0.71	0.242626	0.249639	0.25723	0.265555	0.274849	0.285484	0.298116	0.314108	0.337471
-0.72	0.246997	0.254277	0.262184	0.270899	0.280692	0.292007	0.30566	0.323485	0.352205
-0.73	0.251434	0.258995	0.267241	0.276376	0.286717	0.298797	0.313649	0.333845	0.373749
-0.74	0.255942	0.263802	0.272409	0.281999	0.292944	0.305894	0.322185	0.345633	0
-0.75	0.260526	0.268701	0.277696	0.287781	0.299398	0.313349	0.331412	0.359782	0
-0.76	0.265189	0.2737	0.283112	0.293738	0.306108	0.321228	0.341554	0.379225	0
-0.77	0.269936	0.278806	0.288668	0.29989	0.313111	0.329623	0.352993	0.41043	0
-0.78	0.274773	0.284027	0.294378	0.30626	0.320455	0.338664	0.366484	0	0
-0.79	0.279707	0.289373	0.300256	0.312874	0.328201	0.348545	0.384074	0	0
-0.8	0.284744	0.294854	0.306321	0.319768	0.336429	0.359587	0.421476	0	0

Table B.47: Normalized Power $\hat{p}$ vs Normalized initial resonant current $\hat{I}_0$ in presence of normalized output voltage $\hat{v}$.

				$\hat{v}$				
	0.73	0.74	0.75	0.76	0.77	0.78	0.79	0.8
$\hat{I}_o$				$\hat{p}$				
-0.01	0.00365	0.0037	0.00375	0.0038	0.00385	0.0039	0.00395	0.004
-0.02	0.0073	0.0074	0.0075	0.0076	0.007701	0.007801	0.007901	0.008002
-0.03	0.010949	0.0111	0.010949	0.011401	0.011552	0.011703	0.011854	0.012005
-0.04	0.014398	0.0148	0.015001	0.015203	0.015405	0.015607	0.01581	0.016013
-0.05	0.017995	0.0185	0.018752	0.019006	0.019259	0.019514	0.019769	0.020026
-0.06	0.021896	0.0222	0.022505	0.02281	0.023117	0.023425	0.023734	0.024045
-0.07	0.025545	0.025901	0.026259	0.026618	0.026978	0.027341	0.027705	0.028073
-0.08	0.029195	0.029604	0.029195	0.030429	0.030844	0.031263	0.031685	0.032111
-0.09	0.032845	0.033309	0.033775	0.034244	0.034716	0.035193	0.035674	0.036161
-0.1	0.036497	0.037016	0.037539	0.038065	0.038596	0.039132	0.039675	0.040226
-0.11	0.039581	0.040728	0.041308	0.041893	0.042484	0.043082	0.043689	0.044307
-0.12	0.043811	0.044444	0.045083	0.045728	0.046382	0.047045	0.047719	0.048406
-0.13	0.047473	0.048166	0.048866	0.049574	0.050292	0.051022	0.051765	0.052526
-0.14	0.051141	0.051895	0.052657	0.05343	0.054215	0.055015	0.055832	0.05667
-0.15	0.054816	0.055632	0.056459	0.057299	0.058154	0.059026	0.05992	0.060839
-0.16	0.058498	0.059379	0.060273	0.061182	0.062109	0.063057	0.064031	0.065036
-0.17	0.062189	0.063136	0.064099	0.06508	0.066083	0.067111	0.068169	0.069264
-0.18	0.065889	0.066905	0.06794	0.068996	0.070077	0.071188	0.072335	0.073526
-0.19	0.069601	0.070688	0.071797	0.072931	0.074094	0.075292	0.076533	0.077824
-0.2	0.073325	0.073325	0.075672	0.076886	0.078135	0.079425	0.080763	0.082162
-0.21	0.077064	0.0783	0.079565	0.080864	0.082203	0.083588	0.085031	0.086542
-0.22	0.080817	0.082132	0.08348	0.084867	0.086299	0.087785	0.089337	0.090969
-0.23	0.084587	0.085983	0.087418	0.088896	0.090426	0.092018	0.093686	0.095446
-0.24	0.088374	0.089856	0.09138	0.092953	0.094586	0.09629	0.098081	0.099976
-0.25	0.092182	0.093751	0.095368	0.097041	0.098782	0.100604	0.102524	0.104564
-0.26	0.09601	0.09767	0.099384	0.101162	0.103016	0.104962	0.10702	0.109215
-0.27	0.09986	0.101615	0.10343	0.105318	0.107291	0.109369	0.111573	0.113934
-0.28	0.101939	0.105588	0.107509	0.109511	0.11161	0.113826	0.116186	0.118726
-0.29	0.107634	0.10959	0.111622	0.113745	0.115976	0.118339	0.120865	0.123596
-0.3	0.109571	0.113624	0.115772	0.118021	0.120392	0.122911	0.125615	0.128553
-0.31	0.115518	0.117692	0.119961	0.122343	0.124861	0.127547	0.130442	0.133602
-0.32	0.119506	0.121796	0.124191	0.126713	0.129388	0.132251	0.13535	0.138754
-0.33	0.123526	0.125938	0.128466	0.131135	0.133976	0.137028	0.140349	0.144016
-0.34	0.127581	0.13012	0.132788	0.135613	0.13863	0.141885	0.145444	0.149401
-0.35	0.131673	0.134345	0.137161	0.14015	0.143354	0.146827	0.150645	0.15492
-0.36	0.135805	0.138616	0.141586	0.144751	0.148155	0.151862	0.155962	0.160589
-0.37	0.139977	0.142935	0.146069	0.149419	0.153038	0.156998	0.161407	0.166425
-0.38	0.144195	0.147306	0.150613	0.15416	0.158009	0.162244	0.166992	0.172449
-0.39	0.148458	0.151732	0.155222	0.15898	0.163075	0.167609	0.172732	0.178685
-0.4	0.152772	0.156216	0.1599	0.163883	0.168246	0.173107	0.178647	0.185167

Table B.48: Normalized Power $\hat{p}$ vs Normalized initial resonant current $\hat{I}_0$ in presence of normalized output voltage $\hat{v}$.

				$\hat{v}$				
	0.73	0.74	0.75	0.76	0.77	0.78	0.79	0.8
$\hat{I}_o$				$\hat{p}$				
-0.41	0.157138	0.160763	0.164653	0.168877	0.173529	0.17875	0.184758	0.191932
-0.42	0.16156	0.165375	0.169486	0.173969	0.178936	0.184554	0.191092	0.199034
-0.43	0.166041	0.170059	0.174405	0.179168	0.184479	0.190539	0.197682	0.20654
-0.44	0.170586	0.174818	0.179416	0.184482	0.190171	0.196727	0.20457	0.214548
-0.45	0.175198	0.179659	0.184527	0.189923	0.19603	0.203147	0.211813	0.2232
-0.46	0.179882	0.184587	0.189747	0.195503	0.202075	0.209833	0.219483	0.232725
-0.47	0.184643	0.18961	0.195085	0.201236	0.20833	0.216831	0.227687	0.243526
-0.48	0.189486	0.194733	0.200552	0.20714	0.214823	0.224197	0.236581	0.256484
-0.49	0.194417	0.199967	0.20616	0.213234	0.221592	0.232013	0.24642	0.274587
-0.5	0.199444	0.205321	0.211924	0.219543	0.228682	0.24039	0.257668	
-0.51	0.204573	0.210805	0.217862	0.226096	0.236155	0.249498	0.271386	
-0.52	0.209813	0.216432	0.223994	0.232932	0.244094	0.259615	0.291783	
-0.53	0.215174	0.222218	0.230344	0.240097	0.252617	0.271261		
-0.54	0.220666	0.228178	0.236942	0.247654	0.261903	0.285671		
-0.55	0.226303	0.234334	0.243827	0.25569	0.272251	0.308644		
-0.56	0.232099	0.240711	0.251048	0.264327	0.284224			
-0.57	0.23807	0.247339	0.258667	0.273751	0.299205			
-0.58	0.244238	0.254256	0.266772	0.284272	0.324778			
-0.59	P059'!B45	0.26151	0.275487	0.296482				
-0.6	0.257268	0.269166	0.285002	0.311854				
-0.61	0.264198	0.27731	0.29563	0.339313				
-0.62	0.271465	0.286066	0.307971					
-0.63	0.279131	0.295622	0.323514					
-0.64	0.287283	0.306286	0.35111					
-0.65	0.29604	0.318645						
-0.66	0.305585	0.334123						
-0.67	0.316215	0.360183						
-0.68	0.32848							
-0.69	0.343674							
-0.7	0.367504							

Appendix C

PRC and SRC polynomials in Matlab Codes

C.1 PRC Polynomial Codes

This illustrates PRC polynomials

```
%% Frequency and Duty output with Power and Voltage as Input
% a stands for frequncy polynomial coefficients.
% b stands for duty polynomial coefficients.

function [f,d]=fcn(v,p)
if (v ≥ 1) && (v ≤ 1.2)&&(0.560354057≤p && p ≤1.948584073)
a1=-6.44*v+6.4193;
a2=18.319*v-18.287;
a3=-16.536*v+15.924;
a4=5.349*v-4.1342;

b1=2.5863*v-2.5879;
b2=-7.3565*v+7.3709;
b3=6.8951*v-6.7233;
b4=-2.157*v+2.2782;
```

```
16
17 elseif (v ≥ 1.3) && (v ≤ 1.5)&&(0.773108748≤p && p≤1.498568802)
18
19 a1=-1.59*v+0.73103;
20 a2=7.2865*v-5.5462;
21 a3=-9.536*v+8.1538;
22 a4=4.222*v-3.0346;
23
24 b1=1.4197*v-1.253;
25 b2=-5.573*v+5.5074;
26 b3=6.9235*v-7.1266;
27 b4=-2.8196*v+3.231;
28
29
30 elseif (v ≥ 1.6) && (v ≤ 1.8)&&(0.907865669≤p && p≤1.654088175)
31 a1=-0.675*v-0.27697;
32 a2=5.6585*v-4.4915;
33 a3=-10.486*v+11.393;
34 a4=5.87*v-6.306;
35
36 b1=1.0212*v-0.84879;
37 b2=-5.669*v+6.4327;
38 b3=9.214*v-11.632;
39 b4=-4.713*v+6.5631;
40
41
42 elseif (v ≥ 1.9) && (v ≤ 2.0)&&(1.122564142≤p && p≤1.770743457)
43 a1=-1.095*v+0.5737;
44 a2=8.328*v-9.835;
45 a3=-16.523*v+23.247;
46 a4=10.022*v-14.362;
47
48 b1=1.48*v-1.7409;
49 b2=-8.867*v+12.589;
50 b3=15.965*v-24.54;
51 b4=-9.087*v+14.889;
```

```
52
53 elseif (v ≥ 2.1) && (v ≤ 2.2)&&(1.256339732≤p && p≤1.891467209)
54 a1=2.424*v-6.4033;
55 a2=-9.185*v+24.994;
56 a3=11.445*v-32.488;
57 a4=-4.495*v+14.611;
58
59 b1=-1.4155*v+4.0245;
60 b2=4.987*v-15.045;
61 b3=-5.526*v+18.38;
62 b4=1.776*v-6.8231;
63
64
65 elseif (v ≥ 2.3) && (v ≤ 2.4)&&(1.397247313≤p && p≤2.014631983)
66
67 a1=-0.365*v-0.3347;
68 a2=3.796*v-3.17;
69 a3=-9.153*v+12.106;
70 a4=6.57*v-9.3089;
71
72 b1=0.916*v-1.06;
73 b2=-6.297*v+9.5256;
74 b3=13.015*v-21.959;
75 b4=-8.519*v+15.571;
76
77 elseif (v ≥ 2.5) && (v ≤ 2.6)&&(1.476245431≤p && p≤2.140302049)
78
79 a1=-1.393*v+2.4775;
80 a2=10.211*v-20.46;
81 a3=-22.786*v+48.312;
82 a4=16.191*v-34.545;
83
84 b1=1.8546*v-3.6424;
85 b2=-12.615*v+26.522;
86 b3=27.025*v-58.994;
87 b4=-18.648*v+42;
```

```
88
89
90 elseif (v ≥ 2.7) && (v ≤ 2.8)&&(1.628279553≤p && p≤2.266553158)
91 a1=1.5088*v-5.0318;
92 a2=-7.101*v+24.405;
93 a3=10.879*v-39.025;
94 a4=-5.261*v+21.15;
95
96 b1=-1.2309*v+4.3582;
97 b2=5.429*v-20.312;
98 b3=-7.493*v+30.662;
99 b4=3.007*v-14.273;
100
101
102 elseif (v ≥ 2.9) && (v ≤ 3.0)&&(1.785629982≤p && p≤2.393152588)
103 a1=1.4187*v-5.0571;
104 a2=-7.191*v+26.411;
105 a3=11.834*v-45.351;
106 a4=-6.159*v+ 26.178;
107
108 b1=-1.2665*v+4.7769;
109 b2=6.027*v-23.985;
110 b3=-8.97*v+38.931;
111 b4=3.906*v-19.616;
112
113 elseif (v ≥ 3.1) && (v ≤ 3.2)&&(1.874116055≤p && p≤2.52068241)
114 a1=1.2073*v-4.606;
115 a2=-6.409*v+25.243;
116 a3=11*v-45.349;
117 a4=-5.928*v+27.237;
118
119 b1=-1.1662*v+4.7107;
120 b2=5.796*v-24.789;
121 b3=-8.93*v+41.962;
122 b4=3.946*v-21.928;
123
```

```
124
125 elseif (v ≥ 3.3) && (v ≤ 3.4)&&(2.04026399≤p && p≤2.648888527)
126 a1=1.2193*v-4.9297;
127 a2=-6.94*v+28.953;
128 a3=12.76*v-55.668;
129 a4=-7.38*v+35.5;
130
131 b1=-1.271*v+5.4262;
132 b2=6.787*v-30.625;
133 b3=-11.25*v+55.564;
134 b4=5.38*v-31.26;
135
136
137 elseif (v ≥ 3.5) && (v ≤ 3.6)&&(2.133080856≤p && p≤2.777099761)
138 a1=0.8654*v-3.7104;
139 a2=-5.133*v+22.726;
140 a3=9.82*v-45.536;
141 a4=-5.895*v+30.382;
142
143 b1=-0.9676*v+4.3807;
144 b2=5.378*v-25.769;
145 b3=-9.26*v+48.704;
146 b4=4.56*v-28.434;
147
148
149 elseif (v ≥ 3.7) && (v ≤ 3.8)&&(2.306786125≤p && p≤2.905290807)
150 a1=0.911*v-4.1174;
151 a2=-5.757*v+26.867;
152 a3=11.72*v-57.273;
153 a4=-7.48*v+40.282;
154
155 b1=-1.095*v+5.209;
156 b2=6.505*v-32.697;
157 b3=-11.98*v+65.888;
158 b4=6.34*v-41.151;
159
```

```
160
161 elseif (v ≥ 3.9) && (v ≤ 4.0)&& (2.403633695≤p && p≤3.033446039)
162 a1=0.6699*v-3.19;
163 a2=-4.403*v+21.658;
164 a3=9.31*v-47.998;
165 a4=-6.16*v+35.199;
166
167 b1=-0.8502*v+4.2675;
168 b2=5.238*v-27.824;
169 b3=-9.97*v+58.156;
170 b4=5.4*v-37.535;
171
172 else
173 a1=0;
174 a2=0;
175 a3=0;
176 a4=0;
177
178 b1=0;
179 b2=0;
180 b3=0;
181 b4=0;
182 end
183 f =a1*p^3+a2*p^2+a3*p+a4;
184 d=b1*p^3+b2*p^2+b3*p+b4;
```

C.2 SRC Polynomial Codes

C.2.1 Initial resonant current polynomial

```
1 %% Frequency and Duty output with Power and Voltage as Input
2 % a stands for frequncy polynomial coefficients.
3 % b stands for duty polynomial coefficients.
```

```
4
5  function I = fcn(p,v)
6
7  if (v ≥ 0.01) && (v ≤ 0.02)
8  a0=0;
9  a1=1.14e4*v+341.7;
10 a2=-0.03324*v^2-0.01173*v+0.02147;
11
12 elseif(v>0.02) && (v≤0.04)
13 a0=0;
14 a1=1900*v-132.8;
15 a2=-0.03324*v^2-0.01173*v+0.02147;
16
17 elseif(v>0.04) && (v≤0.06)
18 a0=0;
19 a1=759.7*v-83.39;
20 a2=-0.03324*v^2-0.01173*v+0.02147;
21
22
23 elseif(v>0.06) && (v≤0.08)
24 a0=0;
25 a1=411.4*v-61.18;
26 a2=-0.03324*v^2-0.01173*v+0.02147;
27
28 elseif(v>0.08) && (v≤0.10)
29 a0=0;
30 a1=253.5*v-47.96;
31 a2=-0.03324*v^2-0.01173*v+0.02147;
32
33 elseif(v>0.10) && (v≤0.13)
34 a0=0;
35 a1=159.7*v-38.05;
36 a2=-0.03324*v^2-0.01173*v+0.02147;
37 I=a0*p^2+a1*p+a2;
38 I
39
```

```
40 elseif(v>0.13) && (v≤0.16)
41 a0=0;
42 a1=101.7*v-30.29;
43 a2=-0.03324*v^2-0.01173*v+0.02147;
44
45 elseif(v>0.16) && (v≤0.21)
46 a0=0;
47 a1=64.08*v-24.03;
48 a2=-0.03324*v^2-0.01173*v+0.02147;
49
50 elseif(v>0.21) && (v≤0.26)
51 a0=0;
52 a1=41.81*v-19.32;
53 a2=-0.03324*v^2-0.01173*v+0.02147;
54
55 elseif(v>0.26) && (v≤0.37)
56 a0=0;
57 a1=23.18*v-14.35;
58 a2=-0.0397*v+0.0265;
59
60 elseif(v>0.37) && (v≤0.43)
61 a0=0;
62 a1=14.709*v-11.273;
63 a2=-0.0564*v+0.0327;
64
65 elseif(v>0.43) && (v≤0.49)
66 a0=0;
67 a1=11.57*v-9.918;
68 a2=-0.0783*v+0.0423;
69
70 elseif(v>0.49) && (v≤0.57)
71 a0=0;
72 a1=9.4411*v-8.8613;
73 a2=-0.1141*v+0.0604;
74
75 elseif(v>0.57) && (v≤0.64)
```

```
76 a0=0;
77 a1=8.6549*v-8.4204;
78 a2=-0.2*v+0.1097;
79
80 elseif(v>0.64) && (v≤0.68)
81 a0=0;
82 a1=9.97*v-9.2723;
83 a2=-0.439*v+0.2634;
84
85 elseif(v>0.68) && (v≤0.70)
86 a0=1.1558*v-0.0975;
87 a1=-4.22*v-0.4649;
88 a2=1.0095*v+0.0035;
89
90 elseif(v>0.70) && (v≤0.72)
91 a0=0.9623*v+0.0368;
92 a1=9*v-9.754;
93 a2=1.0179*v-0.0027;
94
95 elseif(v>0.72) && (v≤0.80)
96 a0=5.0657*v-0.3146;
97 a1=5.04*v-6.9612;
98 a2=-0.0807*v+0.0728;
99
100 elseif(v>0.81)
101 a0=0;
102 a1=0;
103 a2=0;
104 else
105 a0=0;
106 a1=0;
107 a2=0;
108 end
109 I=a0*p^2+a1*p+a2;
```

C.2.2 Frequency polynomial

```
%% Frequency and Duty output with Power and Voltage as Input
% a stands for frequncy polynomial coefficients.
% b stands for duty polynomial coefficients.

function T = fcn(i,v)

if (i ≥ -0.10) && (i ≤ -0.01)
a1=-21.46*i^2-6.112*i+0.002965;
a2=15.7*i^2+3.935*i-0.001925;
a3=-3.9458*i^2-1.054*i+0.0005583;
a4=-0.2248*i^2-0.6383*i+0.005342;

elseif(i ≥ -0.20) && (i < -0.10)
a1=-3.894*i^2-3.048*i+0.142;
a2=1.848*i^2+1.415*i-0.1215;
a3=-0.4576*i^2-0.433*i+0.02936;
a4=-0.2248*i^2-0.6383*i+0.005342;

elseif(i ≥ -0.30) && (i < -0.20)
a1=2.182*i^2-0.6247*i+0.3857;
a2=-3.098*i^2-0.584*i-0.3179;
a3=0.697*i^2+0.02788*i+0.07578;
a4=-0.2248*i^2-0.6383*i+0.005342;

elseif(i ≥ -0.40) && (i < -0.30)
a1=7.841*i^2+2.9*i+0.9364;
a2=-8*i^2-3.661*i-0.7979;
a3=1.936*i^2+0.8039*i+0.1978;
a4=-0.2248*i^2-0.6383*i+0.005342;

elseif(i ≥ -0.48) && (i < -0.40)
a1=46.07*i^2+35.04*i+7.696;
```

```
33      a2=-46.86*i^2-36.32*i-7.686;
34      a3=11.98*i^2+9.256*i+1.977;
35      a4=-0.2248*i^2-0.6383*i+0.005342;
36
37      elseif(i ≥ -0.51) && (i < -0.48)
38      a1=-9.7*i-3.424;
39      a2=9.07*i+3.569;
40      a3=-2.32*i-0.8882;
41      a4=-0.2248*i^2-0.6383*i+0.005342;
42
43      elseif(i ≥ -0.54) && (i < -0.51)
44      a1=-10.45*i-4.09;
45      a2=9.655*i+4.154;
46      a3=-2.45*i-1.028;
47      a4=-0.2248*i^2-0.6383*i+0.005342;
48
49      elseif(i≥-0.57) && (i< -0.54)
50      a1=-11*i-4.805;
51      a2=10.26*i+4.783;
52      a3=-2.57*i-1.171;
53      a4=-0.2248*i^2-0.6383*i+0.005342;
54
55      elseif(i≥-0.60) && (i< -0.57)
56      a1=-11.65*i-5.39;
57      a2=10.63*i+5.318;
58      a3=-2.625*i-1.283;
59      a4=-0.2248*i^2-0.6383*i+0.005342;
60
61      elseif(i≥-0.63) && (i< -0.60)
62      a1=-11.75*i-5.79;
63      a2=10.55*i+5.6;
64      a3=-2.575*i-1.335;
65      a4=-0.2248*i^2-0.6383*i+0.005342;
66
67      elseif(i≥-0.66) && (i< -0.63)
68      a1=-11.9*i-6.238;
```

```
69      a2=10.06*i+5.615;
70      a3=-2.43*i-1.323;
71      a4=-0.2248*i^2-0.6383*i+0.005342;
72
73      elseif(i≥-0.69) && (i< -0.66)
74      a1=-10.85*i-5.877;
75      a2=9.425*i+5.505;
76      a3=-2.24*i-1.272;
77      a4=-0.2248*i^2-0.6383*i+0.005342;
78
79      elseif(i≥-0.72) && (i< -0.69)
80      a1=-10.2*i-5.743;
81      a2=8.725*i+5.314;
82      a3=-2.045*i-1.207;
83      a4=-0.2248*i^2-0.6383*i+0.005342;
84
85      elseif(i≥-0.76) && (i< -0.73)
86      a1=-11.81*i-7.237;
87      a2=10.05*i+6.576;
88      a3=-2.327*i-1.482;
89      a4=-0.2248*i^2-0.6383*i+0.005342;
90
91      elseif(i ≥-0.79) && (i < -0.76)
92      a1=-14.8*i-9.931;
93      a2=12.55*i+8.854;
94      a3=-2.87*i-1.983;
95      a4=-0.2248*i^2-0.6383*i+0.005342;
96
97      elseif(i >-0.79) && (v>0.81)
98      a1=0;
99      a2=0;
100     a3=0;
101     a4=0;
102     else
103     a1=0;
104     a2=0;
```

```
105     a3=0;
106     a4=0;
107     end
108     T=a1*v^3+a2*v^2+a3*v+a4;
109     f=1/T;
```

Table C.1: Illustration of the practical validation of the SRC polynomial model as indicated in the figure 5-4

$\hat{p}$	$\hat{v}$	$\hat{I_0}$	$\hat{T}$	$\hat{f}$	f[kHz]	
					Simulated	Practical
0.010	0.09394	-0.2214	0.1429	6.998	234.5	234.3
0.015	0.115	-0.2755	0.1739	5.749	192.7	192.76
0.020	0.1328	-0.3163	0.1971	5.074	170.1	170.07
0.025	0.1485	-0.3606	0.2216	4.513	151.3	151.15
0.030	0.1627	-0.3894	0.2376	4.208	141	140.92
0.035	0.1757	-0.4285	0.2583	3.871	129.8	129.74
0.040	0.1879	-0.4616	0.2773	3.601	120.9	120.95
0.045	0.1993	-0.4889	0.2888	3.463	116.1	116.06
0.050	0.21	-0.5094	0.3015	3.317	111.2	111.06
0.055	0.2203	-0.5387	0.3139	3.186	106.8	106.76
0.060	0.2301	-0.565	0.3224	3.102	104	103.99
0.065	0.2395	-0.5882	0.332	3.012	101	100.93
0.070	0.2485	-0.6085	0.3384	2.955	99.05	99.05
0.075	0.2573	-0.6261	0.3483	2.871	96.23	96.23
0.080	0.2657	-0.6393	0.3509	2.85	95.53	95.53
0.085	0.2739	-0.6645	0.3601	2.777	93.09	93.04
0.090	0.2818	-0.6883	0.3718	2.69	90.15	-
0.095	0.2895	-0.7107	0.379	2.639	88.44	-
0.100	0.2971	-0.7317	0.3858	2.592	86	86.87

Appendix D

FPGA codes for the PRC polynomial model

Contents

D.1 Introduction 257
D.2 The Codes Cuadrado block 258
D.3 The Codes Cubo block 259
D.4 The Codes Mult2 block 262
D.5 The Codes Sumafin block 264
D.6 The Codes Vectorespos block 265

D.1 Introduction

The Figure 6-12 shows the FPGA complete model. The last is made of various blocks, namely: Vectores, Motor, Cubic, Cuadrado, Sumafin, and Mult2. Each iif those blocks holds the control codes as illutrated in various next sections.

D.2 The Codes Cuadrado block

This section covers the codes for the Codes the Cuadrado block shown of the figure 6-12.

```
1  library ieee;
2  use ieee.std_logic_1164.all;
3  use IEEE.numeric_std.ALL;
4
5  entity CUADRADO is
6
7  port
8  (
9  -- Input ports
10 clk : in  std_logic;
11
12 D1  : in    integer range -2147483647 TO 2147483647;
13
14 -- Output ports
15 O1              : out integer range -2147483647 TO 2147483647
16
17 );
18 end CUADRADO;
19
20 -- Library Clause(s) (optional)
21 -- Use Clause(s) (optional)
22
23 architecture SIMPLE of CUADRADO is
24
25 begin
26 process(clk)
27
28 variable D1H: integer range -2147483647 TO 2147483647;
29 variable D1L: integer range -2147483647 TO 2147483647;
30
```

```
31 begin
32 -- vamos calculando los distintos coeficientes por V
33 -- A1 = A11*V+A12
34
35 if (rising_edge(clk)) then
36
37 D1H:= (D1/65536);
38 D1L:= (D1-D1H*65536);
39
40 O1<=((D1H*65536)*D1H+ (D1L*D1H)+(D1H*D1L)+(((D1L/2)*(D1L/2))/16384));
41
42 end if;
43
44 end process;
45
46 end ;
```

D.3 The Codes Cubo block

This section covers the codes for the Cubo block shown of the figure 6-12.

```
1 library ieee;
2 use ieee.std_logic_1164.all;
3 use IEEE.numeric_std.ALL;
4
5 entity CUBO is
6
7
8
9 port
10 (
11 -- Input ports
12 clk : in  std_logic;
13
```

```
14 D1  : in    integer range -2147483647 TO 2147483647;
15
16
17 -- Output ports
18 O1              : out integer range -2147483647 TO 2147483647
19
20
21 );
22 end CUBO;
23
24 -- Library Clause(s) (optional)
25 -- Use Clause(s) (optional)
26
27 architecture SIMPLE of CUBO is
28
29 begin
30
31 process(clk)
32
33
34 variable D1H: integer range -2147483647 TO 2147483647;
35 variable D1L: integer range -2147483647 TO 2147483647;
36 variable INTER: integer range -2147483647 TO 2147483647;
37 variable INTERH: integer range -2147483647 TO 2147483647;
38 variable INTERL: integer range -2147483647 TO 2147483647;
39
40 begin
41
42 -- Calculamos el cuadrado de D1
43 if (rising_edge(clk)) then
44
45 D1H:= (D1/65536);
46 D1L:= (D1-D1H*65536);
47 INTER:=((D1H*65536)*D1H+ ...
      (D1L*D1H)+(D1H*D1L)+(((D1L/2)*(D1L/2))/16384));
48 INTERH:=(INTER/65536);
```

```
49 INTERl:=(INTER-INTERH*65536);
50 O1<=((D1H*65536)*INTERH+ ...
       (D1L*INTERH)+(D1H*INTERL)+(((D1L/2)*(INTERL/2))/16384));
51
52 end if;
53
54
55 end process;
56
57 end ;
```

D.4 The Mult2 block

This section covers the codes for the MULT2 block shown of the figure 6-12.

```
1  library ieee;
2  use ieee.std_logic_1164.all;
3  use IEEE.numeric_std.ALL;
4
5  entity MULT2 is
6
7  port
8  (
9  -- Input ports
10 clk : in  std_logic;
11
12 D1  : in    integer range -2147483647 TO 2147483647;
13 D2  : in  integer range -2147483647 TO 2147483647;
14
15
```

```
16 -- Output ports
17 O1              : out integer range -2147483647 TO 2147483647
18
19 );
20 end MULT2;
21
22 -- Library Clause(s) (optional)
23 -- Use Clause(s) (optional)
24
25 architecture SIMPLE of MULT2 is
26
27
28 begin
29
30 process(clk)
31
32
33 variable D1H: integer range -2147483647 TO 2147483647;
34 variable D1L: integer range -2147483647 TO 2147483647;
35 variable D2H: integer range -2147483647 TO 2147483647;
36 variable D2L: integer range -2147483647 TO 2147483647;
37
38 begin
39 -- vamos calculando los distintos coeficientes por V
40 -- A1 = A11*V+A12
41
42 if (rising_edge(clk)) then
43
44 D1H:= (D1/65536);
45 D1L:= (D1-D1H*65536);
46 D2H:=(D2/65536);
47 D2L:=(D2-D2H*65536);
48 O1<=((D1H*65536)*D2H+ (D1L*D2H)+(D1H*D2L)+(((D1L/2)*(D2L/2))/16384));
49
50 end if;
51
```

```
52 end process;
53
54 end ;
```

D.5 The Codes Sumafin block

This section covers the codes for the sumafin block shown of the figure 6-12.

```
1  library ieee;
2  use ieee.std_logic_1164.all;
3  use IEEE.numeric_std.ALL;
4
5  entity sumafin is
6
7
8
9  port
10 (
11 -- Input ports
12 clk : in  std_logic;
13
14 D1  : in    integer range -2147483647 TO 2147483647;
15 D2  : in    integer range -2147483647 TO 2147483647;
16 D3  : in    integer range -2147483647 TO 2147483647;
17 D4  : in    integer range -2147483647 TO 2147483647;
18 -- Output ports
19 O1              : out integer range -2147483647 TO 2147483647
20
21
22 );
23 end sumafin;
24
25 -- Library Clause(s) (optional)
26 -- Use Clause(s) (optional)
```

```
27
28 architecture SIMPLE of sumafin is
29
30
31 begin
32
33 process(clk)
34
35 begin
36
37 if (rising_edge(clk)) then
38
39
40 O1≤D1+D2+D3+D4;
41
42 end if;
43
44 end process;
45
46 end ;
```

D.6 The Codes Vectorespos block

This section covers the codes for the Vectorespos block shown of the figure 6-12.

```
1 library ieee;
2 use ieee.std_logic_1164.all;
3 use IEEE.numeric_std.ALL;
4
5 entity VECTORESpos is
6
7 port
8 (
9 -- Input ports
```

```
10 clk : in  std_logic;
11 volt    : in  integer;
12
13 A11 : in    integer range -2147483647 TO 2147483647;
14 A12 : in  integer range -2147483647 TO 2147483647;
15 A21 : in    integer range -2147483647 TO 2147483647;
16 A22 : in  integer range -2147483647 TO 2147483647;
17 A31 : in    integer range -2147483647 TO 2147483647;
18 A32 : in  integer range -2147483647 TO 2147483647;
19 A41 : in    integer range -2147483647 TO 2147483647;
20 A42 : in  integer range -2147483647 TO 2147483647;
21
22 -- Output ports
23 h1              : out integer;
24 h2              : out integer;
25 h3              : out integer;
26 h4              : out integer
27
28
29 );
30 end VECTORESpos;
31
32 -- Library Clause(s) (optional)
33 -- Use Clause(s) (optional)
34
35 architecture first of VECTORESpos is
36
37
38 begin
39
40 process(clk)
41
42 variable A1H: integer range -2147483647 TO 2147483647;
43 variable A1L: integer range -2147483647 TO 2147483647;
44 variable A2H: integer range -2147483647 TO 2147483647;
45 variable A2L: integer range -2147483647 TO 2147483647;
```

```
46 variable A3H: integer range -2147483647 TO 2147483647;
47 variable A3L: integer range -2147483647 TO 2147483647;
48 variable A4H: integer range -2147483647 TO 2147483647;
49 variable A4L: integer range -2147483647 TO 2147483647;
50
51 variable VH: integer;
52 variable VL: integer;
53
54 begin
55 -- vamos calculando los distintos coeficientes por V
56 -- A1 = A11*V+A12
57
58 if (rising_edge(clk)) then
59
60 A1H:= (A11/65536);
61 A1L:= (A11-A1H*65536);
62 VH:=(volt/65536);
63 VL:=(volt-VH*65536);
64 h1<=((A1H*65536)*VH+ (A1L*VH)+(A1H*VL)+(((A1L/2)*(VL/2))/16384))+A12;
65
66 -- A2 = A21*V+A22
67
68 A2H:= (A21/65536);
69 A2L:=(A21-A2H*65536);
70 h2<=(A2H*65536)*VH+(A2L*VH)+(A2H*VL)+(((A2L/2)*(VL/2))/16384)+A22;
71
72 -- A3 = A31*V+A32
73 A3H:= (A31/65536);
74 A3L:= (A31-A3H*65536);
75 h3<=((A3H*65536)*VH+(A3L*VH)+(A3H*VL)+(((A3L/2)*(VL/2))/16384))+A32;
76
77 -- A4 = A41*V+A42
78
79 A4H:= (A41/65536);
80 A4L:= (A41-A4H*65536);
81 h4<=(A4H*65536)*VH+(A4L*VH)+(A4H*VL)+(((A4L/2)*(VL/2))/16384)+A42;
```

```
82
83  end if;
84
85  end process;
86  end ;
```

Appendix E

Publications

Contents

E.1 The list of publications 269

This appendix illustrates the list of publications done during the PhD project.

E.1 The list of publications

The publications related to this work:

1. Conference proceedings:

    1. Evode, R. W. A. M. U. R. A. N. G. W. A. (2019, August). High Voltage DC Measurement Through Low-pass Filter Ripples Detection in Parallel Resonant Converters With no-Inductor at Output. In 2019 IEEE PES/IAS PowerAfrica (pp. 379-384). IEEE.

2. Journals:

    1. Rwamurangwa, E., and Mugisha, P. O. (2017). Approach on High Electric Fields for remedying the Micro-organisms attack on Crops. Agricultural Research and Technology, 10 (3).

2. Rwamurangwa, E., González, J. D., Villegas Saiz, P. J., Martín-Ramos, J. A., and Pernía, A. M. (2022). A Parallel Resonant Converter Polynomial Model Implemented in a Digital Signal Controller. Electronics, 11(7), 1085.

The Publications related to the Academic Stay of this work:

1. Conference proceedings:

    1. Evode, R. (2021, October). Modeling of Electric Grid Behaviors having Electric Vehicle charging stations with G2V and V2G Possibilities. In 2021 International Conference on Electrical, Computer, Communications and Mechatronics Engineering (ICECCME) (pp. 1-5). IEEE.

The mentioned publications are enclosed in this work on the pages below.

Agricultural Research & Technology
Open Access Journal
ISSN: 2471-6774

Juniper Publishers
key to the Researchers

Research Article
Volume 10 Issue 3 - August 2017
DOI: 10.19080/ARTOAJ.2017.10.555786

Agri Res & Tech: Open Access J
Copyright © All rights are reserved by Rwamurangwa E

Approach on High Electric Fields for Remedying the Micro-Organisms Attack on Crops

Rwamurangwa E[1]* and Mugisha PO[2]

1Department of Electrical, Electronics and Computer, University of Oviedo, Spain

2Department of Quality, Africa Improved Foods, Rwanda

Submission: June 12, 2017; **Published:** August 24, 2017

***Corresponding author :** Rwamurangwa E, Department of Electrical, Electronics and Computer, University of Oviedo, Spain, Email: ing.rw.evode@gmail.com

Abstract

Mostly, electrical related parameters are capitally understood in energy and industrial like sectors; as a major issue specifically to find out how the sustainable and safe source of energy can be found. However, this battle is not only ending in finding out how to safeguard the energy need, but also touching the agricultural part; where electricity can be one of the tools used for a reliable post-havest handling. The paper in place will tackle the approach to use High Electric Field (HEF) to inhibit the growth of crop's harmful micro-organisms. It will look into the technical approach to design the electrical system, as well as its effective way of use to different storage systems. The Molds and aspyragellus will be the targeted micro-organism, and the crop of our focus will be Maize (Zea Mais) to avoid increase in aflatoxin.

Abbreviations: HEF: High Electric Field; PEF: Pulsed Electric Fields; ZVS: Zero-voltage Switching

Introduction

Cereals, maize especially, are capital source of carbohy-drates; They are one of the major stable crops consumed worldwide. Maize is used in various forms for home con-sumptions and animal feed. They make a bigger part of the raw material in food industries, and major part of export resources for many countries around the globe. Due, crops have to be critically controlled to meet the international standards. Mycotoxin development in many stored cereal grain has constantly affected the grains quality; the major source of the contamination for stored grains is the fungi: *Aspergillus flavus* and *Aspergillus parasiticus*; as they produce aflatoxin. The last is a kind of toxin, its levels on production was found to do not exceed an acceptable level limit of 50ppb stipulated in most export specifications [1]. Aflatoxin is mostly affecting maize and peanuts, it is a group of chemicals similar toxic fungal metabolites (mycotoxins) not affected by heat [2], and is the major source of Aflatoxicoses in humans and animals, and liver cancer among humans. It has been more prevalent in areas where maize constitutes a major part of the diet. Due, the researchers have been focused on identifying causal factors and formulating effective preventive and control measures against aflatoxin [1]. As it was previously shown, the aflatoxin is due to the growth of the fungi: *Aspergillus flavus* and *Aspergillus parasiticus*, as well as the molds. The paper in place will discuss the approach to inhibit the growth of the fungi: *Aspergillus flavus* and *Aspergillus parasiticus* using HEF. Most of the investigations into the bactericidal action of electric fields have been carried out at radio frequencies. In 1949 BURTON reviewed the literature, in which there are accounts both for and against the existance of bactrerial effects [3]. The HEF show some uncertainty concerning heat-ing effects, but non-thermal bactericidal effect occurs if high enough field is applied. The electric field generally can be used either Continuous or Pulsed. The working range of reported used field up to now is 2-50kV =cm [3,4]. The Pulsed electric fields (PEF) is as well a non-thermal method of food conservation that uses short pulses of electricity for microbial inactivation and causes minimal detrimental effect on food quality attributes [4]. The electric field technology mostly PEF shows higher improvement on superiority compared to the traditional methods using thermal processing; as it shows good impact in avoiding or drastically reducing detrimental changes in tastes and physical properties of foods. The main objective of PEF is to provide high-quality foods to consumers.

The PEF technology presents advantageous in comparison to: heat treatments, as it kills mirco-organisms without affecting the ariginal color, flavor, texture and nutritional value of the unprocessed food [4]. PEF in terms of High voltage is suitable to various medium of treatment, as it can be applied to liquids, semi-solid and solid foods between to electrified electrodes, here for instance there are: microbial inactivation in milk and milk products, egg products, juice and several liquid foods. This technology seems to be the most promising non-thermal method for food microbial inactivation; it is counted in the chosen range due to the type of microbes to inactivate. Due, the field intensity and the duration of the pulse can be chosen. In relation to PEF as a promissing non-thermal technology, several technologies were developed, for instance: oscillating magnetic fields, high hydrostatic pressure, light pulses, antimicrobials and bacteriocins [5].

This paper will illustrate the use of electricity as a remedy for post-harvesting, implementing the Electric field as a tool. The suitable prototype for the power supply, electric field generation and control will be tackled. And the general application of the whole system will be illustrated.

Electricity and micro-organisms

Electrical stimulation has been used as a modality for many years for wound healing. Due, one of the mechanisms proposed for why it works is that electrical stimulation is believed to be bacteria static [6]. In medicine, most of the cases of wound healing are really difficult to manage, for instance the wounds due to the diabetes. Several therapies were tried and failed. However, many papers point to the use of electrical stimulation across wound to accelerate healing. Some papers show wound healing with DC micro-current while others show only healing with AC currents [6]. Not only in medecine but also in food processing, where Electric fields and currents have been shown to be capable of desinfecting drinking water and reducing the numbers of bacteria and yeast in food. unfortunately, little research has been conducted regarding the effectiveness of electric fields and currents in the inactivation of viruses. Electric fields are themselves harmful to cells. It has been shown that this is primarily due to the irreversible permeablization of the cell membrane [7].

Fungi make an important group of micro-organisms, due to their positive biochemical abilities as starter cultures in biotechnology to positively modify food characteristics and stability; at the same time play an important role in the development of the products with economical importance. On the other hand, they contribute strongly on the spoilage of food and cause a serious economic issue, therefore the fungi control is drastically important. The use of electric field for microbial inactivation has received much attention in microbiology; Pulsed Electric Field (PEF), as food preservation method, has proved to inactivate the spoilage micro-organisms and pathogens [8]. The PEF application is based on switching for a short duration on HEF to food product, which is placed between the two electrodes. The process succeeds only due to status of the cells morphology and physiology properties, the fluid medium properties, the type and characteristics of the used electric wave-form. From the discussions above, the research have touched almost all of the corners of microbes, as well as the way they are affected by HEF; the same way are the fungi source of aflatoxin.

Principles of electric fields

In order to have a better understanding of the High Electric Field, the attempt to review some basic electrostatic principles; among them, the Electric Field, is the capital point of the research in case. The electric field concept arose in an effort to explain action-at-a-distance forces. All charged objects create an electric field that extends outward into the space that surrounds it. The charge alters that space, causing any other charged object that enters the space to be affected by this field. The strength of the Electric Field is dependent upon how charged the object creating the field is and upon the distance of separation from the charged object.

$$E = \frac{F}{Q} \quad (1)$$

From the eq.1, E being the electric field, F being the electrostatic force and Q being the electric charge. The electric field is a vector quantity with force and direction for which units are Newtons per coulombs or volts per meter; thus defines the electric field. When we move one coulomb of charge from one point to another in an electric field, we do a work on that charge, due the electric potential.

$$V_a - V_b = \int_a^b E.ds \quad (2)$$

Volt can be also considered as the amount of work it takes to move one coulomb of charge a certain distance through an electric field E. This impliedly leads to capacitance; a capacitor is considered as two conductors separated by an insulator; the following illustrates its clear definition. The capacitance C of a capacitor is the ratio of the magnitude of the charge Q on two bodies to the potential difference between the bodies [9].

$$C = \frac{Q}{V} \quad (3)$$

With C in Farads, Q in Coulombs, V in Volts, and the energy stored in a capacitor is as follow:

$$W(work) = \frac{CV^2}{2} \quad (4)$$

From the Eq.2, let the distance from a to b be called d and Va, Vb = V , the the Eq.2 will become as follow:

$$V = E.d \quad (5)$$

Considering the Eq.5, the applied DC voltage to certain parallel plates forms a proportional electric field on a fixed distance between the plates. The DC voltage applied here will work as a control parameter. It is with that voltage, that the

How to cite this article: Rwamurangwa E, Mugisha PO.Approach on High Electric Fields for Remedying the Micro-Organisms Attack on Crops. Agri Res & Tech: Open Access J. 2017; 10(3): 555786. DOI: 10.19080/ARTOAJ.2017.10.555786.

pulsating signal is generated. To insure the right amount of electric field applied, the applied voltage has to be consistently monitored. Here the accurate design of the high voltage DC measuring circuit is implicated. Therefore, the facilitating parameter will be the electrostatic force illustrated in Eq.1. Considering the equations Eq.4, the energy stored in the formed capacitor between the two electrodes is illustrated. The changes that can occur in the energy are showed in Eq.6.

$$dW = \frac{1}{2}v^2 dc = FdX \quad (6)$$

If we consider X to be the spacing between the electrodes or plates. Due, the force will be as

$$F = \frac{1}{2}V^2 \frac{dc}{dX} \quad (7)$$

$$C = \frac{A\varepsilon}{X} \quad (8)$$

$$\frac{dc}{dX} = -\frac{A\varepsilon}{X^2} \quad (9)$$

From the equations Eq.8 and Eq.9, the force F can be found

$$F = -\frac{1}{2}A\varepsilon\frac{V^2}{X^2} \quad (10)$$

From the equation Eq.10, the force is proportional to the square of the potential difference. Due, the potential difference can be monitored through monitoring the force. As the voltage from the sending end will be kept varying to identify the suitable field, based on the application, its values will be continuously monitored through the force measuring. The rest of the work will be to find a way of safe and high voltage application, with the optimum energy density.

Approach to the Prototype Design

In order to achieve reliable results of the research in place, the High Electric Field is needed, this implies High voltage DC. The last as far as energy density and safety are concerned, the design is needed. An adaptive and flexible voltage source is required. To make such flexibility, the source of power will have to be controlled. Reminding back here that the control parameter the field needs is voltage. Due, the voltage in turn has to be controlled and adapted to that high flexibility. The maximum energy density is achieved by tremendously reducing the equipment size without reducing the power capability. The system safety is reached by isolating different steps of the equipment. The three requirements above are achieved by using resonant converters; as they provide flexibility to work at high frquencies, with controllable switching losses and high conversion gain.

The resonant converters are made of voltage source (mostly DC), controlled inverter, resonant tank, transformer, full-wave rectifier, and the load. The resonant tank can be either parallel or series, and each of the structures has its own advantages and drawbacks [10]. As the resonant tank has dynamic behavior based variability of the frequency; the last can even help in reducing the components to use in the building the prototype. The components of the resonant tank can be found considering the parasitics of the transformer. Hence, the total size decreases, and energy density increases. The switching losses can be controlled in Zero-voltage switching (ZVS) mode of functionality [10]. From the Figure 1, the power supply circuit is illustrated; together with Ls and Cp the transformer parasitic. The architecture in Figure 1 fulfill the advantageous configuration discussed in [11,12]. The proper modulation for switching of the controlled inverter, the range of frequencies to be used and the whole analysis behind will be following the discussions in [11]. Hence the controlled high voltage DC is generated. The prototype is safe, as the power source and the output end are on different grounds, the transformer makes a nice isolation. The power density is achieved, as longer as the switching frequency is high, the size of the components will be smaller at higher voltage. Following the Eq.5, the conducting probes will be connected to positive and negative terminal respectively, the distance d between this made fixed, the required voltage is applied, hence the Electric Field, the last is high following the amplitude of the generating voltage. From the discussions above, the prototype will be build specifically following the fungi: *Aspergillus flavus* and *Aspergillus parasiticus* condition of growth, in order to be able to destroy it in maize crops.

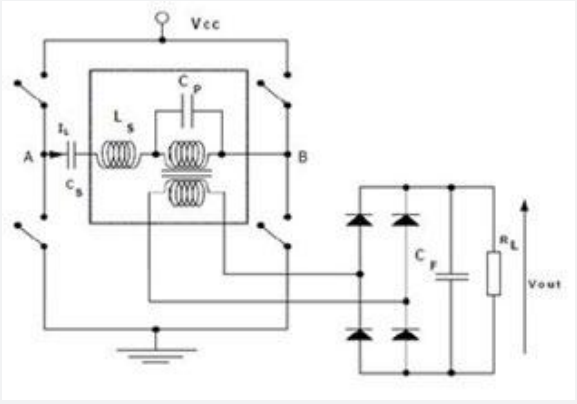

Figure 1: The model of the PRC including all the parasitic component of the step up transformer.

Principles of Application

Micro-organisms are inactivated when they are exposed to factors that substantially alter their cell structure or physiological functionality. Cell functions are altered when the membrane of selectivity is disablaed [13]. Membrane structural or functional damage is generally accepted as the cause of cell death during exposure to High-voltage Electric Field. The best way of exposing the micro-organisms to the High-voltage Electric Field depend on the application in place. Generally, the flexible electric field will be generated, at the required intensity, then it will be aimed

How to cite this article: Rwamurangwa E, Mugisha PO.Approach on High Electric Fields for Remedying the Micro-Organisms Attack on Crops. Agri Res & Tech: Open Access J. 2017; 10(3): 555786. DOI: 10.19080/ARTOAJ.2017.10.555786.

to the micro-organisms environment. Here we can state two among the possible environment: Static storages and Dynamic flow of material (Figure 2).

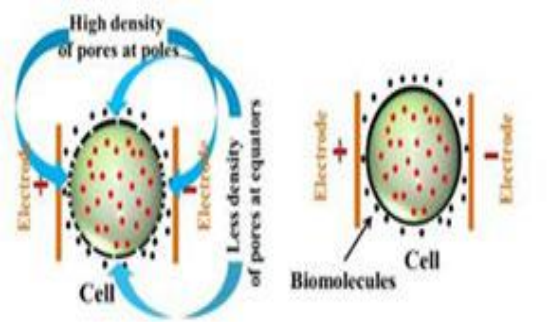

Figure 2: Attack of Electric field to Cell Membrane.

Static storage exposure

This is the in-process storage where the material can take hours kept, and there is high chance of micro biological growth and contamination. This environment can be a silo or a bin. The material inside will be exposed to a suitable electric field intensity. The material in the static state, and exposed to specific electric field intensity, then the existing micro-organisms will die and no new ones will be able to grow. From the Figure 3, the two charged electrodes are place on both sides of the stored material, and the field lines will be going through the storage.

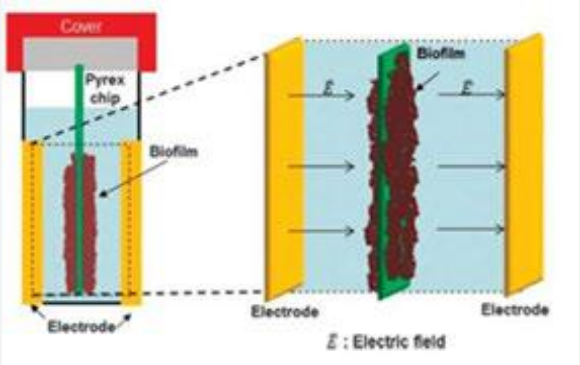

Figure 3: Illustrations of the static storage exposure.

Dynamic flow of material

On the other hand, the material can be in movement instead, and can get contaminated in that route. This is the case when product is under process; in the last, the decontaminants can be applied in process line. The points will be chosen in different routes, on which the electric field will be applied. From the determined using the immune chemical methods (Figure 3) [14]. This will help to ascertain the Pulsed Electric Field on the levels of aflatoxin in maize grains during storage.

Conclusion

In conclusion, the issues of the aflatoxin due, to the growth of the fungi: *Aspergillus flavus* and *Aspergillus parasiticus*; which is the great attack to the maize harvest and a capital handicap of the economy has been discussed. The use of electric Field either pulsed or continuous at high intensity was proposed, and considered as promising technology, taking into account different and possible applications. From different discussions, Electric field looks to be the best way to fight aflatoxin. The only remaining part is to find a suitable, safe and generic way of application, which is the way forward. Figure 4, the treatment chamber can be created at the end of each product rout.

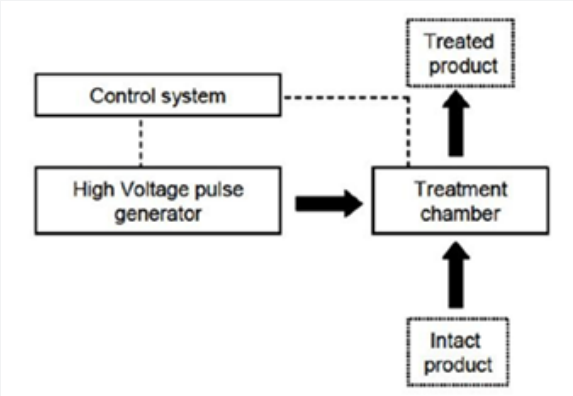

Figure 4: The illustration of the Dynamic flow of material.

Effect of PEF on microorganisms

Molds are fungi whose growth is favored by production of hyphae responsible for colonizing the grain [15]. To determine the effect of PEF on mold growth, the levels of micro-organism in maize before application of PEF needs to be determined. The mold levels can then be determined after the application of PEF. The enumeration of molds can be done following the method according to general guidance for enumeration of yeasts and molds [16]. Till today no clear mechanism is available to explain the inactivation for the exposed biological cells to Pulsed Electric Fields. The micro organisms inactivation by PEF is multi-step process which may cause cell death through multi-mechanisms, the four stages are considered:

A. Increase in trans membrane potential due to charging the cell plasma membrane by external electric field applied.

B. Pore initiation stage.

C. Evolution of the pore population during an electric treatment and

D. Post-treatment stage (pore resealing, cell death) [8]. Primarily, the effects of PEF on microbial cells depend on the pulse amplitude and cell size and including structural fatigue due to induced membrane potential and mechanical stress [17-19]. The whole duration for this is in the range of nanoseconds to milliseconds, on all type of micro-organisms; either spherical, spheroidal, ellipsoidal, cylindrical or the cell with irregular form. Since the molds are the main producers of aflatoxin, the levels of total aflatoxin can be monitored before the application of PEF and later.

How to cite this article: Rwamurangwa E, Mugisha PO.Approach on High Electric Fields for Remedying the Micro-Organisms Attack on Crops. Agri Res & Tech: Open Access J. 2017; 10(3): 555786. DOI: 10.19080/ARTOAJ.2017.10.555786.

References

1. Mycotoxin prevention and control in foodgrains.
2. Richard L (2013) Aflotoxins.
3. Sale A, Hamilton W (1967) Effects of high electric fields on micro organisms: I. killing of bacteria and yeasts. Biochimica et Biophysica Acta (BBA)-General Subjects 148(3): 781-788.
4. Mohamed ME, Ayman H, Eissa A (2012) Pulsed electric fields for food processing technology. In: Eissa AA (Ed.), INTECH Open Access Publisher, Croatia.
5. Zhong K, Chen F, Wu J, Wang Z, Liao X, et al. (2005) Kinetics of inactivation of escherichia coli in carrot juice by pulsed electric field. Journal of food process engineering 28(6): 595-609.
6. Petrofsky J, Laymon M, Chung W, Collins K, Yang TN (2008) Effect of electrical stimulation on bacterial growth. J Orthop Neurolsurg 31: 43.
7. Drees KP, Abbaszadegan M, Maier RM (2003) Comparative electrochemical inactivation of bacteria and bacteriophage. Water research 37(10): 2291-2300.
8. Stoica M, Bahrim G, Carac G Factors that influence the electric field effects on fungal cells. Science against microbial pathogens: communicating current research and technological advances pp. 291-302.
9. Vosteen WE (1984) A review of current electrostatic measurement techniques and their limitations. In Electrical Overstress Exposition pp. 24-26.
10. Choi H, Team PC (2007) Design considerations for an llc resonant converter. In Fairchild Power Seminar pp. 82-83.
11. Rwamurangwa E (2015) High voltage measuring circuits in ac/dc converters for e-beam welding machines.
12. Biela J, Kolar JW (2005) Using transformer parasitics for resonant converters-a review of the calculation of the stray capacitance of transformers, in Industry Applications Conference, 2005. Fourtieth IAS Annual Meeting Conference Record of the IEEE, China 3: 1868-1875.
13. Lado BH, Yousef AE (2002) Alternative food-preservation technologies: efficacy and mechanisms. Microbes and Infection 4(4): 433-440.
14. Wacoo AP, Wendiro D, Vuzi PC, Hawumba JF (2014) Methods for detection of aflatoxins in agricultural food crops. Journal of Applied Chemistry 2014.
15. Stack JP (2000) Grain molds and mycotoxins in corn. Cooperative Extension, Institute of Agriculture and Natural Resources, University of Nebraska-Lincoln, USA.
16. Bird P, Flannery J, Crowley E, Agin J, Goins D, et al. (2015) Evaluation of the 3mâ¢ petrifilmâ¢ rapid yeast and mold count plate for the enumeration of yeast and mold in food: Collaborative study, first action 2014.05. Journal of AOAC International 98(3): 767-783.
17. Min S, Evrendilek GA, Zhang HQ (2007) Pulsed electric fields: processing system, microbial and enzyme inhibition, and shelf life extension of foods. IEEE Transactions on Plasma Science 35(1): 59-73.
18. Santra TS, Tseng FG (2013) Recent trends on micro/nanofluidic single cell electroporation. Micromachines 4(3): 333-356.
19. Kim YW, Subramanian S, Gerasopoulos K, Ben-Yoav H, Wu HC, et al. (2015) Effect of electrical energy on the efficacy of biofilm treatment using the bioelectric effect. Npj Biofilms and Microbiomes 1: 15016.

This work is licensed under Creative Commons Attribution 4.0 License
DOI: 10.19080/ARTOAJ.2017.10.555786

Your next submission with Juniper Publishers will reach you the below assets

- Quality Editorial service
- Swift Peer Review
- Reprints availability
- E-prints Service
- Manuscript Podcast for convenient understanding
- Global attainment for your research
- Manuscript accessibility in different formats

(Pdf, E-pub, Full Text, Audio)

- Unceasing customer service

Track the below URL for one-step submission
https://juniperpublishers.com/online-submission.php

How to cite this article: Rwamurangwa E, Mugisha PO.Approach on High Electric Fields for Remedying the Micro-Organisms Attack on Crops. Agri Res & Tech: Open Access J. 2017; 10(3): 555786. DOI: 10.19080/ARTOAJ.2017.10.555786.

High Voltage DC Measurement Through Low-pass Filter Ripples Detection in Parallel Resonant Converters With no-Inductor at Output

RWAMURANGWA Evode
Department Technology
Africa Improved Foods
Kigali, Rwanda
evode.rwamurangwa@africaimprovedfoods.com
ing.rw.evode@gmail.com

***Abstract*—The parallel resonant converter with an uncontrolled end rectifier, with no inductor at the output, has a low-pass filter for ripple reduction. The ripples in this case has been a serious challenge and various researches were conducted to minimize it. However much the ripples are reduced, they have not been fully removed. Being a drawback, however this paper will use it in another sense, like an advantage of measuring the High Voltage DC (HVDC). In this paper, the Parallel Resonant Converter (PRC) will be discussed, with the HVDC output having different levels based on variation in switching frequencies and duties. The measurement of HVDC has been a challenge in different researches. The proposal of measuring the output DC voltage through ripples detection will be developed and the comparative method as an approving method will be proposed.**

***Index Terms*—Duty, High voltage DC (HVDC), Low Pass Filter, Parallel Resonant Converter(PRC), Ripples, Switching Frequency.**

I. Introduction

Nowadays, due to the development of power electronics and computing; different researches that attempt to propose various options on problems that are being faced when using different systems are being executed. Different systems, like welding machines, high-power converters for x-ray generators etc, use high voltage DC. Mostly the required DC voltage is generated from low voltage that is boosted through converters. Various converters used are mostly grouped in DC-DC, AC-DC, DC-AC and AC-AC. The converters have advantages, disadvantages and different capabilities. In the sense to produce High Voltage DC (in Range of Kilovoltages) from Low Voltage DC (in range of Voltages); the parallel resonant converters (PRC) were preferred in this work. That choice was due to the fact that: it integrates the transformer parasitics as system components of the power topology, it reflects the possibility of Zero-voltage and Zero-current Switching (ZVS and ZCS). In addition, it has the flexibility in varying the frequency and the duty for the targeted power transfer, it is flexible in varying the output voltage; hence, the variation in power transfer, it has the quality of tracking ZVS and ZCS at each variation of switching frequency and duty and it covers a wide range of applications in HVDC equipments. In figure 1, the topology of

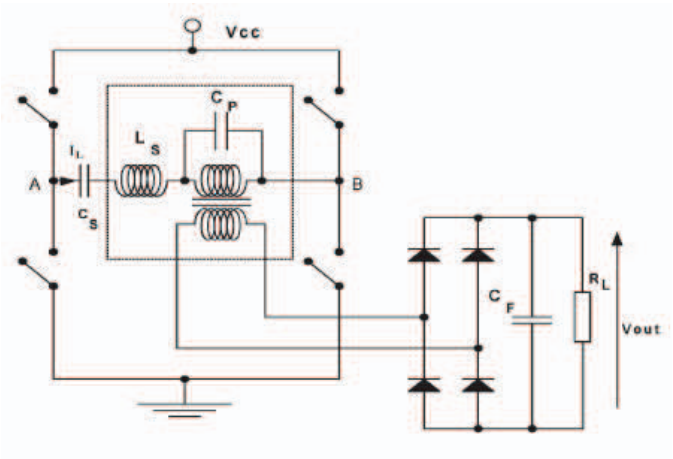

Fig. 1. PRC Topology Without Inductor at the output [1].

the PRC with single-capacitor output filter (without inductor at the output) is illustrated. The mentioned topology itself, it is of high voltage application. The last means that, the input voltage will be low voltage DC, that will be converted into High voltage DC output.

The topology comprises of the controlled inverter, a resonant tank, a step-up transformer, an uncontrolled rectifier and low pass filter. The resonant tank, as a major part of this research, is made of the inductor L_s and the capacitor C_p. Being that the system in place is suggested to work on high frequencies; it was thought to be effective if the resonant tank components are retrieved from the transformer itself instead of additional components. In analysing the transformer, L_s will be replaced by the leakage inductance.The present work aims at operating high voltages, that implies high transformer ratio, due a big number of turns at the secondary of the transformer.

Having that in place, a secondary capacitor (C_p) (parasitic) will appear [1]. The resonant tank is already in place; therefore, it will require to be managed in order to getting a

978-1-7281-1010-3/19/$31.00 © 2019 IEEE

Authorized licensed use limited to: UNIVERSIDAD DE OVIEDO. Downloaded on June 21,2022 at 11:59:28 UTC from IEEE Xplore. Restrictions apply.

varying HVDC at the output due to the changes in one of the following parameters: Input voltage, switching frequency and the switching duty, without compromising the soft switching (ZVS and ZCS). The rest of the components are of various purposes. C_s is not part of the resonant tank, and it is just to filter the DC component of the inverter output. V_{cc}: is the input voltage (DC). C_F and R_L are part of Low pass filter at the output. C_F is a very big capacitor, in the range of ten time the resonant tank capacitor C_p. Having that approach in place, It can be re-called here that before we are able to design the prototype, some of the parameters have to be pre-set. Before starting the design, the following parameters will be set in place: the range of input voltages V_{inmin} and V_{inmax}, output voltages V_{outmin} and V_{outmax}, output power P_{outmin} and P_{outmax}. The next step is to identify the leading parameters, being the switching frequency and the duty; mostly the switching frequency is set to its maximum required value for ease of calculations. Thus, the maximum frequency f_{max} is set together with the duty $d = [0 - 0.5]$, the variation of both respectively which causes the variation of the output voltage and power of the whole converter; without compromising the ZCS and ZVS. From the discussed set points, the prototype will be designed and simulated using Matlab, MathCad and Psim.

II. PRC DESIGN AND HVDC OUTPUT GENERATION

The design in case presents some characteristics: a wide range of variations in the output voltage (in range of Kilovolts) and output power (in the range of Kilowats) [2]. Normally the PRC appears to be a good idea to cope with the resonant net [3]. From the last, the idea described in [1] and [2], series resonant converter (SRC) are commonly used with some modification, due to their better characteristics [4]- [5], although it presents several drawbacks. The SRC itself present the difficulties in changing its output voltage near no-load conditions; it does not cope with the transformer parasitic capacitance, and the output voltage can not be higher than the input voltage without the transformer [2]. As one of the solutions, a parallel resonant converter (PRC) topology was suggested. With C_s and LC filter at the output, it has seemed to be fulfilling the PRC and SRC described in [6]. From the comparison, it was concluded that the PRC with DC component limiting capacitor C_s can combine both the best behaviour of SRC under short-circuit condition and the PRC at no-load, due, the capability to operate with a wide ranges of output voltage and output power [2]. Apart from that, the output inductor is left aside. Actually the PRC used in low output voltage applications have the LC output filter. However, if it goes to high output voltage applications this inductor becomes too large and too expensive component, comparable in size with a high voltage transformer [9]. Fortunately, it was possible to remove it without affecting the performance of the converter [10], [11] and [12]. Based on this, only the low-pass filter capacitor will be at the output (Fig.1). The frequency and duty together were considered as a control parameters [7]- [8]. From the last descriptions, the best variables were illustrated, for the best of trying the DC output measurements. To be able to achieve the required output voltage, having in place the prototype shown in Fig.(1), the adequate switching patterns are required. Above all, in order to approach the design in clear way, some points have to be set. These will determine the designed system limitations, including: minimum and maximum input and output voltage, output power respectively, together and maximum set frequency. In addition, having the set points in place, it implies the identification of the unknowns, hence the equation to use. The last is elaborated based on Fig.2 and it relates the set input and output parameter ranges with the unknown variables. Hence the Eq.1.

$$f_{sw} = f(V_{in}, V_{out}, P_{out}, d, L_s, C_p) \tag{1}$$

The last equation (Eq.1) demonstrate the capability of a PRC to operate in the optimal set ranges, with the changes in frequencies and duty and maintaining soft switching.

A. Prototype Design approach

In approaching the design, all of the calculations will be in per unit value (pu), due, the presence of the base values in the below requirements. Here are the base values:

- $V_{cc} = V_{in}$: Input voltage (Being base voltage)
- $f_{base} = \frac{1}{2\pi\sqrt{L_s C_p}}$: Being the base frequency.
- $Z_{base} = \sqrt{\frac{L_s}{C_p}}$: Being the base impedence
- $P_{base} = \frac{V_{in}^2}{Z_{base}}$: Being the base power.
- $\omega_{base} = \frac{1}{\sqrt{L_s C_p}}$: Being base angular velocity.

Having the ranges of input and output voltages, together with the ranges of the output power and the maximum frequency; all of them being the set points. Fig.2 shows that the variation

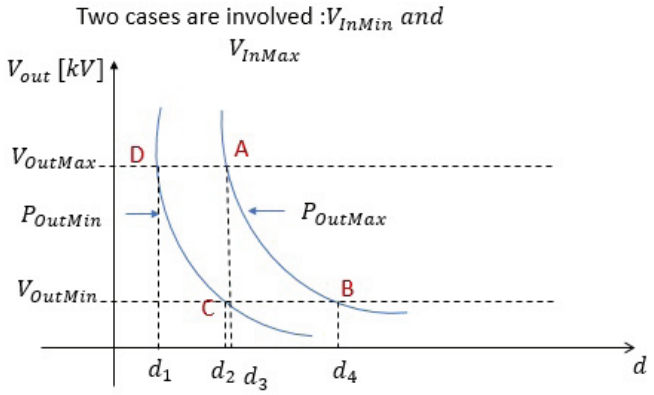

Fig. 2. Illustration of the variation of the PRC output power based on the changes in output voltage and the duty.

of the output power depends on the variation of the output voltage, and is controlled by the changes in duty and switching frequency, without compromising the ZVS and ZCS. The last point raises a question: having our set points, what are the duties and switching frequencies we have to tune to, to have the right output voltage and power without compromising ZVS and ZCS? To be able to answer that question, we refer

Authorized licensed use limited to: UNIVERSIDAD DE OVIEDO. Downloaded on June 21,2022 at 11:59:28 UTC from IEEE Xplore. Restrictions apply.

to a point where we have maximum power and maximum voltage and on that particular point we relate the maximum frequency. In Fig.2, that is point A. The same point corresponds to duty d_3, hence it is possible to calculate the resonant tank components L_s and C_p. Having the last two important points in place, the next step will be now to try different required outputs and see at which frequency and duty they are achieved. Apart from that, the right switching pattern is necessary to have the right modulation and duty.

B. Modulation techniques of the Inverter IGBTs

To achieve the right duties at right frequencies, we need to modulate in a way that we achieve the right output. Things being so, the input inverter has two arms, the first with two switches T_1 and T_2 and the second with T_3 and T_4. The power electronic switches being the IGBTs, are switched on driven square wave signals, following the sequence in Fig.4. It can be noted that the switches S_1 to S_4 shown in Fig.4 correspond to T_1 to T_4 in Fig.3 respectively. Considering the

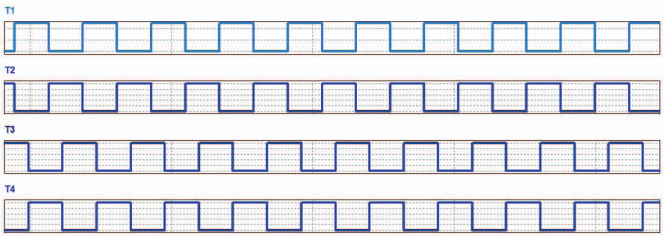

Fig. 3. Illustaration of the switching patterns on PRC to achieve ZVS and ZCS (as shwon in Fig.8), the required output Voltage and Power.

Fig.3, hence the pattern is illustrated in the period of time $T = t_0 + t_1 + t_2 + t_3$, as shown in Fig.4. Having all of

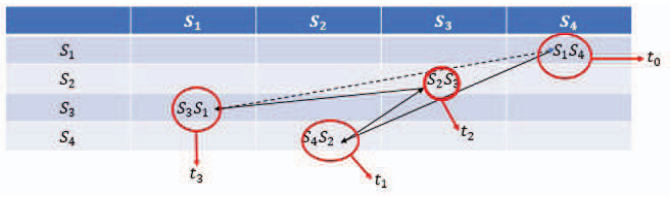

Fig. 4. Illustration of the switching in the time period T.

the methods shown in Fig.2 and the pattern described and illustrated in both Fig.3 and Fig.4, and all applied on the PRC shown in Fig.1, the high voltage DC at the output of the PRC shown in Fig.1 is obtained. As shown that voltage being high enough (in the range of Kilovolts), the next step is to try methods of measuring it.

III. HVDC Measurement Methods

Measuring High Voltage DC, mostly when it is in the range of KiloVolts, it is still a challenge; both safety of the system operators and the accuracy of the measurements. Different researches were conducted on the same case, and tried to show different outputs, that are being applied to date. However, the same researches are still ongoing to have a safe and accurate way of having HVDC measured. That is the reason why this paper tried to go in the same line, and try some techniques that can contribute in accurately and safely measuring the HVDC.

A. Previous Techniques Applied

The High voltages DC have been measured in various ways. Direct measurement of high voltage is possible up to about 200 kV, and several forms of voltmeters have been devised which can be connected directly across the test circuit. The spark-over of sphere gaps and other gaps are also used, especially in calibration of meters in high voltage measurements.

1) Direct Measurement of High Voltage: The direct methods being researched on, and being applied in various application are : Electrostatic voltmeters, Abraham voltmeter, sphare gaps, resistive potential divider, series resistence method, capacitive potential devider. All of the lastly described methods, although being used or researched on to see if they can be used, present some drawbacks: they are not safe as they share the common ground with HVDC source, and their accuracy is not reliable. Having that in mind and as far as the converters are concerned, this paper will propose a method to measure HVDC through output current and RC low pass filter.

B. HVDC measurement through ripple detection at the RC low pass filter.

From Fig.1 illustrating the PRC, the last part described in Fig.5 shows the uncontrolled rectifier, made of assumed silicon

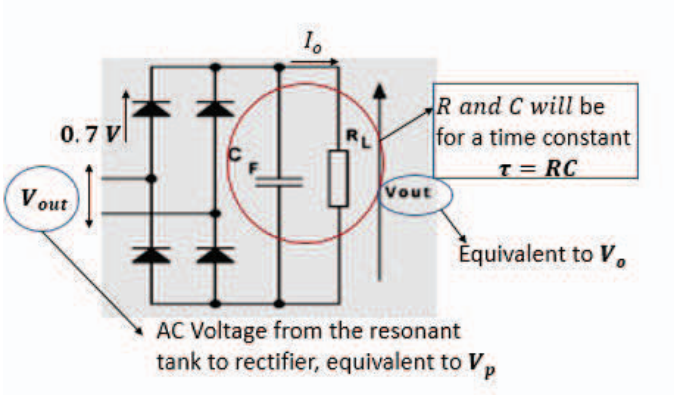

Fig. 5. Illustration of the HVDC measurement through ripple detection.

diodes of $0.7V$ each (as indicated in the Fig. 5). The output of the rectifier is made of the filter capacitor and the load resistance, both of them forming a time constant $\tau = RC$. V_{out} is the output voltage (AC) of the transformer, which is equivalent to V_p (from the output view point), T, being the period of the switching signals and of the AC voltage and current in the resonant tank. Having in place T and τ, then the ripple percentage r can be calculated.

$$r = \frac{\frac{T}{2}}{RC} \tag{2}$$

Authorized licensed use limited to: UNIVERSIDAD DE OVIEDO. Downloaded on June 21,2022 at 11:59:28 UTC from IEEE Xplore. Restrictions apply.

Considering the Eq.2, and the change of the variation of the voltage at the capacitor (charging and discharging), the percentage of ripple r can be calculated as in Eq.3.

$$r = \frac{(V_0 - V_0 e^{-\frac{\frac{T}{2}}{\tau}})}{V_0} = 1 - e^{\frac{T}{2}} \approx 1 - (1 - \frac{T}{2\tau}) = \frac{T}{2\tau} \quad (3)$$

Eq.3 illustrates the percentage of the ripples in the output DC voltage, but the same ripple corresponds to a certain voltage, which can be scaled as indicated in the Eq. 4.

$$V_r = V_0(1 - e^{-\frac{T}{2RC}}) \approx (V_p - (2 * 0.7))(1 - e^{-\frac{T}{2RC}}) \quad (4)$$

From the Eq.4, V_r will approximately results in Eq.5.

$$V_r \approx V_0 \frac{T}{2RC} \quad (5)$$

Apart from the value of the ripple voltage illustrated by the Eq.4 and Eq.5, alternatively, the ripple voltage can be given by Eq.6.

$$V_r = \frac{\frac{V_0}{R}}{2fC} = \frac{I_0}{2fC} \quad (6)$$

In combining both the Eq.4 and Eq.6 result in the eq.7.

$$V_0 = 2f\tau V_r \quad (7)$$

Having in place both Eq.6 and Eq.7, and both being directly proportional, then the high voltage DC (low current DC at the output) at the output can be measured just by measuring a small DC current at the output. This will be a solution for both the HVDC output accurate and safe measurement. The last is due to the reason that, it does not share the common ground with the output voltage, and it is a small signal in value. Therefore, the Eq.7 can be easily written in the microcontroller and with only one input, the output current I_o.

IV. Simulation and Results

The simulations and all of the required calculations were done using Matlab, MathCad, Psim and Pspice. To be able to simulate the PRC, the circuit in Fig.1 was used, as a complete representation of the PRC without inductor at the output. The purpose was to cover the following points: generating the variable output voltage, and being able to measure the same voltage in a safe way, using the ripples and output current sensing.

For the purpose of simulation, described in the introduction (I) and in reference to Fig. 2, we have put the following initial points in place:

- $V_{inmin} = 100V$
- $V_{inmax} = 200V$
- $V_{outmin} = 200V$
- $V_{outmax} = 300V$
- $P_{outmin} = 500W$
- $P_{outmax} = 1000W$
- $f_{max} = 100kHz$

The output voltage was made slightly lower in order to prove the capacity of the PRC to step up the voltage without transformer, so we ignored the transformer ratio. Following the Fig.2, the point ***A*** (of maximum voltage and maximum power), corresponds to the maximum frequency f_{max}. Hence, it is possible to calculate the resonant tank components and the duty required to achieve the output power, without compromising ZVS and ZCS. The calculation done in MathCad, gave the following resonant tank components: $L_s = 2.759 * 10^{-}5$ H and $C_p = 8.375 * 10^{-}8$ F, at the duty $d = 0.3$, with ZVS and ZCS.

The proposed measuring method for HVDC is illustrated in

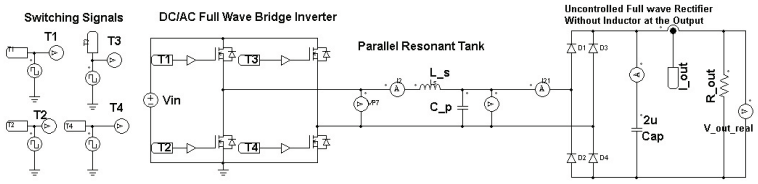

Fig. 6. Illustration of the complete circuit diagram in PSIM as is in Fig.1.

the Fig.7. The model in Fig.6 was run using the previously

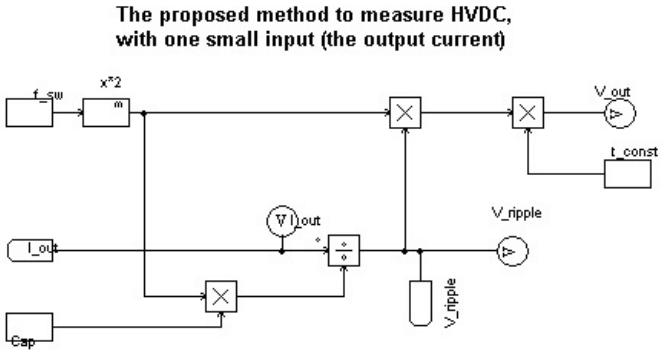

Fig. 7. The method to measure HVDC in PSIM.

shown parameters, to prove the correctness of the switching patterns and the ZVS and ZCS. From the Fig.8, we can

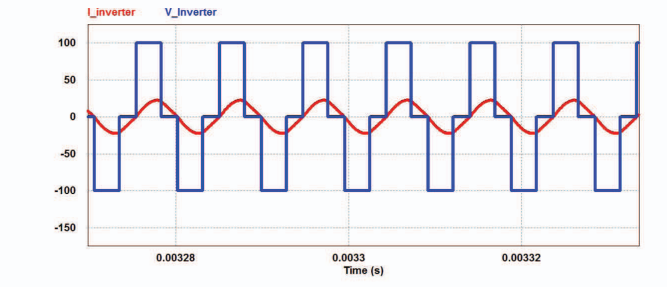

Fig. 8. The illustration of ZVS and ZCS at a frquency of 103.5 kHz and d=0.3.

conclude that, due to uncertainties in ideal calculations, to achieve the targeted power and voltage at the output, the small tune on the frequency is required. This is the reason why we have the switching frequency at $103.5kHz$. The mentioned

Authorized licensed use limited to: UNIVERSIDAD DE OVIEDO. Downloaded on June 21,2022 at 11:59:28 UTC from IEEE Xplore. Restrictions apply.

uncertainties are due to the ideal calculations that may end up missing some small points. Fig.8 illustrates as well the soft-switching and avoid losses during the commutation processes, and unnecessary heating of the power electronic switches. The voltage and current shown, are fed to the resonant tank, that will manage it, to deliver the required voltage and power to the output.

Based on the parameters given, the output DC voltage should be around $300V$, keeping the transformer ratio at unit value.

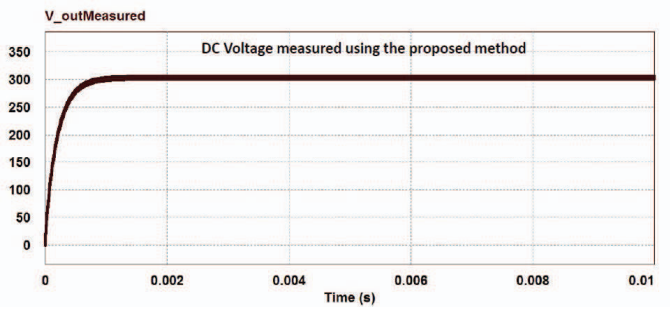

Fig. 9. The measured voltage meets the expected value ($300V$).

To prove the capacity of the parallel resonant tank to step up the voltage without having a transformer ratio; the Fig.9, illustrates that idea clearly. As from the Fig.8, the voltage was $100V$ and in Fig.9, the voltage goes up to $300V$. The PRC, as it was said, accepts a wide range of voltage at the output.

The Fig.9 shows the measured value using the proposed method. In comparing the measured voltage using the proposed method, as shown in Fig.9, and the real output voltage measured using the PSIM probes; we can have from the Fig.10 that both have the linear relationship, and they are the same at the same points. Things being so, then it is a right confirmation of the similarity of the two values. The proposed method track at each point the values of the output voltage. The method described so far, seems to have promising results and many advantages. As illustrated before, it shows the accuracy, converts the ripples (being a drawback before) in a measuring solution. It is a small and simple method as it just uses the system components (the low-pass filter components).

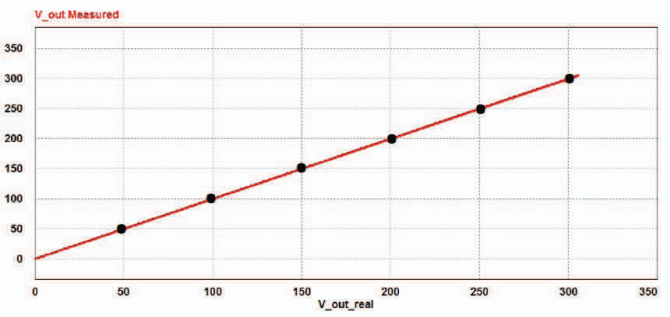

Fig. 10. Illustration of the relationship between the measured and real voltage the output.

It is safer compared to methods described in III(A.1). It is a flexible method as well, as it uses uses only one input from the system (current), and the same input being small in value. As only the current will be measured, then the method will not be sharing the same ground with the measured voltage value, therefore, it is safer. However, it is still a point of challenge to measure from the output. Even if it is clearly illustrated being on accuracy or safety point of view enough, it always much better to measure these types of high voltages from the safest possible sides. For this reason, the next step of this research is to measure the HVDC from the lower part of the system in Fig.1. This means investigating the formula that interprets the Fig.2 in another way around, and having it with the output voltage being a function of all.

$$V_{out} = f(V_{in}, d, I_{prc}, f_{sw}, L_s, C_p, P_{out}) \tag{8}$$

From the Eq.8, the PRC components, based on the principles of use of the transformer parasitics, will be re-calculated. Hence, the same graph like Fig.2 will be drawn for extended calculation references. From this second approach, the objective will be to have a method of indirectly measuring the output HVDC; this implies measuring from the resonant tank itself. Later, the final equation (equivalent to Eq.7) will be elaborated. The last will be easier to be written in the microcontroller. Hence, it will be more flexible and more safer.

V. Conclusions

The parallel resonant converter without inductor at the output demonstrated advantages, as it can allow power transfer from input to output at a wide range of voltage use. It helps in stepping up the voltage levels from input to output with unit transformer ratio. It gives a great opportunity of using transformer parasitics as system components. It helps as well in managing the power transfer from input to output by varying the switching frequency and duty. In additional and being the major purpose of this paper, the use of the output low pass filter ripples as the source of output HVDC measurement. The work in place described all of the discussed and designed points. The method of determining the HVDC at the output, by measuring the parameters of the resonant tank was proposed, and it is the next to be implemented.

References

[1] Diaz, J., Saiz, P. J. V., Martin-Ramos, J. A., Martin-Pernia, A., Martinez, J. A. (2010). A high-voltage AC/DC resonant converter based on PRC with single capacitor as an output filter. IEEE Transactions on Industry Applications, 46(6), 2134-2142.

[2] Martin-Ramos,J.A., Pernia, A. M., Diaz, J., Nuno, F., and Martinez, J. A. (2008).Power supply for a high-voltage application. IEEE Transactions on power electronics, 23(4), 1608-1619.

[3] R. L. Steigerwald, âA comparison of half-bridge resonant converter topologies,â IEEE Trans. Ind. Electron., vol. 3, no. 2, pp. 174â182, Apr.1988.

[4] V. Vlatkovic, M. J. Schutten, and R. L. Steigerwald, âAuxiliary series resonant converter: A new converter for high-voltage, high-power applications,â in Proc. APEC, 96, 1996, pp. 493â499.

[5] H. van der Broek, W. Rexhausen, B.Wagner, and N. Geerkens, âPower supply unit including a PWMinverter, notably for an X-Ray generator,â U.S. Patent 6 072 856, Jun. 2000.

Authorized licensed use limited to: UNIVERSIDAD DE OVIEDO. Downloaded on June 21,2022 at 11:59:28 UTC from IEEE Xplore. Restrictions apply.

[6] R. L. Steigerwald, âA comparison of half-bridge resonant converter topologies,â IEEE Trans. Ind. Electron., vol. 3, no.2,pp.174â182, Apr.1988.
[7] B.-H. Jeong, J.-S. Cho, H.-S. Mok, and G.-H. Choe, âA novel pulse power supply for magnetron using high voltage capacitor embedded high frequency transformer,â in Proc. APEC, 2004, pp. 1819â1824.
[8] F. S. Cavalcante and J. W. Kolar, âSmall signal model of a 5 kW high-output voltage capacitive-loaded series-parallel resonant dcâdc converter,â in Proc. PESC, 2005, pp. 1271â1277.
[9] V. GarcÃa, M. Rico, J. SebastiÃ¡n, and M. Hernando, âUsing the hybrid series parallel resonant converter with capacitive output filter and PWM phase-shifted control for high-voltage applications,â in Proc. IEEE IECON, 1994, pp. 1659â1664.
[10] SD. Johnson, A.F. Witulski and R.W. Erickson. "Comparison of Resonant Topologies in High-Voltage Dc Applications". IEEE Transactions on Aerospace and Electronic Systems. Vol. 24. nQ 3, pp. 263-274, Mayo 1988.
[11] H. Hino, T. Hatakeyama and M. Nakaoka. "Resonant PWM Inverter Linked DC-DC Converter Using Parasitic Impedances of High-Voltage Transformer and Its Applications to X-Ray Generator". IEEE-PESC, pp. 1212-1219, 1988.
[12] H. Hino, T. Hatakeyama, T. Kawase and M. Nakaoka "High-Frequency Parallel Resonant Converter for X-Ray Generator Utilizing Parasitic Circuit Constants of High Voltage-Transformer and Cables". IEEE INTELEC, pp. 20.5.1 - 20.5.8, 1990.

Authorized licensed use limited to: UNIVERSIDAD DE OVIEDO. Downloaded on June 21,2022 at 11:59:28 UTC from IEEE Xplore. Restrictions apply.

Proc. of the International Conference on Electrical, Computer, Communications and Mechatronics Engineering (ICECCME)
7-8 October 2021, Mauritius

2021 International Conference on Electrical, Computer, Communications and Mechatronics Engineering (ICECCME) | 978-1-6654-1262-9/21/$31.00 ©2021 IEEE | DOI: 10.1109/ICECCME52200.2021.9591059

Modeling of Electric Grid Behaviors having Electric Vehicle charging stations with G2V and V2G Possibilities

RWAMURANGWA Evode
Department of Electrical, Electronics and Computer
University of Oviedo
Gijon, Spain
UO241006@uniovi.es or 0000-0003-4861-0812

***Abstract*—The use of green energy has triggered researchers' attention; hence its utilization in transportation and the invention of electric vehicles(EV). They can both be load and storage system to the grid. Therefore, the integration of EVs to the grid has a capital role in grid energy management. This work proposes the grid with EV charging stations which can allow simultaneous multiple charging and bi-directionality. The charging of the vehicles from the grid (Grid-to-Vehicle (G2V)) and the vehicle sending power back to the grid (Vehicle-to-Grid (V2G)) are shown in this work. The behavior of the grid, responding to random charging and discharging of the vehicles, is illustrated. The bi-directional AC-DC converter together with DC-DC off-board charger and the related controls are shown in this work. The complete topology is simulated in Matlab-Simulink and the results are presented in this work.**

***Index Terms*—Bi-directionality, Electric Bicycle (EB), Electric Moto-bicycle (EMB), Electric Vehicle (EV), Grid-to-Vehicle (G2V),Vehicle-to-Grid (V2G), Vehicle-to-Load(V2L) and Vehicle-to-Vehicle(V2V).**

I. Introduction

The use of electric Vehicles (EV) has become a solution, not only as a green transport but also an energy storage system buffering the grid power [1]–[10]. Hence, they play a capital role in integration of intermittent renewable energy sources and grid energy management. The EVs are mostly used in personal transports. Hence, they are parked more than 20 hours each day [1]. They are the idle asset that can potentially support to store excess power(G2V) and send it back to the grid in peak hours (V2G). The EVs have been commonly known in western countries, with new grid technologies and flexibilities. However, recently the same EVs embarked the rest of the world, where the grid capabilities are still lacking alot. In some countries, the power grid can be adapted to charge the EVs, but they have not yet attained the level to accommodate the power from the EVs. The bi-directional flow of power is not yet in use, which might be the next development step to target for. Apart from the EVs, the electric bicycles (EB) and motor-bicycles (EMB) are also in use in the bigger part of the world. The use of EVs, EBs and EMBs represent dynamically increasing and complex load on the power grid. This work aims to show the behaviors of the grid having EV charging stations with bi-directional capabilities in presence of EBs and EMBs.

Special Thanks to Africa Improved Foods and Kigali Collaborative Research Center for supporting this work.

II. Power Grid structure overview

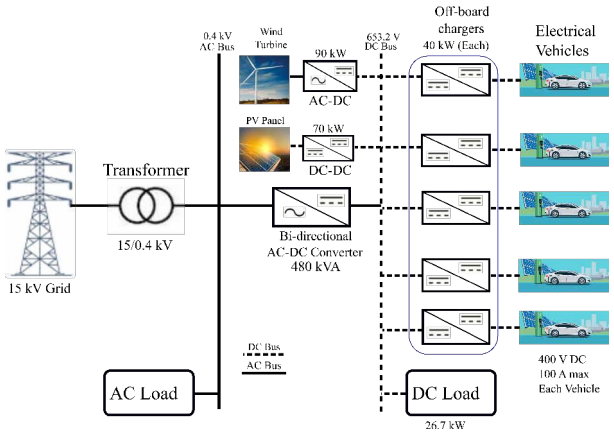

Fig. 1. Illustration of the grid incorporating EV chargers with G2V and V2G feasibility.

The EV, EB or EMB chargers are mostly installed in cities, where in most countries, the Medium voltage transmission grid are 15 kV [11]. The last is converted to low voltage of 0.4kV for distribution through a transformer. The figure 1 presents the 15 kV medium voltage grid. It supplies the DC bus through a bi-directional AC-DC converter. The wind turbine and PV panel supply the same DC bus of 653.2V. In turn, the DC bus supplies the 40kW off-board chargers for the EV charging and discharging and a 26.7 kW DC load. The DC load stands for other DC loads like EBs and EMBs. The 40kW and 100A off-board charger is chosen among the commercially available

978-1-6654-1262-9/21/$31.00 © 2021 IEEE

Authorized licensed use limited to: UNIVERSIDAD DE OVIEDO. Downloaded on June 21,2022 at 12:02:09 UTC from IEEE Xplore. Restrictions apply.

and mostly used charging stations. The indicated off-board chargers are all above level 2 in the levels defined by the Society of Automotive Engineers [1], [7]. They are Electric Vehicle Supply Equipments (EVSE) and categorized as level 3, as they can fast-charge (rated current of 100 A max) [7]. This work considers the grid in figure 1, however the PV panel and wind turbine will be left out. Hence, the study will focus on the grid behavior facing the power flow from/to EVs without PV panel and wind turbine support. Before elaborating in details the behaviors of the grid, this work will first talk about the bi-directional flow of energy, the controls involved and charging and discharging of the EV batteries. Simulink will be used as a tool to simulate and achieve the required results.

III. Simulink models and simulations

Considering the figure 1 from which the figure 2 is retrieved; It illustrates the grid supplying the EV chargers through a DC link. The figure 2 consists of a bi-directional AC-DC grid connected converter, DC link and one off-board charger from the figure 1.

A. Grid Connected Converter

It is a three phase bi-directional AC-DC and controlled converter made of IGBTs. The converter is connected to the grid through an RL choke of $1\mu\Omega$ and $500\mu H$ respectively. The choke stands for a filter to reduce harmonics. The same choke, also known as rectifier choke is reflected as L_{inv} in figure 2. The grid voltage is $400V_{rms}$ phase-to-phase, at the grid frequency of $50H_z$. In Simulink, the grid is mimicked into a three-phase voltage source of the indicated voltage and frequency respectively. It presents the source resistance R_{Source} and source inductance L_{Source} as $100m\Omega$ and $40\mu H$ respectively.

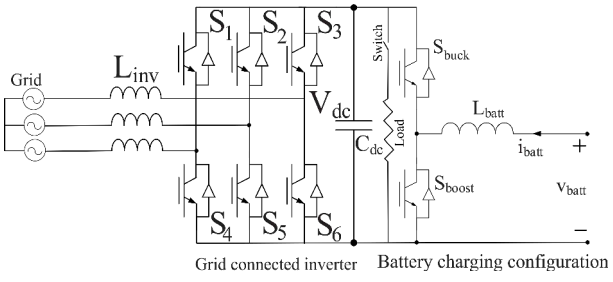

Fig. 2. Bi-directional grid connected converter

The AC-DC converter connected to the grid provides a suitable level of DC link voltage. The appropriate capacitance size is chosen for ripple suppression at optimal level. The expected DC link voltage is retrieved from the grid voltage through the equation 1.

$$V_{dc} = \frac{2\sqrt{2}}{\sqrt{3}} V_{LLrms} \tag{1}$$

With V_{LLrms} being the phase-to-phase rms grid voltage. The DC link voltage control is capital to make the DC link stable. The decoupled $dq0$ control method is applied. It is a cascaded control that consists of outer voltage and inner current loop. The grid voltage and current are captured through voltage and current sensors respectively. On the last, the abc to $\alpha\beta0$, abc to $dq0$ or $\alpha\beta0$ to $dq0$ are performed. The phase locked loop (PLL) is applied to determine the satisfactory synchronous angle ωt. The d-axis outer loop controls the DC bus voltage, while the inner loop controls the active AC current [7]. In case of bi-directional applications, the changes in DC bus voltage are influenced by positive or negative current due to power flow direction. The q-axis outer loop adjusts AC voltage magnitude by regulating the reactive current through the q-axis inner loop control. The decoupling term ωL and the feed-forward voltage signal are added for transient performance improvements. The fore-discussed transformations and PLL

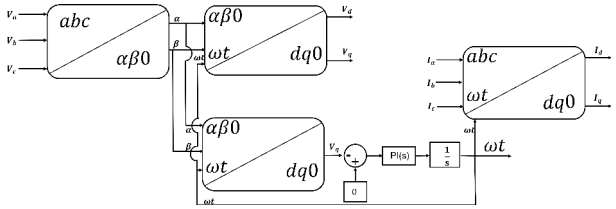

Fig. 3. Illustration of transformation and PLL

are presented in the figure 3. While the control to stabilize the DC link is shown in figure4.

The DC voltage level of 653.2 V with the rated 432 kW rated power are targeted.

B. Off-board battery chargers configuration

The battery charging configuration consists of bi-directional buck and boost converter, that works as buck in G2V and as boost in V2G mode respectively. The battery charging or discharging is made in two modes: Constant Current (CC) and Constant Voltage (CV). Setting up the modes and charging current strongly depends on the State-of-Charge (SOC) of the battery (EV battery). In some practical cases, CC and CV get separated at SOC of 80%, hence the open-circuit battery voltage at 80% SOC plays a cut-off role for charging voltage. Similarly, the nominal discharge current plays cut-off on charging current side.

1) G2V or Charging Mode: The battery in charging mode (G2V) consists of negative current(charging current) at the cut-off level(CC). The charging current starts decreasing toward zero once the charging voltage reaches the cut-off value (CV). The charging current reaches zero once the SOC is approximately 100%. In G2V mode, the off-board charger will be operating as a buck converter. It provides the right level of charging voltage, lower than the DC link voltage. Considering the off-board charger shown in figure 5 in buck mode, the upper switch (S_{buck}) is operated together with the lower switch anti-parallel diode. The off-board charger duty ratio is D and the charging voltage is given by the equation 2.

$$V_{bat} = V_{dc} * D \tag{2}$$

The duty ratio D is in the range of 0.0-1.0, hence the voltage at the battery V_{bat} will be lower than the DC link voltage V_{dc}

Authorized licensed use limited to: UNIVERSIDAD DE OVIEDO. Downloaded on June 21,2022 at 12:02:09 UTC from IEEE Xplore. Restrictions apply.

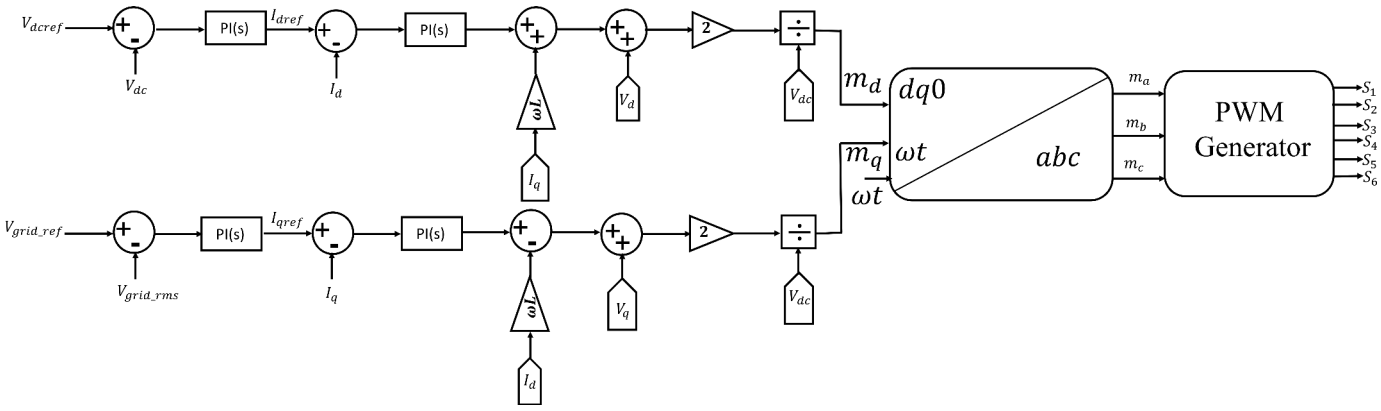

Fig. 4. DC link voltage control

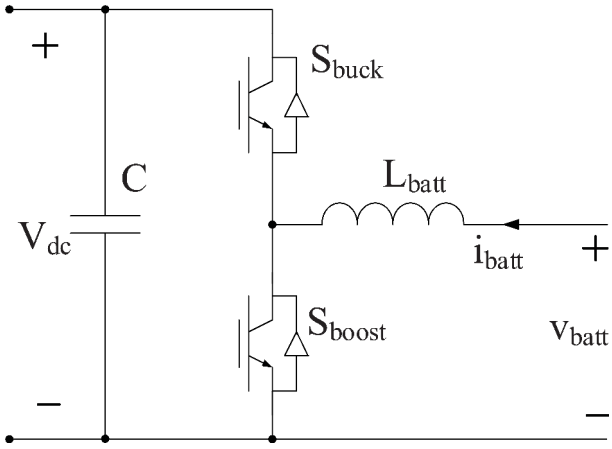

Fig. 5. Bi-directional off-board charger

by the ratio D. Therefore, the last statement illustrates the buck converter functionalities.

2) V2G or discharging Mode: When the EV battery has to send the power back to the grid, or to a certain load (part of the grid); the booster is necessary. The battery voltage is on lower level, it needs to be boosted to a voltage level of the DC link. During the V2G, the battery current is positive(discharging current), the battery voltage is constant(CV) till the current reaches the cut-off (CC). Hence, the voltage starts decreasing. The SOC in this case decreases as well. The battery voltage will keep decreasing till the SOC reaches zero, the battery current will drop to zero and the discharging is completed. Considering the figure 5 in the boost mode, the lower switch (S_{boost}) and the upper-switch ant-parallel diode are operated. The DC link capacitor is enough to stabilize the DC link on the required voltage. And the booster mode is illustrated in equation 3.

$$V_{dc} = \frac{V_{bat}}{1 - D_1} \tag{3}$$

Where D_1 is the duty of the boost mode in the figure 5.

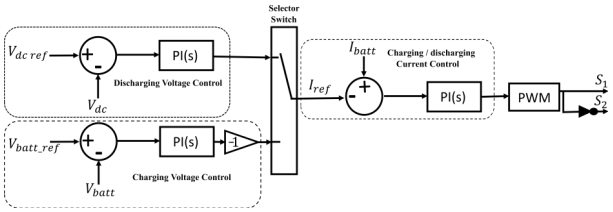

Fig. 6. EV charging or discharging selection and control

C. Simulink Model

The model mimicking the figure 1 was built in simulink. The simulink model considers the figure 1 starting from the AC bus and excluding wind turbine and PV panel contribution. Bearing in mind the mentioned part, will help to assess the behavior of the grid during the random charging and discharging of the EVs. Therefore, the model is made of 0.4 kV voltage source, a 480 kVA AC-DC converter, 653.2 V DC link, 5 off-board chargers of 40 kW each, a 26.7 kW resistive load (for EBs and EMBs) and 5 EVs of 400 V dc and 100 A max battery each. Each off-board charger is connected to the DC link which capacitor is 5mF. The off-board charger inductor, referred to as L_{batt} in figure 5 is of 5.76mH and the battery capacitor of 5.6 nF.The lithium-Iron battery model from Simulink is used as EV battery. The off-board chargers are connected in parallel to the DC link and 5 EVs are connected to the chargers. The Evs are named EV0 up to EV5, with the respective SOC as in the table I. Initially all of the EVs are in V2G mode (discharging to the grid), and

TABLE I
ILLUSTRATION OF THE EVS SOC AND STATES

EV	SOC	Sequence	Mode 1	Mode 2
EV0	15%	5	V2G	-
EV1	20%	4	V2G	G2V
EV2	30%	3	V2G	G2V
EV3	40%	2	V2G	G2V
EV4	60%	1	V2G	G2V
Load	-	6	Off	-

Authorized licensed use limited to: UNIVERSIDAD DE OVIEDO. Downloaded on June 21,2022 at 12:02:09 UTC from IEEE Xplore. Restrictions apply.

the DC load is disconnected. The last process is indicated in table I as Mode 1. As indicated in the same table, the sequence of switching are shown to change from Mode 1 to Mode 2 of presented EVs. However, in Mode 2, the DC load and EV0 were left out as they don't change the mode i.e there are not any EB or EMB charging and EV0 continues discharging. The rest of EVs switch to G2V (charging from the grid) in Mode 2. The switching algorithm and sequence from Mode 1 to Mode 2 and vice-versa, together with the charging and discharging controls are illustrated in the figure 6 and in table I. The off-board charger cut-off voltage is 433V DC, while the cut-off current is $\pm 100A$.

D. Simulations and Results

The simulation was run in Simulink for 2.5 seconds, with focus on: battery charging and discharging modes (CC and CV), DC-link voltage control and the control of Id and Iq-axis current, V2G and G2V as well as the complete power profile of the grid to show the grid behavior. The figure 7 demonstrates

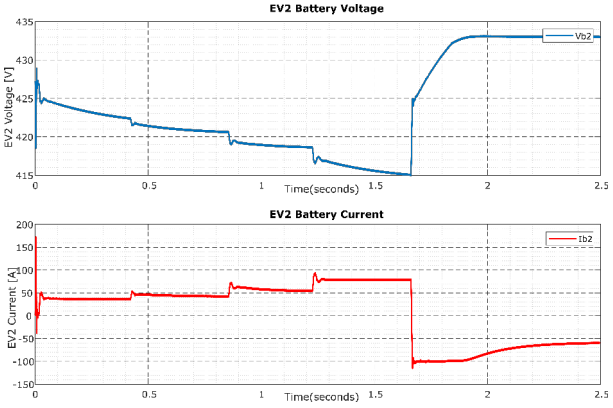

Fig. 7. Illustration of CC and CV in both Mode1 and Mode2

the CC and CV modes of battery charging and discharging. The EV2 is shown in both Mode 1 and 2, illustrates the fact that charging current is constant before the voltage reaches the cut-off, after cut-off voltage is constant and current starts decreasing and Vice-versa.

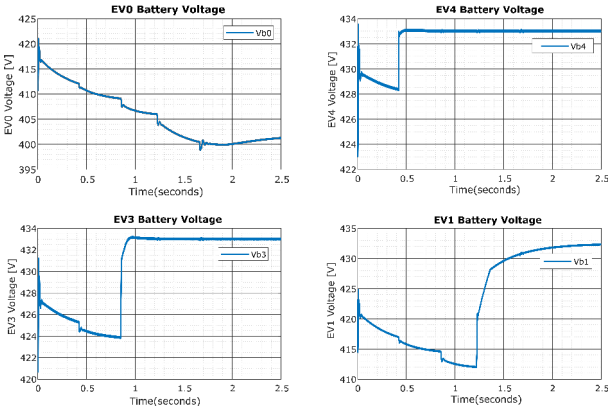

Fig. 8. Battery voltage in both Mode 1 and Mode 2

While the figure 8 and figure 9 display the behavior of different battery in both Mode 1 and 2, respective to their Mode change sequence. In charging of the EV batteries, the voltage increases and the current is negative. In discharging, the voltage decreases and current is positive. In the same figures, the charging and discharging controls are indicated and they respond appropriately. The stabilization of the DC

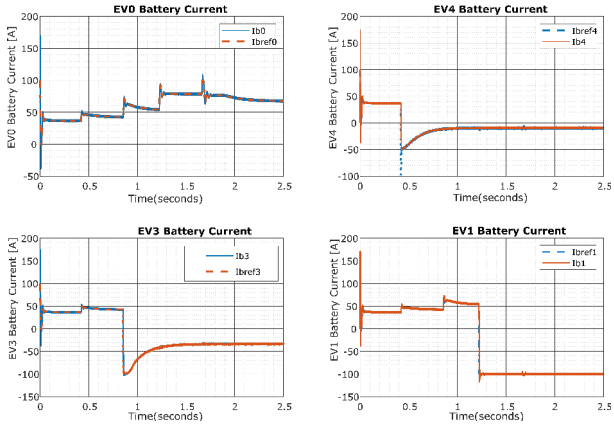

Fig. 9. Battery Current controls in Mode 1 and Mode 2

link was mentioned in this work. It was achieved through the cascaded control in which the inner loop controls the Id-axis current, while the outer loop regulated the DC link voltage. The figure 10 shows the results of both indicated controls and the tracking is as expected. The grid voltage and current

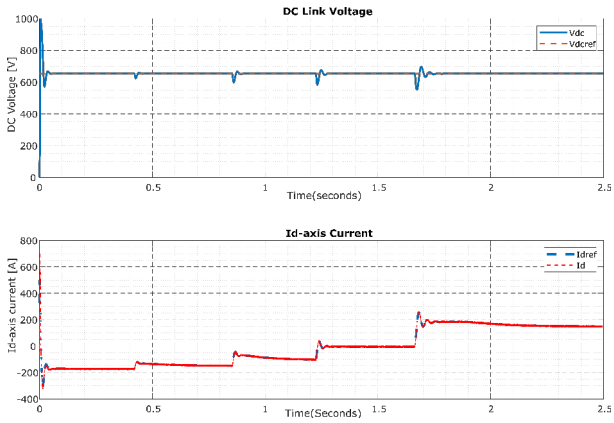

Fig. 10. Vdc link and Id-axis current controls

are presented in figure 11. During the G2V mode, current and voltage are in phase. And they are 180° out-of-phase in V2G. There isn't power supply from the grid when the supply from some EVs in V2G can fulfill the demand of the EVs in G2V and the DC load(charging the EBs and EMBs). In this case the power from the grid is zero and Vehicle-to-Vehicle (V2V) or Vehicle-to-Load (V2L) as new modes of operation are produced. The complete active power profile is illustrated in figure 12. The negative active power from 0 to 1.2 seconds shows the V2G mode i.e the EVs feed the power back to the grid and supply the DC load. The zero active power (from

Authorized licensed use limited to: UNIVERSIDAD DE OVIEDO. Downloaded on June 21,2022 at 12:02:09 UTC from IEEE Xplore. Restrictions apply.

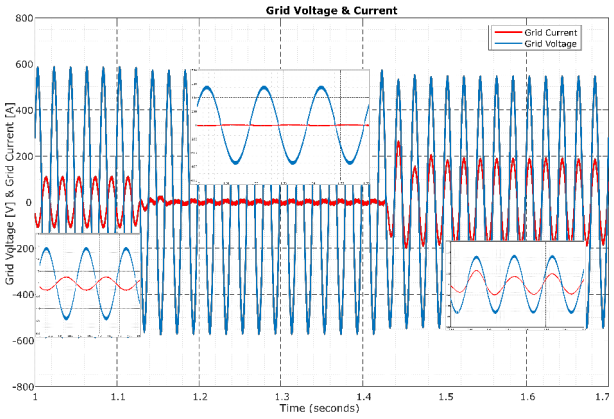

Fig. 11. Grid voltage V_a and Grid current I_a

1.2 to 1.7 seconds) means that the power from some EVs (in V2G) is enough to sustain the rest of the EVs (in G2V) and the DC load. Hence there is neither demand from the grid nor the power back to the grid. From 1.7 to 2.5 sec, the grid active power is positive. It indicates that the power from some EVs (in V2G) is not enough to sustain the demand from the rest of the EVs (in G2V) and the load. The grid intervention is necessary and it illustrates the G2V mode together with some auxiliary modes: V2V, V2L and G2L.

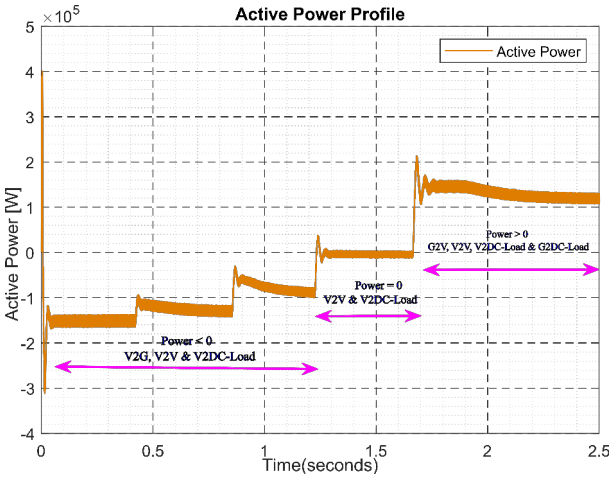

Fig. 12. Grid Active Power Profile

The reactive power injection, regulation and compensation during the AC-DC conversion and vice-versa as well as the effect power and load imbalance are not involved in this study. The further study is being done and these issues will be published in future works.

IV. Conclusions

The model of electric grid behavior in the presence of random charging and discharging of EVs was shown in this work. The bi-directional operation feasibility was demonstrated. EVs battery charging and discharging controls were illustrated. The behavior of the grid in terms of active power contribution and reception was shown in this work. The complete topology built in Simulink illustrated that the G2V, V2G and possible auxiliary modes (V2V, V2L, G2L) are feasible.

References

[1] Shakeel, F. M., and Malik, O. P. (2019, May). Vehicle-To-Grid Technology in a Micro-grid Using DC Fast Charging Architecture. In 2019 IEEE Canadian Conference of Electrical and Computer Engineering (CCECE) (pp. 1-4). IEEE.

[2] Shumei, C., Xiaofei, L., Dewen, T., Qianfan, Z., and Liwei, S. (2011, August). The construction and simulation of V2G system in micro-grid. In 2011 International Conference on Electrical Machines and Systems (pp. 1-4). IEEE.

[3] Yang, Y., and Blaabjerg, F. (2015). Overview of single-phase grid-connected photovoltaic systems. Electric Power Components and Systems, 43(12), 1352-1363.

[4] Chen, T., Jin, Y., Lv, H., Yang, A., Liu, M., Chen, B., ... and Chen, Q. (2020). Applications of lithium-ion batteries in grid-scale energy storage systems. Transactions of Tianjin University, 26(3), 208-217.

[5] Sahoo, B., Routray, S. K., and Rout, P. K. (2020). AC, DC, and hybrid control strategies for smart microgrid application: A review. International Transactions on Electrical Energy Systems, e12683.

[6] Lindstens, J. (2017). Study of a battery energy storagesystem in a weak distributiongrid.

[7] Arancibia, A., and Strunz, K. (2012, March). Modeling of an electric vehicle charging station for fast DC charging. In 2012 IEEE International Electric Vehicle Conference (pp. 1-6). IEEE.

[8] Han, S., Han, S., and Sezaki, K. (2010). Development of an optimal vehicle-to-grid aggregator for frequency regulation. IEEE Transactions on smart grid, 1(1), 65-72.

[9] Tan, K. M., Ramachandaramurthy, V. K., and Yong, J. Y. (2014, May). Bidirectional battery charger for electric vehicle. In 2014 IEEE Innovative Smart Grid Technologies-Asia (ISGT ASIA) (pp. 406-411). IEEE.

[10] M. C. Kisacikoglu, M. Kesler, and L. M. Tolbert, "Single-phase on-board bidirectional PEV charger for V2G reactive power operation," IEEE Trans. Smart Grid, vol. 6, no. 2, pp. 767–775, 2015.

[11] Bimenyimana, S., Asemota, G. N., and Li, L. (2018). The state of the power sector in Rwanda: a progressive sector with ambitious targets. Frontiers in Energy Research, 6, 68.

Authorized licensed use limited to: UNIVERSIDAD DE OVIEDO. Downloaded on June 21,2022 at 12:02:09 UTC from IEEE Xplore. Restrictions apply.

electronics

MDPI

Article

A Parallel Resonant Converter Polynomial Model Implemented in a Digital Signal Controller

Evode Rwamurangwa *, Juan Díaz González, Pedro José Villegas Saiz, Juan Antonio Martín-Ramos and Alberto Martin Pernía

Department of Electric, Electronic, Computer and Systems Engineering (DIEECS), University of Oviedo, 33203 Gijon, Spain; jdiazg@uniovi.es (J.D.G.); pedroj@uniovi.es (P.J.V.S.); jamartin@uniovi.es (J.A.M.-R.); amartinp@uniovi.es (A.M.P.)

* Correspondence: uo241006@uniovi.es or ing.rw.evode@gmail.com; Tel.: +25-078-883-8816

Abstract: Due to their exceptional performance in coping with large variations in output voltage and current, parallel resonant converters (PRC) are commonly used in high-voltage applications. The incorporation of step-up transformer parasitic components as part of a power topology, on the right duty and a suitable switching frequency, determines the high efficiency and wide variety of applications with PRC. Switching losses are reduced in the same topology by tracking and running on the optimum mode for each power and voltage by a set frequency and duty. The PRC's static model behaviors, under optimum operating circumstances, are illustrated. The equivalent polynomial model is used to quickly compute the switching frequency and duty cycle required to achieve the converter's desired output voltage and power. The polynomial model is simple and easy to implement in any form of a digital signal controller (DSC). Normalized parameters are used to widen the operational range and generalize the model. This also offers the essential protection against current and voltage spikes. The work in progress depicts the specific procedures involved in developing a polynomial model. The normalized equations provide a graphical description of the static model, from which the graphical representation of the polynomial are derived. Hence, polynomial equations are obtained. This paper describes the PRC static model, how to convert it to a polynomial model, how to validate it with MATLAB-Simulink, how to program F28335 using Simulink, and how to use it in practice.

Keywords: Code Composer Studio; duty; embedded coder; MATLAB; parallel resonant converter (PRC); polynomial model; Simulink; static model; switching frequency

check for updates

Citation: Rwamurangwa, E.; González, J.D.; Villegas Saiz, P.J.; Martín-Ramos, J.A.; Pernía, A.M. A Parallel Resonant Converter Polynomial Model Implemented in a Digital Signal Controller. *Electronics* **2022**, *11*, 1085. https://doi.org/10.3390/electronics11071085

Academic Editors: Khaled Ahmed and Rui Castro

Received: 4 February 2022
Accepted: 28 March 2022
Published: 30 March 2022

Publisher's Note: MDPI stays neutral with regard to jurisdictional claims in published maps and institutional affiliations.

Copyright: © 2022 by the authors. Licensee MDPI, Basel, Switzerland. This article is an open access article distributed under the terms and conditions of the Creative Commons Attribution (CC BY) license (https://creativecommons.org/licenses/by/4.0/).

1. Introduction

At present, in modern technologies, high voltage is applied in various domains; high voltage levels (tens of KV) are required in a wide range of applications: medical, industrial, environmental, measurement, etc. [1–3]. Due to high efficiency and power density, the use of resonant converters has drastically increased in multiple applications [4–7]. Various power conversion systems have been suggested for decades, as ways of supplying high voltages [8–12]. PRC and PRC-LCC are the most common topologies in high-voltage applications, since, with the inclusion of a high-voltage transformer, they implicate the parasitics as part of the resonant tank [13]. By applying the phase-shifted PWM, it is easier to operate the converter shown in Figure 1 in optimum mode [14], as illustrated in Figure 2. As is well known, in order to operate the converter [14–16], the frequency and duty are modified in such a way that the output voltage and power requirements are achieved. As the duty and frequency are variable, a couple of combinations of power and voltage at the output of the converter are produced and keep the converter operating in the optimum mode. However, at every desired value of output voltage and power, the corresponding frequency and duty have to be pre-calculated [15–19]. The last is a complex process; it renders the implementation more sophisticated. Hence, any algorithm computing it in any

type of DSC is of capital interest. This paper proposes a polynomial model to avoid the static model's complexity. It was first suggested in [15] on a PRC-LCC topology. In [15], a complete model of a parallel resonant converter LCC has been exposed, based on a model that is based on a harmonic approach; the equations and the model used actually are not an approach, and one parameter (frequency) is expressed as a polynomial. In this work, the normalized model is obtained; then, the polynomial equations (frequency and duty cycle) are obtained, and finally, all the steps needed to upload to a digital signal controller are obtained as well. This results in an easy, small, and quick program to implement in the DSC. This work considers the static model of the PRC in Figure 1 as detailed in [14], and limits itself to the optimum mode of operation to elaborate the equivalent polynomial model.

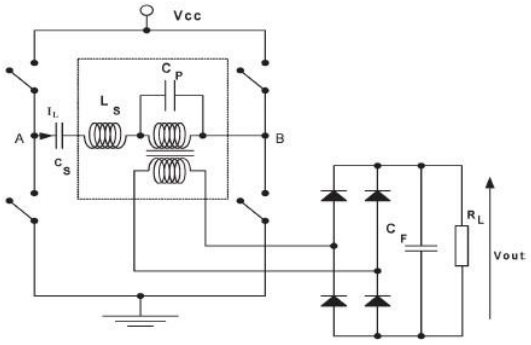

Figure 1. Parallel resonant converter [14].

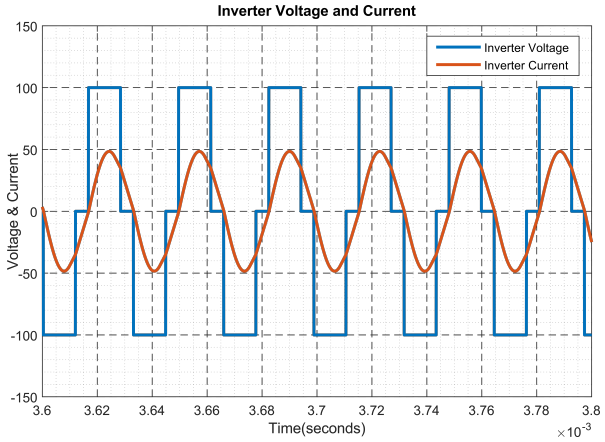

Figure 2. Output of inverter in Figure 1 in terms of voltage and current in optimum mode of operation.

From Figure 1, the L_s and C_p reactive elements are included in the transformer parasitic elements; these parasitics are crucial in high-voltage applications [14–17]. For the ease of application and on a wide range, the normalized parameters are used. Hence, Equations (1) and (2) illustrate the respective base and normalized parameters for the indicated PRC, in which $\hat{f}$, $\hat{v}$, $\hat{\Omega}$, and $\hat{p}$ are the normalized frequency, normalized output voltage, normalized load, and normalized power, respectively.

$$\begin{array}{cc} V_{Base} = V_{CC} & Z_{Base} = \sqrt{\frac{L_S}{C_P}} \quad P_{Base} = \frac{V_{CC}^2}{Z_{Base}} \\ f_{Base} = \frac{1}{2 \cdot \pi \sqrt{L_S \cdot C_P}} & \omega_{Base} = \frac{1}{\sqrt{L_S \cdot C_P}} \end{array} \tag{1}$$

Based on Equation (1), the normalized parameters are illustrated as follows:

$$\hat{v} = \frac{V_{out}}{V_{CC}} \quad \hat{p} = \frac{P_{out}}{P_{Base}} \quad \hat{\Omega} = \frac{R_L}{Z_{Base}} \quad \hat{f} = \frac{f}{f_{Base}} \tag{2}$$

Figure 2 shows the targeted output of the inverter, where the optimum mode operation is observed.

Figure 3 indicates the complete process for developing a polynomial model and its respective DSC control codes from the static model of the PRC. The last includes the static model, its transformation to a polynomial model, control code generation to DSC, and control wave forms generation for the power converter. The mentioned process is illustrated below:

- First, the static model is developed in MathCad and its graphical representations are subsequently illustrated [14]. To extend the operational span and for ease of analysis, the normalized parameters are used. However, this model is complex in that it renders the implementation sophisticated;
- Second, the polynomial model is suggested [15]. It is an alternative to simplify the model and ease the implementation mostly in DSC. The polynomial model is developed by tuning the static model's graphical representation in such away to generate the polynomic form through the numerical data-fitting method. The last gives the equivalent polynomic expression in graphic representation form;
- Third, the polynomial model is processed in MATLAB-Simulink to produce the program used for simulation and validation. The simulation is run for the validation of the polynomial model and to confirm the accuracy of the control codes' output;
- Fourth, the DSC is configured to Simulink and the control codes are generated. They make the control program that fits in a DCS and give the adequate control waveforms to fire the power converter switches (IGBTs);
- Finally, the experimental results are used to confirm the polynomial model's practicability and implementation feasibilities.

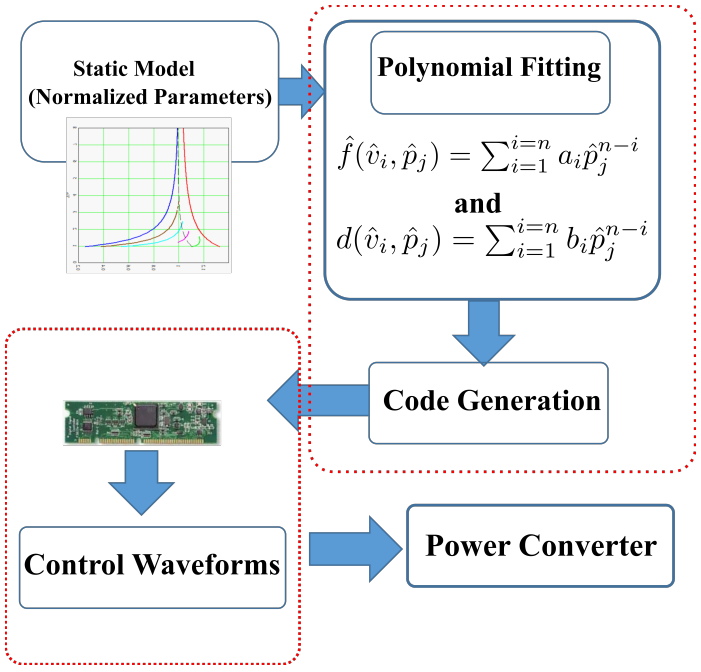

Figure 3. Illustration of the various stages of the project.

2. Grapical Representation of PRC Static Model

The static model normalized equations are detailed in [14]. In those equations, the normalized output voltage $\hat{v}$ is expressed as a function of the normalized frequency $\hat{f}$ in presence of a variable duty cycle d. Meanwhile, the normalized output power $\hat{p}$ is illustrated as a function of the normalized output voltage in presence of a variable duty cycle d.

$$\hat{v} = F(\hat{f}, d) \quad and \quad \hat{p} = F(\hat{v}, d) \tag{3}$$

Equation (3) is represented graphically in Figure 4 to illustrate its behaviors. Figure 4a,b shows the normalized output voltage of the model with respect to the change in normalized switching frequency, and in presence of the suitable value of the duty, while Figure 4c illustrates the normalized power as a function of normalized output voltage in presence of the respective duty values. The mentioned graphs highlight the process of establishing the necessary duty and switching frequency for achieving the targeted output voltage and power. It is a long and complex process that groups the implementation mostly onto low-cost DSCs. Recalling that the target is to determine an appropriate duty and switching frequency for every given output voltage and power, Equation (3) is modified to produce an appropriate normalized frequency and duty for each level of output normalized voltage and normalized power, as shown in Equation (4). For simplification of the task, the static model graphical representation is made in such a way to easily generate the duty and switching frequency once the power and output voltage are provided.

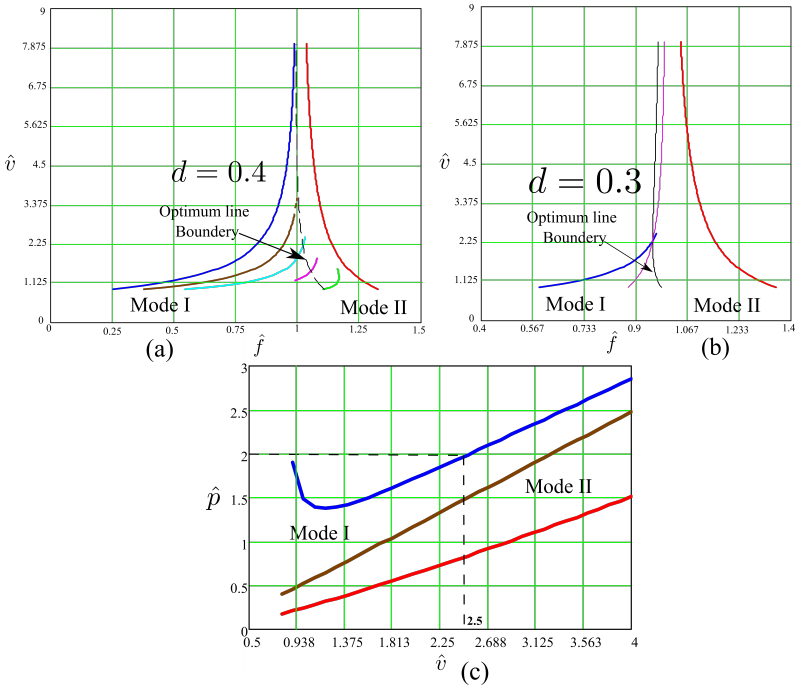

Figure 4. Graphical illustration of Equation (3); where (**a**) and (**b**) show the normalized output voltage vs normalized frequency for the duty $d = 0.4$ and $d = 0.3$ respectively. While (**c**) show the normalize power vs normalized output voltage.

The ideal power switches are used on the topology in Figure 1 to extract the graphs illustrated in Figure 4. This assumption does not significantly affect the final results. However, more complex models will be easily integrated in future work [20–22], in such a way to obtain more accuracy and efficiency. The static model's graphical representation in Figure 4a–c are rectified in a way to give the values of the duty and switching frequency at any set value of output voltage and power. Hence, the new form of graphical representation

is illustrated in Figure 5. In the last, the switching frequency and duty are functions of output voltage and power.

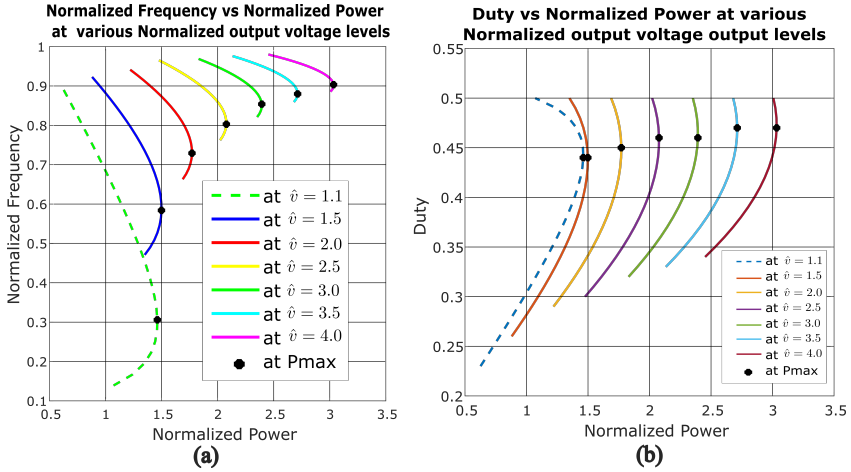

Figure 5. Graphical illustration where: (**a**) shows normalized Frequency vs normalized power, (**b**) shows duty vs normalized power. In presence of various level of normalized output voltage.

Figure 5a indicates the normalized frequency as a function of the normalized output power, in presence of the normalized output voltage. Hence, the normalized frequency is a function of both the normalized output voltage and normalized output power. In Figure 5b, the duty as a function of normalized power, in presence of normalized voltage, is illustrated; it implies that the duty is a function of both the normalized output voltage and the normalized power. Figure 5 can be expressed using Equation (4).

$$\hat{f} = F(\hat{v}, \hat{p}) \quad and \quad d = F(\hat{v}, \hat{p}) \tag{4}$$

Taking Figure 5 into account, the power reaches its maximum at each level of voltage, with a specific frequency or duty, and then begins to fall. Figure 6 depicts the power as a function of the frequency and duty cycle. The power at point **A** has the same value as the power at point **B**. Point **B**, on the other hand, comes after the maximum power point **Pmax**. Similarly, the value of the power at point **C** is the same as the value of the power at point **D**. After the maximum power point **Pmax**, point **D** is attained. The power beyond the maximum level **Pmax** is ignored by the design in place for power maximization at each frequency, duty, and voltage level. Assuming that Equation (4) is made of two polynomials for switching frequency and duty, respectively, the next step is to find their respective coefficients. This process will result in a set of polynomials of the nth order. The last have to be simple and make the control philosophy to run the control topology in Figure 1 on the DSC and in the optimum mode of operation.

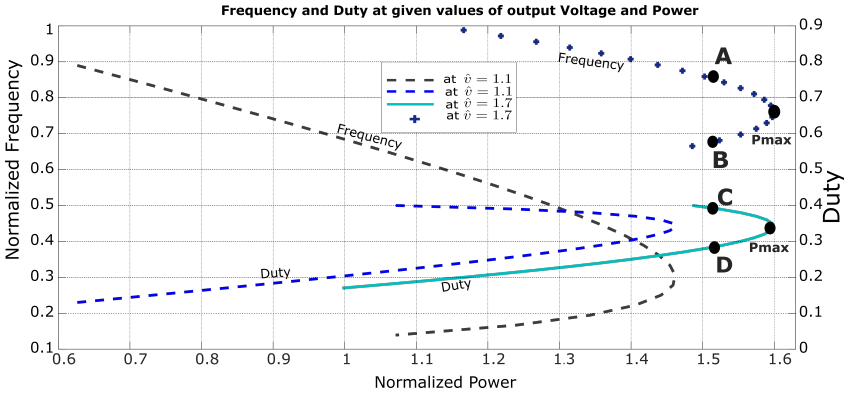

Figure 6. Illustration of normalized frequency vs. normalized power and duty vs. normalized power in presence of normalized voltage with the related behaviors. A and B show the point of same power on a value of frequency, while C and D show the point of same power on a value duty.

3. Polynomial Model of Parallel Resonant Converter

Having concurred with the assumption that Equation (4) is made of two polynomials, the next step is to find the adequate coefficients for each polynomial. In this case, numerical data fitting is applied on Figure 7a,d to retrieve the suitable coefficients for the polynomials. Recalling that, at each level of voltage, the power beyond the maximum is ignored, Figure 7 is a portion of Figure 5 at the normalized output voltage $\hat{v} = 1.1$ and $\hat{v} = 1.7$, respectively.

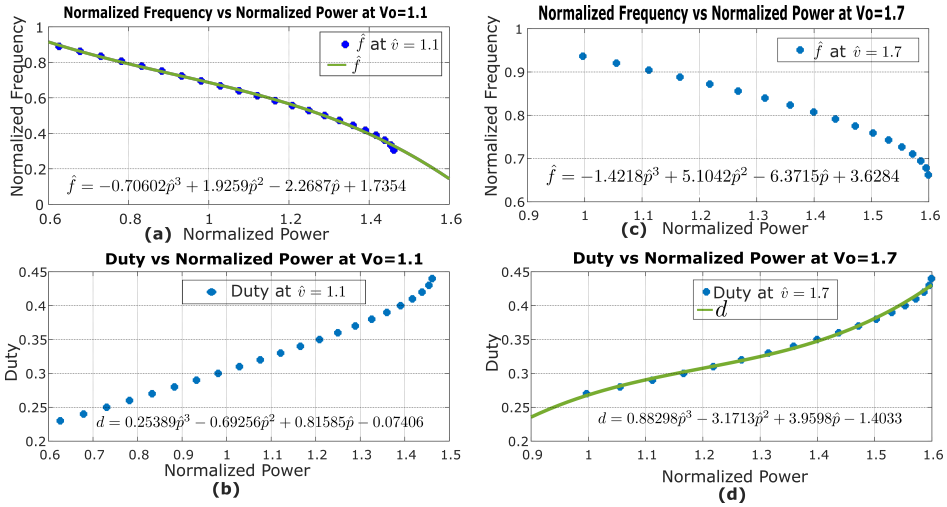

Figure 7. Data-fitting application on frequency and duty in presence of $\hat{v} = 1.1$ and $\hat{v} = 1.7$. (**a**,**b**) show data fitting for frequency and duty at $\hat{v} = 1.1$, while (**c**,**d**) show data fitting for frequency and duty at $\hat{v} = 1.7$.

The data-fitting method is applied to each specific voltage level plot for both frequency and duty, as illustrated in Figure 7, to obtain the equivalent polynomic expression. Various fittings were tried, including each fitting above the cubic over-fitted and each fitting below the cubic under-fitted. Therefore the accurate fitting was realized at the cubic level. This process resulted in the coefficients shown in Tables 1 and 2 for frequency and duty, respectively.

Tables 1 and 2 illustrate the fittings from different frequencies and duties, at various levels of voltage and power. The coefficient a_i is for frequency, while b_i is for duty. Hence, Equation (4) results in Equations (5) and (6) in polynomic form:

$$\hat{f}(\hat{v}, \hat{p}) = a_0\hat{p}^3 + a_1\hat{p}^2 + a_2\hat{p} + a_3 \tag{5}$$

for frequency, and:

$$d(\hat{v}, \hat{p}) = b_0\hat{p}^3 + b_1\hat{p}^2 + b_2\hat{p} + b_3 \tag{6}$$

for duty.

The coefficients a_i and b_i in Tables 1 and 2, respectively, are functions of the output voltage $\hat{v}$ and polynomials as well. They are in the form illustrated in Equation (7). Therefore, their respective coefficients are computed in turn. The data in Tables 1 and 2 are graphically represented and data fitting is applied, as shown in Figure 8a.

$$a_i = F(\hat{v}) \quad and \quad b_i = F(\hat{v}) \tag{7}$$

However, data fitting results in big outliers once applied to coefficients a_i and b_i, as in Figure 8a, which were immediately ignored. Therefore, an alternative was to apply B-spline [23–26]. The last is part of numerical analysis, which is mostly applied in curve-fitting and numerical differentiations of data. By applying B-spline to data in Tables 1 and 2, the coefficients for polynomials a_i and b_i are retrieved. The obtained coefficients are piece-wise linear at each output voltage level, as shown in Figure 8b.

Table 1. The table illustrates various coefficients of different fittings on frequency plots, at specific levels of voltage. a_i: coefficients for frequency fitting.

$\hat{v}$	a_0	a_1	a_2	a_3
1.0	0	0	−0.61102	1.222
1.1	−0.70602	1.9259	−2.2687	1.7354
1.2	−1.288	3.6637	−3.9182	2.2918
1.3	−1.3247	3.9212	−4.2784	2.4819
1.4	−1.5175	4.6649	−5.1259	2.8205
.	.	.	.	.
.	.	.	.	.
.	.	.	.	.
3.6	−0.59499	4.2475	−10.184	9.1596
3.7	−0.74666	5.5661	−13.909	12.606
3.8	−0.65556	4.9904	−12.737	11.858
3.9	−0.57735	4.486	−11.689	11.175
4.0	−0.51036	4.0457	−10.758	10.559

Table 2. The table illustrates various coefficients of different fittings on duty plots, at specific levels of voltage. b_i: coefficients for duty fitting.

$\hat{v}$	b_0	b_1	b_2	b_3
1.0	0	0	0.19449	0.11102
1.1	0.25389	−0.69256	0.81585	−0.07406
1.2	0.51726	−1.4713	1.5735	−0.32038
1.3	0.58838	−1.7417	1.9003	−0.45238
1.4	0.74316	−2.2865	2.5136	−0.68055
.	.	.	.	.
.	.	.	.	.
.	.	.	.	.
3.6	0.89738	−6.408	15.368	−12.018
3.7	1.1575	−8.6289	21.562	−17.693
3.8	1.048	−7.9784	20.364	−17.059
3.9	0.95176	−7.3958	19.273	−16.475
4.0	0.86674	−6.872	18.276	−15.935

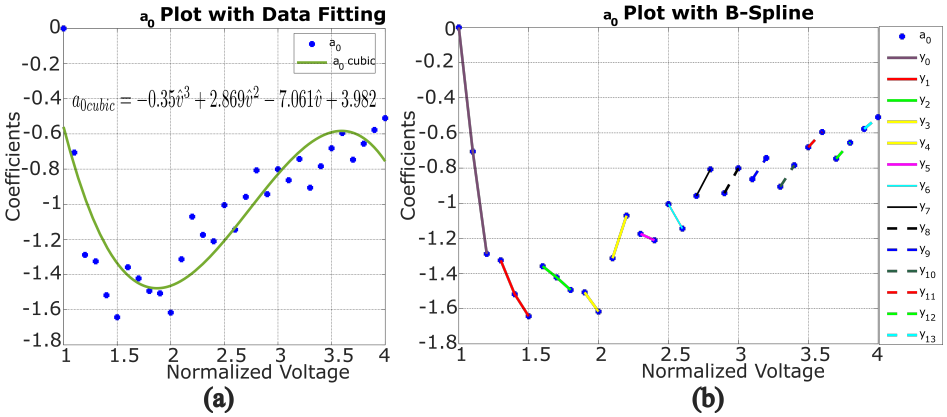

Figure 8. Illustration of a_0 plotting, data fitting and B-spline application; where (**a**) shows data fitting while (**b**) shows its equivalent B-spline representation.

The application of B-spline results in the linear expressions displayed in Equation (8). Tables 3 and 4 give the detailed coefficients obtained through B-spline application from data in Tables 1 and 2, respectively, for Equation (8).

Table 3. This table shows the specific coeffiecients retrieved from the coefficients in Table 1 after B-spline.

$\hat{v}$	a_0		a_1		a_2		a_3	
	α_0	λ_0	α_1	λ_1	α_2	λ_2	α_3	λ_3
1.0–1.2	−6.4400	6.4193	18.3190	−18.2870	−16.5360	15.9240	5.3490	−4.1342
1.3–1.5	−1.5900	0.7310	7.2865	−5.5462	−9.5360	8.1538	4.2220	−3.0346
1.6–1.8	−0.6750	−0.2770	5.6585	−4.4915	−10.4860	11.3930	5.8700	−6.3060
1.9–2.0	−1.0950	0.5737	8.3280	−9.8350	−16.5230	23.2470	10.0220	−14.3620
2.1–2.2	2.4240	−6.4033	−9.1850	24.9940	11.4450	−32.4880	−4.4950	14.6110
2.3–2.4	−0.3650	−0.3347	3.7960	−3.1700	−9.1530	12.1060	6.5700	−9.3089
2.5–2.6	−1.3930	2.4775	10.2110	−20.4600	−22.7860	48.3120	16.1910	−34.5450
2.7–2.8	1.5088	−5.0318	−7.1010	24.4050	10.8790	−39.0250	−5.2610	21.150
2.9–3.0	1.4187	−5.0571	−7.1910	26.4110	11.8340	−45.3510	−6.1590	26.1780
3.1–3.2	1.2073	−4.6060	−6.4090	25.2430	11.0000	−45.3490	−5.9280	27.2370
3.3–3.4	1.2193	−4.9297	−6.9400	28.9530	12.7600	−55.6680	−7.3800	35.5000
3.5–3.6	0.8654	−3.7104	−5.1330	22.7260	9.8200	−45.5360	−5.8950	30.3820
3.7–3.8	0.9110	−4.1174	−5.7570	26.8670	11.7200	−57.2730	−7.4800	40.2820
3.9–4.0	0.6699	−3.1900	−4.4030	21.6580	9.3100	−47.9980	−6.1600	35.1990

Table 4. This table shows the specific coeffiecients retrieved from the coefficients in Table 2 after B-spline.

$\hat{v}$	b_0		b_1		b_2		b_3	
	β_0	ϕ_0	β_1	ϕ_1	β_2	ϕ_2	β_3	ϕ_3
1.0–1.2	2.5863	−2.5879	−7.3565	7.3709	6.8951	−6.7233	−2.1570	2.2782
1.3–1.5	1.4197	−1.2530	−5.5730	5.5074	6.9235	−7.1266	−2.8196	3.2310
1.6–1.8	1.0212	−0.8488	−5.6690	6.4327	9.2140	−11.6320	−4.7130	6.5631
1.9–2.0	1.4800	−1.7409	−8.8670	12.5890	15.9650	−24.5400	−9.0870	14.8890
2.1–2.2	−1.4155	4.0245	4.9870	−15.0450	−5.5260	18.3800	1.7760	−6.8231
2.3–2.4	0.9160	−1.0600	−6.2970	9.5256	13.0150	−21.9590	−8.5190	15.5710
2.5–2.6	1.8546	−3.6424	−12.6150	26.5220	27.0250	−58.9940	−18.6480	42.0000
2.7–2.8	−1.2309	4.3582	5.4290	−20.3120	−7.4930	30.6620	3.0070	−14.2730
2.9–3.0	−1.2665	4.7769	6.0270	−23.9850	−8.970	38.9310	3.9060	−19.6160
3.1–3.2	−1.1662	4.7107	5.7960	−24.7890	−8.9300	41.9620	3.9460	−21.9280
3.3–3.4	−1.2710	5.4262	6.7870	−30.6250	−11.2500	55.5640	5.3800	−31.2600
3.5–3.6	−0.9676	4.3807	5.3780	−25.7690	−9.2600	48.7040	4.5600	−28.4340
3.7–3.8	−1.0950	5.2090	6.5050	−32.6970	−11.9800	65.8880	6.3400	−41.1510
3.9–4.0	−0.8502	4.2675	5.2380	−27.8240	−9.9700	58.1560	5.4000	−37.5350

Equation (7) results in two capital polynomial coefficients, for frequency and duty, respectively, as follows:

$$a_i(\hat{v}) = \alpha_i \hat{v} + \lambda_i \quad and \quad b_i(\hat{v}) = \beta_i \hat{v} + \phi_i \tag{8}$$

Equations (5) and (6) provide the frequency and duty that are able to run the topology on Figure 1 in its optimum mode at a specified level of voltage, power, and load. Combining Equations (5), (6) and (8), the general Equation (9) for frequency and duty, respectively, is obtained. They can fit in any DSC and generate the suitable control signals.

$$\hat{f}(\hat{v}_i, \hat{p}_j) = \sum_{i=0}^{i=n} a_i \hat{p}_j^{n-i} \quad and \quad d(\hat{v}_i, \hat{p}_j) = \sum_{i=0}^{i=n} b_i \hat{p}_j^{n-i} \tag{9}$$

4. Model Building and Simulations

In order to validate the polynomials shown in Equation (9). The model in Figure 1 was built in MATLAB-Simulink R2021a. The polynomials were applied to the mentioned model to confirm the optimum mode of operation. The model validation considers output voltage and power as independent variables, while the switching frequency and duty are dependent. The last is illustrated in Equation (9). Each level of output voltage and power corresponds not only to frequency and duty but also to the load. Hence, the load is dynamic in this case, and governed by Equation (10), which is a polynomial in turn. The control model was built in MATLAB-Simulink as well. It is made of a MATLAB function block to hold Equation (9). This block accepts two inputs (normalized output voltage and normalized power) and generates two outputs (normalized frequency and duty). The two last outputs are used to obtain the required period and phase shift that run the PWM generator. The last, in turn, generates the switching signals that run the IGBTs on the model in Figure 1. The control model is illustrated in both Figures 9 and 10. Both the power and control model are run in MATLAB-Simulink for validation of the polynomials before going for practical implementation.

$$\hat{\Omega} = F(\hat{v}_i, \hat{p}_j) \tag{10}$$

Practically, the load is not always variable; it is fixed in most cases. Therefore, the simulation will be conducted in two ways: two-inputs model simulation and one-input model simulation.

4.1. Two-Inputs Model Simulations

The normalized voltage and normalized power are the capital. They change the independent variables to the polynomials in Equation (9). Hence, they are the two inputs for the model in Figure 9. They are fed to the polynomials' block. The last holds Equation (9); they are written in the form of control codes with the necessary protection and generate from them the necessary duty and frequency. The frequency is converted into an equivalent period and it is fed to PWM generator for PWM signal generation. The duty is used to calculate the shifting time; this is fed to the phase shift block and helps generate the phase-shifted PWM signals.

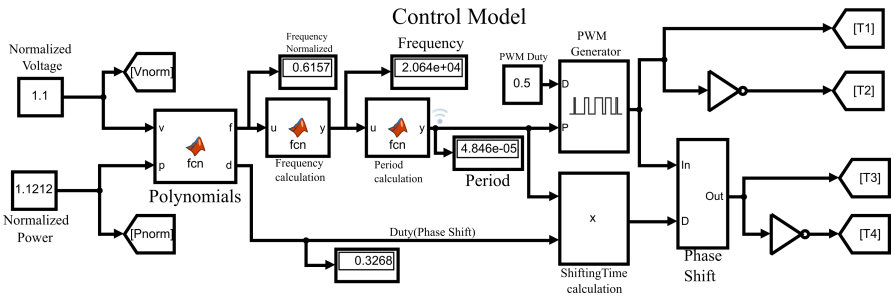

Figure 9. Illustration of Simulink model with normalized voltage and normalized power as inputs.

$$\hat{\Omega} = \frac{\hat{v}^2}{\hat{p}} \tag{11}$$

The normalized load at each level of voltage and power is given by Equation (11). The simulation component values used in the simulation are from the prototype components' values. They are indicated in Table 5.

Equations (5) and (6) were simulated in Simulink. The parameters in Table 5 were used. The input voltage is $V_{in} = 100$ V, while the normalized value of the output voltage is $\hat{v} = 2.5$. Then, the expected value of the output voltage is $V_{out} = 250$ V. If the normalized power $\hat{p} = 1.83177461$ is considered, then the required frequency and duty are obtained by applying Equations (5) and (6) to the model in Figure 3. The frequency $\hat{f} = 0.9086$ and the duty $d = 0.3566$ were obtained and applied in the Simulink model. The load value is given by Equation (11) and the value by $\hat{\Omega} = 3.412$. The results of the simulation are shown in Figure 10. In this case, the optimum mode is fulfilled along the domain of the functions in Equation (9).

Table 5. The parameters used to simulate the model in Figure 9 with dynamic load.

Item	Value	Unit
V_{in}	100	V
L_s	34.232	uH
C_p	658.7	nF
C_f	30	uF
Z_{Base}	7.209	Ω
f_{Base}	33.527	kHz

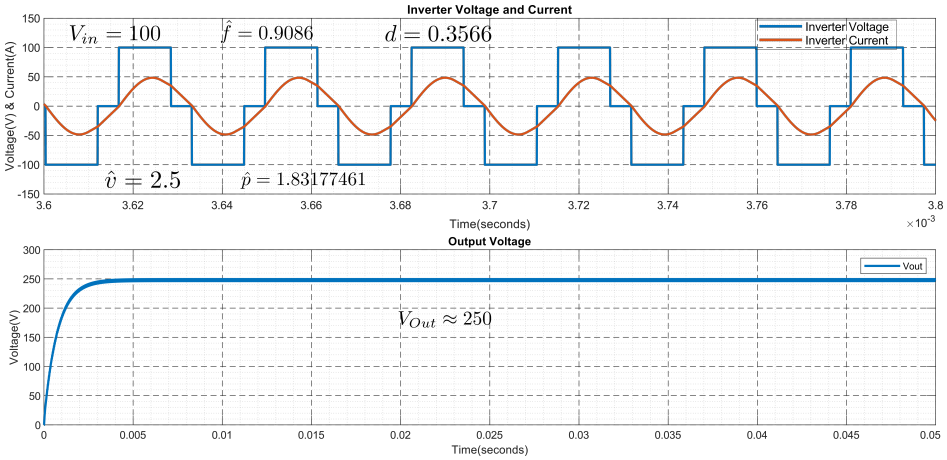

Figure 10. The voltage and current output of the converter with normalized output voltage and normalized power as inputs.

4.2. One-Input Model Simulations

In this case, the load is constant. Any change in the output power results in a different level of output voltage. The power is the only input to the control model, the corresponding voltage is illustrated with respect to the fixed load. Except having one input, the rest of the model components fit the model description in Section 4.1 Figure 11.

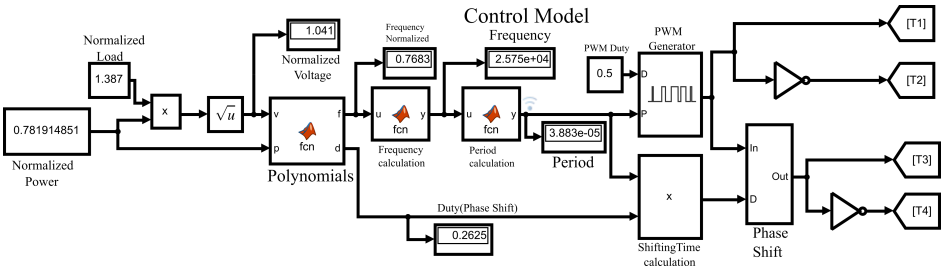

Figure 11. One-input Simulink control model.

Therefore, having the load as a fixed parameter and the power as an input, the corresponding voltage is given by Equation (12).

$$\hat{v} = \sqrt{\hat{p} * \hat{\Omega}} \tag{12}$$

The simulation parameters are given in Table 5.

The power and the load are $\hat{p} = 0.7819$ and $\hat{\Omega} = 1.387$, respectively; hence, the voltage is $\hat{v} = 1.0414$. In this case, the frequency and duty are $\hat{f} = 0.76827$ and $d = 0.2625$, respectively. Figure 12 displays the simulation results. In case of a fixed load, the optimum mode is fulfilled at a fixed range of voltage. Hence, $\hat{\Omega} = 1.387$ runs from $\hat{v} = 1.00664$ to $\hat{v} = 1.441706$.

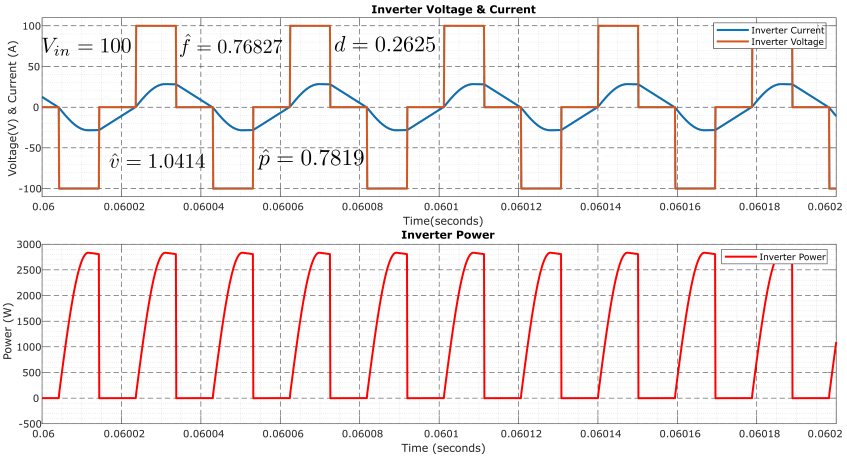

Figure 12. Inverter voltage, current, and power at fixed load

5. DSC Configuration

Due to the aforementioned operations, the indicated controls cannot be easily implemented. The DCS is key, as it is has the computational capability; this work will take advantage of a Texas Instrument (TI) DSC. The last is a TMS320F28335 Peripheral Explorer Kit with high-performance static CMOS technology, a high-performance 32-bit CPU, fast interrupt response processing, on-chip memory, and many more advantages [27]. The shifted pulse-width modulation (PWM) switching signals were generated on a TMS320F28335 Peripheral Explorer Kit using MATLAB-Simulink. In fact, the TMS320F28335 is a Texas Instrument micro-controller, programmed through a Code Composer Studio development environment (CCS). CCS supports C or C++ language. Even if they are common to most control engineers, the mentioned languages are time-consuming and prone to several errors; hence, it is tiresome to code the signals accurately. However, those challenges are responded to by using model-based programming through MATLAB-Simulink. The complete control algorithm is completed in MATLAB-Simulink and, later on, the PWM codes for the F28335 are generated. Some necessary steps are crucial to configure a Peripheral Kit to MATLAB-Simulink. MATLAB-Simulink, with some necessary add-ons such as "Embedded Coder",

"Simulink Coder", and "MATLAB Coder", together with CCS, have to be installed on the PC. In this case, MATLAB R2021a, with the mentioned add-ons, together with CCS 7.3.0, are installed on the PC. Hence, the target hardware (TI Delfino F2833x) is configured. The model is built in Simulink, through which the PWM codes are generated and downloaded to a TMS320F28335 Peripheral Explorer Kit. The codes for backup or any other analysis are retrieved in project form through CCS. Equation (9) is programmed in the F28335 using a MATLAB function block; they are quick and fast-response polynomials. In the same coding is included the protection of the system, in case of mistakes when entering values.

Figure 13 mentions the model-based program to generate PWM for control purposes. The Hex-Encoder on the F28335 serves as the input, as it accepts 16 inputs at different input steps. The Hex-Encoder is linked to four general-purpose input–outputs (GPIO). The last are GPIO15, GPIO14, GPIO13, and GPIO12, in order of most to least significant bit, respectively. They input 16 different values of power with the help of a lookup table. Taking into consideration the fixed load, Equation (12) gives the voltage. Both voltage and power are fed to polynomial block. The last hosts the Equation (9)-related codes. They generate, in turn, the corresponding frequency and duty. The frequency is converted to the corresponding period according to Equation (13). The period is fed to both ePWM1 and ePWM2 at input "T" for PWM signal generation for both converter legs. A half of the period is fed to both ePWM1 and ePWM2 on inputs "WA" and "WB" to maintain a 50% duty cycle for each switching signal. The product of period and duty gives the adequate time-shift between the converter legs, and it is fed to ePWM2 on input "PHS". The PWM-switching signals at adequate frequencies with the necessary duty shifting are generated. The ePMW1A and ePWM1B output the switching signal for the first leg, while ePWM2A and ePWM2B give the shifted switching signal for the second leg.

$$T = \frac{f_{clk}}{2 * f_{sw}} \tag{13}$$

From Equation (13), T is the period, f_{clk} is the F28335 maximum clock frequency, and f_{sw} is the switching frequency.

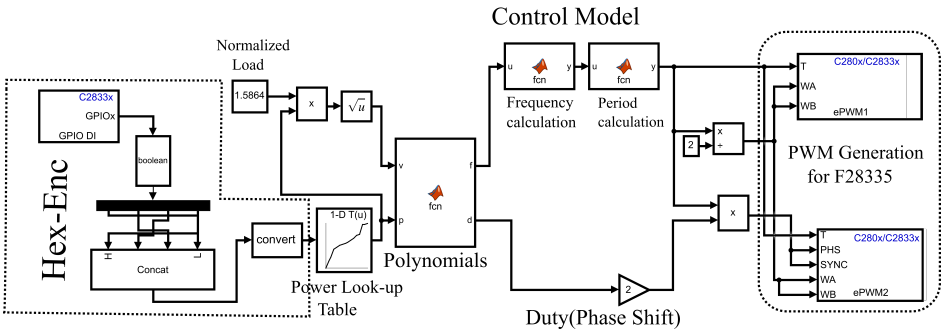

Figure 13. PWM generation model in Simulink.

6. Experimental Prototype

The topology shown in Figure 1 was used to build the prototype for practical experimentations, with the target of obtaining the model illustrated in Figure 14 and to practically prove the polynomial model. It is a topology made of a personal computer for programming purposes. The F28335 micro-controller is used for hosting the control program and to generate the corresponding switching signals, S^*_1, S^*_2, S^*_3, and S^*_4. The drivers are connected to the output of the controller and strengthen the switching signals to a suitable level of S_1, S_2, S_3, or S_4 for firing the IGBTs. The embedded IGBTs are used and provide an adequate commutation for the proper output of the prototype. The IGBTs form a converter and link the input voltage to the resonant tank. The last is made of leakage inductance and parallel capacitance connected in parallel. Both these components can be part of the power transformer

as parasitics. The diode rectifier and the filter capacitor output the DC voltage with proper smoothness. Figure 14 presents the steps and components of the prototype.

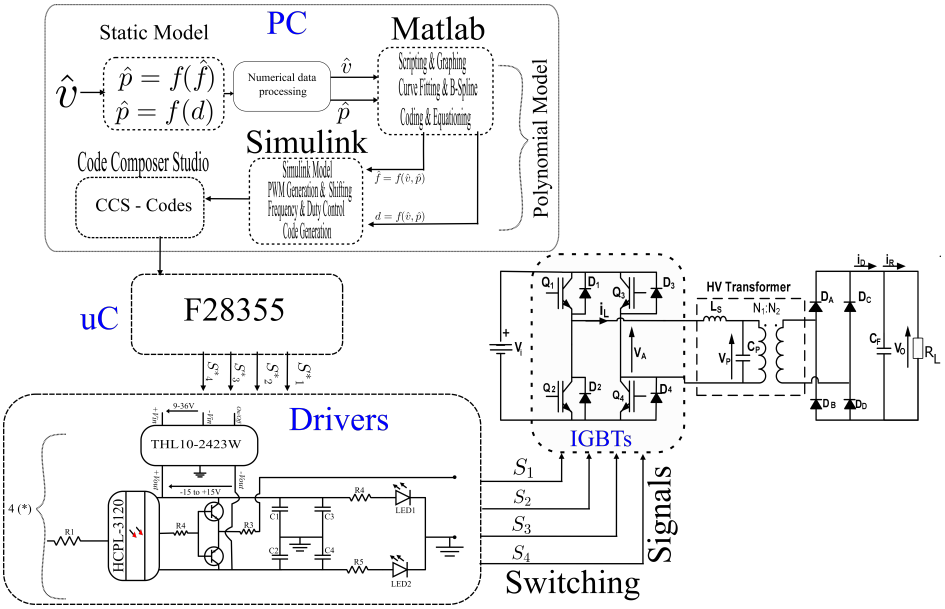

Figure 14. Illustration of the complete model of the practical implementation.

6.1. Driver

The drivers are signal-strengthening circuits. They are fed from the F28335 microcontroller. They give the level necessary to switch the IGBTs to the switching signals. They replicate into four similar drivers: one driver for each signal, as presented in Figure 15. Each driver is made of an HCPL-3120 opto-coupler to electrically decouple the references of input and output signals. The THL10-2423W is a DC–DC power converter that receives 9 V to 36 V and outputs −15 V to +15 V. The complete driver receives a switching signal of 0 to 3.3 V and outputs −15 V to +15 V. Figure 15 shows the driver board. The F4-150R12KS4 is the embedded circuit made of two legs of IGBTs. It is small, compact, and mounted on the driver board, which makes the complete topology small in size.

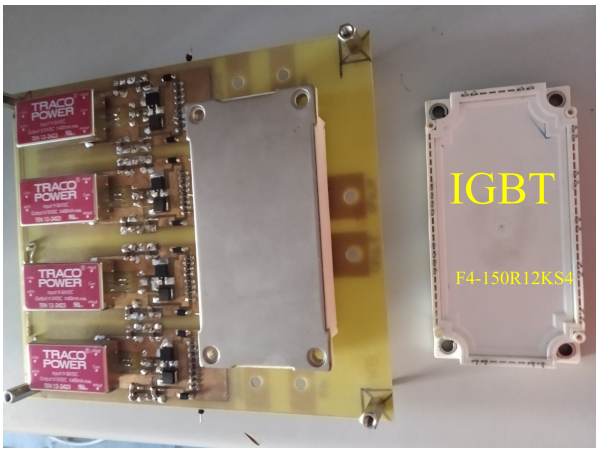

Figure 15. Illustration of the driver model.

The prototype can have different behaviors based on the components of the resonant tank. Two scenarios are tested in this work. The first scenario is the low-voltage prototype, where the resonant tank is made of an independent capacitor and inductor without a power

transformer. This is the low-voltage case. The second option considers the resonant tank with an independent inductor together with the power transformer and its parasitics. This is a high-voltage case.

6.2. Low-Voltage Test

The prototype was made up of an F28335 TI micro-controller for shifted PWM signals, a driver to strengthen the PWM signals to a required switching level, an F4-150R12KS4-embedded IGBT converter, a resonant tank of $L_s = 34.232$ µH and $C_p = 658.7$ nF, an uncontrolled rectifier, a filter capacitor of 30 µF, and a 10 Ω load.

The prototype was tested on a fixed load of 10 Ω by applying Equation (12) on the program model in Figure 13. The power values in Table 6 were applied.

Table 6 shows the data retrieved on the prototype in Figure 16. The same prototype was run $\hat{v} = 1.00664$–1.441706 and $\hat{p} = 0.730587$–1.498569. The resonant frequency of the prototype was $f_r = 33.517$ kHz. The behavior of the prototype at the fixed load is illustrated in Figure 17. As the output voltage increased, the power transfer increased as well. Hence, the switching frequency goes further below resonance, while the duty increases drastically.

Figure 18 shows the behaviors of the prototype in Figure 16 in optimum mode. It was obtained through running the topology in Figure 16 in optimum mode and on the following data: power: $\hat{p} = 0.781915$; normalized load: $\hat{\Omega} = 1.387$. Hence, the voltage becomes $\hat{v} = 1.0414$. At the input voltage $V_{in} = 39.6$ V, the output voltage becomes $V_{out} = 41.24$. Therefore, the obtained frequency and duty are $\hat{f} = 0.76826685 \approx f = 25.75$ kHz and $d = 0.2625$, respectively.

Table 6. This table shows different operating points in the design operating window of the prototype in Figure 16 with a load of 10 Ω ≈ $\hat{\Omega}$ = 1.387.

$\hat{v}$	$\hat{p}$	$\hat{f}$	d
1.00664	0.730587	0.780201	0.2535
1.041401	0.781915	0.768267	0.2625
1.074677	0.832682	0.757526	0.2716
1.120123	0.904597	0.74589	0.2842
1.150194	0.953819	0.74052	0.2925
1.172152	0.990585	0.737835	0.2985
1.30065	1.219677	0.695766	0.3417
1.316569	1.249714	0.685622	0.3488
1.332491	1.280124	0.673986	0.3567
1.348824	1.311699	0.661157	0.3656
1.359014	1.331593	0.652206	0.3716
1.372422	1.357997	0.639675	0.3801
1.389738	1.392481	0.621476	0.3924
1.403329	1.419851	0.605663	0.4032
1.412658	1.438791	0.593729	0.4112
1.441706	1.498569	0.550467	0.4404

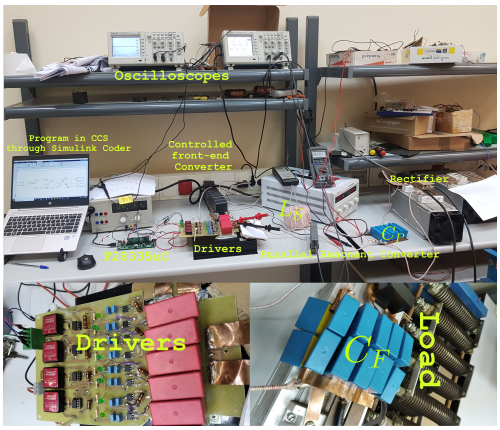

Figure 16. Illustration of the low-voltage prototype.

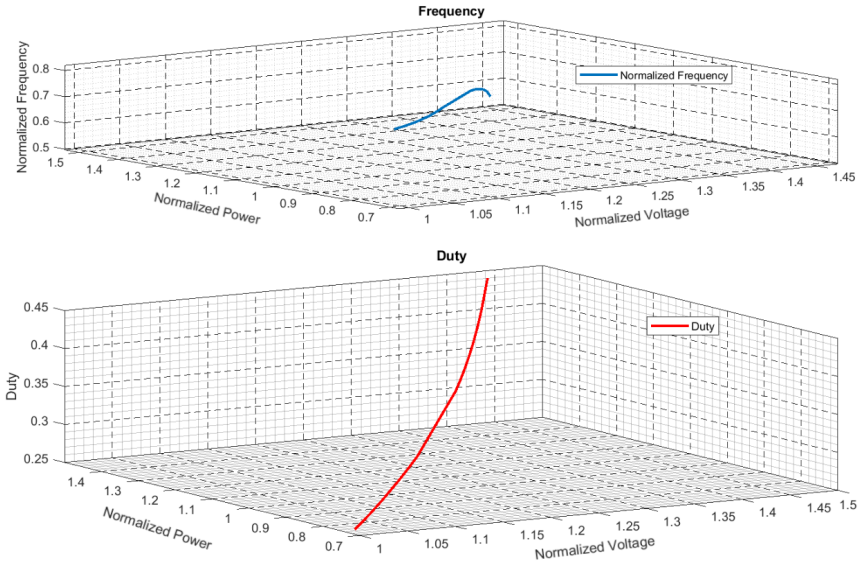

Figure 17. Illustration of normalized frequency and duty at a fixed load of $\hat{\Omega} = 1.387$, corresponding to 10 Ω.

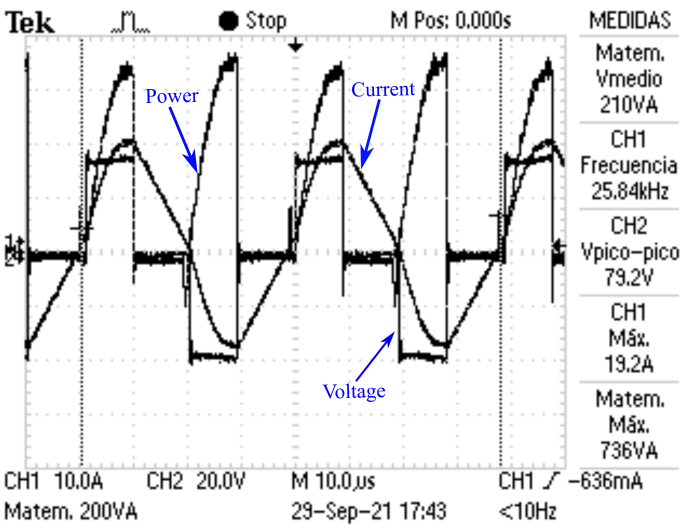

Figure 18. Illustration of the prototype output.

6.3. High-Voltage Test

The high-voltage prototype was built as illustrated in Figure 19. It uses the same components as the low-voltage prototype, with the exception of the high-voltage transformer; this was added for a higher transformation ratio. The inductor $L_S = 110.34$ µH (with 22.4 µH of transformer leakage inductance) and the parasitic capacitor $C_P = 43$ nF, the load is 57.575 Ω, the resonant frequency of $f_r = 73.067$ kHz, $Z_{base} = 50.6561$ Ω, and $n = 400/14$ is the transformer turn ratio. Transformer oil was used to insulate the transformer and the load for safe runs under high-voltage outputs. The maximum output voltage reached was 4 kV. Figure 19 shows the high-voltage transformer and the load immersed in transformer oil for high-voltage insulation.

The prototype in Figure 19 was run at a fixed normalized load of $\hat{\Omega} = 1.1366$. The model-based program illustrated in Figure 13 runs on various power levels, in a range between $\hat{p} = 0.882826$ and $\hat{p} = 1.498569$. Figure 20 shows the output of the high-voltage

test, where the input voltage is $V_{in} = 94$, the input current $I_{in} = 1$ A, the normalized power $\hat{p} = 0.882826$, the normalized frequency $\hat{f} = 0.6862$, the duty $d = 0.283$, and the output voltage $V_{out} = 2$ kV. The optimum mode is realized.

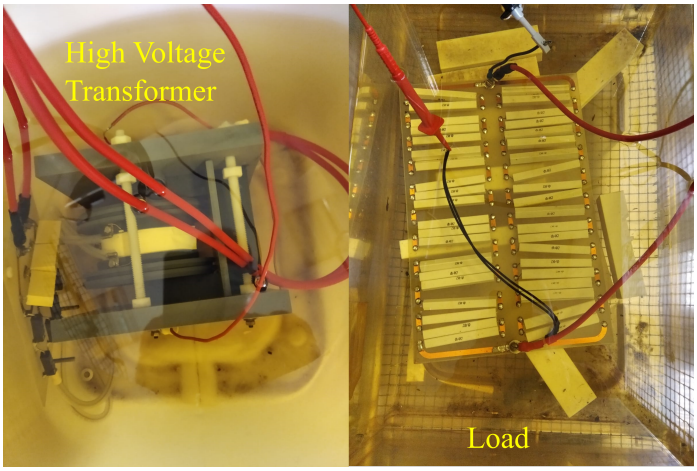

Figure 19. Illustration of the high-voltage prototype.

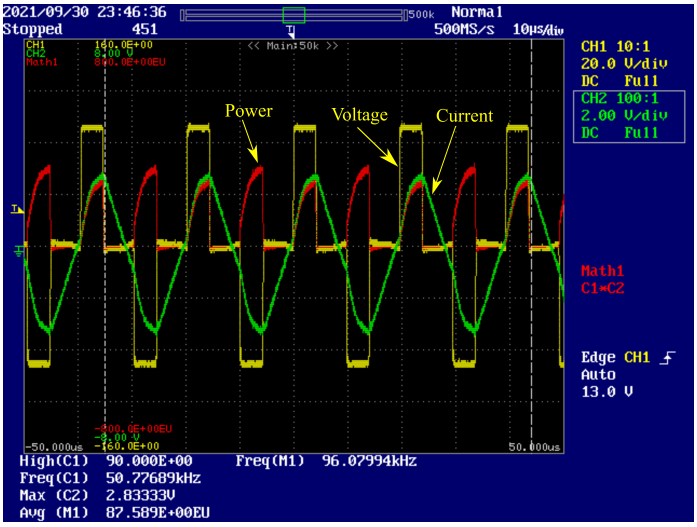

Figure 20. Illustration of converter output at 2 kV output voltage.

7. Conclusions

Parallel resonant converters (PRCs) have acquired popularity and applications in a variety of fields due to their excellent performance. PRCs have been advantageous for years as a result of the utilization of transformer parasitics. They are not, however, challenge-preserved. The intricacy of the models, as well as the challenges of implementing them in small micro-controllers, are among the drawbacks. The goal is to simplify the model such that it may be implemented in a small digital signal controller. This work illustrates the static model graphic representation of PRC. The same model was decomplexed by developing a polynomial model. The last is achieved by applying data-fitting and B-spline methods to static model graphs. Two polynomials were obtained and provide a suitable frequency and duty at any level of output voltage and power. They run the prototype in the optimum mode on F28335 micro-controller. The model was simulated in Simulink and practically tested on both low and high voltages; the results in both cases are shown in this work. The general polynomials were formed, and the corresponding control program

was developed in a model-based manner, using Simulink. The program fits and runs on the F28335 without any problem, and the control waveforms are generated as expected. The same technique illustrated in this paper will be used in further processes, such as implementing the model in FPGA, creating closed-loop fuzzy control, and implementing alternative control strategies, such as constant power control.

Author Contributions: This paper makes up part of the research carried out by the research team that will be here mentioned. The respective contributions of each team member will be mentioned as well. E.R. made conceptualized the research, mathematical models, simulations, and program conception, equationilization, prototyping, and writing. J.D.G. developed the fundemantal relationship among various dependent and independent parameters, supervised, and validated the resaerch. P.J.V.S. tested, upgraded, and validated the prototype. J.A.M.-R. proposed the polynomial concept of generating controlling frequency and duty. A.M.P. designed and developed the used transformer. All authors have read and agreed to the published version of the manuscript.

Funding: This research was funded by FUNDACION PARA LA INVESTIGACION CIENTIFICA Y TECNICA FICYT, grant number SV-PA-21-AYUD/2021/50938 and It was partially supported by Africa Improved Foods https://africaimprovedfoods.com, in the skills development program.

Conflicts of Interest: The authors declare no conflict of interest. The funders had no role in the design of the study; in the collection, analysis, or interpretation of data; in the writing of the manuscript, or in the decision to publish the results.

Abbreviations

The following abbreviations are used in this manuscript:

CCS	Code Composer Studio
IGBT	Insulated Gate Bipolar Transistor
PRC	Parallel Resonant Converters
PWM	Pulse Width Modulation
TI	Texas Instrument

References

1. National Institute of Environmental Health Sciences; National Institutes of Health. Electric and magnetic fields associated with the use of electric power. In *NIEHS/DOE EMF RAPID Program*; 2002.
2. Petri, A.K.; Schmiedchen, K.; Stunder, D.; Dechent, D.; Kraus, T.; Bailey, W.H.; Driessen, S. Biological effects of exposure to static electric fields in humans and vertebrates: a systematic review. *Environ. Health* **2017**, *16*, 41. [CrossRef] [PubMed]
3. Ahlbom, A.; Bridges, J.; De Seze, R.; Hillert, L.; Juutilainen, J.; Mattsson, M.O.; Neubauer, G.; Schüz, J.; Simko, M.; Bromen, K. Possible effects of electromagnetic fields (EMF) on human health–opinion of the scientific committee on emerging and newly identified health risks (SCENIHR). *Toxicology* **2008**, *246*, 248–250. [PubMed]
4. Menke, M.F.; da Silva, M.F.; Bisogno, F.E.; Perdigao, M.S.; Saraiva, E.S.; Alonso, J.M.; Seidel, A.R. Comparative Analysis of Self-Oscillating Electronic Ballast Dimming Methods With Power Factor Correction for Fluorescent Lamps. *IEEE Trans. Ind. Appl.* **2015**, *51*, 770–782. [CrossRef]
5. Kadota, M.; Shoji, H.; Furuya, S. A Dimming Method for Hot Cathode Fluorescent Lamp Using a Resonant Inverter Operating at Fixed Switching Frequency. *IEEE Trans. Power Electron.* **2015**, *30*, 2253–2261. [CrossRef]
6. Sarnago, H.; Lucia, O.; Mediano, A.; Burdio, J.M. Design and Implementation of a High-Efficiency Multiple-Output Resonant Converter for Induction Heating Applications Featuring Wide Bandgap Devices. *IEEE Trans. Power Electron.* **2014**, *29*, 2539–2549. [CrossRef]
7. Kundu, U.; Sensarma, P. Gain-Relationship-Based Automatic Resonant Frequency Tracking in Parallel *LLC* Converter. *IEEE Trans. Ind. Electron.* **2015**, *63*, 874–883. [CrossRef]
8. Garcia, V.; Rico, M.; Sebastian, J.; Hernando, M.; Uceda, J. Study of an optimized resonant converter for high-voltage applications. In Proceedings of the 3rd International Power Electronic Congress. Technical Proceedings (CIEP'94), Puebla, Mexico, 21–25 August 1994; pp. 114–121.
9. Luo, W.; Wang, X. Development of electric control high power medical-use X-ray generator. In Proceedings of the 2009 International Conference on Information Engineering and Computer Science, Wuhan, China, 19–20 December 2009; pp. 1–5.
10. Cavalcante, F. High Output Voltage Series-Parallel Resonant dc-dc Converter for Medical X-ray Imaging Applications. Ph.D. Thesis, These de la Swiss Federal Institute of Technology Zurich, Zurich, Switzerland, 2006.

11. Agamy, M.; Dame, M.; Dai, J.; Li, X.; Cioffi, P.; Sellick, R.; Gupta, R. Resonant converter building blocks for high power, high voltage applications. In Proceedings of the 2015 IEEE Applied Power Electronics Conference and Exposition (APEC), Charlotte, NC, USA, 15–19 March 2015; pp. 2116–2121.
12. Wang, H. Design and Control of Series Resonant Converters for dc Current Power Distribution Applications. Ph.D. Thesis, Utah State University, Logan, UT, USA, 2018.
13. Juan, D.; Villegas, P.J.; Alberto, M.P.; Martín-Ramos, J.A.; Jose-Prieto, M.A. High-voltage DC/DC converter 10KV, 600W with digital output voltage monitoring. In Proceedings of the 2013 IEEE Industry Applications Society Annual Meeting, Lake Buena Vista, FL, USA, 6–11 October 2013; pp. 1–6.
14. Diaz, J.; Saiz, P.J.V.; Martin-Ramos, J.A.; Martin-Pernia, A.; Martinez, J.A. A high-voltage ac/dc resonant converter based on prc with single capacitor as an output filter. *IEEE Trans. Ind. Appl.* **2010**, *46*, 2134–2142. [CrossRef]
15. Martin-Ramos, J.A.; Díaz, J.; Nuño, F.; Villegas, P.J.; López-Hernández, A.; Gutiérrez-Delgado, J.F. A polynomial model to calculate steady-state set point in the PRC-LCC topology with a capacitor as output filter. *IEEE Trans. Ind. Appl.* **2014**, *51*, 2520–2527. [CrossRef]
16. Martín-Ramos, J.A.; Sáiz, P.J.V.; Pernía, A.M.; Díaz, J.; Martínez, J.A. Optimal control of a high-voltage power supply based on the PRC-LCC topology with a capacitor as output filter. *IEEE Trans. Ind. Appl.* **2013**, *49*, 2323–2329. [CrossRef]
17. Yang, R.; Ding, H.; Xu, Y.; Yao, L.; Xiang, Y. An analytical steady state model of LCC type series–parallel resonant converter with capacitive output filter. *IEEE Trans. Power Electron.* **2014**, *29*, 328–338. [CrossRef]
18. Sun, J.M.; Wang, S.P.; Nishimura, T.; Nakaoka, M. Resonant mode PWM DC–DC converter with a high-voltage transformer link and its control methods for medical-use X-ray power supply. In Proceedings of the 8th European Conference on Power Electronics and Applications, Lausanne, Switzerland, 7–9 September 1999; pp. 7–9.
19. Shafiei, N.; Pahlevaninezhad, M.; Farzanehfard, H.; Motahari, S.R. Analysis and implementation of a fixed-frequency LCLC resonant converter with capacitive output filter. *IEEE Trans. Ind. Electron.* **2011**, *58*, 4773–4782. [CrossRef]
20. Nguyen, B.; Zhang, X.; Ferencz, A.; Takken, T.; Senger, R.; Coteus, P. Analytic model for power MOSFET turn-off switching loss under the effect of significant current diversion at fast switching events. In Proceedings of the 2018 IEEE Applied Power Electronics Conference and Exposition (APEC), San Antonio, TX, USA, 4–8 March 2018; pp. 287–291. [CrossRef]
21. Locorotondo, E.; Pugi, L.; Corti, F.; Becchi, L.; Grasso, F. Analytical Model of Power MOSFET Switching Losses due to Parasitic Components. In Proceedings of the 2019 IEEE 5th International forum on Research and Technology for Society and Industry (RTSI), Florence, Italy, 9–12 September 2019; pp. 331–336. [CrossRef]
22. Dobrescu, L.; Smeu, R.; Dobrescu, D. Load switch power MOSFET SPICE model. In Proceedings of the 2016 International Conference and Exposition on Electrical and Power Engineering (EPE), Iasi, Romania, 20–22 October 2016; pp. 644–647. [CrossRef]
23. Yang, Y.; Ma, D.; Yu, T. Interpolation by nonuniform b-spline through uniform b-spline filter banks. In Proceedings of the 2016 IEEE International Conference on Digital Signal Processing (DSP), Beijing, China, 16–18 October 2016; pp. 375–378.
24. Ferrer-Arnau, L.; Parisi-Baradad, V.; Soria, J.; Nasreddine, K.; Benzinou, A. A comparative study between elliptic fourier and b-spline descriptors for object contour representation. In Proceedings of the International Image Processing, Applications and Systems Conference, Sfax, Tunisia, 5–7 November 2014; pp. 1–5.
25. Che, X.; Zong, S.; Che, N.; Gao, Z. The product calculation of linear polynomial and b-spline curve. In Proceedings of the 2009 IEEE 10th International Conference on Computer-Aided Industrial Design & Conceptual Design, Wenzhou, China, 26–29 November 2009; pp. 991–994.
26. Malkowski, M.; Ufnalski, B.; Grzesiak, L.M. B-spline based repetitive controller revisited: Error shift, higher-order polynomials and smooth pass-to-pass transition. In Proceedings of the 2015 19th International Conference on System Theory, Control and Computing (ICSTCC), Cheile Gradistei, Romania, 14–16 October 2015; pp. 19–25.
27. Texas Instrument. *TMS320F2833x, TMS320F2823x Digital Signal Controllers (DSCs)*; Texas Instrument: Brussels Belgium, 2007.

Bibliography

[1] Maysam Abbasi, Ehsan Abbasi, and Li Li. New transformer-less dc–dc converter topologies with reduced voltage stress on capacitors and increased voltage conversion ratio. *IET Power Electronics*, 14(6):1173–1192, 2021.

[2] MS Agamy, ME Dame, J Dai, X Li, PM Cioffi, RL Sellick, and RK Gupta. Resonant converter building blocks for high power, high voltage applications. In *2015 IEEE Applied Power Electronics Conference and Exposition (APEC)*, pages 2116–2121. IEEE, 2015.

[3] Anders Ahlbom, James Bridges, René De Seze, Lena Hillert, Jukka Juutilainen, Mats-Olof Mattsson, Georg Neubauer, Joachim Schüz, Myrtill Simko, and Katja Bromen. Possible effects of electromagnetic fields (emf) on human health–opinion of the scientific committee on emerging and newly identified health risks (scenihr). *Toxicology*, 246(2-3):248–250, 2008.

[4] Mansour Ahmadian, ZJ Nazari, N Nakhaee, and Z Kostic. Model based design and sdr. In *2005 The 2nd IEE/EURASIP Conference on DSPenabledRadio (Ref. No. 2005/11086)*, pages 8–pp. IET, 2005.

[5] J. Marcos Alonso, Marina S. Perdigão, Javier Ribas, David Gacio, and Eduardo Sousa Saraiva. Optimizing universal ballasts using magnetic regulators and digital control. *IEEE Transactions on Industrial Electronics*, 58(7):2860–2871, 2011.

[6] Sanzhong Bai, Zeljko Pantic, and Srdjan Lukic. A comparison study of control strategies for zvs resonant converters. In *IECON 2010-36th Annual Conference on IEEE Industrial Electronics Society*, pages 256–262. IEEE, 2010.

[7] Stephane Bibian and Hua Jin. Time delay compensation of digital control for dc switchmode power supplies using prediction techniques. *IEEE Transactions on power electronics*, 15(5):835–842, 2000.

[8] Britannica. traveling-wave tube, 2022.

[9] byjus. Electrostatic precipitator, 2022.

[10] F Cavalcante. High output voltage series-parallel resonant dc-dc converter for medical x-ray imaging applications. *These de la Swiss Federal Institute of technology Zurich*, 2006.

[11] Ye-Then Chang and Yen-Shin Lai. Effect of sampling frequency of a/d converter on controller stability and bandwidth of digital-controlled power converter. In *2007 7th Internatonal Conference on Power Electronics*, pages 625–629. IEEE, 2007.

[12] Yu-kun Chang. Digital control of a series-loaded resonant converter. 2006.

[13] Steven C Chapra et al. *Applied numerical methods with MATLAB for engineers and scientists*. McGraw-Hill Higher Education, 2008.

[14] Xiangjiu Che, Shiying Zong, Na Che, and Zhanheng Gao. The product calculation of linear polynomial and b-spline curve. In *2009 IEEE 10th International Conference on Computer-Aided Industrial Design & Conceptual Design*, pages 991–994. IEEE, 2009.

[15] Jianfei Chen, Minh-Khai Nguyen, Zhigang Yao, Caisheng Wang, Le Gao, and Gangyi Hu. Dc-dc converters for transportation electrification: Topologies, control, and future challenges. *IEEE Electrification Magazine*, 9(2):10–22, 2021.

[16] Yu-Hsing Chen, Catalin Gabriel Dincan, Philip Kjær, Claus Leth Bak, Xiongfei Wang, Carlos Enrique Imbaquingo, Eduard Sarrà, Nicola Isernia, and Alberto Tonellotto. Model-based control design of series resonant converter based on the discrete time domain modelling approach for dc wind turbine. *Journal of Renewable Energy*, 2018, 2018.

[17] S.A. Chickamenahalli, Jun Liu, and M. Suryakumar. A dsp controlled variable-frequency resonant-commutated converter. *IEEE Transactions on Power Electronics*, 15(3):447–455, 2000.

[18] Tze Wood Ching and KU Chan. Review of soft-switching techniques for high-frequency switched-mode power converters. In *2008 IEEE Vehicle Power and Propulsion Conference*, pages 1–6. IEEE, 2008.

[19] codecruck, 2021.

[20] Steven A Coons. Surface patches and b-spline curves. *Computer Aided Geometric Design*, pages 1–16, 1974.

[21] David R Dance. Diagnostic radiology physics a handbook for teachers and students. 2019.

[22] Mohammad Daryaei, Mohammad Ebrahimi, and Sayed Ali Khajehoddin. Alternative approach to analysis and design of series resonant converter at steady state. *IEEE Transactions on Industrial Electronics*, 66(6):4424–4435, 2019.

[23] Mohammad Daryaei, S. Ali Khajehoddin, Javad Mashreghi, and Khurram K. Afridi. A new approach to steady-state modeling, analysis, and design of power converters. *IEEE Transactions on Power Electronics*, 36(11):12746–12768, 2021.

[24] Dipankar Das, Arijit Chakraborty, and Avik Mitra. Sample based curve fitting computation on the performance of quicksort in personal computer. *vol*, 5:885–891, 2014.

[25] Juan Diaz, Pedro Jose Villegas Saiz, Juan A Martin-Ramos, Alberto Martin-Pernia, and Juan A. Martinez. A high-voltage ac/dc resonant converter based on prc with single capacitor as an output filter. *IEEE Transactions on Industry Applications IEEE*, 46(6):2134 – 2142, 2010.

[26] Electronicsnotes. Traveling wave tube, twt, 2022.

[27] Encyclopedia. Data flow diagram, 2022.

[28] Robert W Erickson and Dragan Maksimovic. *Fundamentals of power electronics*. Springer Science & Business Media, 2007.

[29] RWAMURANGWA Evode. High voltage dc measurement through low-pass filter ripples detection in parallel resonant converters with no-inductor at output. In *2019 IEEE PES/IAS PowerAfrica*, pages 379–384. IEEE, 2019.

[30] Enze Fan, Yaohua Li, Qiongxuan Ge, and Lu Zhao. Time-domain steady-state analysis of phase-shifted full-bridge series resonant converter with light load. In *2020 23rd International Conference on Electrical Machines and Systems (ICEMS)*, pages 1843–1846, 2020.

[31] Ll Ferrer-Arnau, Vicenç Parisi-Baradad, JA Soria, Kamal Nasreddine, and Abdesslam Benzinou. A comparative study between elliptic fourier and b-spline descriptors for object contour representation. In *International Image Processing, Applications and Systems Conference*, pages 1–5. IEEE, 2014.

[32] V Garcia, M Rico, J Sebastian, MM Hernando, and Javier Uceda. Study of an optimized resonant converter for high-voltage applications. *3rd International Power Electronic Congress. Technical Proceedings CIEP'94, IEEE*, pages 114 – 121, 1994.

[33] Fernando Jesús García Díaz, Juan Díaz, Jorge García, Alberto M Pernía, and Pedro J Villegas. A complete control system for a high voltage converter in an electrostatic precipitator. *Electronics*, 10(13):1554, 2021.

[34] Kiran Kumar Geddam and Elangovan Devaraj. Real time hardware-in-loop implementation of llc resonant converter at worst operating point based on time domain analysis. *Energies*, 15(10):3634, 2022.

[35] Joseph A Goguen. L-fuzzy sets. *Journal of mathematical analysis and applications*, 18(1):145–174, 1967.

[36] William J Gordon and Richard F Riesenfeld. B-spline curves and surfaces. In *Computer aided geometric design*, pages 95–126. Elsevier, 1974.

[37] Thales Group. Travelling wave tubes: Timeless precision that goes a long way, 2022.

[38] Sun Guibin and Guo Fei. The data fitting of motor back-to-back test based on least square method. 2018.

[39] Yusuke Hayashi, Hajime Toyoda, and Toshifumi Ise. Contactless dc connector concept for high-power-density 380-v dc distribution system. *IEEJ Journal of Industry Applications*, 4(1):49–58, 2015.

[40] Pavlo Herasymenko and Volodymyr Pavlovskyi. Soft start-up strategy of pulse-density-modulated series-resonant converter for induction heating application. *International Journal of Power Electronics and Drive Systems*, 12(1):258, 2021.

[41] Gabor T Herman. *Fundamentals of computerized tomography: image reconstruction from projections*. Springer Science & Business Media, 2009.

[42] Jun Imaoka, Masayoshi Yamamoto, and Takahiro Kawashima. High-power-density three-phase interleaved boost converter with a novel coupled inductor. *IEEJ Journal of Industry Applications*, 4(1):20–30, 2015.

[43] Gregory Ivensky, Arkadiy Kats, and Sam Ben-Yaakov. A novel rc model of capacitive-loaded parallel and series-parallel resonant dc-dc converters. In *PESC97. Record 28th Annual IEEE Power Electronics Specialists Conference. Formerly Power Conditioning Specialists Conference 1970-71. Power Processing and Electronic Specialists Conference 1972*, volume 2, pages 958–964. IEEE, 1997.

[44] Edwin M. Leidholdt Jr. John M. Boone Jerrold T. Bushberg, J. Anthony Seibert. *The Essential Physics of Medical Imaging (2nd Edition)*. 2.00 edition, 2001.

[45] Óscar Jiménez, Óscar Lucía, Isidro Urriza, Luis A. Barragan, Denis Navarro, and Venkata Dinavahi. Implementation of an fpga-based online hardware-in-the-loop emulator using high-level synthesis tools for resonant power converters applied to induction heating appliances. *IEEE Transactions on Industrial Electronics*, 62(4):2206–2214, 2015.

[46] Steven D Johnson, Arthur F Witulski, and Robert W Erickson. A comparison of resonant topologies in high voltage dc applications. In *1987 2nd IEEE Applied Power Electronics Conference and Exposition*, pages 145–156. IEEE, 1987.

[47] Díaz Juan, Pedro J Villegas, Martín-Pernía Alberto, Juan Antonio Martín-Ramos, and Miguel A Jose-Prieto. High-voltage dc/dc converter 10kv, 600w with digital output voltage monitoring. In *2013 IEEE Industry Applications Society Annual Meeting*, pages 1–6. IEEE, 2013.

[48] Mitsuhiro Kadota, Hiroyuki Shoji, and Sachio Furuya. A dimming method for hot cathode fluorescent lamp using a resonant inverter operating at fixed switching frequency. *IEEE Transactions on Power Electronics*, 30(4):2253–2261, 2014.

[49] Kajanan Kanathipan and John Lam. An electrolytic capacitor-less pv micro-inverter based on cll resonant conversion with a power control scheme using resonant circuit voltage control loops. *CPSS Transactions on Power Electronics and Applications*, 7(2):139–149, 2022.

[50] Keyence. Melting principles and applications, 2021.

[51] Jae Hee Kim, Byung-Song Lee, Jun-Ho Lee, Seung-Hwan Lee, Chan-Bae Park, Shin-Myung Jung, Soo-Gil Lee, Kyung-Pyo Yi, and Jeihoon Baek. Development of 1-mw inductive power transfer system for a high-speed train. *IEEE Transactions on Industrial Electronics*, 62(10):6242–6250, 2015.

[52] Shota Kimura, Kimihiro Nanamori, Taichi Kawakami, Jun Imaoka, and Masayoshi Yamamoto. Allowable power analysis and comparison of high power density dc-dc converters with integrated magnetic components. *IEEJ Journal of Industry Applications*, 6(6):463–472, 2017.

[53] Peter J King and Ehmat H Mamdani. The application of fuzzy control systems to industrial processes. *Automatica*, 13(3):235–242, 1977.

[54] Utsab Kundu and Parthasarathi Sensarma. Gain-relationship-based automatic resonant frequency tracking in parallel llc converter. *IEEE Transactions on Industrial Electronics*, 63(2):874–883, 2015.

[55] C.q. Lee and K. Siri. Analysis and design of series resonant converter by state-plane diagram. *IEEE Transactions on Aerospace and Electronic Systems*, AES-22(6):757–763, 1986.

[56] Wenxin Liu, Zhiqiang Zhang, Weihao Liu, Zhihao Jin, Kedong Zhao, Chao Zhao, Xin Guo, Zhaochuan Zhang, Shengyi Yin, and Zhenxia Zhang. Demonstration of a high-power and wide-bandwidth g-band traveling wave tube with cascade amplification. *IEEE Electron Device Letters*, 42(4):593–596, 2021.

[57] Alexandre Baratella Lugli, Egidio Raimundo Neto, João Paulo Carvalho Henriques, Maureen DAniela Arambulo HERVAS, Max Mauro Dias SANTOS, and Joao Francisco Justo. Industrial application control with fuzzy systems. *International Journal of Innovative Computing, Information and Control*, 12(2 (Web)):665–676, 2016.

[58] Weitao Luo and Xu Wang. Development of electric control high power medical-use x-ray generator. In *2009 International Conference on Information Engineering and Computer Science*, pages 1–5. IEEE, 2009.

[59] JMA Álvarez. High frequency resonant inverters. *Gijón: University of Oviedo*, 1999.

[60] N Madhanakkumar, TS Sivakumaran, G Irusapparajan, and D Sujitha. Closed loop control of llc resonant converter incorporating zvs boost converter. *International Journal of Engineering and Technology*, 6(2), 2014.

[61] Michal Malkowski, Bartlomiej Ufnalski, and Lech M Grzesiak. B-spline based repetitive controller revisited: Error shift, higher-order polynomials and smooth pass-to-pass transition. In *2015 19th International Conference on System Theory, Control and Computing (ICSTCC)*, pages 19–25. IEEE, 2015.

[62] E.H. Mamdani and S. Assilian. An experiment in linguistic synthesis with a fuzzy logic controller. *International Journal of Man-Machine Studies*, 7(1):1–13, 1975.

[63] Sunita Marothiya, Vedant Patel, Divya Jain, Shubhangi Agrawal, Surbhi Joshi, and Vipin Pandey. Cone beam computed tomography in orthodontics: A. 2019.

[64] JA Martin-Ramos, AM Pernia, J Díaz, F Nuño, and JM Alonso. A circuit for the large and small signal dynamic modeling of the prc-lcc resonant topology with a capacitor as output filter. In *2005 IEEE 36th Power Electronics Specialists Conference*, pages 635–641. IEEE, 2005.

[65] Juan A Martin-Ramos, Juan Díaz, Fernando Nuño, Pedro José Villegas, Agustín López-Hernández, and J Francisco Gutiérrez-Delgado. A polynomial model to calculate steady-state set point in the prc-lcc topology with a capacitor as output filter. *IEEE Transactions on Industry Applications*, 51(3):2520–2527, 2014.

[66] Juan A Martín-Ramos, Pedro José Villegas Sáiz, Alberto M Pernía, Juan Díaz, and Juan A Martínez. Optimal control of a high-voltage power supply based on the prc-lcc topology with a capacitor as output filter. *IEEE Transactions on Industry Applications*, 49(5):2323–2329, 2013.

[67] Pernía A. M. Díaz J. Nuno F. Martin-Ramos, J. A. and Martinez J. A. Power supply for a high-voltage application. *IEEE Transactions on power electronics IEEE*, 23(4):1608 – 1619, 2008.

[68] Mathworks. Ip core generation workflow without an embedded arm processor: Arrow deca max 10 fpga evaluation kit, 2022.

[69] Blausen Medical. Medical gallery of blausen medical 2014. *WikiJournal of Medicine*, 1(2):1–79, 2014.

[70] MF Menke, MF Da Silva, FE Bisogno, MS Perdigao, ES Saraiva, JM Alonso, and AR Seidel. Comparative analysis of self-oscillating electronic ballast dimming methods with power factor correction for fluorescent lamps. *IEEE Transactions on Industry Applications*, 51(1):770–782, 2014.

[71] Andrzej Mondzik, Robert Stala, Stanisław Piróg, Adam Penczek, Piotr Gucwa, and Miłosz Szarek. High efficiency dc–dc boost converter with passive snubber and reduced switching losses. *IEEE Transactions on Industrial Electronics*, 69(3):2500–2510, 2021.

[72] Sang Cheol Moon and Chen-Hua Chiu. Hybrid-mode pfm control for llc resonant converter. *IEEE Transactions on Power Electronics*, 37(1):274–284, 2021.

[73] Omid Mostaghimi, Nick Wright, and Alton Horsfall. Design and performance evaluation of sic based dc-dc converters for pv applications. In *2012 IEEE Energy Conversion Congress and Exposition (ECCE)*, pages 3956–3963. IEEE, 2012.

[74] Thomas Nussbaumer, Marcelo Lobo Heldwein, Guanghai Gong, Simon D Round, and Johann W Kolar. Comparison of prediction techniques to compensate time delays caused by digital control of a three-phase buck-type pwm rectifier system. *IEEE transactions on industrial electronics*, 55(2):791–799, 2008.

[75] National Institute of Environmental Health Sciences, National Institutes of Health, et al. Electric and magnetic fields associated with the use of electric power. *NIEHS/DOE EMF RAPID Program*, 2002.

[76] National Institute of Environmental Health Sciences, National Institutes of Health, et al. Electric and magnetic fields associated with the use of electric power. *NIEHS/DOE EMF RAPID Program*, 2002.

[77] Hwa-Pyeong Park, Yesung Kang, Seokhyeong Kang, and Jee-Hoon Jung. Fpga controller design for high-frequency llc resonant converters. *IEEJ Journal of Industry Applications*, 9(5):523–529, 2020.

[78] Miguel J. Prieto Pedro J. Villegas Juan Díaz Pernía, A. Martín and Juan A. Martín-Ramos. Lcc resonant multilevel converter for x-ray applications. *Energies MDPI*, 10(10):1573, 2017.

[79] Anne-Kathrin Petri, Kristina Schmiedchen, Dominik Stunder, Dagmar Dechent, Thomas Kraus, William H Bailey, and Sarah Driessen. Biological effects of exposure to static electric fields in humans and vertebrates: a systematic review. *Environmental Health*, 16(1):1–23, 2017.

[80] Andrzej Piegat. *Modelowanie i sterowanie rozmyte*. Akademicka Oficyna Wydawnicza" Exit", 1999.

[81] Aleksandar Prodic, Dragan Maksimovic, and Robert W Erickson. Design and implementation of a digital pwm controller for a high-frequency switching dc-dc power converter. In *IECON'01. 27th Annual Conference of the IEEE Industrial Electronics Society (Cat. No. 37243)*, volume 2, pages 893–898. IEEE, 2001.

[82] Jacek Rąbkowski, Andrzej Łasica, Mariusz Zdanowski, Grzegorz Wrona, and Jacek Starzyński. Portable dc supply based on sic power devices for high-voltage marx generator. *Electronics*, 10(3):313, 2021.

[83] Akshay K Rathore, Ashoka KS Bhat, and Ramesh Oruganti. A comparison of soft-switched dc-dc converters for fuel cell to utility interface application. *IEEJ Transactions on Industry Applications*, 128(4):450–458, 2008.

[84] Lisandra Kittel Ries, Thiago Batista Soeiro, Márcio Silveira Ortmann, and Marcelo Lobo Heldwein. Analysis of carrier-based pwm patterns for a three-phase five-level bidirectional buck<inline-formula> <tex-math notation="latex">+</tex-math></inline-formula>boost-type rectifier. *IEEE Transactions on Power Electronics*, 32(8):6005–6017, 2017.

[85] Wilhelm Conrad Röntgen. and the glimmer of light. *Physics Today, Nov*, pages 25–31, 1995.

[86] Mohamed Salem, Awang Jusoh, NR Nik Idris, Tole Sutikno, and Yonis M Yonis Buswig. Phase-shifted series resonant converter with zero voltage switching turn-on and variable frequency control. *International Journal of Power Electronics and Drive Systems (IJPEDS)*, 8(3):1184–1192, 2017.

[87] Hector Sarnago, Oscar Lucia, Arturo Mediano, and Jose M Burdio. Design and implementation of a high-efficiency multiple-output resonant converter for induction heating applications featuring wide bandgap devices. *IEEE Transactions on Power Electronics*, 29(5):2539–2549, 2013.

[88] J Anthony Seibert. X-ray imaging physics for nuclear medicine technologists. part 1: Basic principles of x-ray production. *Journal of nuclear medicine technology*, 32(3):139–147, 2004.

[89] Navid Shafiei, Majid Pahlevaninezhad, Hosein Farzanehfard, Alireza Bakhshai, and Praveen Jain. Analysis of a fifth-order resonant converter for high-voltage dc power supplies. *IEEE transactions on power electronics*, 28(1):85–100, 2012.

[90] Navid Shafiei, Majid Pahlevaninezhad, Hosein Farzanehfard, and Seyed Reza Motahari. Analysis and implementation of a fixed-frequency lclc resonant converter with capacitive output filter. *IEEE Transactions on industrial electronics*, 58(10):4773–4782, 2011.

[91] Hossein Shayeghi, Saeed Pourjafar, Seyed Majid Hashemzadeh, and Frede Blaabjerg. A high efficiency soft-switched dc–dc converter with high voltage conversion ratio. *International Journal of Circuit Theory and Applications*, 49(2):244–266, 2021.

[92] David C Shelledy and Jay I Peters. *Respiratory care: Patient assessment and care plan development*. Jones & Bartlett Learning, 2021.

[93] David C Shelledy and Jay I Peters. *Respiratory care: patient assessment and care plan development*. Jones & Bartlett Learning, 2021.

[94] Benjamin K Sovacool and Christopher J Cooper. *The governance of energy megaprojects: politics, hubris and energy security*. Edward Elgar Publishing, 2013.

[95] Robert L Steigerwald. A comparison of half-bridge resonant converter topologies. *IEEE transactions on Power Electronics*, 3(2):174–182, 1988.

[96] Guibin Sun and Fei Guo. The data fitting of motor back-to-back test based on least square method. In *2018 8th International Conference on Manufacturing Science and Engineering (ICMSE 2018)*, pages 204–209. Atlantis Press, 2018.

[97] JM Sun, SP Wang, T Nishimura, and M Nakaoka. Resonant mode pwm dc-dc converter with a high-voltage transformer link and its control methods for medical-use x-ray power supply. In *Proc. EPE*, volume 99, pages 1–7, 1999.

[98] Amirehsan Sarabadani Tafreshi, Verena Klamroth-Marganska, Silvio Nussbaumer, and Robert Riener. Real-time closed-loop control of human heart rate and blood pressure. *IEEE Transactions on Biomedical Engineering*, 62(5):1434–1442, 2015.

[99] Shuilin Tian, Fred C. Lee, and Qiang Li. A simplified equivalent circuit model of series resonant converter. *IEEE Transactions on Power Electronics*, 31(5):3922–3931, 2016.

[100] Shuilin Tian, Fred C Lee, Qiang Li, and Bin Li. Small-signal equivalent circuit model of series resonant converter. In *2015 IEEE Energy Conversion Congress and Exposition (ECCE)*, pages 172–179. IEEE, 2015.

[101] TMS320F28334 TMS320F28335 and TMS320F28332 TMS320F28333. Tms320f2833x, tms320f2823x digital signal controllers (dscs), 2007.

[102] Roland Unruh, Frank Schafmeister, and Joachim Böcker. 11kw, 70khz llc converter design with adaptive input voltage for 98efficiency in an mmc. In *2020 IEEE 21st Workshop on Control and Modeling for Power Electronics (COMPEL)*, pages 1–8, 2020.

[103] Michael Unser, Akram Aldroubi, and Murray Eden. B-spline signal processing. i. theory. *IEEE transactions on signal processing*, 41(2):821–833, 1993.

[104] Vlatko Vlatkovic, Michael J Schutten, and Robert L Steigerwald. Auxiliary series resonant converter: A new converter for high-voltage, high-power applications. In *Proceedings of Applied Power Electronics Conference. APEC'96*, volume 1, pages 493–499. IEEE, 1996.

[105] Ge Wang, Hengyong Yu, and Bruno De Man. An outlook on x-ray ct research and development. *Medical physics*, 35(3):1051–1064, 2008.

[106] Guozhao Wang, Qinyu Chen, and Minghua Zhou. Nuat b-spline curves. *Computer Aided Geometric Design*, 21(2):193–205, 2004.

[107] Hongjie Wang. *Design and control of series resonant converters for dc current power distribution applications*. PhD thesis, Utah State University, 2018.

[108] Brian C Williams and Michel D Ingham. Model-based programming: Controlling embedded systems by reasoning about hidden state. In *International Conference on Principles and Practice of Constraint Programming*, pages 508–524. Springer, 2002.

[109] Mengwei Xu, Xin Yang, and Jiawen Li. C-rc snubber optimization design for improving switching characteristics of sic mosfet. *IEEE Transactions on Power Electronics*, 2022.

[110] Tatsuya Yamamoto, Yinggang Bu, Tsutomu Mizuno, Yutaka Yamaguchi, and Tomoyoshi Kano. Loss reduction of transformer for llc resonant converter using a magnetoplated wire. *IEEJ Journal of Industry Applications*, 7(1):43–48, 2018.

[111] Bo Yang, Fred C Lee, AJ Zhang, and Guisong Huang. Llc resonant converter for front end dc/dc conversion. In *APEC. Seventeenth Annual IEEE Applied Power Electronics Conference and Exposition (Cat. No. 02CH37335)*, volume 2, pages 1108–1112. IEEE, 2002.

[112] Chengzi Yang, Yunqing Pei, Laili Wang, Longyang Yu, Fan Zhang, and Braham Ferreira. Overvoltage and oscillation suppression circuit with switching losses optimization and clamping energy feedback for sic mosfet. *IEEE transactions on power electronics*, 36(12):14207–14219, 2021.

[113] Eric X Yang, Fred C Lee, and MM Jovanovic. Small-signal modeling of power electronic circuits by extended describing function concept. In *Proc. Virginia Power Electronics Center Seminar*, pages 167–178, 1991.

[114] Rui Yang, HongFa Ding, Yun Xu, Lei Yao, and YingMeng Xiang. An analytical steady-state model of lcc type series–parallel resonant converter with capacitive output filter. *IEEE Transactions on Power Electronics*, 29(1):328–338, 2013.

[115] Yanli Yang, De Ma, and Ting Yu. Interpolation by nonuniform b-spline through uniform b-spline filter banks. In *2016 IEEE International Conference on Digital Signal Processing (DSP)*, pages 375–378. IEEE, 2016.

[116] Lotfi A Zadeh. Fuzzy sets. *Information and control*, 8(3):338–353, 1965.

[117] Mostafa Zarghani, Saeed Peyghami, Francesco Iannuzzo, Frede Blaabjerg, and Shahriyar Kaboli. An energy recovery scheme for rcd snubber in the series configuration of igbts. In *2021 IEEE Energy Conversion Congress and Exposition (ECCE)*, pages 5183–5189. IEEE, 2021.

[118] Li Zhai, Shuangjie Yang, Guixing Hu, and Mengyuan Lv. Optimal design method of high voltage dc power supply emi filter considering source impedance of motor controller for electric vehicle. *IEEE Transactions on Vehicular Technology*, 2022.

[119] Yiming Zhang, Kainan Chen, Fanbo He, Zhengming Zhao, Ting Lu, and Liqiang Yuan. Closed-form oriented modeling and analysis of wireless power transfer system with constant-voltage source and load. *IEEE Transactions on Power Electronics*, 31(5):3472–3481, 2016.

[120] Zhennan Zhao, Shanlu Zhang, Lei Li, Shengfang Fan, and Cheng Wang. Digital implementation of lcc resonant converters for x-ray generator with optimal trajectory startup control. *World Electric Vehicle Journal*, 13(5):71, 2022.